Modelling Ciliopathies in the Zebrafish:

Elucidating the Role of Cc2d2a and Talpid3 in Photoreceptor Development and Function

---

Dissertation

zur

Erlangung der naturwissenschaftlichen Doktorwürde

(Dr. sc. nat.)

vorgelegt der

Mathematisch-naturwissenschaftlichen Fakultät

der

Universität Zürich

von

Irene Ojeda Naharros

aus

Spanien

Promotionskommission

Prof. Dr. Stephan NEUHAUSS (Vorsitz)
Prof. Dr. Ruxandra BACHMANN-GAGESCU
Prof. Dr. Esther STOECKLI
Prof. Dr. Ronald ROEPMAN

Zürich, 2017

«I don´t know anything, but I do know that everything is interesting if you go into it deeply enough»

Richard Feynman

To my family, to Fabian.

Summary

Ciliopathies are a group of human disorders caused by primary cilium dysfunction and unified by a wide array of overlapping phenotypes: cystic kidney disease, central nervous system (CNS) malformations and retinal degeneration among others. Primary cilia are crucial ubiquitous organelles consisting of a centriole-derived basal body (BB), a microtubule-based axoneme and a specialized membrane that harbors proteins required for signal detection. Indeed, the main function of primary cilia is detection and transduction of signals critical for embryonic development and adult tissue homeostasis, including important morphogens such as Hedgehog (Hh) or environmental stimuli such as light. Given their role at the crux of multiple biological and developmental processes, the study of primary cilia has broad implications for our understanding of cell biology, embryonic development and human disease.

Joubert syndrome (JBTS) is a canonical ciliopathy, characterized by a pathognomonic cerebellar malformation, the Molar Tooth Sign (MTS), with variable association of additional ciliopathy phenotypes including retinal disease. Retinal photoreceptors are highly polarized sensory neurons with a modified primary cilium called the outer segment (OS), which contains the opsin-photopigment responsible for light detection. Opsin enrichment in the OS was thought to be enabled by polarized vesicle trafficking controlled by the small GTPase Rab8, a model that has been recently questioned. JBTS displays prominent genetic heterogeneity as mutations in >30 different genes, including *CC2D2A* and *TALPID3/KIAA0586*, can cause this disorder. Most of the protein products of JBTS genes localize in functional networks at the transition zone (TZ) (CC2D2A) or the BB (TALPID3). The TZ has been proposed to act as a gatekeeper, controlling the protein content of the ciliary membrane, while the BB is thought to be responsible for extending the cilium, serving as a microtubule organizing center (MTOC) and possibly participating in sorting of incoming cargo destined to the ciliary compartment. The link between cytoplasmic polarized vesicle transport, the TZ and the BB has been unexplored to date.

In my thesis, I have used the unique advantages offered by the zebrafish model to investigate the function and disease mechanisms of JBTS proteins Cc2d2a and Talpid3 in the retina.

Focusing on a *cc2d2a* zebrafish mutant, I identified a role for Cc2d2a as a periciliary membrane organizer, demonstrating a link between polarized vesicle trafficking and the TZ (chapter 2). My results support a model whereby Cc2d2a controls localization of vesicle fusion machinery components such as t-SNAREs and provides a docking point for opsin-carrier incoming vesicles. This work relied in part on a novel imaging technology called Correlative Light and Electron Microscopy (CLEM), that I adapted to the zebrafish system (chapter 3), which allows precise localization of proteins at the ultrastructural level without the limitations encountered with immunogold staining. An additional strength of this project lies in live imaging of

fluorescently-tagged Rab8 proteins, which provides the very first characterization of Rab8 trafficking in photoreceptors in a whole tissue context. My results support for a role for Rab8 in opsin trafficking, a key finding in the current controversy about Rab8 function.

KIAA0586/TALPID3 (TA3) is a novel ciliopathy protein required for ciliogenesis in various model organisms through a Rab8-dependent role in BB docking. The requirement during ciliogenesis precluded the investigation of potential additional roles for Ta3 in ciliary function in other models. In this project (chapter 4), I analyze the role of Ta3 in retinal photoreceptors of zygotic *ta3*$^{-/-}$ zebrafish mutants, in which maternally-derived Ta3 contribution partially rescues ciliogenesis. My results confirm the role of Ta3 in BB docking and suggest in addition a Rab8-independent role in cell-shape maintenance, possibly linked to the MTOC function of the BB.

Zusammenfassung

Ciliopathien sind eine Gruppe von Erkrankungen im Menschen, die durch Dysfunktion von primären Cilien ausgelöst werden, und durch eine Reihe an gemeinsamen Phänotypen verbunden sind. Dazu zählen die Zystenniere, Fehlbildungen des zentralen Nervensystems und Degeneration der Retina. Bei primären Cilien handelt es sich um äusserst wichtige ubiquitäre Organellen, die aus einem Centriol-basierten Basalkörperchen (BK), einem Mikrotubuli-basierten Axonem und einer spezialisierten Membran, welche signaldetektierende Proteine trägt, bestehen. Tatsächlich ist es die Hauptfunktion von primären Cilien, kritische Signale für die Embryonalentwicklung und für die Homöostase von adulten Geweben zu detektieren und weiterzuleiten. So werden etwa wichtige Morphogene wie Hedgehog (Hh) oder Umgebungs-Stimuli wie Licht durch Cilien detektiert. Da Cilien eine essentielle Rolle in einer Vielzahl von (entwicklungs-)biologischen Prozessen spielen, hat die Untersuchung dieser Organellen weitreichende Auswirkungen auf unser Wissen über Zellbiologie, Embryonalentwicklung und Erkrankungen im Menschen.

Das Joubert Syndrom (JBTS) ist eine kanonische Ciliopathie, welche durch eine pathogene, als Molar Tooth Sign (MTS) bezeichnete, Fehlbildung des Cerebellums und zusätzliche variierende Ciliopathie-Phänotypen, etwa Erkrankungen der Retina, charakterisiert ist. Die Photorezeptoren der Retina sind sensorische Neuronen mit ausgeprägter Polarisierung. Sie tragen ein modifiziertes primäres Cilium, welches als Aussensegment (AS) bezeichnet wird und das für die Lichtdetektion verantwortliche Photopigment Opsin trägt. Es wurde angenommen, dass die Anreicherung von Opsin im AS über den polarisierten und durch die GTPase Rab8 regulierten Transport von Vesikeln erfolgt. Jedoch wurde dieses Modell kürzlich in Frage gestellt. JBTS kann durch Mutationen in über 30 Genen, darunter *CC2D2A* und *TALPID3/KIAA0586*, verursacht werden und ist daher genetisch äusserst heterogen. Ein Grossteil der von JBTS Genen codierten Proteine sind entweder in funktionellen Proteinnetzwerken an der Transitionszone (TZ; CC2D2A), oder am BK (TALPID3/KIAA0586) lokalisiert. Es wird spekuliert, dass die TZ ähnlich einem Schrankenwärter wirkt, und somit das Proteinrepertoire der ciliären Membran kontrolliert. Das BK ist hingegen wahrscheinlich für das Wachstum des Ciliums verantwortlich ist, indem er als Zentrum für die Organisation von Mikrotubuli (ZOMT) funktioniert, und möglicherweise auch am Sortieren von Molekülen, welche für den Transport in das ciliäre Kompartiment bestimmt sind, beteiligt ist. Der Zusammenhang zwischen cytoplasmischem polarisierten Vesikeltransport, der TZ und dem BK ist bis zum heutigen Zeitpunkt unerforscht.

In meiner Arbeit machte ich mir die einzigartigen Vorteile des Modellorganismus Zebrafisch zunutze, um die Funktionen und die krankheitsauslösenden Mechanismen der JBTS Proteine Cc2d2a und Talpid3 in der Retina zu untersuchen.

Indem ich *cc2d2a*-mutante Zebrafisch untersuchte, konnte ich eine Funk-

tion von Cc2d2a als Organisator der periciliären Membran identifizieren, was ein Zusammenspiel von polarisiertem Vesikeltransport und der TZ offenlegt (Kapitel 2). Diese Resultate unterstützen ein Modell, in welchem Cc2d2a die Lokalisierung von Komponenten der Vesikel-Fusionsmaschinerie, wie etwa t-SNAREs, kontrolliert, und eine Andockstelle für Opsin-beladene Transportvesikel bietet. Dieser Teil der Arbeit beruht zum Teil auf einem neuartigen Bildgebungsverfahren für korrelative Licht- und Elektronenmikroskopie, welches ich für den Modellorganismuss Zebrafisch adaptierte (Kapitel 3). Diese Methode ermöglicht die genaue Lokalisierung von Proteinen auf ultrastrukureller Ebene, ohne dabei auf Limitationen wie bei Immunogold-Färbungen zu stossen. Eine weitere Stärke dieses Projektes liegt in der Lebendbeobachtung von fluoreszent markierten Rab8 Proteinen, wodurch zum ersten Mal Rab8 Trafficking in Photorezeptoren innerhalb eines intakten Gewebes charakterisiert werden konnte. Meine Resultate unterstützen die Rolle von Rab8 im Trafficking von Opsin, ein Schlüsselergebnis in der derzeitigen Kontroverse über die Funktion von Rab8.

TALPID3/KIAA0586 (TA3) is ein neuartiges Ciliopathie-Protein, welches in verschiedenen Modellorganismen für die Ciliogenese durch Rab8-vermitteltes Vesikel-Andocken benötigt wird. Wegen dieser wichtigen Rolle in der Ciliogenese war es bisher nicht möglich, potentielle zusätzliche Rollen von Ta3 in der Funktion von Cilien zu untesuchen. In diesem Projekt (Kapitel 4) analysierte ich die Rolle von Ta3 in Photorezeptoren der Retina von zygotischen *ta3*$^{-/-}$ Zebrafisch-Mutanten, in welchen durch maternal beigesteuertes Ta3 die Ciliogenese teils erhalten bleibt. Meine Resultate bekräftigen die Rolle von Ta3 im Andocken an das BK, und deuten ausserdem auf eine Rab8-unabhängige Funktion in der Aufrechterhaltung der Zellmorpologie hin, welche möglicherweise im Zusammenhang mit der ZOMT Funktion des BK steht.

Contents

Summary VII
Zusammenfassung IX

Chapter 1. General introduction 17

Motile and primary cilia 19
Ciliopathies 21
Joubert syndrome 23
Retinal involvement in ciliopathies 25
Polarized protein transport towards the cilium 26
Ciliogenesis 29
Zebrafish as a model for retinal ciliopathy research 32
Aims of the thesis 33
References 33

Chapter 2. The ciliopathy protein CC2D2A organizes the vesicle fusion machinery at the periciliary membrane of Zebrafish photoreceptors 41

Abstract 43
Introduction 44
Results 46
Vesicles accumulate progressively from the onset of outer segment formation in the apical portion of cc2d2a-/- photoreceptors 46
Accumulated vesicles are opsin-carrier vesicles 46
The small GTPase Rab8 associates with opsin-carrier vesicles 48
Overexpressed mCherry-Rab8a partially mislocalizes in cc2d2a-/- cones 51
Dynamics of Rab8-directed trafficking in zebrafish photoreceptors display complex patterns 51
Loss of Cc2d2a function results in mislocalization of the t-SNARE SNAP25 at the periciliary membrane 54
Decreased levels of the t-SNARE syntaxin3 and of the Exocyst in cc2d2a-/- retina 55
Discussion 56
Acknowledgements 60
Methods 60
Zebrafish maintenance and breeding 60
Zebrafish lines 60
Construct and transgenic line generation 61
Annotation of Rab cDNAs 61
Phylogenetic Analysis 61
Transmission electron microscopy (TEM) 62
Correlative light and electron microscopy (CLEM) 62

Live imaging 63
Tracking and video analysis 63
Immunohistochemistry 64
Western blot 64
Quantitative reverse transcription polymerase chain reaction (qRT-PCR) 65
Statistics 65
References 65
Supplemetary material 70

Chapter 3. Correlative super-resolution and electron microscopy to resolve protein localization in zebrafish retina 77

Keywords 79
Short abstract 79
Long abstract 79
Introduction 80
Protocol 81
Representative results 85
Discussion 85
Acknowledgements 86
Disclosures 86
References 86
Supplementary material 88

Chapter 4. The ciliopathy protein TALPID3/KIAA0586 acts upstream of Rab8 activation in zebrafish photoreceptor outer segment formation and maintenance 91

Abstract 93
Author summary 94
Introduction 94
Results 96
Normal PR differentiation followed by progressive degeneration in ta3 zebrafish mutants 96
Marked intracellular opsin mislocalization as a cause for PR cell death 99
Loss of Ta3 leads to visual function loss 99
Deficient outer segment development in ta3-/- larvae 99
Abnormal BB localization and impaired docking in ta3-/- PR underlie the OS development defect 101
Maternal Ta3 contribution rescues OS development in a subset of PRs of zygotic ta3-/- 102
Opsin mislocalization and cell shape abnormalities in PRs with normally formed OSs support roles for Ta3 beyond BB docking 104
Outer segment development is rescued by constitutively active Rab8a 104
Discussion 106

Material and methods 109
Zebrafish 109
Immunohistochemistry and Light microscopy 110
Transmission electron microscopy 110
Ta3 antibody generation 110
Electroretinography (ERG) 110
Quantifications and stats 111
Acknowledgements 111
References 111
Supplementary material 115

Chapter 5. General discussion 123

The role of the TZ protein Cc2d2a in photoreceptor ciliary function 125
The role of Rab8 in ciliary transport 127
The hidden roles of Talpid3 in photoreceptor cell shape maintenance 129
Genetic heterogeneity and phenotypic variability in ciliopathies 131
Concluding remarks and perspective 133
References 133

Appendix I. Transgenic lines and constructs 139

Materials and methods 139
Results 140

Appendix II. List of Abbreviations 143

Appendix III. Curriculum Vitae 147

Acknowledgements 151

Chapter 1. General introduction

Motile and primary cilia

Cilia are thin cell protrusions that were first observed in protozoa in 1675 by Antonie van Leeuwenhoek, who described them as «*tiny feet that move very nimbly*». However, it is believed that the term "cilia" (meaning "eyelash" in latin) was coined by Otto Müller in 1786 (Bloodgood, 2010b). Since their discovery, cilia were defined by their motility, their only ascribed purpose for centuries. When solitary non-motile cilia were found on the surface of mammalian cells, they were considered a vestigial organelle remnant of the unicellular past, and they were named primary cilia because they appear in brain tissue earlier in development than multiciliated cells (Beales and Jackson, 2012). It was not until the 1950-1960s that the primary cilia regained scientific interest and started being characterized; and not until year 2000, when the first clear association between primary cilium dysfunction and disease was reported. Ever since, primary cilia research field has been on expansion (Bloodgood, 2010a).

Cilia are present apically in most eukaryotic cells with the exception of higher plants and fungi. In invertebrates, they are restricted to sensory neurons, whereas in vertebrates they are present throughout each tissue (Baker and Beales, 2009). While motile cilia are present as several extensions protruding from very specific cell types (e.g. ependymal cells in the brain, epithelial cells of the airways and reproductive tracts) and beat in concert to generate extracellular fluid flow, primary cilia are ubiquitous organelles present as solitary sessile extensions on most cells of the body (Mitchison and Valente, 2017). There are very few but notable exceptions of vertebrate cells without a cilium: intercalated cells in the kidney collecting duct, hepatocytes, the female gamete and circulating blood cells (Temiyasathit and Jacobs, 2010).

Primary cilia are evolutionarily conserved organelles consisting of a centriole-derived basal body (BB), a microtubule-based axoneme and a specialized membrane (Fig. 1), and they are devoted to extracellular and environmental signal detection both during development and adult tissue homeostasis (Singla and Reiter, 2006). Primary cilia can detect a big panoply of signals, including mechanical stimuli, light and morphogens of the Hedgehog (Hh) family and the non-canonical Wnt PCP pathway (Goetz and Anderson, 2010).

Centrioles are highly organized structures built on a barrel-like scaffold formed by 9 triplets of microtubules arranged in a cartwheel (Garcia and Reiter, 2016). In quiescent cells, there is always a pair of centrioles intimately associated with each other –an entity known as centrosome–, which has a complex and cell cycle-dependent dynamic protein composition still not fully elucidated that allows them to cover a plethora of cytoskeletal regulatory functions, including microtubule organization center (MTOC), mitotic spindle formation or ciliary BB (Keeling et al., 2016). The BB works as a template from which the axoneme nucleates and is extended to form cilia (see ciliogenesis section for more information).

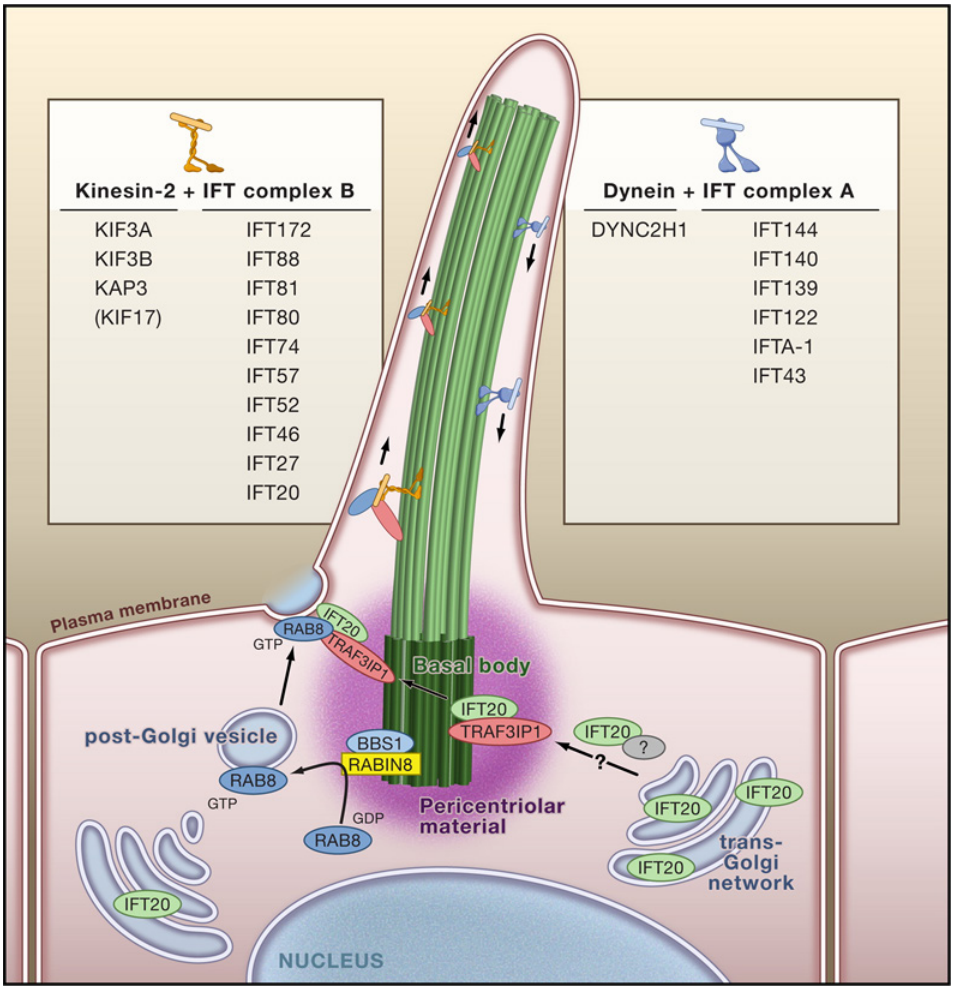

Figure 1. Primary cilium components (modified Gerdes et al., 2010)
The axoneme (light green) nucleates from the basal body (dark green). Incorporation of vesicles from the Golgi apparatus carrying ciliary proteins occurs at the ciliary base via RAB8 (dark blue). Regulation of protein content and trafficking inside the cilium happens at the transition zone, between the axoneme and the basal body. Ciliary proteins are shuttled inside the compartment by the IFT complex B, whereas material is recycled back to the cytoplasm via IFT complex A.

The axoneme is typically formed by 9 doublets of microtubules. In motile cilia, there is an additional central pair (constituting a "9+2" arrangement) connected to the outer doublets by radial spokes. In these cilia, small dynein arms provide the motor-driving force required to bend the outer microtubules relative to the inner microtubules. Thus, the beating motion can be generated. However, most primary cilia have a "9+0" axoneme arrangement, without the central pair. Therefore, with the exception of the primary cilia in the embryonic left-right organizer, they are immotile (Baker and Beales, 2009).

The ciliary membrane sheaths the axoneme. Despite being continuous to the plasma membrane, the ciliary membrane constitutes a highly specialized compartment, as it harbors and concentrates a unique set of proteins devoted to signal detection and transduction (Nachury et al., 2010). Because many cells are specialized in detecting signals of specific nature, ciliary protein composition is different between different cell types; moreover, it can also change dynamically within one cell type depending on the signaling status (Goetz and Anderson, 2010). Recently, it has been shown that the lipid composition of this compartment, rich in phosphatidylinositol 4-phosphate (PIP or PI(4)P), is also distinct from the adjacent membrane, where phosphatidylinositol 4,5-bisphosphate (PIP_2 or $PI(4,5)P_2$) is more prominent. The maintenance of this lipidic configuration is required for proper ciliary function and enabled by at least one known ciliary phospha-

tase INPP5E, which converts PIP_2 into PIP (Garcia-Gonzalo et al., 2015). The ciliary compartment is devoid of protein synthesis machinery. Thus, the aforementioned protein enrichment is enabled by a combination of polarized vesicle trafficking towards the cilium and a septin-containing diffusion barrier at the periciliary membrane (Hu and Nelson, 2011). The transition zone (TZ) is a region between the BB and the axoneme, which has been proposed to participate in the regulation of ciliary protein composition, although the details of protein sorting remain unknown. The TZ is characterized by the presence of Y-shaped linkers and the ciliary necklace that bind the microtubule doublets to the surrounding membrane. Futhermore, the TZ has been proposed to play both a gatekeeper role, preventing non-ciliary proteins from entering the compartment, and a facilitator role, allowing ciliary proteins to go in (Szymanska and Johnson, 2012).

Once proteins have been successfully sorted to the ciliary compartment, transport along the axoneme and turnover to the cell body are guaranteed by the intraflagellar transport complexes (IFT). IFT complexes constitute an evolutionary conserved mechanism, first described in *Chlamydomonas reinhardtii* (Hao and Scholey, 2009; Ishikawa and Marshall, 2011). The IFT is formed by at least 20 proteins named according to their masses and distributed in two complexes, functioning as adaptors between motor proteins and ciliary cargo. The core of the IFT-A complex functions in the dynein-dependent retrograde aspect of IFT. The IFT-B particle is required for the kinesin-mediated anterograde aspect of IFT. Anterograde and retrograde transport of proteins respectively allow incorporation of new material and protein recycling/turnover (Pearring et al., 2013). The IFT is required both for ciliary extension (see ciliogenesis section for more information) as well as ciliary maintenance.

Understanding primary cilia structure, composition and function is crucial to appreciate their role in embryonic development, adult tissue homeostasis and pathogenesis.

Ciliopathies

Ciliopathies are an expanding group of human disorders caused by cilium dysfunction. *Sensu lato*, ciliopathies encompass both the molecular diseases caused by motile and primary cilia dysfunction. However, strictly speaking, the term ciliopathies refers to the disorders arisen from primary cilia dysfunction (Mitchison and Valente, 2017). Due to the ubiquitous presence of primary cilia, dysfunction of this organelle has multiple pleiotropic effects in very diverse organ systems. Therefore, primary ciliopathies –from now on, simply "ciliopathies"– are characterized and unified by a wide array of overlapping features: central nervous system (CNS) malformations, retinal degeneration, anosmia, hearing loss; pancreatic, hepatic or renal cysts; obesity, polydactyly, left-right asymmetry defects and skeletal dysplasia/malformations (Fig. 2) (Badano et al., 2006; Hildebrandt et al., 2011). Ci-

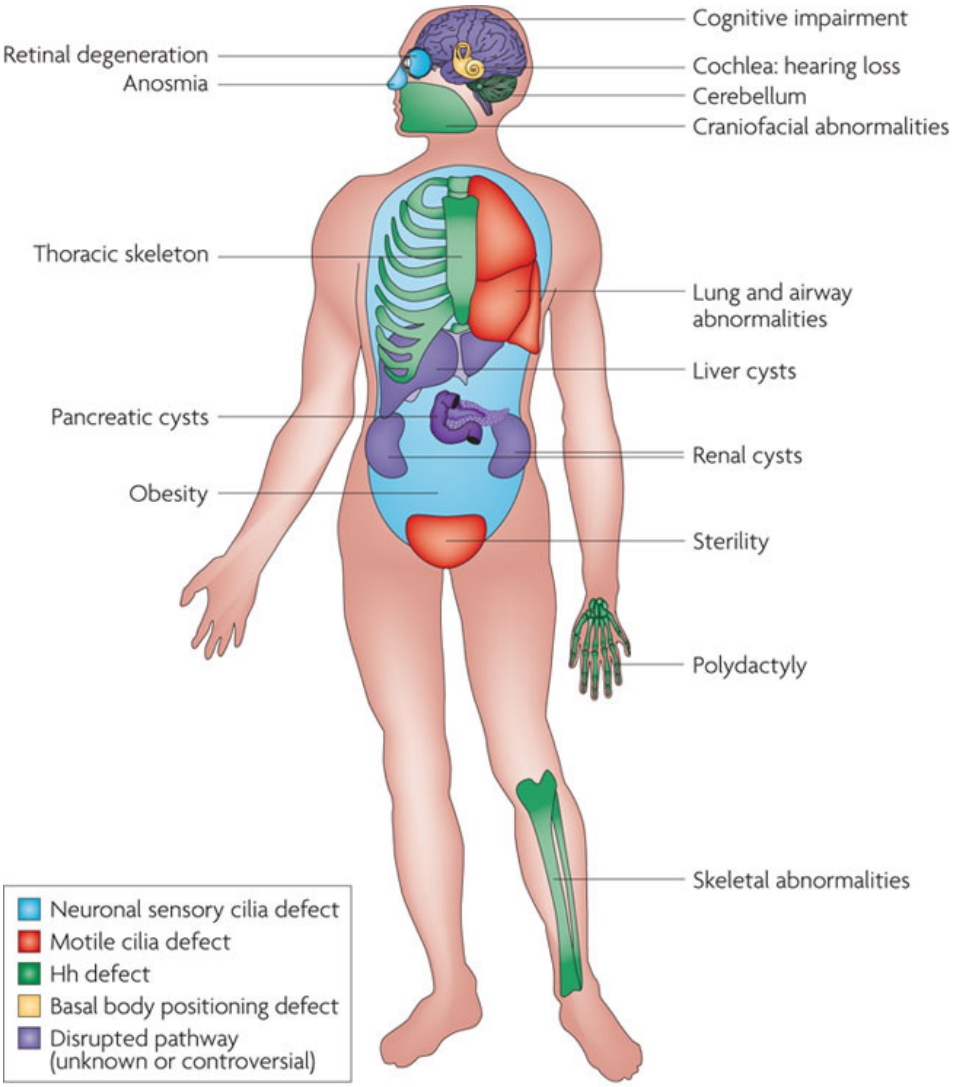

Figure 2. Ciliopathy phenotypes (modified from Goetz and Anderson, 2010)
Color-coded schematic depicting specific ciliary functions or pathways involved for each phenotype. Some aspects of these syndromes, such as the polydactyly in BBS and MKS and the skeletal abnormalities that affect the limbs of patients with SRTD, have been attributed to defective hedgehog (Hh) signaling (green). Other attributes of human disorders result from defective sensory cilia (blue). The special case of hearing loss is due to a requirement for the primary cilia of the cochlea downstream of the PCP pathway in establishing the correct polarity of sensory hair cells (yellow). Infertility and lung and airway abnormalities/dysfunction are a result of defective motile cilia or "primary cilia dyskinesia" (red). The most severe and common abnormalities associated with ciliopathies, such as cyst formation in the kidneys, liver, biliary duct and pancreas, the underlying molecular causes downstream of the cilium remain unclear or controversial (purple), the Molar Tooth Sign belongs to this category, although it is presumably related to defective Hh signaling.

liopathies can be characterized and classified based on their clinical features, presence of core phenotypes and a constellation of symptoms (presumably arisen from the biological role of the protein involved) into different disorders: Short-rib thoracic dysplasia with or without polydactyly (SRTD, OMIM 617405, encompassing Jeune asphyxiating thoracic dystrophy, Ellis van Creveld and Short rib polydactyly) is characterized by constricted thoracic cage; Bardet-Biedl syndrome (BBS, OMIM 209900) is characterized by retinitis pigmentosa, obesity, kidney dysfunction and polydactyly; autosomal dominant polycystic kidney disease, (ADPKD, OMIM 173900), autosomal recessive polycystic kidney disease (ARPKD, OMIM 263200) and nephronoptisis (NPHP, OMIM 256100) are characterized by cystic kidney disease; Meckel-Gruber syndrome (MKS, OMIM 249000) is a severe disorder causing fetal or perinatal decease; Alström syndrome (ALMS, OMIM 203800) and Leber congenital amaurosis (LCA, OMIM 204000) are both coursing with retinal dysfunction as main hallmark; and Joubert syndrome (JBTS, OMIM 213300) is characterized by a specific cerebellar malformation (carefully described in the next section) (Baker and Beales, 2009).

Ciliopathies are phenotypically and genetically heterogenous disorders, i.e.

multiple genes can cause similar clinical phenotypes, and each disorder can be caused by mutations in many different genes. In addition, prominent genotypic and phenotypic overlap exists between different ciliopathies. Most of these disorders are inherited in an autosomal recessive Mendelian fashion, with some autosomal dominant or sex-linked exceptions. Oligogenicity has also been proposed as a possible inheritance mechanism (Katsanis, 2004), supported in the concept of mutational load and meaning that mutations in three or more alleles of different loci are disease causing. However, there has been no evidence of triallelism found on mutation screenings on large cohorts of patients so far (Nakane and Biesecker, 2005; Laurier et al., 2006; Smaoui et al., 2006; Phelps et al., unpublished).

The broad genetic heterogeneity and phenotypic variability of ciliopathies have led to various hypotheses to explain genotype and phenotype correlations (Tobin and Beales, 2009): 1) the mutated genetic locus itself can determine disease severity. 2) The nature of the mutation can lead to seemingly different disorders: loss-of-function mutations cause severe, early-onset multiorganic disease; whereas hypomorphic mutations cause milder, late-onset disease with limited organ involvement (Mougou-Zerelli et al., 2009; Bachmann-Gagescu et al., 2012). 3) The presence of a genetic modifier, a third heterozygous mutation on top of the two recessive mutations affecting the same locus, could worsen a phenotype (Bachmann-Gagescu et al., 2015a).

Although many genes whose protein product localizes or is associated to cilia have been identified as causal for ciliopathies, many patients remain diagnosed with an unidentified genetic cause (Waters and Beales, 2011). Efforts have been recently directed towards the assembly of the ciliary proteome or "ciliome" and the connections between these proteins, and now we know that > 1200 proteins localize or associate to this cell compartment (Gherman et al., 2006; Inglis et al., 2006; Boldt et al., op. 2009; van Reeuwijk et al., 2011; Roepman et al., 2012; Boldt et al., 2016). It is likely that many of these genes harbor disease mutations. Functional characterization of these proteins will help to dissect primary cilia function and disease mechanisms and will likely improve the prognosis, medical and educational management and development of potential therapies for ciliopathies (Tobin and Beales, 2009).

Joubert syndrome

Joubert syndrome (JBTS, OMIM 213300) is an inherited congenital cerebellar ataxia and a prototypical ciliopathy, characterized by a specific cerebellar malformation that is exclusive to this disease and renders a pathognomonic imaging finding called the Molar Tooth Sign (MTS) (Poretti et al., 2014b). The MTS received this name because the brainstem of the patient acquires the shape of a molar tooth in axial MRI. This is due to cerebellar vermis hypodysplasia, thickened and elongated superior cerebellar

peduncles, deep interpeduncular fossa at the level of the isthmus and upper pons. Despite JBTS was described in 1969 by Marie Joubert, the MTS was not determined as its main hallmark until 1997 (Romani et al., 2013).

It is believed that the cerebellar malformation can be caused by an underlying axon guidance defect (Engle, 2010; Romani et al., 2013). This assumption is based on the facts that most neuronal types possess a primary cilium and primary cilia are crucial for the transduction of Shh (which determines the neuronal fate and constitutes a guidance cue for axons). However, this hypothesis remains untested and the cerebellar phenotype is unexplained so far. Other central nervous system (CNS) defects have been associated with JBTS, mostly in the midbrain and tectum (Doherty, 2009; Poretti et al., 2014a).

Clinically, JBTS can be suspected in the first months of life and presents with hypotonia, abnormal ocular movements and changes in the respiratory pattern, alternating apnea and tachypnea, that are potentially life-threatening. Later on, intellectual disability usually manifests (although some cases with normal cognitive function have been reported) (Poretti et al., 2009). However, in addition to the core clinical hindbrain malformation causing all these symptoms, JBTS exhibits substantial phenotypic variability and 60% of JBTS patients display additional features that span the whole spectrum of ciliopathy phenotypes, giving rise to the term "Joubert Syndrome and Related Disorders" (JSRD), to highlight that they are variable clinical manifestations of one disease and do not represent distinct clinical syndromes (Brancati et al., 2010). Retinal defects, renal defects and congenital liver fibrosis are the most common extracerebellar symptoms (Bachmann-Gagescu et al., 2015a).

JBTS follows a recessive inheritance pattern, mostly autosomal (except for *OFD1*), with prominent genetic heterogeneity, since mutations in over 30 genes have been reported so far to cause this disorder: *INPP5E, TMEM216, AHI1, NPHP1, CEP290, TMEM67, RPGRIP1L, ARL13B, CC2D2A, OFD1, TTC21B, KIF7, TCTN1, TMEM237, CEP41, TMEM138, C5ORF42, TCTN3, ZNF423, TMEM231, CSPP1, PDE6D, KIAA0586, TCTN2, CEP104, KIAA0556, B9D1, MKS1* and the novel genes *KIAA0753* (Stephen et al., 2017), *CELSR2* (Vilboux et al., 2017), *CEP120* (Roosing et al., 2016), *HYLS1* (Oka et al., 2016). Because there is no genetic cause found in ca. 38% of the patients diagnosed with JBTS, it is likely that this list will further expand in the next years (Bachmann-Gagescu et al., 2015a). The polypeptide products of all these genes localize to the cilium, most of them in functional networks at the TZ or the BB (Szymanska et al., 2014). Mutations in the aforementioned genes can also cause the more severe Meckel-Gruber syndrome (MKS). This genetic overlap suggests that JBTS and MKS are allelic diseases, the milder and severe versions of the same disease spectrum (Valente et al., 2013; Szymanska et al., 2014).

It is intriguing that dysfunction of TZ and BB proteins leads to the same phenotype with the same core malformation. Comparison of models for dysfunction in each region may allow identifying the common downstream

pathogenic mechanism leading to JBTS and address the possible therapeutical management (Ware et al., 2011).

Retinal involvement in ciliopathies

Ciliopathies can course with retinal dystrophy or retinal degeneration, most times with an unclear mechanism. 25% of JBTS patients present retinal involvement (Bachmann-Gagescu et al., 2015a). The retina is placed at the back of the vertebrate eye and is involved in image-forming vision. This process is not only limited to light detection but there is also local sophisticated processing of the information before it is conveyed to higher brain centers, where it gets integrated with other sensory inputs. Despite its peripheral localization, the retina is considered part of the central nervous system, as optic vesicles are formed out of an evagination of the diencephalon during embryonic development (Purves et al., 2008).

Canonical vertebrate retinae are composed of three nuclear layers and two synaptic layers (Perry et al., 2010). The outermost (most distal to the light source) nuclear layer contains two types of photoreceptors: cones that mediate day-light vision and rods, which are very sensitive and detect low luminance levels (Holcman and Korenbrot, 2005). Upon the absorption of a photon by the photoreceptors, the biochemically coupled phototransduction cascade machinery ultimately leads to hyperpolarization of the photoreceptor. The visual information transformed into an electrical signal is transmitted from the photoreceptors to the bipolar cells of the next layer, and from the bipolar cells to the retinal ganglion cells in the innermost nuclear layer. The axons of ganglion cells converge to form the optic nerve, which exits the eye and transmits the retinal output to other brain areas. This is the so called vertical pathway of signal transmission; however, there is also horizontal information flow at the synaptic layers mediated by horizontal cells in the outer plexiform layer, believed to maintain retina's sensitivity to contrast, and amacrine cells in the inner plexiform layer, which among other functions are involved in the detection of directional motion (Purves et al., 2008).

Light detection and transduction is carried out by the retinal photoreceptors, which are highly polarized sensory neurons with a synaptic terminal, a cell body, an inner segment (IS) and a modified primary cilium called the outer segment (OS) (Kennedy and Malicki, 2009; Bloodgood, 2013). The OS consists of stacks of membranous disks which are organized around a microtubule-based axoneme and which contain proteins required for phototransduction, such as the light-absorbing chromophore-coupled pigment opsin (Khanna, 2015). The connecting cilium, equivalent to the transition zone in other primary cilia (Bloodgood, 2013), joins the OS with the IS. The OS is, like all cilia, devoid of protein synthesis machinery (Nachury et al., 2010; Khanna, 2015). Thus, the specialized protein enrichment of the OS membranes is enabled by the polarized vesicle trafficking from the IS

explained in the previous section (Deretic et al., 1995; Nachury et al., 2007; Ward et al., 2011).

Rhodopsin is detected at the trans-Golgi network by Arf4 through a ciliary-targeting sequence (CTS) encoded in the C-terminus of the protein (VxPx) that is conserved with Polycystin1, but does not seem to be shared with other transmembrane ciliary proteins (Ward et al., 2011; Pearring et al., 2013). Then, the factor cascade ASAP1-Rab11-FIP3-Rabin8-Rab8 (thoroughly discussed in the next section) is recruited for its transport to the base of the outer segment (Wang and Deretic, 2015), where the carrier vesicles fuse using Syntaxin3 and SNAP25 as t-SNAREs (Mazelova et al., 2009). Photoreceptors shed the most distal portions of their OSs to be degraded by retinal epithelial cells. Therefore, rhodopsin is continuously synthesized and transported in high rates to the OSs to replenish the lost pool (Pearring et al., 2013). This makes of the PRs a very suitable cell model to study polarized protein trafficking to the cilium and offer the unique opportunity to investigate the function of ciliopathy proteins in this context.

Polarized protein transport towards the cilium

In 2013, the Nobel Prize in Physiology and Medicine was awarded to Thomas C. Südhof, James E. Rothman and Randy W. Schekman for the discovery of the underlying mechanisms and pathways of polarized vesicle trafficking (Mellman and Emr, 2013; Rothman, 2014). Cells invest a great deal of energy in keeping the identity and exclusivity of their membranous compartments to propagate the spatial organization of biochemical events (McNew et al., 2000). Nowadays we know that vesicular transport is an exquisitely complex process that is genetically conserved from yeast to humans and has an enormous amount of proteins and regulatory layers involved. Vesicle trafficking can be viewed as a four-step process: vesicle budding, movement of the vesicle towards the target compartment, docking and ultimately fusion of the lipid bilayers. Coating molecules, motor proteins propelling the vesicles along cytoskeleton tracks and specific membrane fusion complexes have been identified serving in each of these processes (Stenmark, 2009). Two major protein groups must be mentioned: the small RabGTPase and SNARE protein superfamilies.

RabGTPases are the largest family of small cytoplasmic GTPases, with close to 70 members in humans. They work as molecular switches alternating between an active GTP-bound and an inactive GDP-bound conformational state to deliver membrane from one compartment to another. When RabGTPases are active, they recruit several types of specific effector molecules, including adaptors, tethering factors or motor proteins. Although RabGTPases have an intrinsic catalytic activity to hydrolyze GTP to GDP, there are proteins that can activate them by removing the GDP (guanidine exchange factors or GEFs) or inactivate them by accelerating

the GTP catalysis (GTPase activating protein or GAPs), adding another layer of regulation (Zerial and McBride, 2001). RabGTPases are reversibly associated with membranes via hydrophobic geranylgeranyl groups at their carboxy-termini. They localize to distinct intracellular compartments in an incompletely understood way, although it is believed that, besides their own structural determinants (Schimmoller et al., 1998; Pfeffer, 2005), yet another set of regulators play a role in this salient feature: GDP dissociation inhibitors (GDIs) bind the cytosolic Rabs encapsulating the geranylgeranyl groups in a hydrophobic pocket and GDI displacement factors (GDFs) release the GDP-Rab complex facilitating the binding to the membrane (Pfeffer, 2005; Pfeffer, 2013). RabGTPases are dispensable in most cases for vesicle budding; however, their specific localization and their capacity to direct trafficking make them the main membrane organizers of the cell (Zerial and McBride, 2001).

Rab8 is the most prominent RabGTPase involved in ciliary transport. Rab8 exists in humans in the form of two paralogs, RAB8A and RAB8B. Both have been demonstrated to be necessary for ciliogenesis in cell culture (Westlake et al., 2011). Indeed, Rab8 enters the cilium in cultured cells in a BBSome-dependent way to promote ciliary membrane extension (Nachury et al., 2007). It is not working alone but coordinated with Rab11, which recruits the GEF activator of Rab8, Rabin8 (Knodler et al., 2010). Furthermore, it was found in zebrafish that Rab8 binds to Rabaptin5, which in turn binds Elipsa (zebrafish ortholog of mammalian IFT54), providing a molecular link between Rab8-mediated trafficking and the IFT machinery (Omori et al., 2008).

The first link between Rab8 and ciliary transport was demonstrated in photoreceptors, which are very specialized ciliated cells with a modified primary cilium, the outer segment (see retina section for further information). Rab8 was found to be crucial for rhodopsin transport as rhodopsin-carrier-vesicles accumulated in the presence of a dominant negative form of Rab8 in frog photoreceptors (Deretic et al., 1995; Moritz et al., 2001). The current model for rhodopsin transport involves recognition of rhodopsin by Arf4 in the trans-Golgi network. Arf4 recruits the adaptor protein ASAP1, which in turn recruits Rab11. Arf4 abandons the complex and Rab11 binds its effectors FIP3 and Rabin8. FIP3 is known to interact with specific PIPs at the target membrane, probably providing stability during fusion. Rabin8 recruits and activates Rab8 (Wang et al., 2012; Wang and Deretic, 2015). A double knock-out mouse model for *rab8a* and *rab8b* without a ciliogenesis phenotype was published, but the authors found that the closest orthologue of Rab8, Rab10, could be taking over this function, as knock-down of Rab10 in the double mutant MEFs abolished ciliogenesis (Sato et al., 2014). Interestingly, Rab10 has been associated with the primary cilia of renal epithelial cells (Babbey et al., 2010). However, a recent publication presented a double *rab11a;rab8a* mouse mutant with additional expression of dominant negative Rabs without any evident trafficking defects in the retina (Ying et al., 2016). Although it could be that a different

species-specific mechanism governs rhodopsin transport in mammals compared to amphibians, it is also plausible that other RabGTPases take over this function.

Supporting this notion, Rab8, Rab11 and Rab10 are not the only RabGTPases involved in ciliary trafficking. Rab17-positive endosomal compartment contributes to the ciliary compartment (Yoshimura et al., 2007). Rab23 is required for retrograde transport from primary cilia and is involved in Shh signaling (Boehlke et al., 2010; Lim et al., 2011). Recently, the cone-rod dystrophy-associated Rab28 protein was found to concentrate at the periciliary membrane in its active form, associate with the BBSome and the IFT (Jensen et al., 2016). Nevertheless, it is not easy to disregard the function of Rab8 in ciliary transport, as it has been demonstrated to interact with many ciliopathy proteins, including Ahi1, ODF2 (Lim et al., 2011), the BBSome (Nachury et al., 2007) and the Exocyst complexes (Das and Guo, 2011).

The Exocyst is a multiprotein complex that works as a vesicle tethering factor involved in many exocytosis processes. Its components are well conserved from yeast to human, some of them localizing at specific membrane sites, where fusion occurs (Novick and Guo, 2002). The Exocyst has been reported to bind RabGTPases and act upstream of SNARE fusion, as mutations in any of the eight proteins (Sec3p, Sec5p, Sec6p, Sec8p, Sec10p, Sec15p, Exo70p and Exo84p in yeast) cause vesicle accumulation (Lipschutz and Mostov, 2002). It is unclear, however, how the Exocyst triggers the SNARE-mediated fusion, but it seems it is not a simple tethering factor that brings the vesicle in close proximity to the SNARE proteins. Some authors have reported a direct interaction between the Exocyst and SNARE proteins (Dubuke et al., 2015; Yue et al., 2017) or an indirect interaction by binding their inhibitors, to prevent premature SNARE complex formation (Morgera et al., 2012).

SNAREs (short for Soluble N-ethylmaleimide-sensitive factor Attachment protein REceptors) are a superfamily of small proteins with around 36 members in humans. All of them have at least one SNARE motif, an evolutionarily conserved stretch of 60-70 amino acids arranged in heptad repeats (Hong, 2005). Most SNAREs have a single C-terminal transmembrane domain for their membrane insertion, which can co-exist with hydrophobic post-translational modifications that prevent from degradation. Some of them have regulatory N-terminal groups that can cap the SNARE domain. The small subfamily of SNAREs comprising SNAP25, SNAP23 and SNAP29 contains two SNARE motifs joined by a palmitoylated flexible linker, without a transmembrane domain (Jahn and Scheller, 2006).

When appropriate sets of SNAREs are combined, the SNARE motifs bind spontaneously in a helical core complex of extraordinary stability that brings the bilayers in close proximity and allow fusion. Four helices/SNARE motifs are required to form this complex, the center of which contains largely hydrophobic chains except for three highly conserved glutamine (Q) residues and one arginine (R) residue (one residue per helix). This gives

rise to the classification of SNAREs into Qa-, Qb-, Qc- and R-SNAREs, depending on their contribution to the complex (Fasshauer et al., 1998). This classification is more informative than the traditional classification sorting SNAREs into t-SNAREs (target membrane) or v-SNAREs (vesicle membrane), although the latter one is still in use for orientation purposes (Hong, 2005). Formation of the core complex uses the free energy provided by the exothermic SNARE pairing reaction. However, once the SNAREs are bundled, they remain in a super-stable *trans*-complex (i.e. all of them in the same membrane) that renders them biologically inactive. Disassembly and recycling of the fusion components is mediated by NSF (N-ethylmaleimide-sensitive factor) and SNAPs (soluble NSF attachment proteins, not to be confused with the nomenclature of the SNAP25 SNARE subfamily) and involves several cycles of ATP hydrolysis (Sollner et al., 1993).

Although SNAREs can form core complexes in a promiscuous way *in vitro*, it was demonstrated that *in vivo* only certain combinations have the intrinsic capacity of mediating fusion of very specific compartments (Scales et al., 2000). This is further supported by the distinct topology and distribution of SNAREs between membranes, which is partly encoded in their N-termini (Nakanishi et al., 2004) and their transmembrane domain (Watson & Pessin, 2001). However, in addition to this intrinsic capacity, SNAREs are associated with a large number of regulators that prevent their fusion unless the triggering conditions are given.

The t-SNAREs Syntaxin3 (Qa-SNARE) and SNAP25 (Qbc-SNARE) have been demonstrated to mediate rhodopsin-carrier-vesicle fusion in frog and mammalian photoreceptors (Greenlee et al., 2001; Mazelova et al., 2009). These t-SNAREs would be pairing up with the v-SNARE VAMP7 present on the RTC surface (Ray et al., 2013). It still remains unknown if this is a conserved mechanism for the ciliary transport of all cell types. However, this appears unlikely, given the preferential neuronal expression of SNAP25 (Jahn and Scheller, 2006). On the other hand, Syntaxin3 is present in the plasma membrane of multiple cell types (Fujita et al., 1998; Lehtonen et al., 1999; Knowles et al., 2015; Soo Hoo et al., 2016) and could represent a common mechanism of ciliary material delivery. Furthermore, Rab11 was found to be required for Syntaxin3 proper localization in enterocytes (Knowles et al., 2015), which could represent the bridge binding the ciliary-targeting vesicle apparatus with the fusion machinery.

Ciliogenesis

The assembly of primary cilia, also known as ciliogenesis, is a multi-step process that is strongly regulated and tightly coupled to the cell cycle. Indeed, because the mother centriole has to be released from the centrosomal function of building the mitotic spindle, presence of a cilium is incompatible with cell division (Keeling et al., 2016). Thus, when a cell re-enters the cell cycle, primary cilia are disassembled and the centrosome migrates near

the nucleus. When the cell exits the cell cycle (G1 or G0), the centriole migrates to the cell surface and nucleates the cilium. These mutually exclusive states of the centriole require a conversion in which cell-cycle dependent transcription of proteins and dynamic centrosomal protein localization participate (Lessman, 2012).

Before cell division, centrosomes duplicate in a way that remarkably resembles DNA replication: 1) centriole duplication occurs during S phase and is terminated by the maturation and separation of the two pairs of centrosomes during M phase, concomitant to DNA replication and segregation respectively. 2) It is a semi-conservative process, in which each daughter cell inherits one of the old centrioles and a newly formed one, and 3) it is regulated by cyclin-dependent kinases (CDKs) (Brownlee and Rogers, 2013). Centriole duplication or centriologenesis occurs normally via the canonical pathway, in which each one of the centrioles serves as a platform to nucleate a procentriole at their base (Bauer et al., 2016). In multiciliated cells, the *de novo* pathways operate, where the daughter centriole builds structures called deuterosomes with incipient and latent procentrioles and releases them in the cytoplasm. New centrioles grow from both the mother centriole and the deuterosomes. These centrioles are matured and dock to extend the motile cilia (Al Jord et al., 2014).

Many proteins have been associated with the human centrosome and its full protein composition is not known yet (Andersen et al., 2003). Some of these proteins are anti-ciliogenic and prevent the centrosome to build a cilium, some of them are pro-ciliogenic and prime the centrioles to build a cilium. Differential expression of both factors throughout the cell cycle, protein-protein interactions that block or reduce the function of one of the factors and sequestration of factors in different locations within the centrosome are some of the known mechanisms that regulate ciliogenesis (Kobayashi and Dynlacht, 2011). For instance, protein CP110 –substrate of CDK– is known to interact with Cep97 and form a complex that caps the distal end of centrioles in a Kif24-dependent manner during centriole assembly to regulate centriole size (Kobayashi et al., 2011; Pearson, 2011). CP110 binds Talpid3 and Cep290 and suppresses their pro-ciliogenic activity (Kobayashi et al., 2014). When the cell enters G1, CP110 protein levels decrease and inactivation of Kif24 (presumably via phosphorylation by Aurora kinases, although the mechanism is unknown so far) restricts the expression of CP110 to the daughter centriole (Pearson, 2011). Consequently, the mother centriole is free to extend the axoneme (Fig. 3).

Once the cell exits the cell cycle, the oldest centriole of the inherited pair, called mother centriole, matures into the basal body (BB). This transition requires recruitment and formation of both distal (transition fibers) and subdistal appendages (basal feet) and other accessory structures such as ciliary rootlets. The formation of appendages is independent of ciliogenesis but is required for it. Examples illustrating this notion include loss of cilia upon depletion of the appendage proteins OFD2, Cep164 or ninein. Distal appendages appear to play a role in the docking of the BB to the plas-

ma membrane and docking of the IFT machinery to the BB for axoneme extension (Kobayashi and Dynlacht, 2011).

After centriole maturation, a Golgi-derived vesicle or ciliary vesicle docks onto the BB, from which the nascent axoneme begins to emerge in an IFT-dependent manner. The ciliary vesicle subsequently fuses with secondary vesicles and invaginates, leading to the formation of a ciliary sheath around the assembling axoneme and eventually forming a ciliary membrane. The nascent shaft acquires transition zone-like features (Pedersen et al., 2008). The small RabGTPase, Rab8a localizes near centrosomes during the early phase of ciliogenesis, playing an important role in ciliary vesicle docking and membrane elongation (Fig. 3) (Kobayashi et al., 2014). The membrane-surrounded nascent cilium structure migrates to the apical cell surface in an actin-dependent manner. Subsequently, the ciliary vesicle fuses with the plasma membrane and further extension occurs via the IFT (Reiter et al., 2012).

Many of the proteins involved in ciliogenesis are also involved in protein transport to cilia or ciliary maintenance (Kobayashi and Dynlacht, 2011). The cilium lacks ribosomes and therefore ciliary proteins are transported from the cytoplasm. Transmembrane proteins are transported in Rab8-associated vesicles from the Golgi apparatus to the ciliary base, where they fuse (Nachury et al., 2010). IFT mediates further transport into the ciliary compartment. Despite its intraciliary role, the bulk of the IFT components localizes at the base of the cilium, an important selective filter for trans-

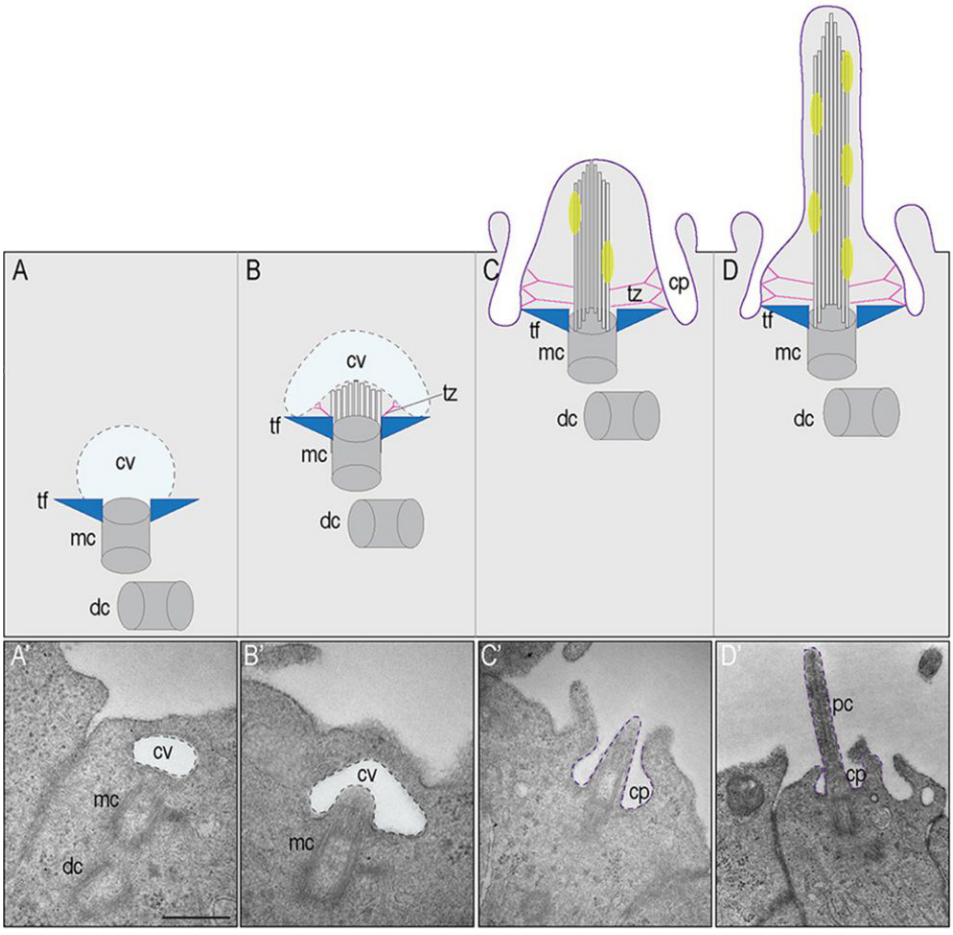

Figure 3. Hypothesized steps of canonical ciliogenesis (modified from Chang et al., 2014)
(A) A ciliary vesicle (cv) binds to the distal end of the mother centriole (mc), via associations with transition fibers (tf). (B) Microtubule and transition zone (tz) outgrowth emerges and invaginates the cv. (C) Docking of the centriolar/cv complex to the plasma membrane. (D) Axonemal outgrowth. (A'-D') Steps of intracellular ciliogenesis in wild-type chicken embryos. dc, daughter centriole; pc, primary cilium; cp, ciliary pocket. Scale bars: 500 nm in A'-D'.

port, where other proteins can regulate the traffic (Pedersen et al., 2008).
In conclusion, ciliogenesis is a complex and fascinating process that is only now starting to be understood. Determination of the enzymatic functions and interactions of individual proteins at the BB, TZ and IFT will be crucial to generate integrative models to understand how the huge and still-increasing number of ciliary components work together to regulate assembly and disassembly of the small sensory organelle, the primary cilium (Ishikawa and Marshall, 2011).

Zebrafish as a model for retinal ciliopathy research

The zebrafish is a small tropical freshwater teleost, which emerged as a promising new model organism due to the pioneering efforts of George Streisinger to use zebrafish in developmental genetic studies and due to Christiane Nusslein-Vollhard, Wolfgang Driever and their teams, who applied forward genetics to elicit a number of mutant lines (Lessman, 2012). Because of its high fecundity, amenability to genetic manipulations and rapid development of externally fertilized and translucent embryos, the zebrafish allows for experiments not easily done in other vertebrates.
In addition to the aforementioned forward genetic approaches, reverse genetic approaches are possible as complete genomic information of the zebrafish is available (Howe et al., 2013). Gene knockdown with antisense morpholino oligonucleotides has been used extensively and since the development of ZFN, TALENs and CRISPR/Cas9 technologies, it is now possible to mutate virtually any gene of interest (Hwang et al., 2013). To complete the genetic toolkit, Tol2 transposon mediated transgenesis can be efficiently applied (Kawakami, 2007) with ease to produce transgenic lines, often with the use of fluorescent reporters to label cells or proteins of interest in a spatiotemporal-controlled manner.
The zebrafish has a body plan shared by vertebrates including humans, providing added significance to the existing lines of zebrafish as human disease models (Lessman, 2012). Ciliopathy-causing genes are well conserved between zebrafish and humans in terms of nucleotide identity, function and localization of their protein products (Zaghloul and Katsanis, 2011) and exist as 1:1 orthologues despite the extra whole genome duplication event undergone in the teleost lineage. Furthermore, the zebrafish canonical vertebrate retina exhibiting *quasi* adult morphology at 5 days post fertilization (dpf), extraordinarily fast development of zebrafish diurnal vision, which is more similar to human vision than the one of mice of nocturnal lifestyle, makes zebrafish very suitable for the study of ciliopathy proteins in retinal function (Perry et al., 2010).

Aims of the thesis

My aim is to shed light on the pathogenesis mechanisms underlying JBTS by studying mutants in two genes, *KIAA0586/TALPID3* and *CC2D2A*. The protein product of these genes localizes respectively to the BB and the TZ, the two affected compartments in JBTS (Baker and Beales, 2009). This kind of approach allows us to compare and extract the common mechanistic links, which could potentially be shared by other proteins in these compartments.

KIAA0586/TALPID3 (TA3) is a novel ciliopathy gene (Bachmann-Gagescu et al., 2015b). Ta3 localizes to both mother and daughter centrioles and is required for ciliogenesis in various model organisms through a Rab8-dependent role in BB docking (Kobayashi et al., 2014). The requirement for Ta3 during ciliogenesis precludes the investigation of potential additional roles in ciliary function in mouse or chick models. In Chapter 4, we analyze the role of Ta3 in retinal photoreceptors of zygotic *talpid3*$^{-/-}$ zebrafish mutants, in which maternally-derived Ta3 contribution partially rescues ciliogenesis at early developmental stages, which allowed us to uncover another Rab8-independent role in cell-shape maintenance through a yet unknown mechanism.

CC2D2A is a transition zone protein whose dysfunction is one of the most common causes for JBTS (Bachmann-Gagescu et al., 2015a). Cc2d2a loss-of-function leads to loss of ciliary protein localization in fibroblasts from knock-out mice (Garcia-Gonzalo et al., 2011). Similarly, we previously reported intracellular opsin mislocalization and massive vesicle accumulation in PRs of the *cc2d2a*^{uu38} mutant zebrafish, suggesting the involvement of Cc2d2a in ciliary trafficking and supporting the role of the TZ in ciliary protein content regulation (Bachmann-Gagescu et al., 2011). In Chapter 2, we describe a role for Cc2d2a in periciliary membrane organization as a selective gatekeeper for the fusion machinery t-SNARE SNAP25, using a novel Correlative Light and Electron Microscopy technique (thoroughly described in Chapter 3). In this study we also provide the very first characterization of Rab8 trafficking through live imaging in PRs and evidence in its involvement in opsin trafficking, resolving the recent controversy around this function (Ying et al., 2016).

References

Al Jord, A., Lemaitre, A.-I., Delgehyr, N., Faucourt, M., Spassky, N., and Meunier, A. (2014). Centriole amplification by mother and daughter centrioles differs in multiciliated cells. Nature ***516***, 104-107.

Andersen, J.S., Wilkinson, C.J., Mayor, T., Mortensen, P., Nigg, E.A., and Mann, M. (2003). Proteomic characterization of the human centrosome by protein correlation profiling. Nature ***426***, 570-574.

Babbey, C.M., Bacallao, R.L., and Dunn, K.W. (2010). Rab10 associates with primary cilia and the exocyst complex in renal epithelial cells. American journal of physiology. Renal physiology ***299***, F495-506.

Bachmann-Gagescu, R., Dempsey, J.C., Phelps, I.G., O'Roak, B.J., Knutzen, D.M., Rue, T.C., Ishak, G.E., Isabella, C.R., Gorden, N., and Adkins, J., et al. (2015a). Joubert syndrome: a model for untangling recessive disorders with extreme genetic heterogeneity. Journal of medical genetics ***52***, 514-522.

Bachmann-Gagescu, R., Ishak, G.E., Dempsey, J.C., Adkins, J., O'Day, D., Phelps, I.G., Gunay-Aygun, M., Kline, A.D., Szczaluba, K., and Martorell, L., et al. (2012). Genotype-phenotype correlation in CC2D2A-related Joubert syndrome reveals an association with ventriculomegaly and seizures. Journal of medical genetics ***49***, 126-137.

Bachmann-Gagescu, R., Phelps, I.G., Dempsey, J.C., Sharma, V.A., Ishak, G.E., Boyle, E.A., Wilson, M., Marques Lourenco, C., Arslan, M., and Shendure, J., et al. (2015b). KIAA0586 is Mutated in Joubert Syndrome. Human mutation ***36***, 831-835.

Bachmann-Gagescu, R., Phelps, I.G., Stearns, G., Link, B.A., Brockerhoff, S.E., Moens, C.B., and Doherty, D. (2011). The ciliopathy gene cc2d2a controls zebrafish photoreceptor outer segment development through a role in Rab8-dependent vesicle trafficking. Human molecular genetics ***20***, 4041-4055.

Badano, J.L., Mitsuma, N., Beales, P.L., and Katsanis, N. (2006). The ciliopathies: an emerging class of human genetic disorders. Annual review of genomics and human genetics ***7***, 125-148.

Baker, K., and Beales, P.L. (2009). Making sense of cilia in disease: the human ciliopathies. American journal of medical genetics. Part C, Seminars in medical genetics ***151C***, 281-295.

Bauer, M., Cubizolles, F., Schmidt, A., and Nigg, E.A. (2016). Quantitative analysis of human centrosome architecture by targeted proteomics and fluorescence imaging. The EMBO journal ***35***, 2152-2166.

Beales, P., and Jackson, P.K. (2012). Cilia - the prodigal organelle. Cilia ***1***, 1.

Bloodgood, R. (2013). Ciliary and Flagellar Membranes (Springer US).

Bloodgood, R.A. (2010a). From Central to Rudimentary to Primary: The History of an Underappreciated Organelle Whose Time Has Come.The Primary Cilium. In Primary cilia, R.D. Sloboda, ed. (London: Academic), pp. 2–52.

Bloodgood, R.A. (2010b). Sensory reception is an attribute of both primary cilia and motile cilia. Journal of cell science ***123***, 505-509.

Boehlke, C., Bashkurov, M., Buescher, A., Krick, T., John, A.-K., Nitschke, R., Walz, G., and Kuehn, E.W. (2010). Differential role of Rab proteins in ciliary trafficking: Rab23 regulates smoothened levels. Journal of cell science ***123***, 1460-1467.

Boldt, K., van Reeuwijk, J., Gloeckner, C.J., Ueffing, M., and Roepman, R. (op. 2009). Tandem Affinity Purification of Ciliopathy-Associated Protein Complexes. In Cilia. Structure and motility, S.M. King and G.J. Pazour, eds. (Amsterdam: Academic Press), pp. 143–160.

Boldt, K., van Reeuwijk, J., Lu, Q., Koutroumpas, K., Nguyen, T.-M.T., Texier, Y., van Beersum, S.E.C., Horn, N., Willer, J.R., and Mans, D.A., et al. (2016). An organelle-specific protein landscape identifies novel diseases and molecular mechanisms. Nature communications ***7***, 11491.

Brancati, F., Dallapiccola, B., and Valente, E.M. (2010). Joubert Syndrome and related disorders. Orphanet journal of rare diseases ***5***, 20.

Brownlee, C.W., and Rogers, G.C. (2013). Show me your license, please: deregulation of centriole duplication mechanisms that promote amplification. Cellular and molecular life sciences : CMLS ***70***, 1021-1034.

Das, A., and Guo, W. (2011). Rabs and the exocyst in ciliogenesis, tubulogenesis and beyond. Trends in cell biology ***21***, 383-386.

Deretic, D., Huber, L.A., Ransom, N., Mancini, M., Simons, K., and Papermaster, D.S. (1995). rab8 in retinal photoreceptors may participate in rhodopsin transport and in rod outer segment disk morphogenesis. Journal of cell science ***108 (Pt 1)***, 215-224.

Doherty, D. (2009). Joubert syndrome: insights into brain development, cilium biology, and complex disease. Seminars in pediatric neurology ***16***, 143-154.

Dubuke, M.L., Maniatis, S., Shaffer, S.A., and Munson, M. (2015). The Exocyst Subunit Sec6 Interacts with Assembled Exocytic SNARE Complexes. The Journal of biological chemistry ***290***, 28245-28256.

Engle, E.C. (2010). Human genetic disorders of axon guidance. Cold Spring Harbor perspectives in biology ***2***, a001784.

Fasshauer, D., Sutton, R.B., Brunger, A.T., and Jahn, R. (1998). Conserved structural features of the synaptic fusion complex: SNARE proteins reclassified as Q- and R-SNAREs. Procee-

dings of the National Academy of Sciences of the United States of America ***95***, 15781-15786.

Fujita, H., Tuma, P.L., Finnegan, C.M., Locco, L., and Hubbard, A.L. (1998). Endogenous syntaxins 2, 3 and 4 exhibit distinct but overlapping patterns of expression at the hepatocyte plasma membrane. Biochemical Journal ***329***, 527-538.

Garcia, G.3., and Reiter, J.F. (2016). A primer on the mouse basal body. Cilia ***5***, 17.

Garcia-Gonzalo, F.R., Corbit, K.C., Sirerol-Piquer, M.S., Ramaswami, G., Otto, E.A., Noriega, T.R., Seol, A.D., Robinson, J.F., Bennett, C.L., and Josifova, D.J., et al. (2011). A transition zone complex regulates mammalian ciliogenesis and ciliary membrane composition. Nature genetics ***43***, 776-784.

Garcia-Gonzalo, F.R., Phua, S.C., Roberson, E.C., Garcia, G.3., Abedin, M., Schurmans, S., Inoue, T., and Reiter, J.F. (2015). Phosphoinositides Regulate Ciliary Protein Trafficking to Modulate Hedgehog Signaling. Developmental cell ***34***, 400-409.

Gherman, A., Davis, E.E., and Katsanis, N. (2006). The ciliary proteome database: an integrated community resource for the genetic and functional dissection of cilia. Nature genetics ***38***, 961-962.

Goetz, S.C., and Anderson, K.V. (2010). The primary cilium: a signalling centre during vertebrate development. Nature reviews. Genetics ***11***, 331-344.

Greenlee, M.H., Roosevelt, C.B., and Sakaguchi, D.S. (2001). Differential localization of SNARE complex proteins SNAP-25, syntaxin, and VAMP during development of the mammalian retina. The Journal of comparative neurology ***430***, 306-320.

Hao, L., and Scholey, J.M. (2009). Intraflagellar transport at a glance. Journal of cell science ***122***, 889-892.

Hildebrandt, F., Benzing, T., and Katsanis, N. (2011). Ciliopathies. The New England journal of medicine ***364***, 1533-1543.

Holcman, D., and Korenbrot, J.I. (2005). The limit of photoreceptor sensitivity: molecular mechanisms of dark noise in retinal cones. The Journal of general physiology ***125***, 641-660.

Hong, W. (2005). SNAREs and traffic. Biochimica et Biophysica Acta (BBA) - Molecular Cell Research ***1744***, 120-144.

Howe, K., Clark, M.D., Torroja, C.F., Torrance, J., Berthelot, C., Muffato, M., Collins, J.E., Humphray, S., McLaren, K., and Matthews, L., et al. (2013). The zebrafish reference genome sequence and its relationship to the human genome. Nature ***496***, 498-503.

Hu, Q., and Nelson, W.J. (2011). Ciliary diffusion barrier: the gatekeeper for the primary cilium compartment. Cytoskeleton (Hoboken, N.J.) ***68***, 313-324.

Hwang, W.Y., Fu, Y., Reyon, D., Maeder, M.L., Tsai, S.Q., Sander, J.D., Peterson, R.T., Yeh, J.-R.J., and Joung, J.K. (2013). Efficient genome editing in zebrafish using a CRISPR-Cas system. Nature biotechnology ***31***, 227-229.

Inglis, P.N., Boroevich, K.A., and Leroux, M.R. (2006). Piecing together a ciliome. Trends in genetics : TIG ***22***, 491-500.

Ishikawa, H., and Marshall, W.F. (2011). Ciliogenesis: building the cell‘s antenna. Nature reviews. Molecular cell biology ***12***, 222-234.

Jahn, R., and Scheller, R.H. (2006). SNAREs--engines for membrane fusion. Nature reviews. Molecular cell biology ***7***, 631-643.

Jensen, V.L., Carter, S., Sanders, A.A.W.M., Li, C., Kennedy, J., Timbers, T.A., Cai, J., Scheidel, N., Kennedy, B.N., and Morin, R.D., et al. (2016). Whole-Organism Developmental Expression Profiling Identifies RAB-28 as a Novel Ciliary GTPase Associated with the BBSome and Intraflagellar Transport. PLoS genetics ***12***, e1006469.

Katsanis, N. (2004). The oligogenic properties of Bardet-Biedl syndrome. Human molecular genetics ***13 Spec No 1***, R65-71.

Kawakami, K. (2007). Tol2: a versatile gene transfer vector in vertebrates. Genome biology ***8 Suppl 1***, S7.

Keeling, J., Tsiokas, L., and Maskey, D. (2016). Cellular Mechanisms of Ciliary Length Control. Cells ***5***.

Kennedy, B., and Malicki, J. (2009). What drives cell morphogenesis: a look inside the vertebrate photoreceptor. Developmental dynamics : an official publication of the American Association of Anatomists ***238***, 2115-2138.

Khanna, H. (2015). Photoreceptor Sensory Cilium: Traversing the Ciliary Gate. Cells ***4***, 674-686.

Knodler, A., Feng, S., Zhang, J., Zhang, X., Das, A., Peranen, J., and Guo, W. (2010). Coordination of Rab8 and Rab11 in primary ciliogenesis. Proceedings of the National Academy of Sciences of the United States of America ***107***, 6346-6351.

Knowles, B.C., Weis, V.G., Yu, S., Roland, J.T., Williams, J.A., Alvarado, G.S., Lapierre, L.A., Shub, M.D., Gao, N., and Goldenring, J.R. (2015). Rab11a regulates syntaxin 3 localization and microvillus assembly in enterocytes. Journal of cell science ***128***, 1617-1626.

Kobayashi, T., and Dynlacht, B.D. (2011). Regulating the transition from centriole to basal body. The Journal of cell biology ***193***, 435-444.

Kobayashi, T., Kim, S., Lin, Y.-C., Inoue, T., and Dynlacht, B.D. (2014). The CP110-interacting proteins Talpid3 and Cep290 play overlapping and distinct roles in cilia assembly. The Journal of cell biology ***204***, 215-229.

Kobayashi, T., Tsang, W.Y., Li, J., Lane, W., and Dynlacht, B.D. (2011). Centriolar kinesin Kif24 interacts with CP110 to remodel microtubules and regulate ciliogenesis. Cell ***145***, 914-925.

Laurier, V., Stoetzel, C., Muller, J., Thibault, C., Corbani, S., Jalkh, N., Salem, N., Chouery, E., Poch, O., and Licaire, S., et al. (2006). Pitfalls of homozygosity mapping: an extended consanguineous Bardet-Biedl syndrome family with two mutant genes (BBS2, BBS10), three mutations, but no triallelism. European journal of human genetics : EJHG ***14***, 1195-1203.

Lehtonen, S., Riento, K., Olkkonen, V.M., and Lehtonen, E. (1999). Syntaxin 3 and Munc-18-2 in epithelial cells during kidney development. Kidney international ***56***, 815-826.

Lessman, C.A. (2012). Centrosomes in the zebrafish (Danio rerio): a review including the related basal body. Cilia ***1***, 9.

Lim, Y.S., Chua, C.E.L., and Tang, B.L. (2011). Rabs and other small GTPases in ciliary transport. Biology of the cell ***103***, 209-221.

Lipschutz, J.H., and Mostov, K.E. (2002). Exocytosis. The Many Masters of the Exocyst. Current Biology ***12***, R212-R214.

Mazelova, J., Ransom, N., Astuto-Gribble, L., Wilson, M.C., and Deretic, D. (2009). Syntaxin 3 and SNAP-25 pairing, regulated by omega-3 docosahexaenoic acid, controls the delivery of rhodopsin for the biogenesis of cilia-derived sensory organelles, the rod outer segments. Journal of cell science ***122***, 2003-2013.

McNew, J.A., Parlati, F., Fukuda, R., Johnston, R.J., Paz, K., Paumet, F., Sollner, T.H., and Rothman, J.E. (2000). Compartmental specificity of cellular membrane fusion encoded in SNARE proteins. Nature ***407***, 153-159.

Mellman, I., and Emr, S.D. (2013). A Nobel Prize for membrane traffic: vesicles find their journey‘s end. The Journal of cell biology ***203***, 559-561.

Mitchison, H.M., and Valente, E.M. (2017). Motile and non-motile cilia in human pathology: from function to phenotypes. The Journal of pathology ***241***, 294-309.

Morgera, F., Sallah, M.R., Dubuke, M.L., Gandhi, P., Brewer, D.N., Carr, C.M., and Munson, M. (2012). Regulation of exocytosis by the exocyst subunit Sec6 and the SM protein Sec1. Molecular biology of the cell ***23***, 337-346.

Moritz, O.L., Tam, B.M., Hurd, L.L., Peranen, J., Deretic, D., and Papermaster, D.S. (2001). Mutant rab8 Impairs docking and fusion of rhodopsin-bearing post-Golgi membranes and causes cell death of transgenic Xenopus rods. Molecular biology of the cell ***12***, 2341-2351.

Mougou-Zerelli, S., Thomas, S., Szenker, E., Audollent, S., Elkhartoufi, N., Babarit, C., Romano, S., Salomon, R., Amiel, J., and Esculpavit, C., et al. (2009). CC2D2A mutations in Meckel and Joubert syndromes indicate a genotype-phenotype correlation. Human mutation ***30***, 1574-1582.

Nachury, M.V., Loktev, A.V., Zhang, Q., Westlake, C.J., Peränen, J., Merdes, A., Slusarski, D.C., Scheller, R.H., Bazan, J.F., and Sheffield, V.C., et al. (2007). A Core Complex of BBS Proteins Cooperates with the GTPase Rab8 to Promote Ciliary Membrane Biogenesis. Cell ***129***, 1201-1213.

Nachury, M.V., Seeley, E.S., and Jin, H. (2010). Trafficking to the ciliary membrane: how to get across the periciliary diffusion barrier? Annual review of cell and developmental biology ***26***, 59-87.

Nakane, T., and Biesecker, L.G. (2005). No evidence for triallelic inheritance of MKKS/BBS loci in Amish Mckusick-Kaufman syndrome. American journal of medical genetics. Part A ***138***, 32-34.

Nakanishi, H., Ios Santos, P. de, and Neiman, A.M. (2004). Positive and negative regulation of a SNARE protein by control of intracellular localization. Molecular biology of the cell ***15***, 1802-1815.

Novick, P., and Guo, W. (2002). Ras family therapy: Rab, Rho and Ral talk to the exocyst. Trends in cell biology ***12***, 247-249.

Oka, M., Shimojima, K., Yamamoto, T., Hanaoka, Y., Sato, S., Yasuhara, T., Yoshinaga, H., and Kobayashi, K. (2016). A novel HYLS1 homozygous mutation in living siblings with Joubert syndrome. Clinical genetics ***89***, 739-743.

Omori, Y., Zhao, C., Saras, A., Mukhopadhyay, S., Kim, W., Furukawa, T., Sengupta, P., Veraksa, A., and Malicki, J. (2008). Elipsa is an early determinant of ciliogenesis that links the IFT particle to membrane-associated small GTPase Rab8. Nature cell biology ***10***, 437-444.

Pearring, J.N., Salinas, R.Y., Baker, S.A., and Arshavsky, V.Y. (2013). Protein sorting, targeting and trafficking in photoreceptor cells. Progress in retinal and eye research ***36***, 24-51.

Pearson, C.G. (2011). A kinesin in command of primary ciliogenesis. Cell ***145***, 817-819.

Pedersen, L.B., Veland, I.R., Schroder, J.M., and Christensen, S.T. (2008). Assembly of primary cilia. Developmental dynamics : an official publication of the American Association of Anatomists ***237***, 1993-2006.

Perry, S.F., Ekker, M., Farrell, A.P., and Brauner, C.J. (2010). Fish Physiology: Zebrafish (Elsevier Science).

Pfeffer, S. (2005). A model for Rab GTPase localization. Biochemical Society transactions ***33***, 627-630.

Pfeffer, S.R. (2013). Rab GTPase regulation of membrane identity. Current opinion in cell biology ***25***, 414-419.

Poretti, A., Boltshauser, E., and Doherty, D. (2014a). Cerebellar hypoplasia: differential diagnosis and diagnostic approach. American journal of medical genetics. Part C, Seminars in medical genetics ***166C***, 211-226.

Poretti, A., Boltshauser, E., and Valente, E.M. (2014b). The molar tooth sign is pathognomonic for Joubert syndrome! Pediatric neurology ***50***, e15-6.

Poretti, A., Dietrich Alber, F., Brancati, F., Dallapiccola, B., Valente, E.M., and Boltshauser, E. (2009). Normal cognitive functions in joubert syndrome. Neuropediatrics ***40***, 287-290.

Purves, D., Augustine, G.J., Fitzpatrick, D., Hall, W.C., LaMantia, A.-S., McNamara, J.O. and White, L.E. (2008). Neuroscience. 4th edition.

Ray, B., Tam, B., Moritz, O., and Deretic, D. (2013). VAMP7 as a Regulator of Rhodopsin Transport Carrier Fusion in Photoreceptors. Invest. Ophthalmol. Vis. Sci. ***54***, 706.

Reiter, J.F., Blacque, O.E., and Leroux, M.R. (2012). The base of the cilium: roles for transition fibres and the transition zone in ciliary formation, maintenance and compartmentalization. EMBO reports ***13***, 608-618.

Roepman, R., Ueffing, M., Kremer, H., Huynen, M.A., Gibson, T.J., Katsanis, N., Walz, G.T., Wolfrum, U., Franco, B., and Giles, R.H., et al. (2012). SYSCILIA, "A systems biology approach to dissect cilia function and its disruption in human genetic disease". Cilia ***1***, P41.

Romani, M., Micalizzi, A., and Valente, E.M. (2013). Joubert syndrome. Congenital cerebellar ataxia with the molar tooth. The Lancet Neurology ***12***, 894-905.

Roosing, S., Romani, M., Isrie, M., Rosti, R.O., Micalizzi, A., Musaev, D., Mazza, T., Al-Gazali, L., Altunoglu, U., and Boltshauser, E., et al. (2016). Mutations in CEP120 cause Joubert syndrome as well as complex ciliopathy phenotypes. Journal of medical genetics ***53***, 608-615.

Rothman, J.E. (2014). The principle of membrane fusion in the cell (Nobel lecture). Angewandte Chemie (International ed. in English) ***53***, 12676-12694.

Sato, T., Iwano, T., Kunii, M., Matsuda, S., Mizuguchi, R., Jung, Y., Hagiwara, H., Yoshihara, Y., Yuzaki, M., and Harada, R., et al. (2014). Rab8a and Rab8b are essential for several apical transport pathways but insufficient for ciliogenesis. Journal of cell science ***127***, 422-431.

Scales, S.J., Chen, Y.A., Yoo, B.Y., Patel, S.M., Doung, Y.C., and Scheller, R.H. (2000). SNAREs contribute to the specificity of membrane fusion. Neuron ***26***, 457-464.

Schimmoller, F., Simon, I., and Pfeffer, S.R. (1998). Rab GTPases, Directors of Vesicle Docking. Journal of Biological Chemistry ***273***, 22161-22164.

Singla, V., and Reiter, J.F. (2006). The primary cilium as the cell's antenna: signaling at a sensory organelle. Science (New York, N.Y.) ***313***, 629-633.

Smaoui, N., Chaabouni, M., Sergeev, Y.V., Kallel, H., Li, S., Mahfoudh, N., Maazoul, F., Kammoun, H., Gandoura, N., and Bouaziz, A., et al. (2006). Screening of the eight BBS genes in Tunisian families: no evidence of triallelism. Investigative ophthalmology & visual science ***47***, 3487-3495.

Sollner, T., Bennett, M.K., Whiteheart, S.W., Scheller, R.H., and Rothman, J.E. (1993). A protein assembly-disassembly pathway in vitro that may correspond to sequential steps of synaptic vesicle docking, activation, and fusion. Cell ***75***, 409-418.

Soo Hoo, L., Banna, C.D., Radeke, C.M., Sharma, N., Albertolle, M.E., Low, S.H., Weimbs, T., and Vandenberg, C.A. (2016). The SNARE Protein Syntaxin 3 Confers Specificity for Polarized Axonal Trafficking in Neurons. PloS one ***11***, e0163671.

Stenmark, H. (2009). Rab GTPases as coordinators of vesicle traffic. Nat Rev Mol Cell Biol ***10***, 513-525.

Stephen, J., Vilboux, T., Mian, L., Kuptanon, C., Sinclair, C.M., Yildirimli, D., Maynard, D.M., Bryant, J., Fischer, R., and Vemulapalli, M., et al. (2017). Mutations in KIAA0753 cause Joubert syndrome associated with growth hormone deficiency. Human genetics ***136***, 399-408.

Szymanska, K., Hartill, V.L., and Johnson, C.A. (2014). Unraveling the genetics of Joubert and Meckel-Gruber syndromes. Journal of pediatric genetics ***3***, 65-78.

Szymanska, K., and Johnson, C.A. (2012). The transition zone: an essential functional compartment of cilia. Cilia ***1***, 10.

Temiyasathit, S., and Jacobs, C.R. (2010). Osteocyte primary cilium and its role in bone mechanotransduction. Annals of the New York Academy of Sciences ***1192***, 422-428.

Tobin, J.L., and Beales, P.L. (2009). The nonmotile ciliopathies. Genetics in medicine : official journal of the American College of Medical Genetics ***11***, 386-402.

Valente, E.M., Dallapiccola, B., and Bertini, E. (2013). Joubert syndrome and related disorders. Handbook of clinical neurology ***113***, 1879-1888.

van Reeuwijk, J., Arts, H.H., and Roepman, R. (2011). Scrutinizing ciliopathies by unraveling ciliary interaction networks. Human molecular genetics ***20***, R149-57.

Vilboux, T., Malicdan, M.C.V., Roney, J.C., Cullinane, A.R., Stephen, J., Yildirimli, D., Bryant, J., Fischer, R., Vemulapalli, M., and Mullikin, J.C., et al. (2017). CELSR2, encoding a planar cell polarity protein, is a putative gene in Joubert syndrome with cortical heterotopia, microophthalmia, and growth hormone deficiency. American journal of medical genetics. Part A ***173***, 661-666.

Wang, J., and Deretic, D. (2015). The Arf and Rab11 effector FIP3 acts synergistically with ASAP1 to direct Rabin8 in ciliary receptor targeting. Journal of cell science ***128***, 1375-1385.

Wang, J., Morita, Y., Mazelova, J., and Deretic, D. (2012). The Arf GAP ASAP1 provides a platform to regulate Arf4- and Rab11-Rab8-mediated ciliary receptor targeting. The EMBO journal ***31***, 4057-4071.

Ward, H.H., Brown-Glaberman, U., Wang, J., Morita, Y., Alper, S.L., Bedrick, E.J., Gattone, V.H.2., Deretic, D., and Wandinger-Ness, A. (2011). A conserved signal and GTPase complex are required for the ciliary transport of polycystin-1. Molecular biology of the cell ***22***, 3289-3305.

Ware, S.M., Aygun, M.G., and Hildebrandt, F. (2011). Spectrum of clinical diseases caused by disorders of primary cilia. Proceedings of the American Thoracic Society ***8***, 444-450.

Waters, A.M., and Beales, P.L. (2011). Ciliopathies: an expanding disease spectrum. Pediatric nephrology (Berlin, Germany) ***26***, 1039-1056.

Watson, R.T. & Pessin, J.E. (2001). Transmembrane domain length determines intracellular membrane compartment localization of syntaxins 3, 4 and 5. Am J Physiol Cell Physiol ***281***, 215-223.

Westlake, C.J., Baye, L.M., Nachury, M.V., Wright, K.J., Ervin, K.E., Phu, L., Chalouni, C., Beck, J.S., Kirkpatrick, D.S., and Slusarski, D.C., et al. (2011). Primary cilia membrane assembly is initiated by Rab11 and transport protein particle II (TRAPPII) complex-dependent trafficking of Rabin8 to the centrosome. Proceedings of the National Academy of Sciences of the United States of America ***108***, 2759-2764.

Ying, G., Gerstner, C.D., Frederick, J.M., Boye, S.L., Hauswirth, W.W., and Baehr, W. (2016). Small GTPases Rab8a and Rab11a Are Dispensable for Rhodopsin Transport in Mouse Photoreceptors. PloS one ***11***, e0161236.

Yoshimura, S.-I., Egerer, J., Fuchs, E., Haas, A.K., and Barr, F.A. (2007). Functional dissection of Rab GTPases involved in primary cilium formation. The Journal of cell biology ***178***, 363-369.

Yue, P., Zhang, Y., Mei, K., Wang, S., Lesigang, J., Zhu, Y., Dong, G., and Guo, W. (2017). Sec3 promotes the initial binary t-SNARE complex assembly and membrane fusion. Nature communications ***8***, 14236.

Zaghloul, N.A., and Katsanis, N. (2011). Zebrafish assays of ciliopathies. Methods in cell

biology *105*, 257-272.

Zerial, M., and McBride, H. (2001). Rab proteins as membrane organizers. Nature reviews. Molecular cell biology *2*, 107-117.

Chapter 2. The ciliopathy protein CC2D2A organizes the vesicle fusion machinery at the periciliary membrane of Zebrafish photoreceptors

Ojeda Naharros, I., Gesemann, M., Mateos, J.M., Barmettler, G., Ziegler, U., Neuhauss, S.C.F. and Bachmann-Gagescu, R.*

University of Zurich, Institute of Molecular Life Sciences
Winterthurerstrasse 190, 8057
Zurich, Switzerland
Life Science Zurich Graduate School, PhD. Program in Neurosciences

* Corresponding author
Ruxandra Bachmann-Gagescu
ruxandra.bachmann@imls.uzh.ch

In submission

Personal contribution: Conceptualization and experimental design, performed experiments, figure preparation, drafting and writing of the manuscript

Abstract

Ciliopathies are human disorders caused by dysfunction of primary cilia, ubiquitous organelles involved in transduction of environmental signals such as light sensation in photoreceptors. Concentration of signal detection proteins in the ciliary membrane is achieved by regulated polarized vesicle trafficking and a selective barrier at the ciliary base, the transition zone (TZ). Dysfunction of the TZ protein CC2D2A causes ciliopathies in humans and loss of ciliary protein localization in animal models. Using correlative light and electron microscopy and live imaging in zebrafish photoreceptors, we identify a role for Cc2d2a in the latest step of opsin-carrier vesicle (OCV) trafficking, namely vesicle fusion, through organization of the vesicle fusion machinery components SNAP25, Syntaxin3 and Exoc4 at the periciliary membrane. We further provide the first live characterization of Rab8-trafficking in rod and cone photoreceptors, supporting the recently questioned role of Rab8 in OCV trafficking and suggesting redundancy between Rab8 paralogs in this process.

Introduction

Ciliopathies are an expanding group of human disorders caused by primary cilium dysfunction and unified by a wide array of overlapping phenotypes: cystic kidneys, central nervous system (CNS) malformations and retinal degeneration among others (Badano et al., 2006; Goetz and Anderson, 2010; Hildebrandt et al., 2011). Primary cilia are ubiquitous organelles that consist of a mother centriole-derived basal body (BB) and a microtubule-based axoneme ensheathed by a specialized membrane. Primary cilia are involved in transduction of a variety of environmental signals to the cell, depending on the cell type, including morphogens and light. To serve this purpose, the ciliary membrane is enriched with specific receptors and channels required for signal detection (Singla and Reiter, 2006). Cilia are devoid of protein synthesis machinery (Nachury et al., 2010), thus the ciliary membrane compartmentalization is enabled by highly controlled polarized vesicle trafficking subject to RabGTPase regulation (Hsiao et al., 2012) and by a selective barrier at the base of the cilium likely formed by the transition zone (TZ) (Szymanska and Johnson, 2012), a region localized between the BB and the axoneme. Mutations in several genes encoding TZ proteins lead to Joubert syndrome (JBTS; OMIM: 213300), a representative ciliopathy characterized by a very specific cerebellar malformation –the molar tooth sign– and associated in 30% of cases with retinal involvement due to photoreceptor (PR) dysfunction (Bachmann-Gagescu et al., 2015a).

Light transduction takes place in PRs, which are highly polarized sensory neurons harboring a highly specialized primary cilium, the outer segment (OS) (Bloodgood, 2013). OSs consist of stacks of membranous disks containing proteins required for phototransduction, such as the photopigment opsin, and organized around a microtubule-based axoneme (Kennedy and Malicki, 2009). Trafficking of opsins towards the OSs is thought to be controlled by the small GTPase Rab8, based on expression of a dominant negative GDP-locked Rab8 form in frog PRs that led to opsin-carrier vesicle (OCV) accumulation at the base of the PR OS (Deretic et al., 1995; Moritz et al., 2001). Further work in frog PRs identified a complex initiated by Arf4 in the trans-Golgi network and formed by ASAP1-Rab11-FIP3-Rabin8-Rab8 involved in opsin delivery to the ciliary compartment (Wang et al., 2012; Wang and Deretic, 2015). In addition, Rab11 and Rabin8, the guanidine exchange factor for Rab8, were shown to promote ciliary membrane biogenesis in RPE-hTERT cells (Nachury et al., 2007; Knodler et al., 2010; Ward et al., 2011). While two RAB8 paralogs exist in humans (RAB8A and RAB8B) which were both found to be involved in ciliogenesis in RPE cells (Westlake et al., 2011), it remains unclear which paralogue is important in OCV trafficking in PRs. In fact, since a double *rab8a;rab8b* knock-out mice, which revealed mislocalization of apical proteins in intestinal cells, developed ciliogenesis defects only after additional knock-out of the closest Rab8-relative Rab10 in MEFs (Sato et al., 2014), it appears that

various Rabs can compensate for loss of function of each other. However, in contrast to all these results, a recent study questioned the role of Rab8 in opsin trafficking in PRs based on double mouse *rab8a;rab11a* knock-outs which displayed no retinal phenotype, reopening the question of the role of Rab8 in OCV trafficking in PRs (Ying et al., 2016).

Once OCVs have reached their target membrane, vesicle fusion is thought to be mediated by the Exocyst and by SNARE (Soluble N-ethylmaleimide-sensitive factor Attachment Protein REceptor) proteins. SNAREs present on the vesicle surface (v-SNAREs) and on the target membrane (t-SNAREs) pair up and work as catalysts to provide the mechanical force required to mediate membrane fusion (Jahn and Scheller, 2006). The Exocyst, a multisubunit protein complex, is implicated in tethering of secretory vesicles to the plasma membrane in several exocytosis processes including ciliogenesis (Das and Guo, 2011; Heider and Munson, 2012). The Exocyst localizes at the ciliary base in cell culture (Rogers et al., 2004) and in the ciliary stalk of PRs in frog retina (Mazelova et al., 2009) and one of its components, Sec15, has been found to interact directly with Rab8 (Das and Guo, 2011). Exocyst components Sec8, Sec10 and Exo84 have been involved in the pathogenicity of various ciliopathies, including Joubert syndrome and the related Meckel syndrome (Fogelgren et al., 2011; Dixon-Salazar et al., 2012; Shaheen et al., 2013; Martin-Urdiroz et al., 2016; Seixas et al., 2016).

Joubert syndrome is caused by mutations in one of at least 30 genes, many of which encode TZ proteins interacting with each other in large multi-protein complexes, as is the case for *CC2D2A*. CC2D2A dysfunction is one of the most common causes for JBTS, accounting for 10% of JBTS families. As for other TZ proteins, its dysfunction leads to loss of ciliary protein localization in fibroblasts from knock-out mice (Garcia-Gonzalo et al., 2011). Similarly, we previously reported intracellular opsin mislocalization and massive vesicle accumulation in PRs of the zebrafish *cc2d2a*^{uw38} mutant, suggesting the involvement of Cc2d2a in ciliary trafficking and supporting the role of the TZ in ciliary protein content regulation (Owens et al., 2008; Bachmann-Gagescu et al., 2011). Although we observed loss of Rab8 puncta in absence of Cc2d2a function, the mechanistic link between the TZ protein Cc2d2a, Rab8 and ciliary-directed trafficking remained obscure.

In this study, we show that ciliary-directed vesicles containing opsins and coated by Rab8 accumulate progressively at the apical portion of *cc2d2a-/-* PRs as a result of a vesicle fusion defect. Using Correlative Light and Electron Microscopy (CLEM) and live imaging in zebrafish PRs, we provide a detailed analysis of the movement kinetics of Rab8-tagged vesicles, supporting a role for Rab8 in OCV trafficking and demonstrating redundancy between Rab8a and Rab8b-like paralogs in both rods and cones of wild-type fish. Time-lapse analysis of Rab8-tagged puncta in *cc2d2a-/-* PRs reveals no substantial difference compared to wild-type PRs, suggesting that the observed OCV accumulation is not secondary to a defect in trafficking

but rather in vesicle fusion. In support of this hypothesis, we observe mislocalization and/or depletion of elements of the vesicle fusion machinery, including the t-SNAREs SNAP25 and Syntaxin3 and the Exocyst component Sec8, at the apical membrane of PRs consequent to Cc2d2a loss of function. Together, these results indicate that Cc2d2a plays a crucial role in the organization of the vesicular docking sites at the periciliary membrane, allowing OCVs to fuse and deliver their cargo at the base of the OSs.

Results

Vesicles accumulate progressively from the onset of outer segment formation in the apical portion of cc2d2a-/- photoreceptors

Our previous studies of the *cc2d2a*^{uw38} zebrafish mutant, which harbors a non-sense mutation upstream of the C2 domain of Cc2d2a (Owens et al., 2008), identified massive accumulation of vesiculo-tubular structures in the apical portion of zebrafish photoreceptors (PRs) co-existing with misshapen outer segments (OSs) at 5 days post fertilization (dpf) (Bachmann-Gagescu et al., 2011). To rule out the possibility that these structures are the result of a degenerative process we analyzed the ultrastucture of mutant retinae at earlier time points spanning OS formation by transmission electron microscopy (TEM). At 60 hpf, wild-type (wt) PRs have taken on their typical cell morphology including an apico-basally elongated nucleus, a recognizable inner segment containing the forming mitochondrial cluster (Fig. 1 A) and an already docked basal body (BB) to the apical membrane with extension of the connecting cilium (Fig. 1 C). At this stage, *cc2d2a-/-* PRs are indistinguishable from wt based on cell morphology, distribution of organelles (Fig. 1B) and docking of the BB to the apical membrane with extension of the connecting cilium (Fig. 1 D and Fig. S1). However, at later stages we observe that ciliary membrane stacking is impaired in *cc2d2a-/-* PRs. Nascent OSs are observed in a majority of wt PRs at 75 hpf (Fig. 1 E and G) but are mostly absent in *cc2d2a-/-* retinae where vesicular structures begin to appear instead (Fig. 1 F and H). While wt PRs extend OSs of increasing length at 4dpf (Fig. 1 I and K), vesicular accumulation increases progressively over time in *cc2d2a-/-* PRs (Fig. 1 J and L) and becomes massive at 5 dpf, as previously reported (Bachmann-Gagescu et al., 2011). Therefore, we conclude that accumulation of vesicles is progressive from onset of OS formation.

Accumulated vesicles are opsin-carrier vesicles

To ensure that these accumulated membranous structures are opsin-carrier vesicles (OCVs) and thus were ciliary targeted, we used a recently developed Correlative Light and Electron Microscopy (CLEM) method (Mateos

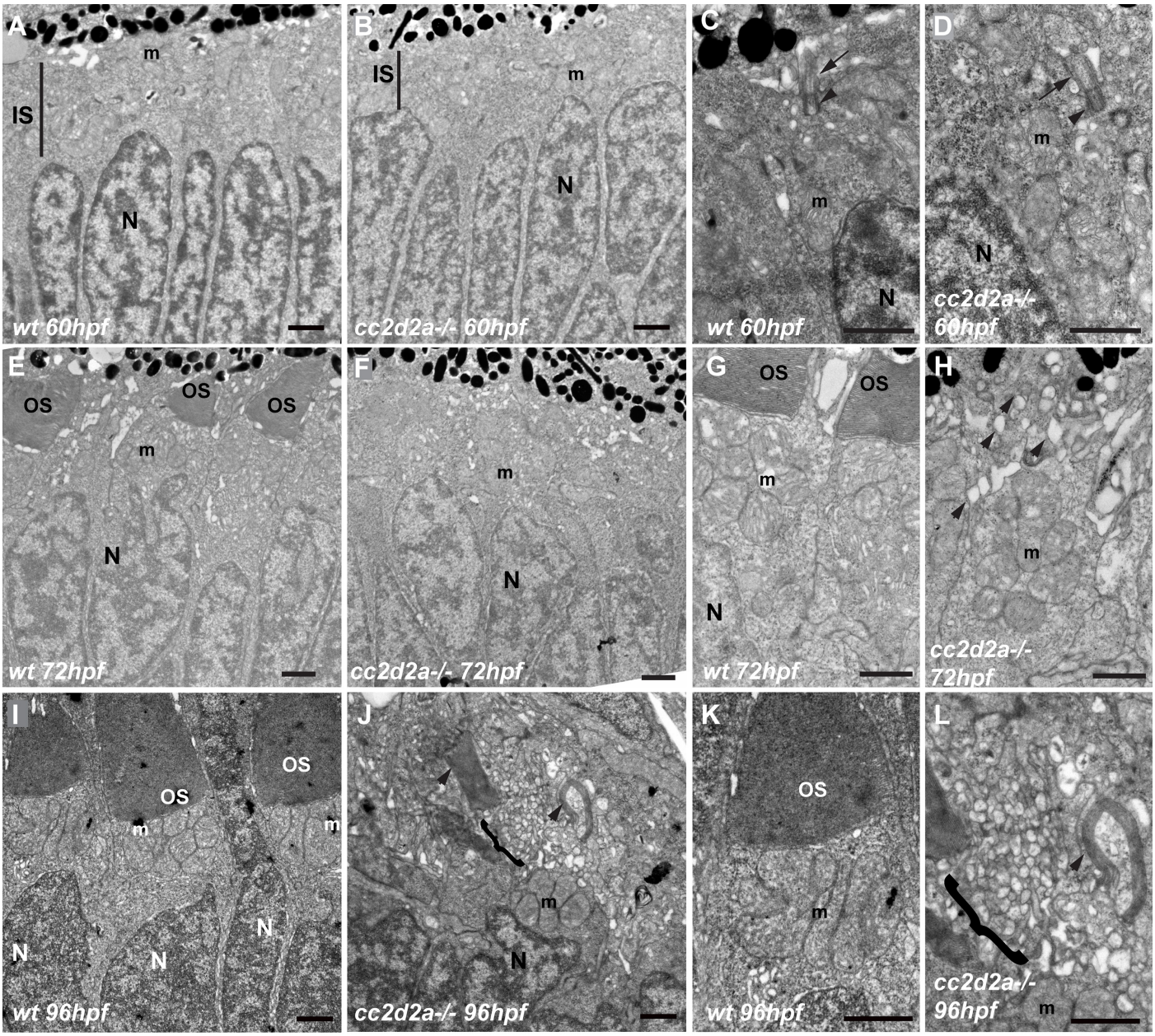

Figure 1. Vesicle accumulation is progressive from the onset of OS formation in *cc2d2a-/-* PRs
(A-D) Transmission Electron Microscopy (TEM) of retinal sections at 60hpf is indistinguishable between wild-type (wt) (A, C) and *cc2d2a-/-* (B, D), including with respect to basal body docking (arrowheads in C-D) and extension of the connecting cilium (arrows in C-D). (E-H) TEM of retinal sections at 72 hpf: Note the nascent Outer Segments (OS) in wt (E, G), but the quasi-absence of OSs in *cc2d2a-/-* with onset of apical accumulation of vesicular structures (F, H, arrowheads). (I-L) TEM of retinal sections at 96 hpf: Well-formed OSs are present apical to the mitochondrial cluster in wt (I, K), while in mutant photoreceptors an increased number of vesicles (brackets) are found in the apical portion of the cell together with misshapen membrane stacks (arrowheads) instead of OSs (J, L). Scale bars are 1 µm in all panels. M mitochondria, N nuclei, OS outer segments, wt wild-type.

et al., 2016), which enables us to overlay immunodetected opsin on ultrathin sections with scanning electron microscopy (SEM) images to determine the precise ultrastructural localization of the opsins. Structures of interest such as OSs (Fig. 2 A' and B'), accumulated vesicles (Fig. 2 D' and E', arrows) or cilia (Fig. 2 D'' and E'', arrowhead) are easily recognizable on the SEM images. Using the 4D2 antibody which recognizes rod and red-green cone opsin, we found opsin signal in OSs of wild-type PRs (Fig. 2 A and C and A'-B'). In *cc2d2a-/-* PRs, opsins localize to aberrant membrane stacks of dysmorphic OSs as well as to the accumulated vesicles

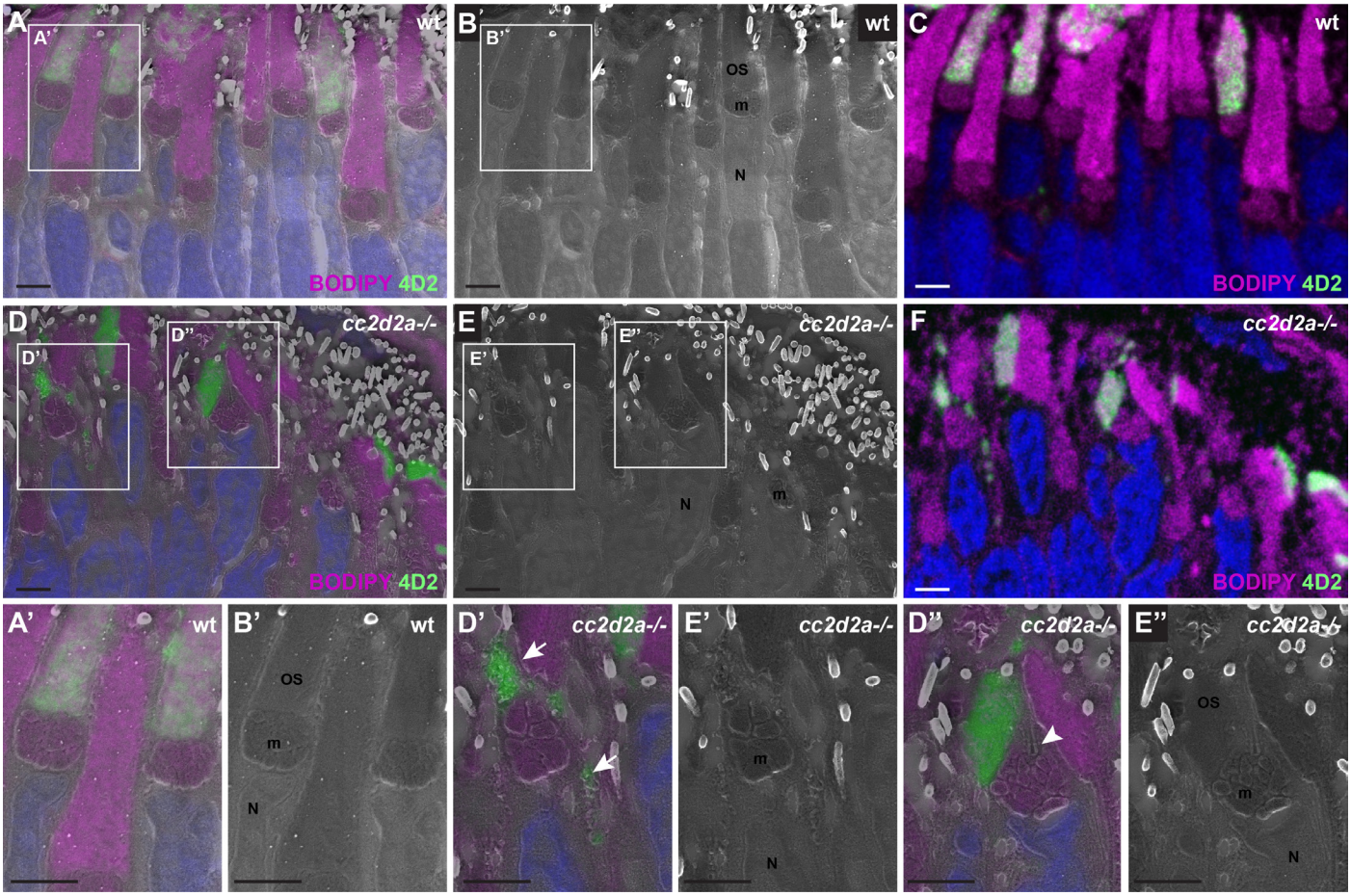

Figure 2. Accumulated vesicles in *cc2d2a-/-* PR are opsin-carrier-vesicles

(A-C) 5 dpf Correlative Light and Electron Microscopy (CLEM) image of a wildtype (wt) retina stained with BODIPY (magenta) to mark the outer segment membranes and the mitochondrial cluster and with 4D2 (green) to label rhodopsin and red-green opsin. (A) is the overlay of the Scanning Electron Microscopy (SEM) image (B) and the immuno-histochemistry image (IHC) (C). (D-E) 5 dpf CLEM sections of a *cc2d2a-/-* retina. Note that while 4D2 staining only localizes at the outer segments of wildtype PRs (A"), it is visible in accumulated vesicles in *cc2d2a-/-* PRs (D', arrows). Also note normal cilium docking in *cc2d2a-/-* PRs (D"-E", arrowhead). Scale bars are 2 µm in all images.

(Fig. 2 D and F and D'-E"). In comparison, transport of transmembrane proteins such as Cacna1fa to other cellular compartments than the OS (synapse) is unaffected in *cc2d2a-/-* PRs (Fig. S2). Collectively, our data indicate that OCVs accumulate progressively in *cc2d2a-/-* PRs as a result of a ciliary-specific trafficking or a vesicle fusion defect.

The small GTPase Rab8 associates with opsin-carrier vesicles

Our previous study of the zebrafish *cc2d2a*^{uw38} mutant described mislocalization of the small GTPase Rab8 in PRs lacking Cc2d2a. This suggested that a defect in Rab8-mediated trafficking could underlie the observed vesicle accumulation, given the ascribed roles for Rab8 in regulation of polarized vesicle trafficking to cilia (Nachury et al., 2007; Knodler et al., 2010; Westlake et al., 2011) and in delivery of opsin-carrier-vesicles (OCVs) in PRs (Wang and Deretic, 2015). However, recent work has questioned this role for Rab8 paralogues in OCV transport in mouse (Ying et al., 2016). To elucidate whether Rab8 participates in opsin transport in zebrafish and to investigate the consequences of Cc2d2a loss-of-function on Rab8-mediated trafficking, we generated transgenic fish lines stably expressing tagged Rab8 in PRs.

Zebrafish have 3 Rab8 paralogues: Rab8a, Rab8b and Rab8b-like. While zebrafish Rab8a (NM_001089562) appears to be the true orthologue of human RAB8A (NM_005370) based on synteny and on sequence comparisons (93.2% identity at the amino acid level), the situation is more

complex for RAB8B (NM_016530). Indeed, zebrafish have a Rab8b gene (NM_001099259) on chromosome 7, with conserved synteny compared to human, and a Rab8b-like gene (XM_017354313.1) (Fig. S3) on chromosome 25, a region where uncertainties in the zebrafish genome assembly currently limit further investigation. In any case, all three zebrafish Rab8 paralogues share very high sequence similarity with each other and with the human RAB8A and B paralogues (Fig. S4).

To characterize Rab8-directed trafficking in zebrafish photoreceptors, we chose to use the zebrafish Rab8a sequence, given the large body of literature concerning ciliary-directed trafficking focused on this paralogue, as well as the Rab8b-like sequence, to test whether other Rab8 paralogues could also play a role in OCV trafficking. We generated lines expressing N-terminal mCherry-tagged Rab8a in rods (*tg(rhod:mCherry-Rab8a)*) and cones (*tg(tacp:mCherry-Rab8a)*) as well as Rab8b-like in rods (*tg(rhod:mCherry-Rab8b-like)*). To test if the different Rab8 paralogues co-localized with opsin-carrier vesicles, we transiently co-expressed heat-shock inducible GFP-tagged rhodopsin (Zhao and Malicki, 2011) in our Rab8 transgenic fish or stained them for endogenous opsin (4D2 antibody). We observed co-localization of both Rab8 paralogues with GFP-tagged rhodopsin and endogenous opsins in both cones and rods (Fig. 3 A-J). Moreover, using CLEM, we observed that opsin signal is associated with mCherry-Rab8a in vesicular-like structures (Fig. 3 J-N). Together, these results confirm that the small GTPase Rab8 is present at the surface of OCVs in both cones and rods and suggest possible redundancy between Rab8 paralogs in the transport of opsins.

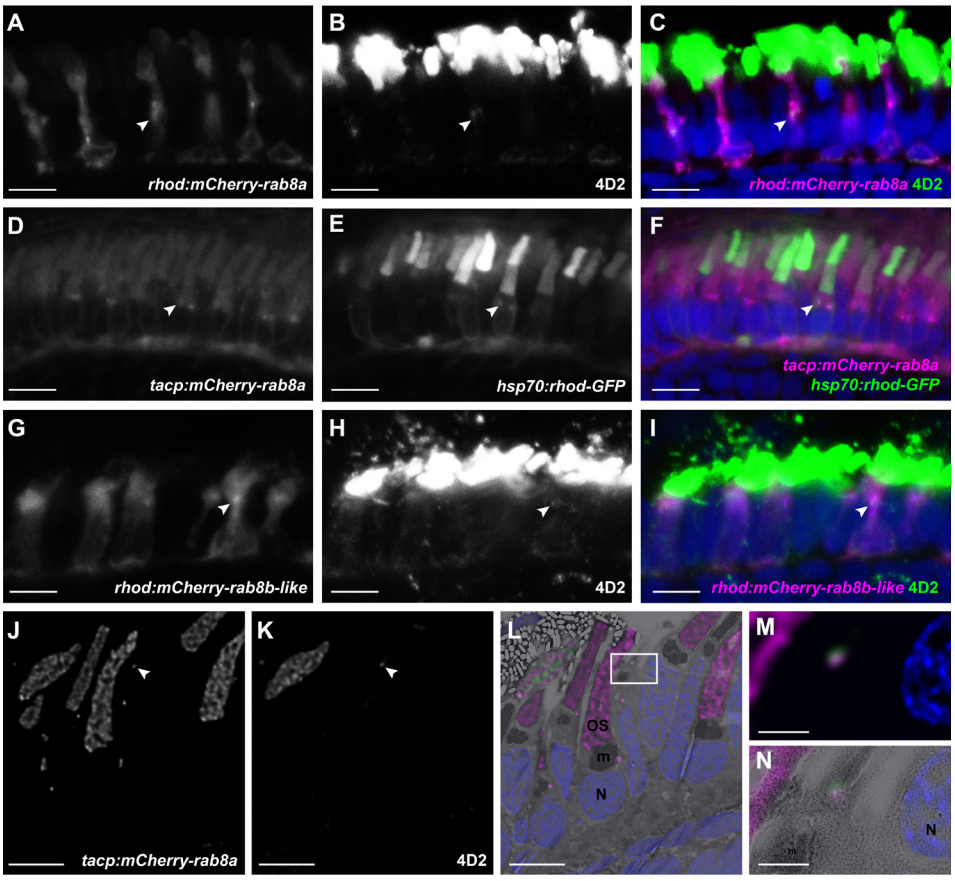

Figure 3. Rab8a and Rab8-like associate with rhodopsin-carrier vesicles

(A-C) 5 dpf cryosections of wildtype (wt) zebrafish expressing mCherry-tagged Rab8a in rods *(tg(rhod:mCherry-rab8a))* (magenta), stained with the anti-opsin antibody 4D2 (green). Note co-localization of the signals (arroheads). (D-F) 5 dpf cryosections of wt zebrafish stably expressing mCherry-tagged Rab8a in cones *(tg(-Tacp:mCherry-rab8a))* (magenta), and transiently expressing GFP-tagged rhodopsin (green). Note co-localization of the signals. (G-I) 5 dpf cryosections of wt zebrafish stably expressing mCherry-tagged Rab8-like in rods *tg(rhod:mCherry-rab8like)* (magenta), stained with the anti-opsin antibody 4D2 (green). Arrowheads indicate examples of co-localization in all cases. (J-N) CLEM image of wt zebrafish stably mCherry-tagged Rab8a in cones *(tg(-Tacp:mCherry-rab8a))* (J) stained with anti-opsin antibody 4D2 (K). (L) shows the merged image of Rab8a (magenta) and 4D2 (green) over the SEM image. (M) Zoom of the co-localized Rab8a and opsin signals surrounded by membrane (N), indicating a vesicular structure. Scale bars are 5 µm in A-I, 5 µm in J-L, 1 µm in M-N.

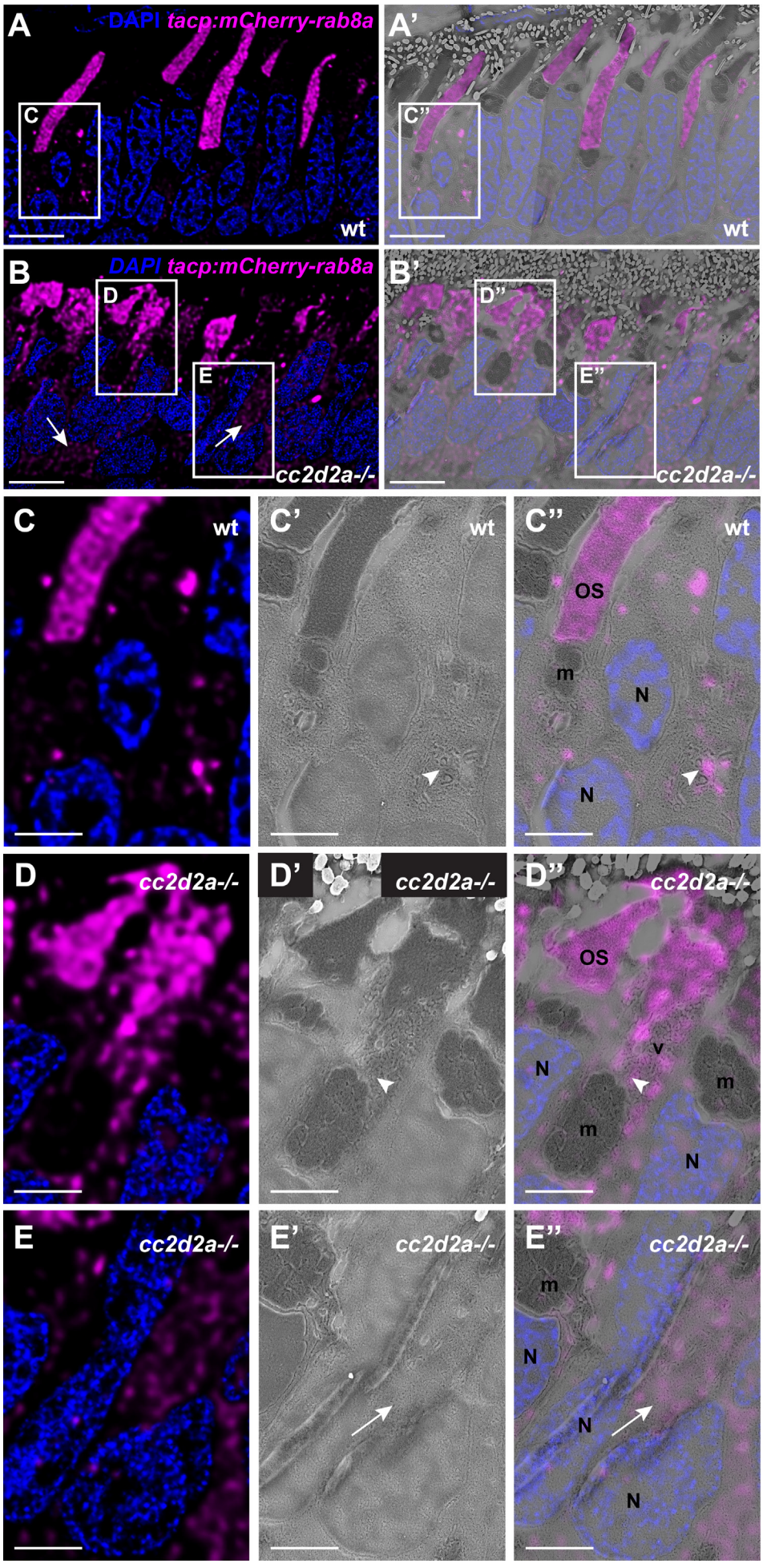

Figure 4. Rab8a is diffusely mislocalized in *cc2d2a-/-* cones
(A-A') 5 dpf Correlative Light and Electron Microscopy (CLEM) retinal section of a wildtype (wt) zebrafish expressing mCherry-tagged Rab8a in cones *(tg(-tacp:mCherry-rab8a))*. (A) is the immunohistochemistry image (IHC) stained for mCherry (magenta) and counterstained with DAPI (blue) and (A') is the overlay of the Scanning Electron Microscope (SEM). (B-B') CLEM of a *cc-2d2a-/-* retina. (C-E") are higher magnification images of the boxed areas in A-B'). Note the localization of Rab8a (magenta) to outer segments (OSs) and to vesicular structures (arrowhead) in wt (C-C"). In *cc2d2a-/-* cones, Rab8a (magenta) localizes to in dysmorphic OSs and to accumulated vesicles (v, arrowheads) in (D-D") as well as to non-membrane-delimited cytoplasmic areas (arrow in E"). Scale bars are 5 µm in A-B' and 3 µm in C-E". OS outer segment, m mitochondria, N nuclei, v vesicular structures.

Overexpressed mCherry-Rab8a partially mislocalizes in cc2d2a-/- cones

We previously published that Cc2d2a is required for punctate localization of Rab8, since transiently expressed mCherry-Rab8 was diffusely localized in a majority of *cc2d2a-/-* cone PRs (Bachmann-Gagescu et al., 2011). We confirmed these observations in transgenic lines stably expressing mCherry-Rab8, which we subjected to CLEM to ascertain the structures where Rab8 mislocalizes within the mutant PRs. In wt PRs, using an anti-mCherry antibody to enhance the signal, we could observe discrete mCherry-positive puncta (Fig. 4 A and A') that localized to membrane-delimited vesicular structures (Fig. 4 C-C'', arrowheads) as well as diffuse mCherry signal in the outer segments (OS). Immunostaining using an anti-Rab8 antibody confirmed that these mCherry-signals contain Rab8 (Fig. S5 A-F). In *cc2d2a-/-* PRs, mCherry signal was localized to accumulated vesicles and to dysmorphic OSs (Fig. 4 D' and D''). In addition, we observed a weaker diffuse signal in the cytoplasm of mutant PRs, not delimited by membrane (Fig. 4 B and B' and E-E'', arrows). Collectively, these data indicate that loss of Cc2d2a function leads to partial mislocalization of Rab8 to the cytoplasmic compartment, while vesicles coated with Rab8 also remain present.

Dynamics of Rab8-directed trafficking in zebrafish photoreceptors display complex patterns

Taking advantage of the stable transgenic lines expressing mCherry-tagged Rab8 paralogues in rods and cones, we went on to characterize Rab8-trafficking in PRs *in vivo* in a whole tissue context. For that purpose, we obtained time-lapse videos of live 5 dpf old transgenic larvae stably co-expressing mCherry-Rab8 with GFP-hCentrin, the latter serving as an immobile cellular reference to label the basal body (BB) (Video #1). We found Rab8-tagged puncta to display a complex shuffling apico-basal movement, mostly localized to the inner segment but spanning up the entire length of the PR from the BB to the synapse, with a subset of puncta approaching the BB (Fig. 5 A-F). To ensure that this movement was not an artifact driven by the overexpression of Rab8, we transiently overexpressed mCherry-Rab3aa and analyzed its behavior via live imaging. mCherry-Rab3aa strongly localizes at the PR synapse as predicted (Fischer von Mollard et al., 1990), with only localized movement over the 10 minute duration of the time-lapse (Video #2 and Fig. 5 F-H'), indicating that overexpressed Rabs exhibit the predicted endogenous behavior. Furthermore, overexpression of Rab8 did not substantially affect retinal ultrastucture in the transgenic animals at 5 dpf, despite some increase in vesiculo-tubular structure in a subset of PRs (Fig. S5 G-G'').

We thus pursued to track the movement of Rab8-tagged particles (Fig. 5 A'-C') to compare the kinetics of the different Rab8 paralogues in wt cones

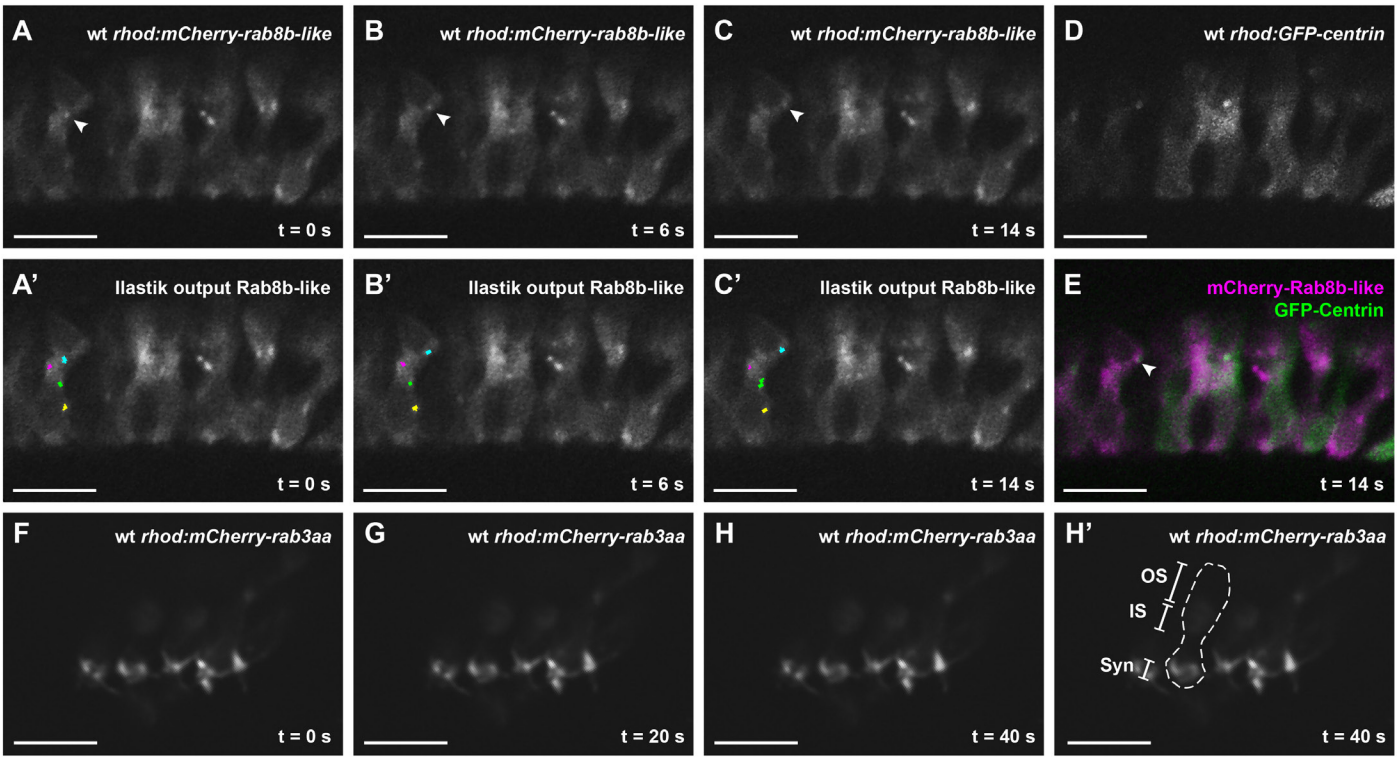

Figure 5. Rab8-particles display dynamic movement patterns and transiently approach the BB
(A-C) Time-lapse imaging of a 5 dpf wt zebrafish retina expressing Rab8like in rods *(tg(rhod:mCherry-rab8like))*. The Rab8like punctum marked with an arrowhead in all time frames can be recognized and followed by the Ilastik tracking software (cyan overlay) (A'-C'). This punctum transiently approaches the GFP-tagged basal body (D and merge in E). The movement is specific for Rab8 as transiently expressed Rab3aa in rods *(rhod:mCherry-rab3aa)* (F-H') exhibits the expected endogenous synaptic localization (H'). Scale bars are 10 µm in all images. OS outer segment, IS inner segment, Syn Synapse.

and rods over 10 minutes (videos acquired at a rate of 1 frame per second) (Videos #3 to #6). Important kinetic parameters analyzed for each particle included displacement (distance between initial and final coordinates), directionality (ratio displacement in the lateral axis/displacement in the apico-basal axis) and maximum speed. We observed no significant difference between the Rab8a and Rab8b-like paralogs or between rods and cones: average displacement was 890±28 nm (Fig. 6 A); maximum speed was 1016±98 nm/s (Fig. 6 B) and directionality was 0.60±0.08, i.e. mostly apico-basal (Fig. 6 C). The only significantly differing variables included particle size of Rab8a particles in rods (7.86±1.41 pixels) which was larger than in cones (10.08±2.19 pixels) ($p=0.0121$, Student's t-test) (Fig. 6 D). While statistical significance was achieved for this parameter, it is questionable whether these differences are biologically relevant. In particular, the different strengths of the promoters used to express Rab8a in these two PR types may at least partially explain these differences, as the weaker transducin promoter used in cones leads to a lower signal-to-noise ratio, making segmentation more difficult. This hypothesis is further supported by the higher number or Rab8a particles in rods than in cones (Fig. 6 E; minimum of 8.76±3.66 particles in rods vs 3.84±1.09 in cones; $p=0.001$ Student's t-test). Altogether, our data suggest that Rab8a and Rab8b-like have a similar behavior in PRs, which could indicate possible functional redundancy, and that Rab8a-controlled trafficking occurs similarly in rods and cones.

Rab8-mediated trafficking is not directly affected by loss of Cc2d2a function

To determine whether the observed vesicle accumulation in *cc2d2a-/-* photoreceptors (PRs) is secondary to a defect in Rab8-mediated trafficking, we compared Rab8a and Rab8b-like kinetics in wt and *cc2d2a-/-* rods, focusing on those mutant PRs that did express puncta. Using the same video

duration and acquisition rate paradigm described above, we observed no major differences in movement kinetics in mutant PRs compared to wt including particle size, trajectory, displacement and speed. The only variable differing significantly in mutant PRs was the directionality of Rab8b-like puncta (Fig. 6 C) (0.52±0.12 in wt, 0.73±0.19 in *cc2d2a-/-; p=0.0025*, Student's t-test, n=13 PRs per condition). Directionality was measured as the ratio between the maximum distance spanned in each of the axes (lateral/apico-basal) and while predominantly apico-basal in wt PRs, it is shifted towards a more lateral movement in *cc2d2a-/-* rods *(p=0.005, Student's t-test)*. Given that cell-shape is grossly maintained in *cc2d2a-/-* PRs, this difference could be explained by enhanced difficulty to move through accumulated vesicles.

Given the model whereby Rab8 coats opsin-carrier vesicles delivering op-

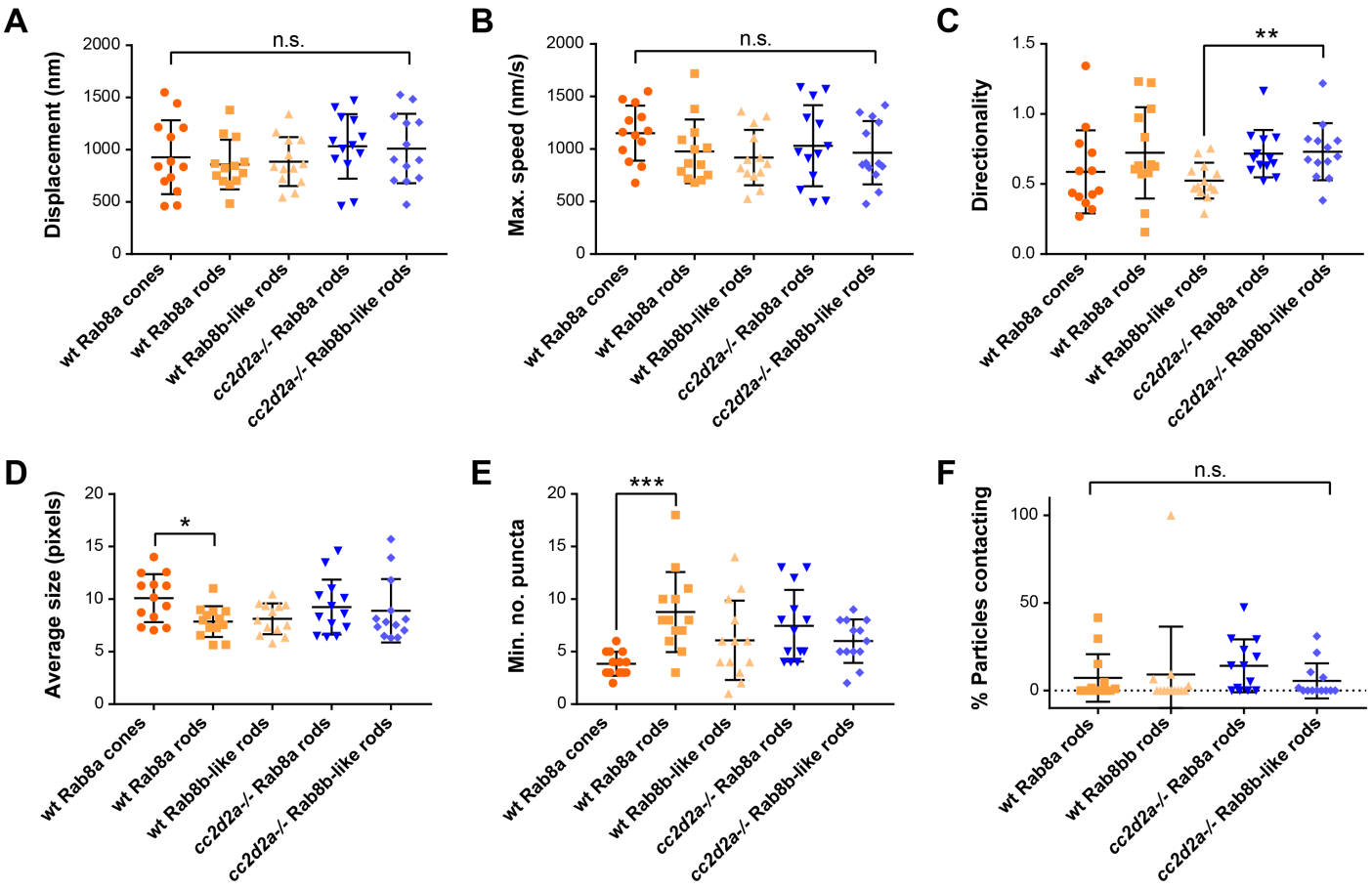

Figure 6. Rab8-trafficking kinetics are conserved between different paralogs in wt rods and cones and in *cc2d2a-/-* photoreceptors

(A-F) Quantification for various parameters generated by tracking of tagged Rab8 particles on 10-minute long videos recorded at 1 frame/second. 13 photoreceptors (PRs) per group (5 different conditions) were analyzed: PRs expressing mCherry-Rab8a in wt cones (orange circles), wt rods (orange squares) and *cc2d2a-/-* rods (blue inverted triangles) as well as PRs expressing mCherry-tagged Rab8-like in wt rods (orange triangles) and *cc2d2a-/-* rods (blue diamonds). Each dot in the scatter plots represents the average value of all the particles present in 1 PR. Only particles present in ≥10 frames were analyzed. (A) Puncta displacement measured as the distance between the first set of coordinates and the last set of coordinates. Average displacement was close to 1 µm for all conditions. (B) Maximum speed of puncta was about 1 µm/s in all conditions. (C) Puncta directionality measured as the ratio of distance spanned in the lateral axis over the distance spanned in the apico-basal axis indicates a predominantly apico-basal movement in all conditions. (D) Puncta size. (E) Minimum number of puncta per PR present in any one frame: on average, 4-8 puncta per PR were present at a given time. (F) Proportion of puncta contacting the BB. * $p < 0.05$, ** $p < 0.01$, *** $p < 0.001$, n.s. not significant. Note consistent results between Rab8a-puncta in cones and rods, between Rab8a and Rab8-like puncta in rods and between wt and *cc2d2a-/-* rods for both paralogues for the majority of parameters.

sins to the base of the ciliary compartment, supported by our findings so far, we next quantified the relative number of particles reaching the periciliary membrane region and approaching the basal body (BB) (Fig. 6 F). We did not observe a significant difference between wt and *cc2d2a-/-* PRs for either of the Rab8 paralogs with respect to BB-contacting over the 10 minute duration of the movies. The absolute number of Rab8 particles coming in proximity with the BB varied widely between different PRs in both wt and mutants, ranging from 0 to 10 in wt and 0 to 28 in mutants. We conclude that loss of Cc2d2a function does not directly affect Rab8-trafficking.

Loss of Cc2d2a function results in mislocalization of the t-SNARE SNAP25 at the periciliary membrane

Because the massive accumulation of vesicles in *cc2d2a-/-* PRs occurs only apically and Rab8-trafficking seems unaffected, we hypothesized that the trafficking defect observed in these mutants must happen at late steps of the trafficking process, namely vesicle fusion. Therefore, we focused on the fusion machinery components at the ciliary base. It was previously shown

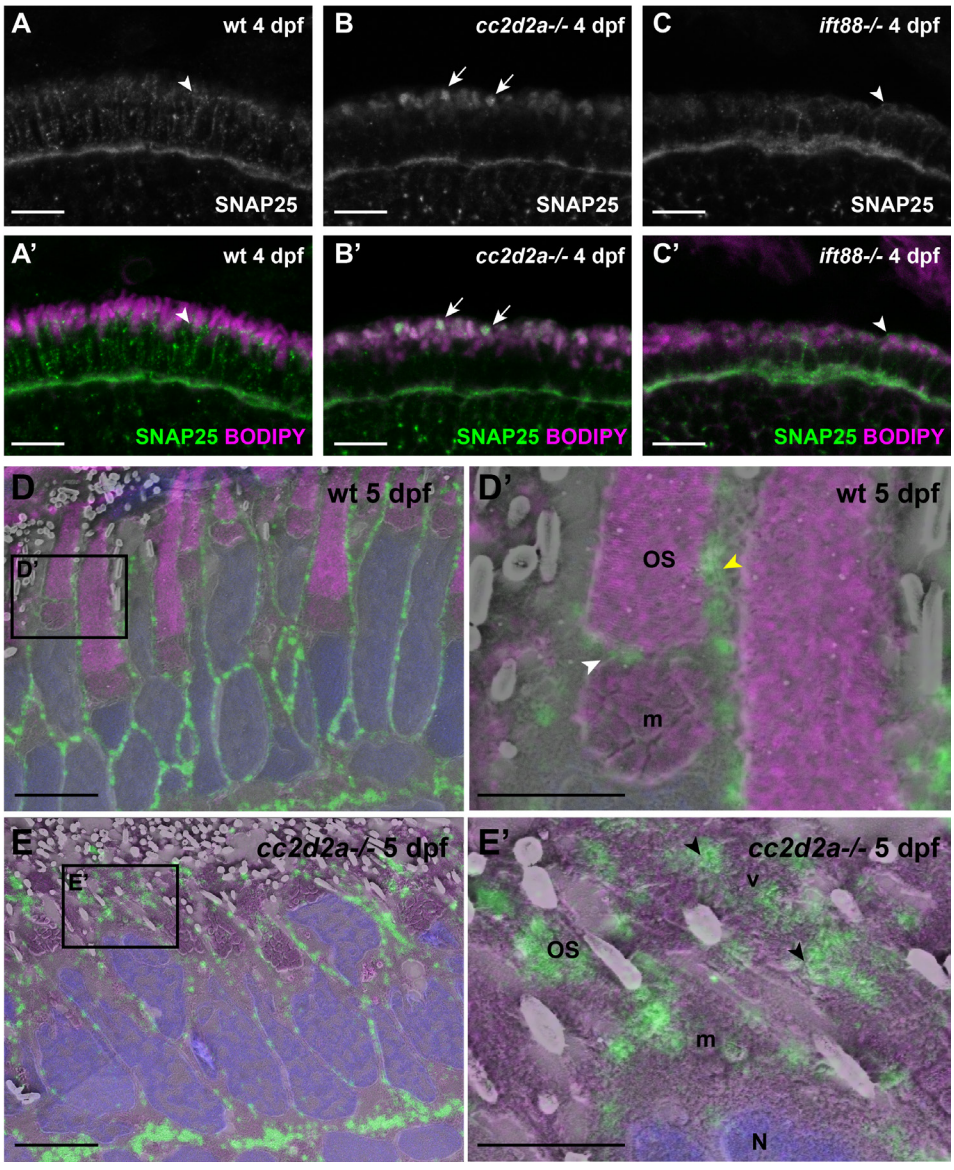

Figure 7. SNAP25 mislocalizes in OSs and accumulated vesicles of *cc2d2a-/-* PRs

(A-C') 4 dpf cryosections of wildtype (wt) (A-A'), *cc2d2a-/-* (B-B') and *ift88-/-* (C-C') retinae stained for SNAP25 (grayscale in A-C and green in A'-C') and counterstained with BODIPY (magenta). Note that in wt (A-A') SNAP25 localizes between the mitochondrial cluster and the outer segment (OS) (arrowhead), along the plasma membrane and at the synapse. In *cc2d2a-/-* (B and B'), SNAP25 synaptic localization is preserved but apical mislocalization to a membrane-rich compartment (BODIPY, arrows) is obvious. (C and C') Despite absence of OSs in the *ift88-/-* ciliary mutant, SNAP25 localizes correctly at the apical membrane of PRs. (D-E') 5 dpf Correlative Light and Electron Microscopy (CLEM) retinal sections stained for SNAP25 (green), counterstained with BODIPY (magenta) and DAPI (blue). (D' and E') are higher magnification images of the boxed areas in (D and E). In wt PRs, SNAP25 signal is found at the IS apical membrane (white arrowhead) and along the calycal processes (yellow arrowhead) (D and D'). In contrast, in *cc2d2a-/-* PRs (E and E'), SNAP25 prominently mislocalizes in dysmorphic OSs and in accumulated vesicles (black arrowheads, v). Scale bars are 10 µm in A-C', 5 µm in D and E; and 2 µm in D' and E'. OS outer segment, m mitochondria, N nuclei, v vesicles.

that the t-SNAREs required for the delivery of OCVs in frog (Mazelova et al., 2009) and mammalian (Greenlee et al., 2001) retina are SNAP25 and Syntaxin3. We therefore performed immunostaining to determine the localization of these proteins at 4 dpf and 6 dpf. We found SNAP25 localization along the plasma membrane, including the periciliary membrane (white arrowheads Fig. 7 A-A' and D'), the inner segment (IS) membrane, the calycal process membrane (yellow arrowhead Fig. 7 D') and at the synapse (Fig. 7 A-A', D) in wt animals, consistent with previous reports. In *cc2d2a-/-* PRs, however, SNAP25 was mislocalized apically in a membranous compartment (Fig. 7 B-B') that we identified as dysmorphic OSs and accumulated vesicles by CLEM (black arrowheads in Fig. 7 E'). On the other hand, the synaptic localization of SNAP25 was unaffected in *cc2d2a-/-* PR, suggesting again a ciliary-specific effect. This effect was primary and specific to loss of Cc2d2a, as it was observed at early stages (4 dpf) in *cc2d2a-/-* retina and was not present in PRs of the ciliary mutant *oval/ift88,* defective for intraflagellar transport (IFT) and unable to form OSs (Fig. 7 C-C'). Taken together, our data suggest that Cc2d2a is required for the correct localization of SNAP25 at the periciliary membrane.

Decreased levels of the t-SNARE Syntaxin3 and of the Exocyst in cc2d2a-/- retina

We next turned to the second known t-SNARE involved in fusion of OCVs in PRs, Syntaxin3. We found Syntaxin3 localization to mirror SNAP25 localization in wild-type PRs at the plasma membrane, including the periciliary membrane and the calycal processes and at the synapse both at 4 dpf and 6 dpf (Fig. 8 A-A', C-C'). In 4 dpf *cc2d2a-/-* PRs we observed minor mislocalization of Syntaxin3 (Fig. 8 B-B', arrowhead), which was much less prominent than for SNAP25 and decreased further at 6 dpf (Fig. 8 D-D'). However, at both time points we consistently observed a strong decrease in fluorescence intensity. We confirmed that Syntaxin3 protein levels were depleted by 20% by western blot *($p=0.019$,* Student's t-test after normalization to wt levels) on whole 6 dpf larval eyes (Fig. 8 E and Fig. S6) and qRT-PCR revealed that the Syntaxin3 mRNA levels were similarly decreased by 20% *($p=0.0061$,* Student's t-test after normalization to wt levels) at this time point. In contrast, transcript levels for other fusion or tethering machinery components were unaffected, including SNAP25 (Fig. 8 F). We next focused our analysis on components of the Exocyst, which is a tethering complex involved in most exocytosis processes, downstream of Rab-mediated targeting and upstream of SNARE-mediated fusion. Specifically, we measured levels of the Sec8 homolog Exoc4, which is a predicted interactor of Rab8, as a surrogate for the whole Exocyst complex and found these to be decreased by 45% by western blot at 6 dpf (Fig. 8 E and Fig. S6) *($p=0.033$,* Student's t-test after normalization to wt levels), while *Exoc4* transcript levels were unaffected (Fig. 8 F). Thus, Exoc4 is degraded and Syntaxin3 is downregulated in *cc2d2a-/-* eyes. Collectively, our data

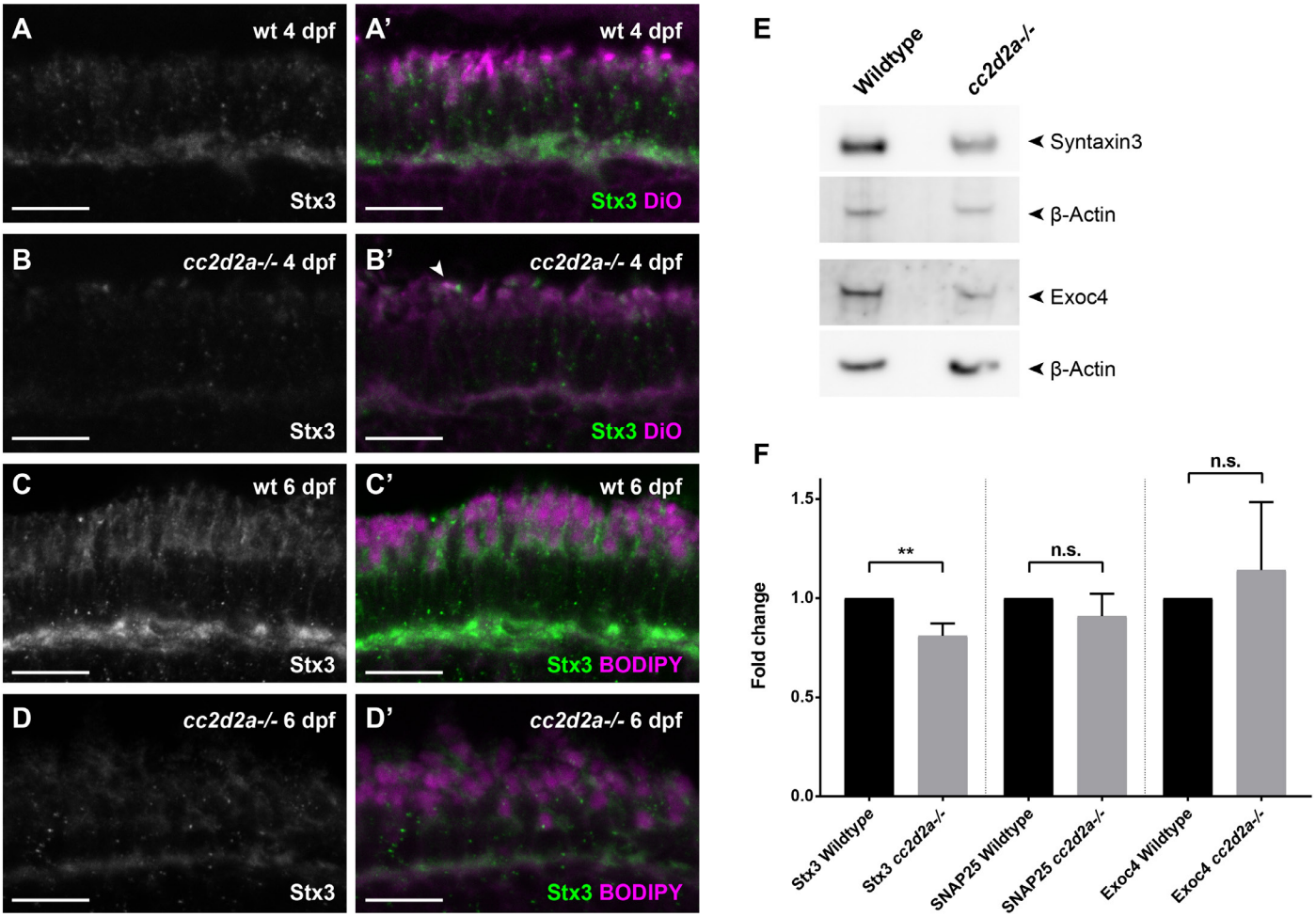

Figure 8. Proteins involved in OCV fusion are affected by loss of Cc-2d2a function

4 dpf cryosections of wildtype (wt) (A-A') and *cc2d2a-/-* retinae (B-B') and 6 dpf cryosections of wildtype (C-C') and *cc2d2a-/-* retinae (D-D'), all stained for Syntaxin3 (Stx3) (grayscale in A-D and green in A'-D') and counterstained with DiO (A',B') or BODIPY (C',D') (both magenta) to label membranes. Note that in wt PRs at both timepoints, Stx3 localizes between the mitochondrial cluster and the OS, along the plasma membrane and at the synapse (A', C'), similar to SNAP25. While minimal Stx3 mislocalization to a membraneous compartment is visible in *cc2d2a-/-* (arrowhead B'), the most striking difference in the mutant is the decreased fluorescent intensity (B', D'). (E) Western blot on whole eye lysates at 6 dpf confirms depletion of Stx3 by approx. 20% in *cc2d2a-/-*. In addition, protein levels of the Exocyst component Exoc4 are decreased by approx. 45%. (F) qRT-PCR shows a significant decrease in the transcript levels of Stx3 in *cc2d2a-/-* whole eyes, mirroring the 20% depletion found by western blot. SNAP25 and Exoc4 transcripts are not significantly affected in *cc2d2a-/-*. ** $p < 0.01$.

suggest that loss of Cc2d2a leads to mislocalization and/or downregulation of various components required for fusion of OCVs at the periciliary membrane.

Discussion

Primary cilia are devoted to the transduction of a plethora of signals crucial for embryonic development, adult tissue homeostasis and interpretation of environmental stimuli, such as light (Baker and Beales, 2009). Therefore, regulation of ciliary protein content, in particular of the transmembrane signal receptors and channels, is indispensable for primary cilium function (Singla and Reiter, 2006). While the ciliary transition zone (TZ) is thought to act as a gatekeeper in this process (Szymanska and Johnson, 2012), its link to upstream protein sorting mechanisms provided by polarized vesicular trafficking has not been elucidated so far. Our study using CC2D2A as a representative TZ protein and relying on novel imaging technology with CLEM and live imaging of Rab8-trafficking in photoreceptors in a whole tissue context, identifies a role for CC2D2A in the last steps of trafficking, namely vesicle fusion. Furthermore, our work provides novel evidence in support of a role for Rab8a in opsin-carrier vesicle (OCVs) trafficking in photoreceptors and suggests that this trafficking is only indirectly affected by dysfunction of the TZ, which is in agreement with the fact that Rab8

and motor protein recruitment to opsin-carrier vesicles occurs in the cytoplasm, upstream of the TZ (Wang and Deretic, 2015).

The vesicle fusion defects observed in *cc2d2a-/-* PRs are secondary to mislocalization (SNAP25), downregulation (Syntaxin3) and degradation (Exoc4) of the vesicle fusion machinery at the periciliary region. These vesicle fusion defects are ciliary-specific, despite the broader localization of the analyzed SNAREs along the PR cell membrane, since delivery of non-ciliary proteins to other highly organized membrane compartments such as the synapse remains unaffected. Furthermore, SNAP25 mislocalization as seen in *cc2d2a-/-* PRs is not observed in the non-TZ ciliary mutant *ift88-/-*, which also lacks vesicle accumulation ((Sukumaran and Perkins, 2009) and data not shown), strongly suggesting that the fusion machinery defects are specific to loss of Cc2d2a/TZ function.

We have previously shown CC2D2A to interact with NINL (Bachmann-Gagescu et al., 2015b), a centrosomal protein that also interacts with dynein-dynactin motor proteins and MICAL3, a proposed Rab8 effector (Grigoriev et al., 2011). Both Rab8 and MICAL3 have catalytic properties that can modify cortical actin cytoskeleton (Peranen et al., 1996; Grigoriev et al., 2011; Giridharan and Caplan, 2014), thus facilitating vesicle docking (Williams, 2004). In addition, Rab8 recruits the Exocyst to initiate vesicle fusion (Essid et al., 2012; Heider and Munson, 2012). Taken together with the data presented in this work, we propose a model whereby Cc2d2a at

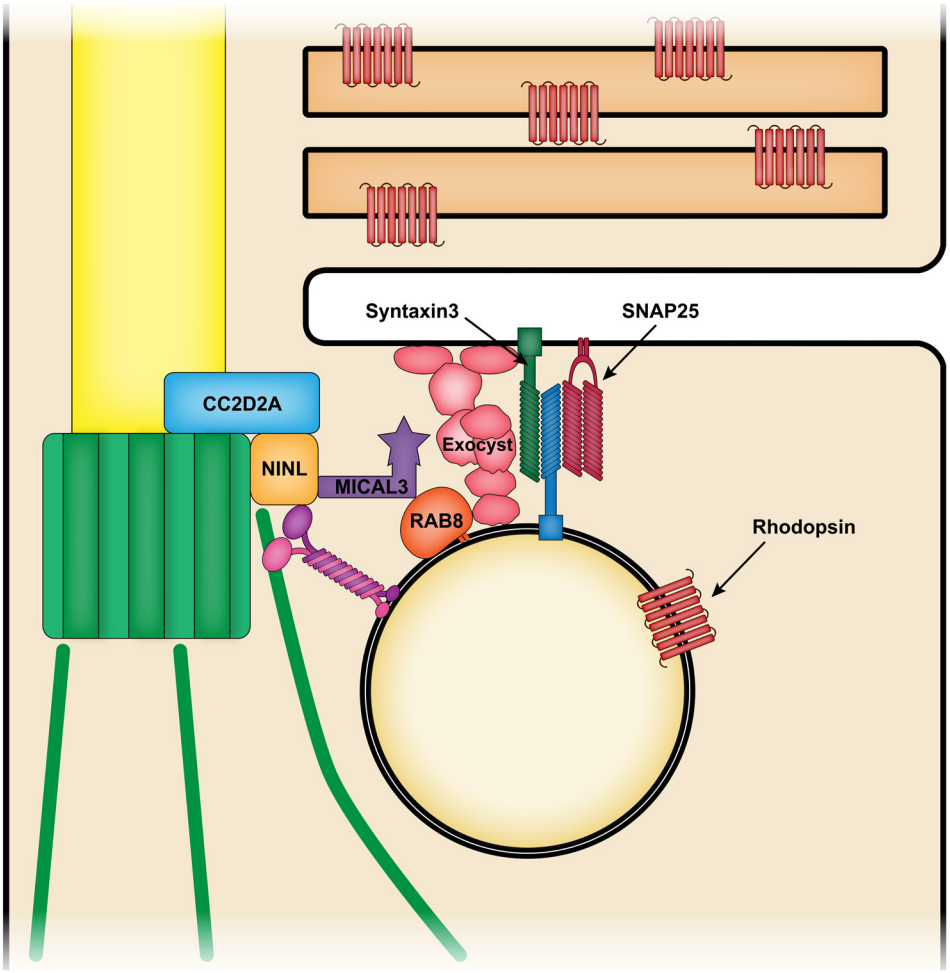

Figure 9. Model
Rab8 coats opsin-carrier-vesicles and targets them to the periciliary membrane, where their fusion is mediated by the Exocyst and by SNAREs including SNAP25 and Syntaxin 3 (and by an as yet undefined v-SNARE). CC2D2A at the transition zone is required for correct localization of SNAP25 to the periciliary membrane and provides a docking point for incoming vesicles through its interaction with NINL, which also binds the dynein motor and the Rab8 effector MICAL3. Thus, CC2D2A plays a role in concentrating all components required for correct vesicle fusion at the periciliary membrane.

the TZ may provide a docking point for incoming OCVs through its interaction with NINL and control the localization of the t-SNAREs required for fusion, thereby bringing all components required for vesicle fusion in proximity with each other at the periciliary region (Fig. 9).

The mechanisms underlying SNAP25 mislocalization, and Syntaxin3 downregulation/Exoc4 degradation, remain to be elucidated. Previous work has shown that SNAREs can be downregulated if their interactors are missing or not appropriately localized (Toonen and Verhage, 2003). Given the observed mislocalization of SNAP25, the cell might try to prevent aberrant fusion of OCVs to the wrong membranes by downregulating Syntaxin3, depleting the Exocyst and reducing the amount of Rab8 engaged on OCVs. SNARE mislocalization was described in the ciliopathy *bbs17-/-* mouse model, where Syntaxin3 and Stx1bp are mislocalized in the OSs of mutant PRs (Datta et al., 2015). The authors propose that Bbs17 is required for retrograde transport of proteins out of the ciliary compartment. In our experiments, accumulation of SNAP25-positive vesicles occurred in *cc2d2a-/-* PRs even before and in the absence of formation of OSs, speaking against a role for Cc2d2a in active retrograde transport.

SNAP25 does not possess a transmembrane domain but is inserted in the target membrane through palmitoylation; thus, its localization might be influenced by the lipid composition of the periciliary membrane (Loranger and Linder, 2002). Other proteins regulating intracellular trafficking such as FIP3 or Exocyst subunits contain phosphatidylinositol (PIP)-binding domains that can be highly specific for certain phospholipids (Novick and Guo, 2002; Williams, 2004) and SNAREs are arranged around cholesterol and PIP2-rich membrane microdomains (Lang et al., 2001; Davletov et al., 2007; Balla et al., 2012). OCV delivery was shown to depend on PIP2 recognition by FIP3 and to be enhanced by providing docosahexaenoic acid to the PRs (Mazelova et al., 2009; Wang and Deretic, 2015). Moreover, MICAL3 recognizes membrane-associated proteins bound to specific PIPs as the vesicle "landing site" (Lansbergen et al., 2006; Grigoriev et al., 2011). Finally, the JBTS protein INPP5E, whose ciliary localization depends on the TZ (Garcia-Gonzalo et al., 2015; Slaats et al., 2016), plays a crucial role in regulating ciliary PIP content. Loss of Cc2d2a at the TZ could therefore impact the balance of phosphoinositides not only in the ciliary, but also in the periciliary membrane, which could in turn lead to mislocalization of SNAP25, a hypothesis that requires further investigations.

A large body of work has characterized OCV trafficking and opsin delivery to the OSs. The generally accepted model for OCV sorting stipulates that Rhodopsin is recognized at the trans-Golgi network by Arf4 which recruits ASAP1, allowing the OCVs to bud off from the Golgi apparatus. While being transported along the microtubule network to the periciliary membrane using a dynein motor, Rab11 substitutes Arf4 and recruits its effector FIP3, which in turn recruits Rabin8, which binds and activates Rab8, priming the OCV for its fusion (Wang and Deretic, 2015). However, a recent publication has questioned this model, suggesting that Rab8a and

Rab8b paralogs are dispensable for Rhodopsin transport, based on lack of a retinal phenotype in double knockout mice with additional expression of dominant negative forms of the Rab8 activator protein Rab11 and the closest Rab8 relative Rab10 (Ying et al., 2016). Our study relying on live imaging of tagged Rab8 in photoreceptors supports a role for Rab8 paralogs in rhodopsin transport, based on co-localization of tagged Rabs with opsins on vesicular structures and on the movement pattern of Rab8 particles with apico-basal directionality towards the BB (as expected with movement along microtubules) at a speed consistent with dynein-driven transport (Howard, 2001). Moreover, our work investigated for the first time both rod and cone PRs with respect to Rab8-trafficking, and found no biologically relevant difference, indicating that OCV trafficking occurs similarly in both PR types. Our findings also support redundancy between Rab8 paralogs, which might extend to other Rabs as well. While one of the Rab8 paralogs might dominate in the physiologic situation, the other Rab8 paralogs, and potentially additional Rabs such as the closest Rab8-relatives Rab10 and Rab13, may be able to take over in case of loss-of-function of one Rab8 paralog. While Rabs are thought to provide membrane specificity, given the high amount of genes (close to 70 in humans) and their high degree of sequence conservation, redundancy may be operating in case of disruptions. In this framework, where many of the components could be redundant in trafficking, the function of the TZ would be bringing all the components together to engage fusion.

Association of mutations in Exocyst components with ciliopathies, in particular JBTS (Dixon-Salazar et al., 2012; Martin-Urdiroz et al., 2016), suggest that the mechanisms uncovered in this work to explain the ciliary dysfunction in *cc2d2a-/-* PRs, might represent a more general mechanism underlying JBTS. Since about half of JBTS proteins are TZ proteins, abnormal ciliary protein composition through a similar trafficking/fusion defect could represent a common pathogenic mechanism underlying JBTS. Initial studies of JBTS genes often suggested ciliogenesis defects for TZ proteins based on cell culture experiments. Likewise, for *Cc2d2a*, one mouse model showed a BB docking defect leading to complete absence of cilia (Veleri et al., 2014). On the other hand, another *Cc2d2a* mouse knock-out had deficient ciliogenesis in only a subset of cell types, while others formed normal cilia, albeit with abnormal protein content (Garcia-Gonzalo et al., 2011). Given that vertebrate animal models display very early embryonic lethality in complete absence of cilia, it is unlikely that major ciliogenesis defects could lead to the relatively milder phenotypes of JBTS in humans. In accordance with this, our zebrafish *cc2d2a* model does not display BB docking or ciliogenesis defects, despite being a null mutant (Bachmann-Gagescu et al., 2011).

Taken together, our findings suggest that dysfunction of the TZ leads to disorganization of the vesicle fusion machinery, causing accumulation of ciliary-bound vesicles, secondary trafficking defects and aberrant protein content of the ciliary membrane. This is consistent with the ascribed

gate-keeper function of the TZ, but suggests a more complex and active role, influencing both sides of the barrier. Further work will be required to elucidate the precise mechanisms through which individual TZ proteins affect the periciliary membrane, in our quest to uncovering the pathogenesis underlying JBTS.

Acknowledgements

The authors thank Pablo Sánchez Bosch, Lorenzo Gatti and the Centre for Microscopy and Image Analysis, University of Zurich (ZMB), in particular Moritz Kirschmann, for their help with image and data analysis and the entire Ilastik team for their support with the tracking software. We also thank Kara Dannenhauer and Martin Walther for expert fish care and members of the Neuhauss lab for constructive discussions. Many thanks for reagents go to research groups mentioned in the text (Robert Molday for the 4D2 antibody, Michael Taylor for the Cacna1fa antibody, Brian Link for the 5'E Rhod promoter, the 3'E Rab8b-like and the 3'E hCentrin clones, Philip Beales for the 3'E Rab8a clone, Brian Perkins for the *ift88*^{tz288} mutant line, Jarema Malicki for the *hsp70:rhod-GFP* construct and Susan Brockerhoff for the TaCP promoter 5'E clone).

Methods

Zebrafish maintenance and breeding

Zebrafish *(Danio rerio)* were maintained as described (Mullins et al., 1994). Embryos were obtained through natural matings, raised at 28°C in embryo medium and staged according to development in days post fertilization (dpf) (Kimmel et al., 1995). 0.003% PTU (1-phenyl-2-thiourea) in embryo medium was used to inhibit melanin synthesis during larval development and facilitate fluorescent microscopy. All animal protocols were in compliance with internationally recognized guidelines for the use of fish in biomedical research and all experiments were approved by the local authorities (Veterinäramt Zürich TV4206).

Zebrafish lines

The *cc2d2a*^{uw38}, the *ift88*^{tz288} and the *casper* mutants were previously described (Owens et al., 2008; White et al., 2008; Sukumaran and Perkins, 2009; Bachmann-Gagescu et al., 2011). Stable zebrafish transgenic lines used in this study included *Tg(rhod:mCherry-rab8a)*, *Tg(rhod:mCherry-rab8b-like)* (Bachmann-Gagescu et al., 2011), *Tg(tacp:mCherry-rab8a)*, *Tg(rhod:hCentrin-GFP)*, *Tg(tacp:hCentrin-GFP*); the latter three lines were generated in this

study (see next paragraph). Constructs injected transiently included *rhod:m-Cherry-rab3aa* (generated in this study) and *hsp70:rhod-GFP* (a gift from J. Malicki (Zhao and Malicki, 2011)).

Construct and transgenic line generation

RT-PCR was performed using cDNA obtained from whole larvae at 5 dpf to generate a Gateway® (Invitrogen) p3' entry clone including the full length coding sequence for Rab3aa (NM_001003419.1). The following primers were used (attB site sequences are written in lowercase):
Rab3aa attB2r:
5'-ggggacagctttcttgtacaaagtggcgATGGCTTCAGCGAATGATGC-3'
Rab3aa attB3:
5'- ggggacaactttgtataataaagttgtTTAGCAAGCGCAGTCCTTGT-3'
Gateway® (Invitrogen) recombination was performed using the Tol2 system (Kwan et al., 2007). p5' entry clones included the rod-specific rhodopsin promoter (gift from the Link lab) or the cone-specific alpha-transducin promoter (tacp, (Lewis et al., 2010)). mCherry or GFP middle-entry clones and p3' entry clones containing the human Centrin sequence (gift from the Link lab), the Rab3aa and the Rab8a zebrafish sequence (NM_001089562; gift from Beales lab) were used to generate N-terminal fusions of Rab proteins or Centrin. The resulting constructs were co-injected with Tol2 transposase mRNA as previously described (Kawakami, 2007) into 1-cell stage embryos. Injected fish were either imaged (transients) or raised and further outcrossed to *casper* zebrafish for at least two generations.

Annotation of Rab cDNAs

As gene predictions within GenBank are produced by automated processes which have been shown to contain numerous errors, Rab cDNA sequences used in this study were manually annotated. Sequences were identified and annotated using combined information from expressed sequence tags and genome databases (GeneBank, http://www.ncbi.nlm.nih.gov; Ensembl, http://www.ensembl.org/index.html). Human and mouse sequences were used as initial query (for more details on sequence annotation see Gesemann et al. 2010).

Phylogenetic Analysis

The phylogenetic analysis was performed on the Phylogeny.fr platform (http://www.phylogeny.fr/) comprising the following steps (Dereeper et al. 2008). Sequences were aligned using MUSCLE (v3.7) (Edgar, 2004) configured for highest accuracy (MUSCLE with default settings). Sequences length varied between 700 and 214 amino acids. After alignment, ambiguous regions (i.e. containing gaps and/or poorly aligned) were removed using Gblocks (v0.91b) (Castresana, 2000). The following parameters were

implemented: The minimum length of a block after gap cleaning was set to 5; positions with a gap in less than 50% of the sequences were selected in the final alignment if they were within an appropriate block; all segments with contiguous non-conserved positions bigger than 8 were rejected; minimum number of sequences for a flank position were 55%. After curation 203 amino acids were chosen for further analysis. The phylogenetic tree was reconstructed using the maximum likelihood method implemented in the PhyML program (v3.0 aLRT) (Guindon and Gascuel, 2003). The default substitution model was selected assuming an estimated proportion of invariant sites (of 0.000) and 4 gamma-distributed rate categories to account for rate heterogeneity across sites. The gamma shape parameter was estimated directly from the data (gamma=0.728). Reliability for internal branch was assessed using the aLRT test (Anisimova and Gascuel, 2006). Graphical representation and edition of the phylogenetic tree were performed with TreeDyn (v198.3) and the .svg file imported into CorelDraw (version x5; Corel Corporation Ottawa, Canada) for final editing.

Transmission electron microscopy (TEM)

Zebrafish larvae were fixed overnight at 4°C in a freshly prepared mixture of 2.5% glutaraldehyde and 2% paraformaldehyde in 0.1 M sodium cacodylate buffer (pH 7.4). After rinsing in buffer, specimens were washed in 1% osmiumtetroxide and 1% potassiumferrocyanide in 0.1 M sodiumcacodylate buffer (pH 7.4), during 2 h at room temperature. After rinsing, tissues were dehydrated through a graded series of ethanol and embedded in epon. Ultrathin sections (70 nm) comprising zebrafish eyes were collected on formvar coated grids, subsequently stained with 2% uranyl acetate and Reynold's lead citrate, and examined with a Philips CM-100 scope.

Correlative light and electron microscopy (CLEM)

A detailed protocol will be available at JoVE (manuscript in press). Briefly, 5 dpf old larvae were euthanised in Tricaine (ethyl 3-aminobenzoate methanesulfonate, Sigma-Aldrich) and their sectioned heads fixed in 4% formaldehyde/0.025% glutaraldehyde in cacodylate buffer overnight at 4°C. Eyes were dissected out in fixative, washed in PBS, embedded in 12% gelatin in 0.1 M PBS at 40°C, cooled down and immersed and stored in 2.3 M sucrose at 4°C. Prepared samples were frozen in liquid nitrogen and sectioned with a cryo-ultramicrotome (Ultracut EM FC6, Leica Microsystems). 100 nm ultrathin sections were transferred to a 7 x 7 mm silicon wafer (Si-Mat Silicon Materials) and stored at 4°C.
Sections were stained with mouse anti-rhodopsin (4D2, gift from R. Molday, University of British Columbia) 1:100, rabbit anti-SNAP25 1:250 (StressGen Biotechnologies), chicken anti-mCherry 1:50 (Abcam) and counterstained when necessary with BODIPY®TR methyl ester (Invitrogen) 1:100 and DAPI (4′,6-diamidino-2-phenylindole dihydrochloride)

1:100. Alexa Fluor 488-conjugated secondary antibodies (Life Technologies) were used at 1:200. After confocal microscopy, samples were postfixed with 0.1% glutaraldehyde in PBS, covered with a thin layer of methylcellulose and coated with 10 nm Platinum/Carbon by rotary shadowing at an angle of 8 degrees. SEM images were taken using a Zeiss Supra 50 VP and a Zeiss Auriga 40 SEM. Alignment of light and electron microscopy images was done with the open-source platform Fiji, based on manually inserted landmarks from the nuclear DAPI signal and using the TrakEM2 plugin. At least 3 animals per condition were used for CLEM.

Live imaging

Transiently injected *Tg(rhod:mCherry-rab3aa)* and stable *Tg(rhod:mCherry-rab8a ; rhod:GFP-hCentrin), Tg(rhod:mCherry-rab8b-like ; rhod:GFP-hCentrin)* and *Tg(tacp:mCherry-rab8a)* 5 dpf zebrafish larvae were anesthetized in Tricaine, embedded in 1.8% low melting agarose (Lonza), mounted on glass-bottom Petri dishes and covered with Tricaine-supplemented embryo medium. Time-lapse videos were obtained in a single focal plane using a 60x objective in a Nikon Eclipse Ti spinning disk microscope. The acquisition lasted for 10 min at a rate of 1 frame per second including both channels (488 nm and 561 nm). 13 photoreceptors from 4-7 animals per condition were imaged.

Tracking and video analysis

Time-lapse live imaging videos were registered using the MultiStackReg plugin in Fiji. To avoid sampling error carryover, only three to four photoreceptors (PRs) were selected per animal for analysis. The analyzed PRs were randomly picked (random.org) from the pool of eligible PRs in the videos. The chosen PRs were first isolated using Fiji followed by signal segmentation and automated tracking using the respective pipelines in the open-source software Ilastik (versions 1.1.5, 1.1.7 and 1.2.0 (Sommer et al., 2011)). Segmentation cues were provided every 5 to 10 frames. Segmented videos were processed for tracking using sigma values of 0.1 for Gaussian blurring and a threshold between 0.29 and 0.31. Potential objects were only considered when they had a minimum size of 2 pixels. Optimized tracking parameters were: max. number of objects per merger = 1, division weight = 10, transition weight = 3, appearance cost = 9, disappearance cost = 47. Objects were not considered divisible. The minimum number of particles per PR was determined by counting the highest number of particles visible in any one frame.

The selected software outputs were the particle pixel count per frame (used to determine the average size of particles) and the raw coordinates of the particle barycenter in each frame (used to calculate the distance, maximum speed, displacement (measured as the distance between the first and the last set of coordinates of a particle), and trajectory (measured as the

summation of all the distances travelled by a particle)). Directionality was expressed as the quotient of the maximum distance spanned in the lateral X axis over the maximum distance spanned in the apico-basal Y axis (after correcting the coordinates in the reference Cartesian system using Euler angle rotations: $x_{new} = x_{original} \cdot cos\theta + y_{original} \cdot sin\theta$; and $y_{new} = y_{original} \cdot cos\theta - x_{original} \cdot sin\theta$). Thus, results <1 represent apico-basally directed movement. A particle approaching the BB was considered to reach the periciliary membrane (determined as a "contact") when the barycenter coordinates of the particle were within a 3 pixel radius (630nm) from the barycenter of the BB.

Immunohistochemistry

Zebrafish larvae were fixed in 4% PFA at room temperature (RT) for 30 min, embedded in Neg50 (Richard-Allan Scientific) and cryosectioned following standard protocols. Non-specific binding was blocked using PBDT (PBS, 1% DMSO, 0.5% Triton X-100, 2mg/ml BSA) with 10% goat serum for 30 minutes at RT before incubation with primary antibodies overnight at 4°C. Primary antibodies were rabbit anti-Syntaxin3 (1:400, Alomone labs), rabbit anti-SNAP25 (1:1000, StressGen Biotechnologies), mouse monoclonal anti-Rab8a (1:100, Novus Biologicals), rabbit anti-Cacna1fa (1:5000, a gift from Michael Taylor, UW Wisconsin) (Jia et al., 2014). Secondary antibodies were Alexa Fluor-conjugated goat anti-rabbit or goat anti-mouse IgG (1:400, Life Technologies). BODIPY®TR methyl ester (1:300, Invitrogen) was applied for 20 min and nuclei were counterstained with DAPI. Confocal imaging was performed on a Leica HCS LSI or a Leica SP5 microscope. All IHC experiments were performed at least in duplicate with at least 10 animals per condition.

Western blot

6 dpf zebrafish larvae were anesthetized in Tricaine. Whole larval eyes were dissected and collected in PBS. Samples were lysated using a Sonopuls HD 2070 sonicator in urea buffer (65 mM Tris HCl pH 6.75, 8 M urea, 20% glycerine, 5% SDS, 5% β-mercaptoethanol) in the presence of protease inhibitors (cOmplete EDTA-free Protease Inhibitor Cocktail, Roche) and electrophoresed under reducing conditions on Mini-PROTEAN TGX 4-15% precast polyacrylamide gels (Bio-Rad). Proteins were transferred to a polyvinylidene difluoride (PVDF) membrane (Invitrogen). Nonspecific antibody binding was inhibited by incubation in PBST (PBS, 0.05% Tween-20) supplemented with 3% skimmed milk powder. Membranes were probed using antibodies against Syntaxin3 (rabbit, 1:2000, Alomone labs), rSec8 (mouse, 1:1000, Enzo) and β-actin (mouse, 1:1000, Sigma). HRP-conjugated goat anti-mouse (1:3000, Merck) or anti-rabbit (1:5000, Merck) were used to detect proteins of interest, visualized by chemiluminescence using luminol/peroxide substrate (SuperSignal West Dura Extended Duration Substrate, Life Technologies) and an ImageQuant LAS

4000 imager.

Quantitative reverse transcription polymerase chain reaction (qRT-PCR)

6 dpf zebrafish larvae were anesthetized in Tricaine. Whole larval eyes were dissected and collected in RNAlater (Sigma-Aldrich). RNA was extracted with the NucleoSpin RNA II kit (Macherey-Nagel) and reverse transcription was performed with 150 ng RNA using the Superscript III kit (Life Technologies). qRT-PCR was performed in a transcriptor (Applied Biosystems Prism SDS 7900HT, Life Technologies) using the MESA Green kit (Eurogentec, Seraing, Belgium). Primer pairs were specifically designed to generate short amplicons spanning exon-exon boundaries to avoid unspecific amplification of genomic DNA. Primer sequences are the following (amplicon size stated next to the reverse primer):
Syntaxin3 forward: 5'-CAACGTCAGACCAGAAAAC-3'
Syntaxin3 reverse: 5'-GGCCGATACTCTTTCCAC-3'. 137 bp
SNAP25 forward: 5'-GGATATGCGCAATGAGC-3'
SNAP25 reverse: 5'-CCTGATACCAGCATCTTTAC-3'. 121 bp
Exoc4 forward: 5'-CAGCCGCGTAGTTCAAC-3'
Exoc4 reverse: 5'-ACGCAAGCTGGATGTTC-3'. 148 bp
As reference for normalization, the previously published primers (Tang et al., 2007) for the housekeeping genes *rpl-13a* (ribosomal protein L-13a), *EF1a* (elongation factor 1 alpha), and *beta-actin* were used.

Statistics

All statistical tests were run using GraphPad Prism. Student's t-tests were used for pairwise comparisons between wild-type (wt) and *cc2d2a-/-* to analyze tracking, western blot and qRT-PCR results. Western blot and qRT-PCR results were first normalized to the wt levels. Because parameters relative to periciliary membrane contact do not have a normal distribution, we used a Mann-Whitney U-test instead of a t-test. ANOVA was used to compare kinetic parameters between wt Rab8a cones, wt Rab8a rods and wt Rab8b-like rods.

References

Anisimova, M., and Gascuel, O. (2006). Approximate likelihood-ratio test for branches: A fast, accurate, and powerful alternative. Systematic biology 55, 539-552.

Bachmann-Gagescu, R., Dempsey, J.C., Phelps, I.G., O'Roak, B.J., Knutzen, D.M., Rue, T.C., Ishak, G.E., Isabella, C.R., Gorden, N., and Adkins, J., et al. (2015a). Joubert syndrome: a model for untangling recessive disorders with extreme genetic heterogeneity. Journal of medical genetics *52*, 514-522.

Bachmann-Gagescu, R., Dona, M., Hetterschijt, L., Tonnaer, E., Peters, T., Vrieze, E. de, Mans, D.A., van Beersum, S.E.C., Phelps, I.G., and Arts, H.H., et al. (2015b). The Ciliopathy Protein CC2D2A Associates with NINL and Functions in RAB8-MICAL3-Regulated Vesicle Trafficking. PLoS genetics *11*, e1005575.

Bachmann-Gagescu, R., Phelps, I.G., Stearns, G., Link, B.A., Brockerhoff, S.E., Moens, C.B., and Doherty, D. (2011). The ciliopathy gene cc2d2a controls zebrafish photoreceptor outer segment development through a role in Rab8-dependent vesicle trafficking. Human molecular genetics ***20***, 4041-4055.

Badano, J.L., Mitsuma, N., Beales, P.L., and Katsanis, N. (2006). The ciliopathies: an emerging class of human genetic disorders. Annual review of genomics and human genetics *7*, 125-148.

Baker, K., and Beales, P.L. (2009). Making sense of cilia in disease: the human ciliopathies. American journal of medical genetics. Part C, Seminars in medical genetics ***151C***, 281-295.

Balla, T., Wymann, M., and York, J.D. (2012). Phosphoinositides II: The Diverse Biological Functions (Springer).

Bloodgood, R. (2013). Ciliary and Flagellar Membranes (Springer US).

Castresana, J. (2000). Selection of conserved blocks from multiple alignments for their use in phylogenetic analysis. Molecular biology and evolution 17, 540-552.

Das, A., and Guo, W. (2011). Rabs and the exocyst in ciliogenesis, tubulogenesis and beyond. Trends in cell biology ***21***, 383-386.

Datta, P., Allamargot, C., Hudson, J.S., Andersen, E.K., Bhattarai, S., Drack, A.V., Sheffield, V.C., and Seo, S. (2015). Accumulation of non-outer segment proteins in the outer segment underlies photoreceptor degeneration in Bardet-Biedl syndrome. Proceedings of the National Academy of Sciences of the United States of America ***112***, E4400-9.

Davletov, B., Connell, E., and Darios, F. (2007). Regulation of SNARE fusion machinery by fatty acids. Cellular and molecular life sciences : CMLS ***64***, 1597-1608.

Deretic, D., Huber, L.A., Ransom, N., Mancini, M., Simons, K., and Papermaster, D.S. (1995). rab8 in retinal photoreceptors may participate in rhodopsin transport and in rod outer segment disk morphogenesis. Journal of cell science ***108 (Pt 1)***, 215-224.

Dereeper, A., Guignon, V., Blanc, G., Audic, S., Buffet, S., Chevenet, F., Dufayard, J.-F., Guindon, S., Lefort, V., and Lescot, M., et al. (2008). Phylogeny.fr: robust phylogenetic analysis for the non-specialist. Nucleic acids research 36, W465-9.

Dixon-Salazar, T.J., Silhavy, J.L., Udpa, N., Schroth, J., Bielas, S., Schaffer, A.E., Olvera, J., Bafna, V., Zaki, M.S., and Abdel-Salam, G.H., et al. (2012). Exome sequencing can improve diagnosis and alter patient management. Science translational medicine *4*, 138ra78.

Edgar, R.C. (2004). MUSCLE: multiple sequence alignment with high accuracy and high throughput. Nucleic acids research 32, 1792-1797.

Essid, M., Gopaldass, N., Yoshida, K., Merrifield, C., and Soldati, T. (2012). Rab8a regulates the exocyst-mediated kiss-and-run discharge of the Dictyostelium contractile vacuole. Molecular biology of the cell ***23***, 1267-1282.

Fischer von Mollard, G., Mignery, G.A., Baumert, M., Perin, M.S., Hanson, T.J., Burger, P.M., Jahn, R., and Sudhof, T.C. (1990). rab3 is a small GTP-binding protein exclusively localized to synaptic vesicles. Proceedings of the National Academy of Sciences of the United States of America ***87***, 1988-1992.

Fogelgren, B., Lin, S.-Y., Zuo, X., Jaffe, K.M., Park, K.M., Reichert, R.J., Bell, P.D., Burdine, R.D., and Lipschutz, J.H. (2011). The exocyst protein Sec10 interacts with Polycystin-2 and knockdown causes PKD-phenotypes. PLoS genetics *7*, e1001361.

Garcia-Gonzalo, F.R., Corbit, K.C., Sirerol-Piquer, M.S., Ramaswami, G., Otto, E.A., Noriega, T.R., Seol, A.D., Robinson, J.F., Bennett, C.L., and Josifova, D.J., et al. (2011). A transition zone complex regulates mammalian ciliogenesis and ciliary membrane composition. Nature genetics ***43***, 776-784.

Garcia-Gonzalo, F.R., Phua, S.C., Roberson, E.C., Garcia, G.3., Abedin, M., Schurmans, S., Inoue, T., and Reiter, J.F. (2015). Phosphoinositides Regulate Ciliary Protein Trafficking to Modulate Hedgehog Signaling. Developmental cell ***34***, 400-409.

Gesemann, M., Lesslauer, A., Maurer, C.M., Schönthaler, H.B., and Neuhauss, S.C.F. (2010). Phylogenetic analysis of the vertebrate Excitatory/Neutral Amino Acid Transporter (SLC1/EAAT) family reveals lineage specific subfamilies. BMC Evol Biol 10, 117.

Giridharan, S.S.P., and Caplan, S. (2014). MICAL-family proteins: Complex regulators of the actin cytoskeleton. Antioxidants & redox signaling ***20***, 2059-2073.

Goetz, S.C., and Anderson, K.V. (2010). The primary cilium: a signalling centre during vertebrate development. Nature reviews. Genetics ***11***, 331-344.

Greenlee, M.H., Roosevelt, C.B., and Sakaguchi, D.S. (2001). Differential localization of SNARE complex proteins SNAP-25, syntaxin, and VAMP during development of the mammalian

retina. The Journal of comparative neurology ***430***, 306-320.

Grigoriev, I., Yu, K.L., Martinez-Sanchez, E., Serra-Marques, A., Smal, I., Meijering, E., Demmers, J., Peränen, J., Pasterkamp, R.J., and van der Sluijs, P., et al. (2011). Rab6, Rab8, and MICAL3 Cooperate in Controlling Docking and Fusion of Exocytotic Carriers. Current Biology ***21***, 967-974.

Guindon, S., and Gascuel, O. (2003). A simple, fast, and accurate algorithm to estimate large phylogenies by maximum likelihood. Systematic biology 52, 696-704.

Heider, M.R., and Munson, M. (2012). Exorcising the exocyst complex. Traffic (Copenhagen, Denmark) ***13***, 898-907.

Hildebrandt, F., Benzing, T., and Katsanis, N. (2011). Ciliopathies. The New England journal of medicine ***364***, 1533-1543.

Howard, J. (2001). Mechanics of Motor Proteins and the Cytoskeleton (Sinauer Associates, Publishers).

Hsiao, Y.-C., Tuz, K., and Ferland, R.J. (2012). Trafficking in and to the primary cilium. Cilia ***1***, 4.

Jahn, R., and Scheller, R.H. (2006). SNAREs--engines for membrane fusion. Nature reviews. Molecular cell biology ***7***, 631-643.

Jia, S., Muto, A., Orisme, W., Henson, H.E., Parupalli, C., Ju, B., Baier, H., and Taylor, M.R. (2014). Zebrafish Cacna1fa is required for cone photoreceptor function and synaptic ribbon formation. Human molecular genetics ***23***, 2981-2994.

Kawakami, K. (2007). Tol2: a versatile gene transfer vector in vertebrates. Genome biology ***8 Suppl 1***, S7.

Kennedy, B., and Malicki, J. (2009). What drives cell morphogenesis: a look inside the vertebrate photoreceptor. Developmental dynamics : an official publication of the American Association of Anatomists ***238***, 2115-2138.

Kimmel, C.B., Ballard, W.W., Kimmel, S.R., Ullmann, B., and Schilling, T.F. (1995). Stages of embryonic development of the zebrafish. Developmental dynamics : an official publication of the American Association of Anatomists ***203***, 253-310.

Knodler, A., Feng, S., Zhang, J., Zhang, X., Das, A., Peranen, J., and Guo, W. (2010). Coordination of Rab8 and Rab11 in primary ciliogenesis. Proceedings of the National Academy of Sciences of the United States of America ***107***, 6346-6351.

Kwan, K.M., Fujimoto, E., Grabher, C., Mangum, B.D., Hardy, M.E., Campbell, D.S., Parant, J.M., Yost, H.J., Kanki, J.P., and Chien, C.-B. (2007). The Tol2kit: a multisite gateway-based construction kit for Tol2 transposon transgenesis constructs. Developmental dynamics : an official publication of the American Association of Anatomists ***236***, 3088-3099.

Lang, T., Bruns, D., Wenzel, D., Riedel, D., Holroyd, P., Thiele, C., and Jahn, R. (2001). SNAREs are concentrated in cholesterol-dependent clusters that define docking and fusion sites for exocytosis. The EMBO journal ***20***, 2202-2213.

Lansbergen, G., Grigoriev, I., Mimori-Kiyosue, Y., Ohtsuka, T., Higa, S., Kitajima, I., Demmers, J., Galjart, N., Houtsmuller, A.B., and Grosveld, F., et al. (2006). CLASPs attach microtubule plus ends to the cell cortex through a complex with LL5beta. Developmental cell ***11***, 21-32.

Lewis, A., Williams, P., Lawrence, O., Wong, R.O.L., and Brockerhoff, S.E. (2010). Wild-type cone photoreceptors persist despite neighboring mutant cone degeneration. The Journal of neuroscience : the official journal of the Society for Neuroscience ***30***, 382-389.

Loranger, S.S., and Linder, M.E. (2002). SNAP-25 traffics to the plasma membrane by a syntaxin-independent mechanism. The Journal of biological chemistry ***277***, 34303-34309.

Martin-Urdiroz, M., Deeks, M.J., Horton, C.G., Dawe, H.R., and Jourdain, I. (2016). The Exocyst Complex in Health and Disease. Frontiers in cell and developmental biology ***4***, 24.

Mateos, J.M., Guhl, B., Doehner, J., Barmettler, G., Kaech, A., and Ziegler, U. (2016). Topographic contrast of ultrathin cryo-sections for correlative super-resolution light and electron microscopy. Scientific reports ***6***, 34062.

Mazelova, J., Ransom, N., Astuto-Gribble, L., Wilson, M.C., and Deretic, D. (2009). Syntaxin 3 and SNAP-25 pairing, regulated by omega-3 docosahexaenoic acid, controls the delivery of rhodopsin for the biogenesis of cilia-derived sensory organelles, the rod outer segments. Journal of cell science ***122***, 2003-2013.

Moritz, O.L., Tam, B.M., Hurd, L.L., Peranen, J., Deretic, D., and Papermaster, D.S. (2001). Mutant rab8 Impairs docking and fusion of rhodopsin-bearing post-Golgi membranes and causes cell death of transgenic Xenopus rods. Molecular biology of the cell ***12***, 2341-2351.

Mullins, M.C., Hammerschmidt, M., Haffter, P., and Nusslein-Volhard, C. (1994). Large-scale mutagenesis in the zebrafish: in search of genes controlling development in a vertebrate. Current biology : CB *4*, 189-202.

Nachury, M.V., Loktev, A.V., Zhang, Q., Westlake, C.J., Peränen, J., Merdes, A., Slusarski, D.C., Scheller, R.H., Bazan, J.F., and Sheffield, V.C., et al. (2007). A Core Complex of BBS Proteins Cooperates with the GTPase Rab8 to Promote Ciliary Membrane Biogenesis. Cell *129*, 1201-1213.

Nachury, M.V., Seeley, E.S., and Jin, H. (2010). Trafficking to the ciliary membrane: how to get across the periciliary diffusion barrier? Annual review of cell and developmental biology *26*, 59-87.

Novick, P., and Guo, W. (2002). Ras family therapy: Rab, Rho and Ral talk to the exocyst. Trends in cell biology *12*, 247-249.

Owens, K.N., Santos, F., Roberts, B., Linbo, T., Coffin, A.B., Knisely, A.J., Simon, J.A., Rubel, E.W., and Raible, D.W. (2008). Identification of genetic and chemical modulators of zebrafish mechanosensory hair cell death. PLoS genetics *4*, e1000020.

Peranen, J., Auvinen, P., Virta, H., Wepf, R., and Simons, K. (1996). Rab8 promotes polarized membrane transport through reorganization of actin and microtubules in fibroblasts. The Journal of cell biology *135*, 153-167.

Rogers, K.K., Wilson, P.D., Snyder, R.W., Zhang, X., Guo, W., Burrow, C.R., and Lipschutz, J.H. (2004). The exocyst localizes to the primary cilium in MDCK cells. Biochemical and biophysical research communications *319*, 138-143.

Sato, T., Iwano, T., Kunii, M., Matsuda, S., Mizuguchi, R., Jung, Y., Hagiwara, H., Yoshihara, Y., Yuzaki, M., and Harada, R., et al. (2014). Rab8a and Rab8b are essential for several apical transport pathways but insufficient for ciliogenesis. Journal of cell science *127*, 422-431.

Seixas, C., Choi, S.Y., Polgar, N., Umberger, N.L., East, M.P., Zuo, X., Moreiras, H., Ghossoub, R., Benmerah, A., and Kahn, R.A., et al. (2016). Arl13b and the exocyst interact synergistically in ciliogenesis. Molecular biology of the cell *27*, 308-320.

Shaheen, R., Faqeih, E., Alshammari, M.J., Swaid, A., Al-Gazali, L., Mardawi, E., Ansari, S., Sogaty, S., Seidahmed, M.Z., and AlMotairi, M.I., et al. (2013). Genomic analysis of Meckel-Gruber syndrome in Arabs reveals marked genetic heterogeneity and novel candidate genes. European journal of human genetics : EJHG *21*, 762-768.

Singla, V., and Reiter, J.F. (2006). The primary cilium as the cell‘s antenna: signaling at a sensory organelle. Science (New York, N.Y.) *313*, 629-633.

Slaats, G.G., Isabella, C.R., Kroes, H.Y., Dempsey, J.C., Gremmels, H., Monroe, G.R., Phelps, I.G., Duran, K.J., Adkins, J., and Kumar, S.A., et al. (2016). MKS1 regulates ciliary INPP5E levels in Joubert syndrome. Journal of medical genetics *53*, 62-72.

Sommer, C.,Strähle, C., Köthe, U., Hamprecht, F.A. (2011). ilastik: Interactive Learning and Segmentation Toolkit. Eighth IEEE International Symposium on Biomedical Imaging (ISBI). Proceedings,, 230-233.

Sukumaran, S., and Perkins, B.D. (2009). Early defects in photoreceptor outer segment morphogenesis in zebrafish ift57, ift88 and ift172 Intraflagellar Transport mutants. Vision research *49*, 479-489.

Szymanska, K., and Johnson, C.A. (2012). The transition zone: an essential functional compartment of cilia. Cilia *1*, 10.

Tang, R., Dodd, A., Lai, D., McNabb, W.C., and Love, D.R. (2007). Validation of zebrafish (Danio rerio) reference genes for quantitative real-time RT-PCR normalization. Acta biochimica et biophysica Sinica *39*, 384-390.

Toonen, R.F., and Verhage, M. (2003). Vesicle trafficking: pleasure and pain from SM genes. Trends in cell biology *13*, 177-186.

Veleri, S., Manjunath, S.H., Fariss, R.N., May-Simera, H., Brooks, M., Foskett, T.A., Gao, C., Longo, T.A., Liu, P., and Nagashima, K., et al. (2014). Ciliopathy-associated gene Cc2d2a promotes assembly of subdistal appendages on the mother centriole during cilia biogenesis. Nature communications *5*, 4207.

Wang, J., and Deretic, D. (2015). The Arf and Rab11 effector FIP3 acts synergistically with ASAP1 to direct Rabin8 in ciliary receptor targeting. Journal of cell science *128*, 1375-1385.

Wang, J., Morita, Y., Mazelova, J., and Deretic, D. (2012). The Arf GAP ASAP1 provides a platform to regulate Arf4- and Rab11-Rab8-mediated ciliary receptor targeting. The EMBO journal *31*, 4057-4071.

Ward, H.H., Brown-Glaberman, U., Wang, J., Morita, Y., Alper, S.L., Bedrick, E.J., Gattone,

V.H.2., Deretic, D., and Wandinger-Ness, A. (2011). A conserved signal and GTPase complex are required for the ciliary transport of polycystin-1. Molecular biology of the cell ***22***, 3289-3305.

Westlake, C.J., Baye, L.M., Nachury, M.V., Wright, K.J., Ervin, K.E., Phu, L., Chalouni, C., Beck, J.S., Kirkpatrick, D.S., and Slusarski, D.C., et al. (2011). Primary cilia membrane assembly is initiated by Rab11 and transport protein particle II (TRAPPII) complex-dependent trafficking of Rabin8 to the centrosome. Proceedings of the National Academy of Sciences of the United States of America ***108***, 2759-2764.

White, R.M., Sessa, A., Burke, C., Bowman, T., LeBlanc, J., Ceol, C., Bourque, C., Dovey, M., Goessling, W., and Burns, C.E., et al. (2008). Transparent adult zebrafish as a tool for in vivo transplantation analysis. Cell stem cell ***2***, 183-189.

Williams, D.S. (2004). Photoreceptor Cell Biology and Inherited Retinal Degenerations (World Scientific Pub).

Ying, G., Gerstner, C.D., Frederick, J.M., Boye, S.L., Hauswirth, W.W., and Baehr, W. (2016). Small GTPases Rab8a and Rab11a Are Dispensable for Rhodopsin Transport in Mouse Photoreceptors. PloS one ***11***, e0161236.

Zhao, C., and Malicki, J. (2011). Nephrocystins and MKS proteins interact with IFT particle and facilitate transport of selected ciliary cargos. The EMBO journal ***30***, 2532-2544.

Supplemetary material

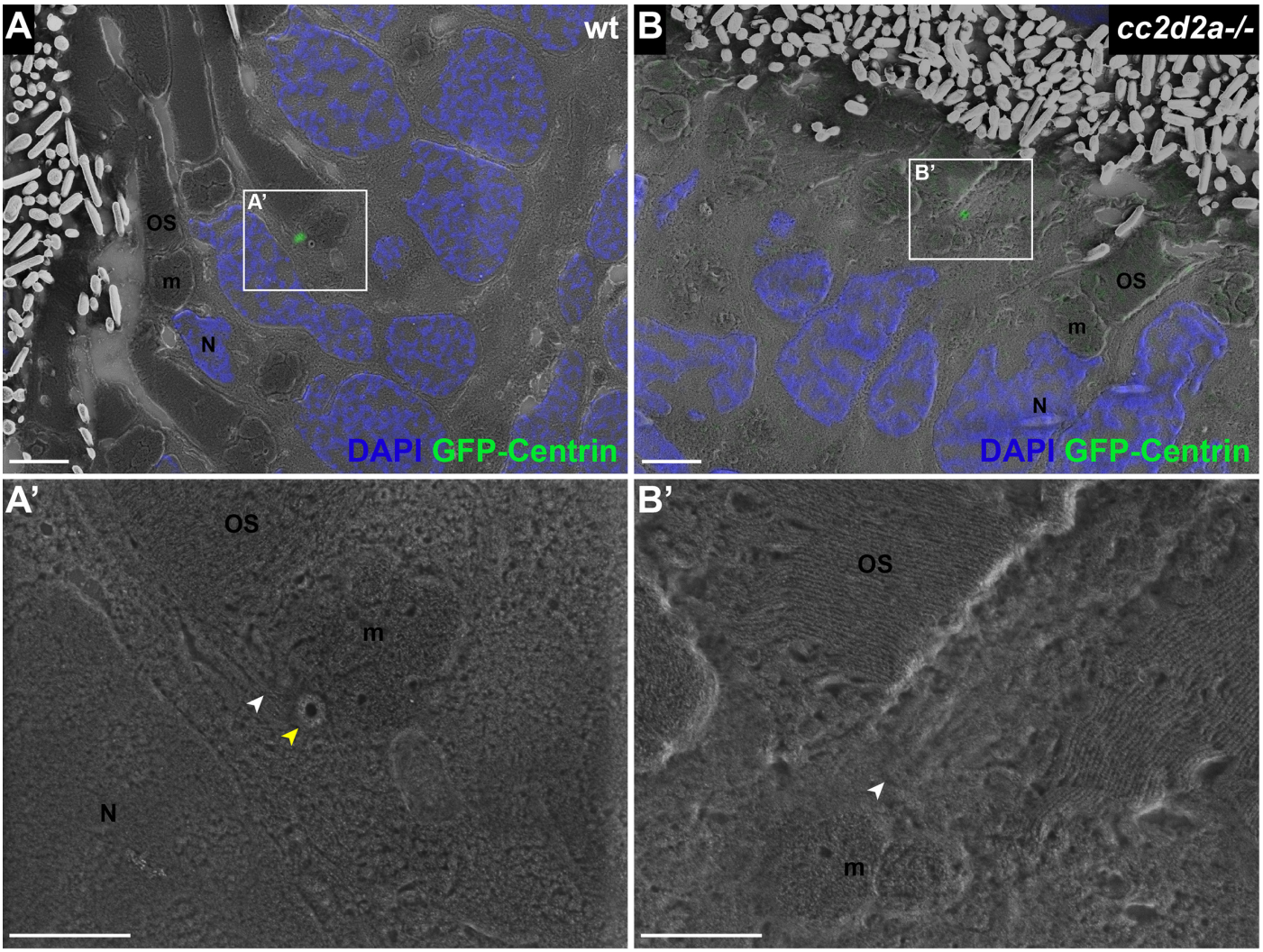

Supplementary figure 1. BB docking occurs normally in *cc2d2a-/-* PRs
5 dpf CLEM sections of a *tg(TaCP:GFP-hCentrin)* wildtype (A) and *cc2d2a-/-* (B) fish counterstained with DAPI (blue, nuclei). GFP-Centrin-labeled basal bodies (BBs) (green) localize at the apical membrane of both wildtype and mutant animals. (A') BB is docked right below the outer segment (white arrowhead), apical to the daughter centriole (yellow arrowhead) in wt. (B') BB (white arrowhead) is localized correctly in *cc2d2a-/-* PRs even when the OSs appear dysmorphic and disorganized. Scale bars are 4 µm in A-B and 2 µm in A'-B'.

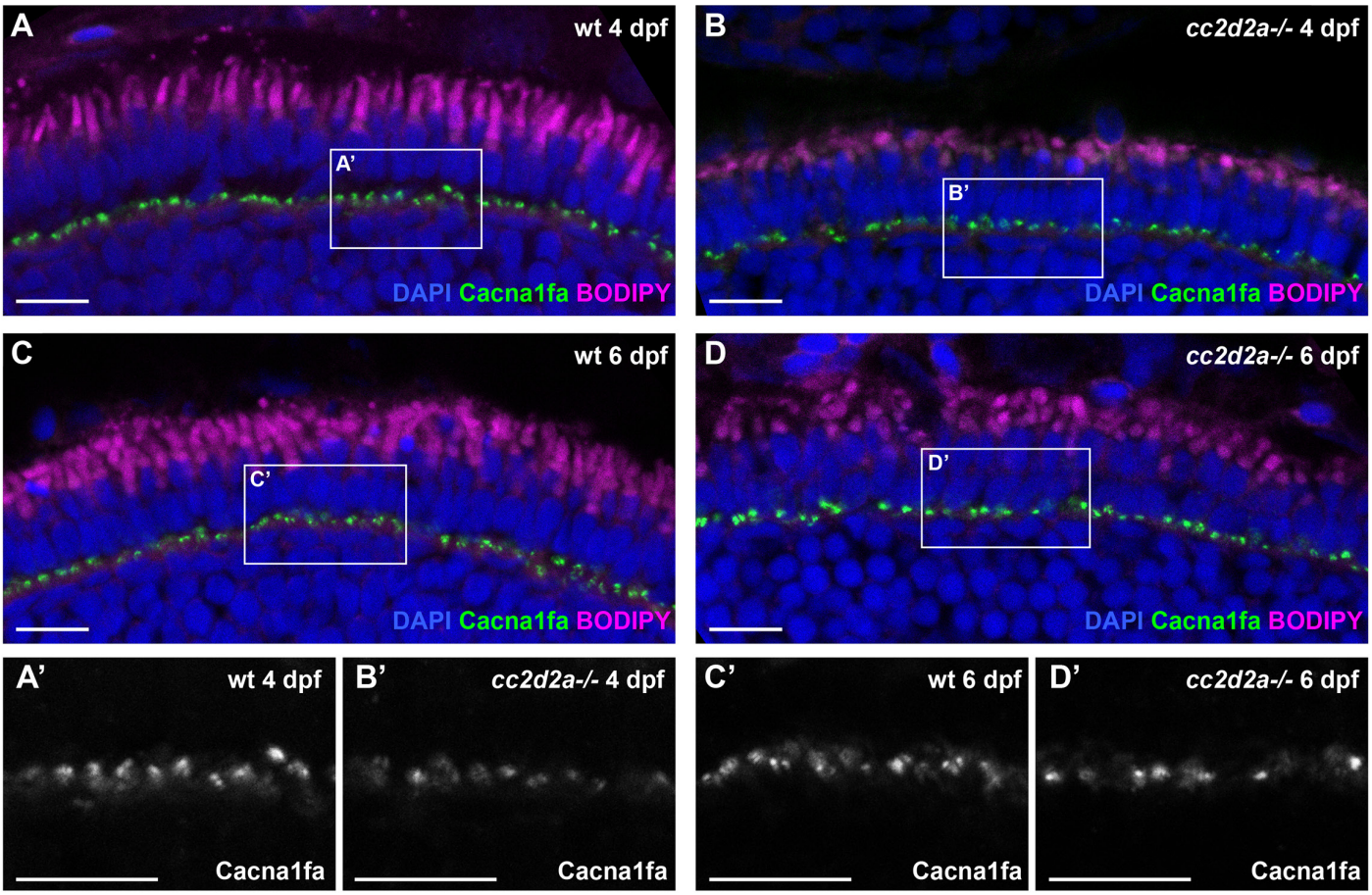

Supplementary figure 2. Polarized trafficking of transmembrane proteins not targeted to cilium occurs normally in *cc2d2a-/-* PRs

Retinal cryosections of 4 dpf (A-B) and 6 dpf (C-D) wildtype (A, C) and *cc2d2a-/-* (B, D) zebrafish, stained with an antibody against Cacna1fa (green), an L-type calcium channel that localizes to the synapse, and counterstained with DAPI (nuclei, blue) and BODIPY (outer segments and mitochondrial cluster, magenta). (A'-D') Close-ups of the synaptic regions boxed in A-D. Note how Cacna1fa (grey) localizes normally in mutant synapses (B' and D') compared to wildtype synapses (A' and C'). Scale bars are 10 µm in all figures.

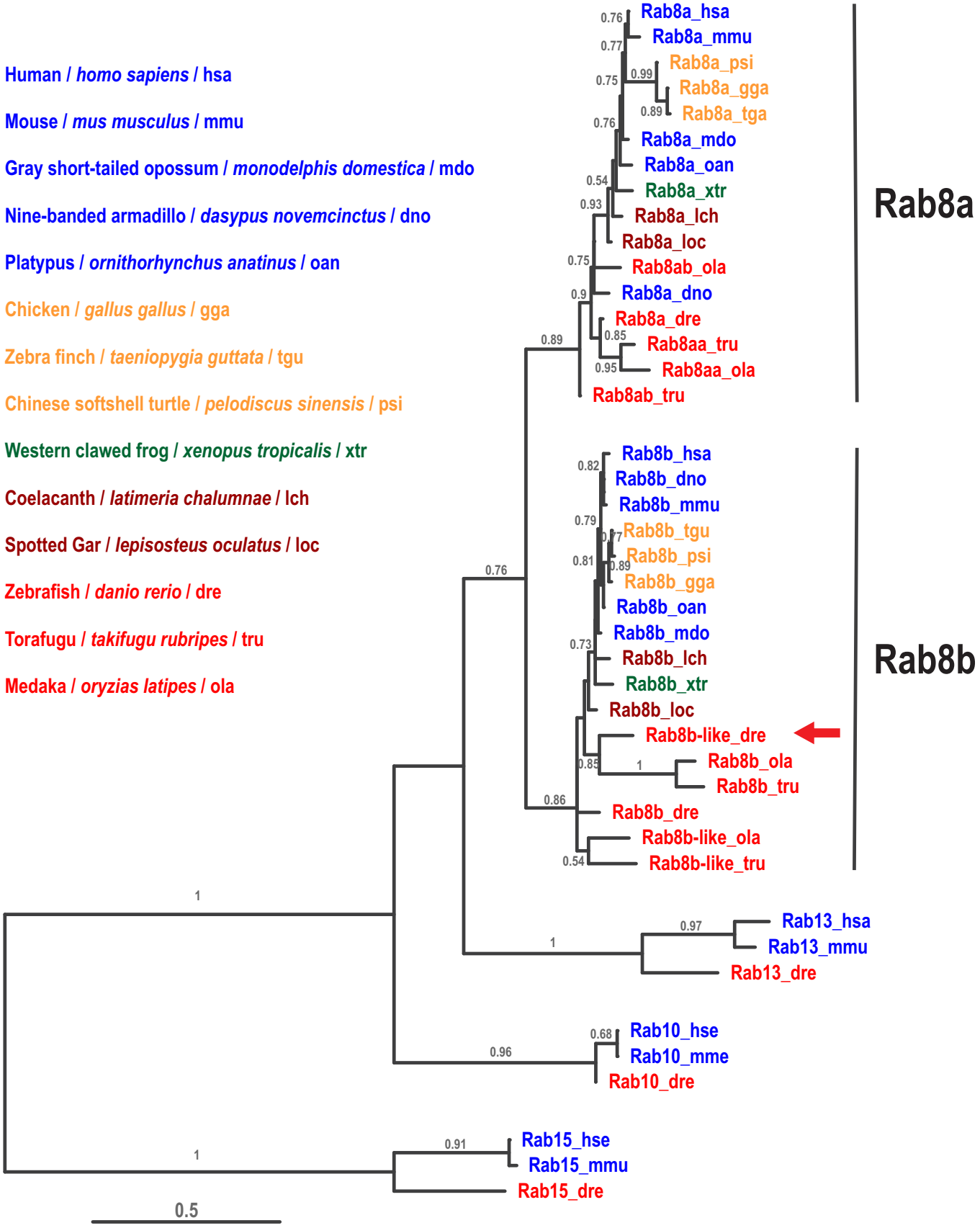

Supplementary figure 3. The zebrafish possess two Rab8b paralogs
Rab sequences of the species indicated were used for phylogenetic reconstructions. Ancient fish species (lacking the teleost specific whole genome duplication) are shown in dark red, teleost species are given in bright red, the amphibian species *Xenopus tropicalis* is shown in green, Sauropsidia are marked in orange and mammals are depicted in blue. As an outgroup to root the tree Rab15 sequences from the three major species were included. Note that all teleosts have two Rab8b-like genes. The Rab8b variant used in our studies is highlighted by a red arrow.

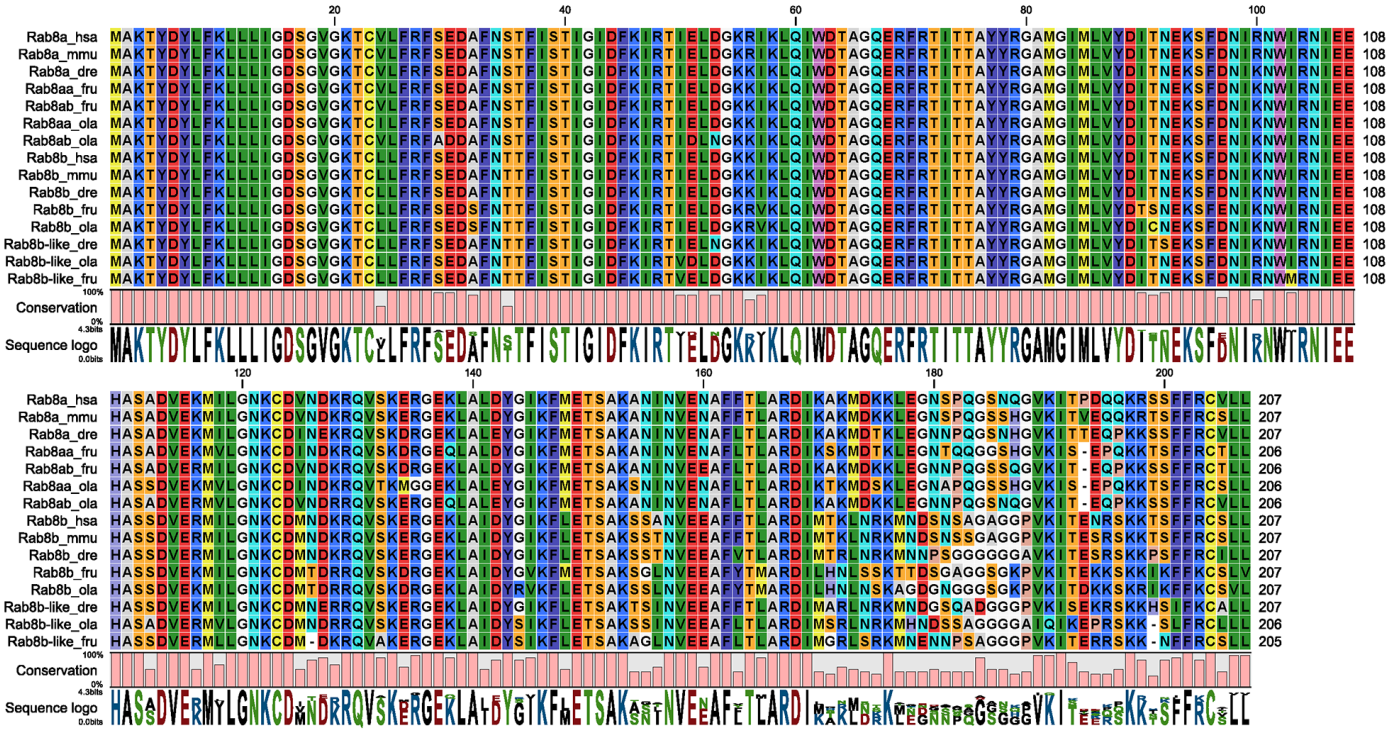

Supplementary figure 4. Homology between Rab8 proteins

Amino acid sequences of the the following species were aligned using CLC Main Workbench program (version 6), configured for high accuracy: Human *(Homo sapiens)* has, mouse *(Mus musculus)* mmu, zebrafish *(Danio rerio)* dre, torafugu (*Takifugu rubripes)* tru, medaka *(Oryzias latipes)* ola. Conservation is given by bar graph (pink boxes) and the sequence logo (occurring amino acids at a given position and their relative abundance are indicated by letter size). Note that variations in the first 110 amino acids are very rare and are only observed in very few of the included sequences.

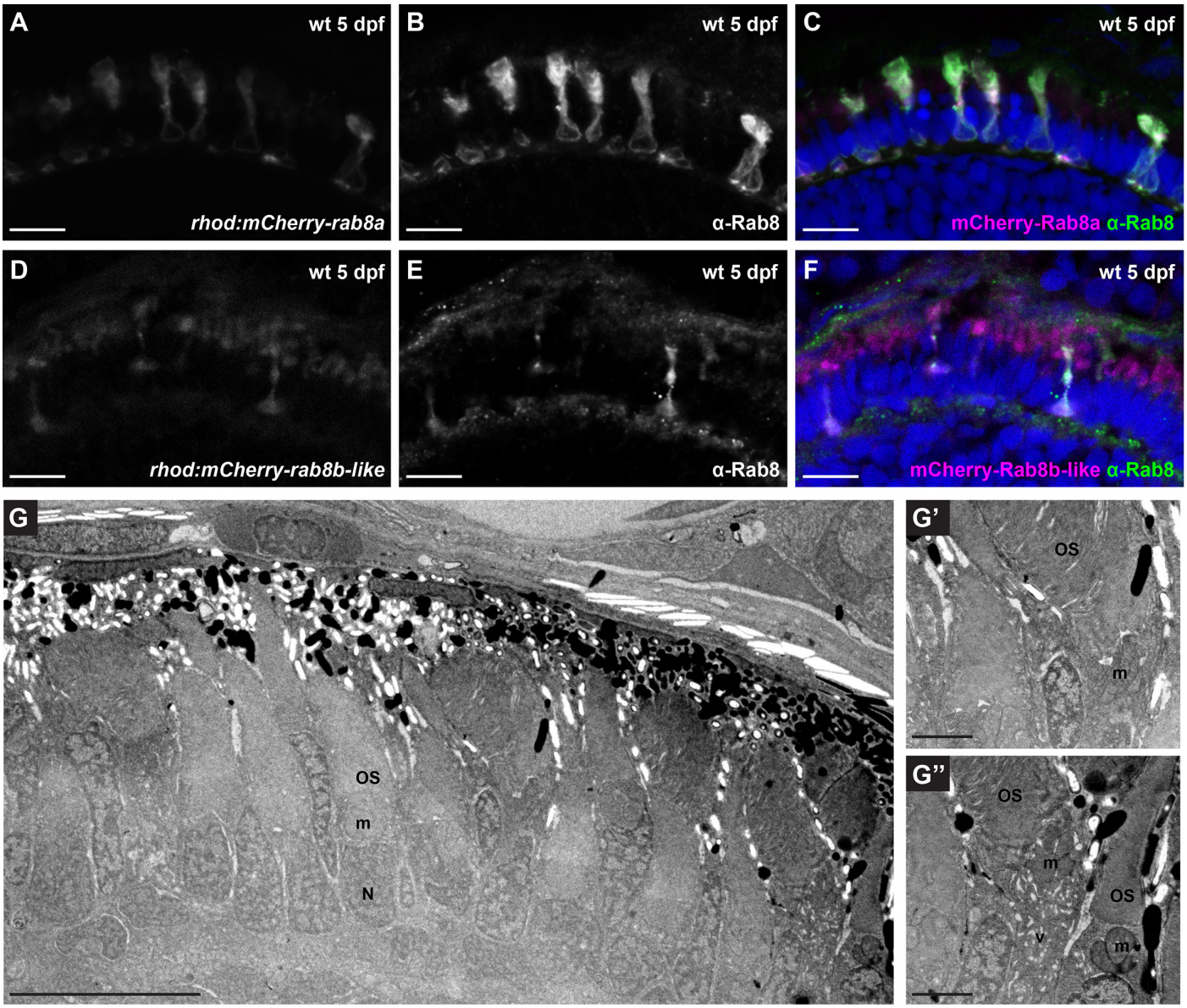

Supplementary figure 5. Validation of transgenic Rab8 lines

An anti-Rab8 antibody (B, E and green in C, F) recognizes mCherry-tagged Rab8a (A, magenta in C) and mCherry-tagged Rab8b-like (D, magenta in F) on retinal cryosections of 5 dpf zebrafish. (G) Transmission Electron Microscopy overview of a *tg(rhod:mCherry-rab8a)* retina. Despite variable accumulation of membrane-bound structures in inner segment regions secondary to overexpression of the transgenic construct in a subset of PRs (absent in G', present in G"), the retinal structure remains normal and extension of outer segments is unaffected. Scale bars are 10 µm in A-G and 2 µm in G' and G". OS outer segment, m mitochondria, v vesiculo-tubular structures.

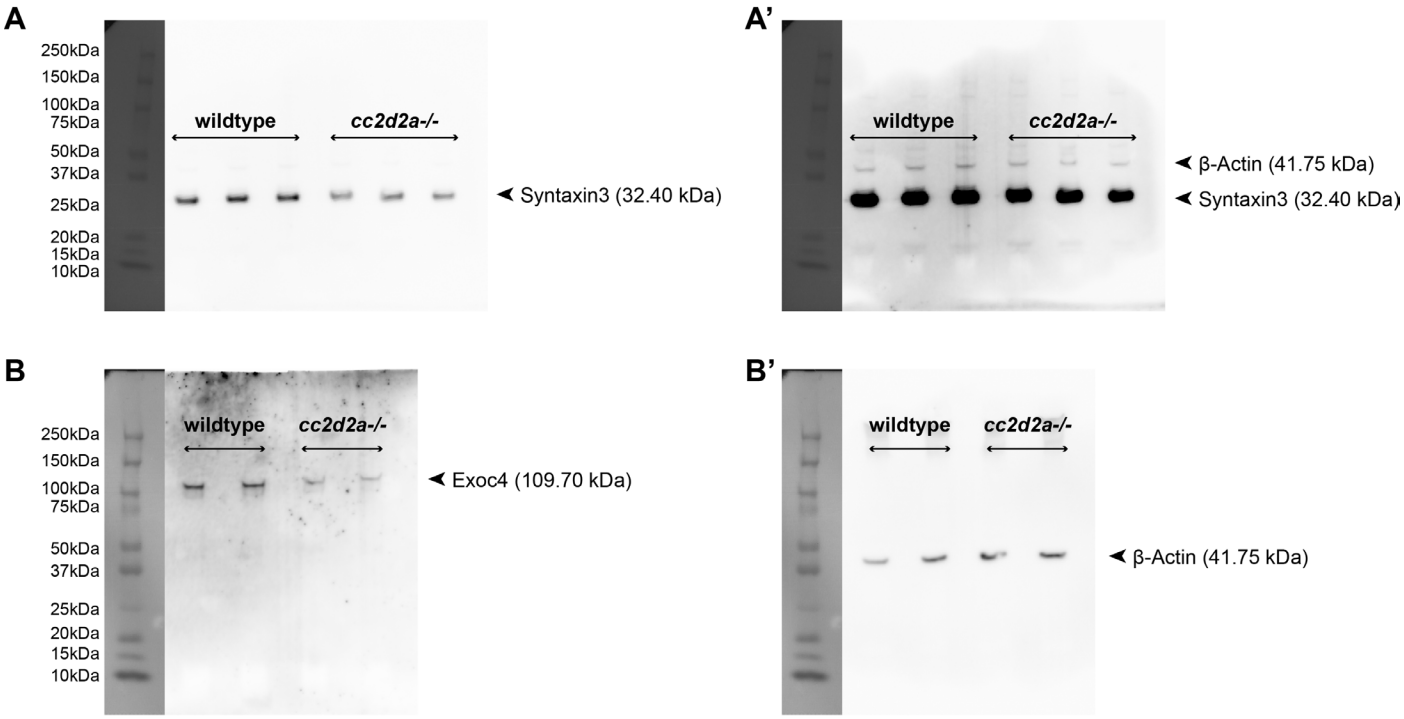

Supplementary figure 6. Complete western blots for Syntaxin3 and Exoc4

(A and A') Lysate triplicates of wt and *cc2d2a-/-* whole eyes probed for (A) Syntaxin3 and (A') beta-actin in the same blot. beta-actin appears at later exposure times. (B and B') Lysate duplicates of wt and *cc2d2a-/-* whole eyes probed for (B) Exoc4 and (B') beta-actin after stripping. Fold change was calculated as the band intensity relative to the housekeeping protein control, averaged for all the replicates and repeated in 3 independent blots.

Chapter 3. Correlative super-resolution and electron microscopy to resolve protein localization in zebrafish retina

Mateos, J.M.*, Barmettler, G., Doehner, J., **Ojeda Naharros, I.**, Guhl, B., Kaech, A., Bachmann-Gagescu, R., Ziegler, U.

University of Zurich, Institute of Molecular Life Sciences
Winterthurerstrasse 190, 8057
Zurich, Switzerland
Life Science Zurich Graduate School, PhD. Program in Neurosciences

* Corresponding author
José María Mateos Melero
mateos@zmb.uzh.ch

In press

Personal contribution: Sample preparation and imaging, participation in manuscript preparation

Keywords

CLEM, immunofluorescence, super-resolution light microscopy, scanning electron microscopy, subcellular localization, zebrafish, retina

Short abstract

This protocol describes the necessary steps to obtain subcellular protein localization results on zebrafish retina by correlating super-resolution light microscopy and scanning electron microscopy images.

Long abstract

We present a method to investigate the subcellular protein localization in the larval zebrafish retina by combining super-resolution light microscopy and scanning electron microscopy. The sub-diffraction limit resolution capabilities of super-resolution light microscopes allow improving the accuracy of the correlated data. Briefly, 110 nm thick cryo-sections are transferred to a silicon wafer and, after immunofluorescence staining, are imaged by super-resolution light microscopy. Subsequently, the sections are preserved in methylcellulose and platinum shadowed prior to imaging in a scanning electron microscope (SEM). The images from these two microscopy modalities are easily merged using tissue landmarks with open source software. Here we describe the adapted method for the larval zebrafish retina. However, this method is also applicable to other types of tissues and organisms. We demonstrate that the complementary information obtained by this correlation is able to resolve the expression of mitochondrial proteins in relation with the membranes and cristae of mitochondria as well as to other compartments of the cell.

Introduction

Methods to determine the subcellular localization of proteins and their relationship to different compartments of the cell are essential tools to understand their functions and possible interactions. Super-resolution microscopy in combination with electron microscopy provides such information (Hauser et al., 2017). Ground state depletion microscopy followed by individual molecule return (GSDIM) is a super-resolution microscopy technology compatible with a wide range of organic and genetically encoded fluorophores (Dempsey et al., 2011) and achieves a lateral resolution up to 20 nm (Fölling et al., 2008). The incorporation of methods with higher resolution than standard diffraction-limited microscopy improves the accuracy of the correlation (Betzig et al., 2006; Kopek et al., 2013; Paez-Segala et al., 2015). In order to achieve the best correlation of protein expression with a specific subcellular compartment and to reduce the volume of uncertainty (Narayan and Subramaniam, 2015) the use of the same ultrathin section for light and electron microscopy is recommended. Among the different sectioning methods, Tokuyasu cryo-section protocol does not require dehydration or resin embedding and, in addition, preserves the antigenicity of many epitopes and provides good tissue ultrastructure (Tokuyasu et al., 1980). Several methods have demonstrated the applicability of these sections in correlative light and electron microscopy (CLEM) (Betzig et al., 2006; Suleiman et al., 2013; Kopek et al., 2012; Kopek et al., 2013).

The zebrafish retina is a valuable model to study visual development and human disease mechanisms given its highly conserved structure and function across vertebrates. In particular, retinal photoreceptors display the same architecture as mammalian photoreceptors, with a basal synapse, an apico-basally elongated nucleus, clustering of mitochondria in the more apical inner segment and an outer segment composed of membrane disks in the most apical position (Avanesov and Malicki, 2010). Protein localization to the diverse cellular compartments is conserved between zebrafish and human, allowing investigation of the biological function of human disease-relevant proteins (Bachmann-Gagescu et al., 2011; Bachmann-Gagescu et al., 2015).

Here we present a protocol to prepare larval zebrafish retina samples to resolve the localization of the mitochondrial outer membrane protein Tom20 by correlative super-resolution light and electron microscopy. The method is based on collecting cryo-sections on silicon wafers and obtaining contrast by topographical information produced after application of a thin layer of platinum. These steps are clear technical improvements in terms of ease of use, reproducibility, and time to complete experiments. We have recently demonstrated the applicability of the method to detect nuclear pores and mitochondria proteins in mouse tissue (Mateos et al., 2016).

Protocol

All experiments were performed in accordance with the ARVO Statement for the Use of Animals in Ophthalmic and Vision Research and were approved by the local authorities (Veterinäramt Zürich TV4206).

1. Preparation of ultrathin sections on silicon wafers

1.1. Sample fixation

1.1.1. Prepare the fixative solution containing 0.1% glutaraldehyde, 4% formaldehyde in 0.1 M cacodylate buffer.

Note: **CAUTION!** Use caution when working with glutaraldehyde, formaldehyde and cacodylate buffer, wear appropriate personal protective equipment and work in a fume hood.

1.1.2. Euthanize 5 days post fertilization (5 dpf) zebrafish larvae with tricaine (ethyl 3-aminobenzoate methanesulfonate, 0.4% w/v in PBS, pH 7)) as previously described (Westerfield, 2000).

1.1.3. Fix the larvae by immersion in pre-chilled fixative solution on ice. Remove the head and incubate overnight at 4°C with gentle rocking.

1.1.4. Dissect the eyes by trimming the tissue around the eye using fine forceps and a microdissection scalpel (under a binocular) in chilled fixative solution on a 1% agarose-bedded plate. Transfer the eyes to a tube with fresh pre-chilled fixative.

1.1.5. Wash twice in PBS (Phosphate buffer saline, pH 7.4) for 5 min each wash at room temperature (RT).

1.2. Gelatin infiltration and mounting.

1.2.1. Warm up 1 mL local food brand gelatin 12% w/v in PB (Phosphate buffer, 0.1 M pH 7.4) at 40°C. Remove the PBS and add gelatin solution to the tubes containing the eyes. Tap the tube gently to ensure the gelatin infiltrates the sample and incubate for 10-30 min at 40°C in a thermoblock with gentle shaking or in a water bath.

1.2.2. Fill 12 mm x 5 mm x 3 mm silicon or polyethylene flat embedding molds with warm gelatin in a 40°C water bath. Add two eyes per mold using a pipette, align them properly under a binocular using a dissection needle and let the gelatin cool down at room temperature for 1 min and harden at 4°C for 20 min.

1.2.3. Re-trim the gelatin block under the binocular to fit one eye per block using a razor blade.

1.2.4. Transfer the gelatin embedded eyes to 2.3 M sucrose in PBS on ice. Incubate at 4 °C overnight.

1.2.5. Exchange to new 2.3 M sucrose solution and store at 4 °C or -20°C after this step, samples are ready for sectioning or can be stored at -20°C for several weeks to months.

1.2.6. Re-trim the gelatin block to almost the size of the eye before transferring to a cryo-pin.

1.2.7. Freeze in liquid nitrogen and transfer to a cryo-ultramicrotome.
1.3. Cryosectioning
1.3.1. Cut 110 nm thick-sections at -120 °C with a diamond knife in the cryo-ultramicrotome.
1.3.2. Pick the sections with a wired loop containing a droplet of 2% methylcellulose (in water) and 2.3 M sucrose solution (1:1).
1.3.3. Transfer sections to a 7 mm x 7 mm silicon wafer. Store sections at 4°C until further processing.

2. Immunolabelling

2.1. Wash wafers with PBS at 0°C for 20 on two drops by placing the wafers upside down on the drops. Wash in PBS 2 x 2 min at room temperature.
2.2. Incubate 3 times in 0.15% glycine in PBS, for 1 min each. Wash 3x for 1 min/wash with PBS.
2.3. Pre-incubate with PBG (PBS with 0.5 % Bovine Serum Albumin BSA and 0.2 % Gelatin type B) for 5 min.
2.4. Incubate with rabbit anti-Tom20 (see the **Table of Materials**) in PBG (4 µg/mL) for 30 min at room temperature.
2.5. Wash 6x for 1 min/wash in PBG. Pre-incubate with PBG for 5 min at RT.
2.6. Incubate with anti-rabbit Alexa 647 F(ab') (see the **Table of Materials**) in PBG (7.5 µg/mL) for 30 min.
2.7. Wash 6x for 1 min/wash in PBG. Wash 3x 2 min in PBS.
2.8. Incubate with DAPI (4 µg/mL) in PBS for 10 s. Wash 2x 2 min in PBS.

3. Super-resolution microscopy

3.1. Incubate the wafer briefly (10 s) by placing it on a droplet of a 1:1 solution of glycerol (80%) and imaging buffer containing an oxygen scavenging system (200 mM Phosphate buffer containing 10% glucose, 0.5 mg/mL glucoseoxidase, 40 µg/mL catalase, 15 mM beta-mercaptoethylamine hydrochloride (MEA HCL), pH 8.0).
3.2. Transfer the wafers (section facing down) to a glass bottom (thickness 170 ± 5 µm) Petri dish onto a fresh drop of the 1:1 mixture of glycerol (80%) and imaging buffer (as in step 3.1).
3.3. Remove from one side, with a pipette, most of the liquid underneath the wafer.
3.4. Use silicone stripes to fix the wafer to the bottom of the Petri dish.
Note: Silicone stripes are made out of two-component silicone-glue (3 mm x 12 mm).
3.5. Image sections on an inverted microscope using a high numerical aperture (*e.g.* 160x / NA 1.43; see the **Table of Materials**) oil immersion super resolution dedicated objective.

3.5.1. Prior to imaging, let the sample equilibrate to microscope temperature in order to minimize/reduce lateral and axial drift.

3.6. Center the area of interest and acquire first widefield epifluorescence reference images.

3.7. Change to the super resolution operation mode. Adjust the exposure time of the camera to 15 ms and set the electron multiplying (EM) gain to the maximum of 300.

3.8. Illuminate sample with the 642 nm continuous wave laser at maximum laser power (corresponding to ~2.8 kW/cm^2) in epifluorescence mode. As soon as the single molecule blinks are well separated in each frame, so that the probability is low that individual signals overlap, set the laser power to ~0.7 kW/cm^2.

3.9. Record the raw image in epifluorescence mode by acquiring a minimum of 30,000 frames.

Note: All these parameter can vary depending on different specimens and labeling densities.

3.10. From the raw data generate a reconstruction event list (localizations of each single molecule blink in the raw image) using a detection threshold of 30 photons (needs to be adjusted according to your sample) by clicking "Evaluate" in the t-series analysis under tools.

3.11. Visualize the super resolution image by Gaussian fitting (Thompson et al., 2002) applying a rendering pixel size of 4 nm by clicking "Create Image" in the event list processing panel under tools.

Note: For generating the super resolved image the integrated software tools of the system used in this study was employed. However, the described super resolution imaging could be done on any other single localization based system, as well as the data could be processed with open source software tools as thunderSTORM (Ovesny et al., 2014).

4. Platinum shadowing

4.1. Remove silicon stripes and add a drop of PBS close to the edges of the wafer to lift it up from the Petri dish.

4.2. Wash the wafer 2 x 2 min in PBS, then post fix it with 0.1% glutaraldehyde in PBS for 5 min. Wash 2x for 2 min/wash in PBS.

4.3. Incubate the wafer twice for 5 min/incubation in 1 drop of methylcellulose 2% in water on ice.

4.4. Insert the wafer in a centrifuge tube and centrifuge at 14,100 x g for 90 s.

4.5. Mount it on a SEM aluminum stub with conducting carbon cement.

4.6. Add a layer of 2 to 10 nm of platinum/carbon on the sample by rotary shadowing at 8° using an electron beam evaporation device settings: 1.55 KV, 55 mA, at 0.3 nm/s, and an angle of 8°, rotation level 4.

5. Scanning electron microscopy

5.1. Image sections with a scanning electron microscope at 1.5 kV, 2 mm working distance and with an In lens secondary electron detector.

6. Alignment of light and electron microscopy images

6.1. Open both types of images with Fiji (Schindelin et al., 2012) by clicking "File/open". Adjust canvas size by clicking Image/Adjust/Canvas size and bring both images to a stack by clicking "Image/Stacks/Images to stack". Save the stack as tiff file type.

6.2. In Fiji, open a new TrackEM2 (Cardona et al., 2012) interface by clicking "File/new/TrackEM2 (new)". Import the stack with both images by right click on the black window and select "import stack".

6.3. Align light microscopy image to electron microscopy image manually with landmarks by right mouse click on the image and select "Align/Align layer manually with landmarks".

6.3.1. Pick the select tool (the black arrow) to add landmarks.

6.3.2. Use the shape of nuclei as reference to select the same edges in both images (Supplementary Figure 1). Add several points (minimum three points need to be selected). Apply alignment with an affine model by right mouse click "apply transform" and select "affine model".

6.4. Change layer transparency (Supplementary Figure 1) to assess the quality of the alignment.

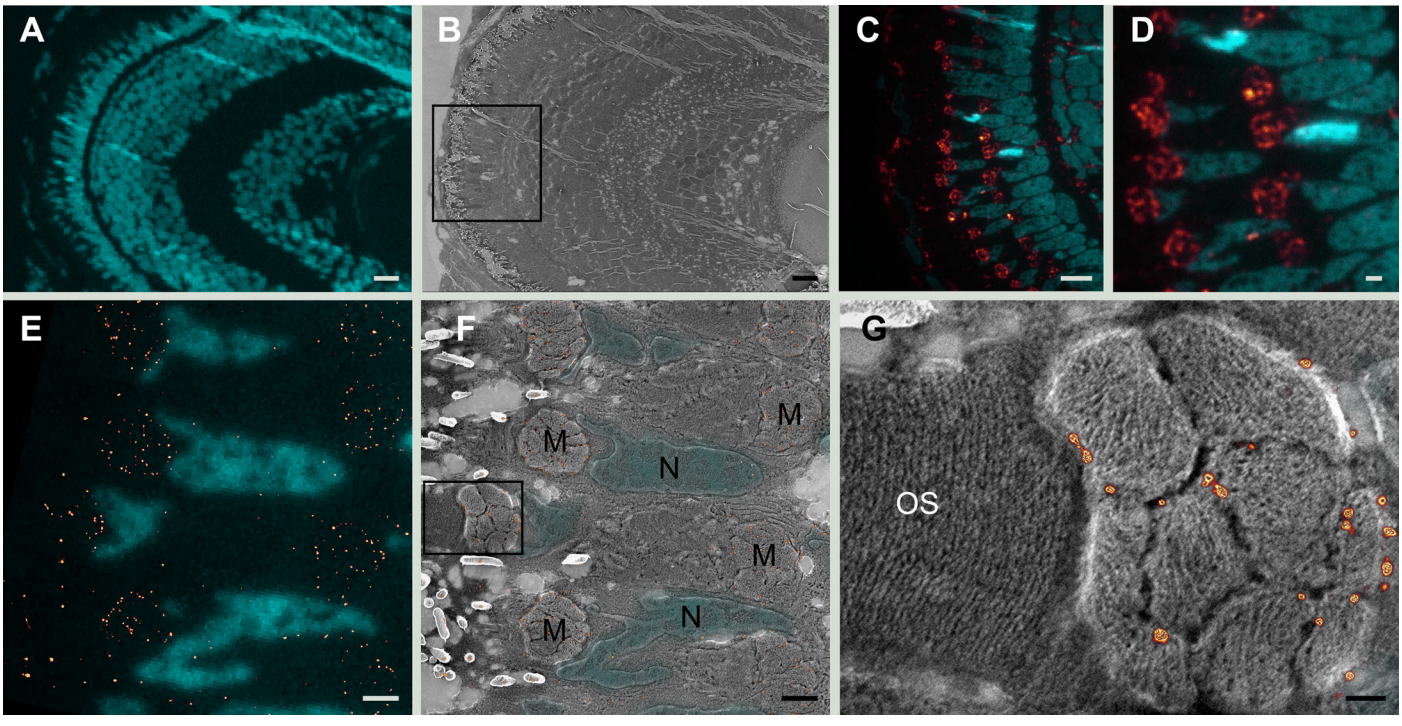

Figure 1: CLEM on zebrafish retina
(A) Low magnification widefield image of a 5 dpf zebrafish retinal section, nuclei stained with DAPI (cyan). (B) Scanning electron microscopy of the same area. (C) Higher magnification widefield image of frame in B. Nuclei stained with DAPI (cyan) and Tom20 mitochondrial staining appears in red. (D) Widefield image of same section at higher magnification. The pattern of Tom20 expression is at the clusters of mitochondria. (E) Expression of Tom20 (red dots) detected by GSDIM microscopy. Nuclei stained with DAPI (cyan). (F) Same section as E combining correlative super-resolution and scanning electron microscopy. Tom20 staining (red dots) appears at the mitochondrial cluster (M) at the outer membranes of mitochondria. Fluorescence DAPI signal in the nuclei (N) corresponds with the topography of the SEM image. (G) High magnification image of frame in F. The scanning electron microscopy image provides context to the GSDIM image (red dots). Mitochondrial cristae are clearly visible and the Tom20 staining is localized to the outer membranes of mitochondria. The membranes of the outer segment the photoreceptors (OS) are clearly resolved. Image pixel size 5 nm. Scale bars: A, B and C: 10 µm; D: 2 µm; E and F: 1 µm and G: 0.2 µm.

Representative results

The expression of the protein Tom20, a subunit of the translocase mitochondrial outer membrane complex (Wurm et al., 2011), was determined, in thin sections of larval zebrafish retina, by super-resolution light microscopy (Fig. 1)and this information was complemented with the topographical signal obtained by scanning electron microscopy after platinum shadowing of the same sections. These correlative data confirm the localization of a protein in association with a particular compartment, the outer mitochondrial membrane and, in addition provide information about the relation of the protein with other organelles of the cell.

Discussion

This method combines super-resolved protein localization with context information to determine the precise position of proteins in an organelle. We demonstrate here the completion of the experiment to visualize the expression of Tom20 in the outer membrane of mitochondria, and its relation to other organelles like nuclei or outer segments of the photoreceptor in the larval zebrafish retina.

Tokuyasu cryo-sectioning requires some training to acquire well-preserved sections. However, this is a method employed in many laboratories with demonstrated success (Slot and Geuze, 2007). Transfer of the sections to the silicon wafer is very simple and no special considerations are needed. The use of glycerol in the imaging buffer is a very critical step to avoid drying of the sections. For super-resolution imaging the best results are obtained when the wafer is very close to the glass bottom of the Petri dish. The silicone stripes help maintaining the wafer in this position. Special care has to be taken while removing the stripes in order to avoid damaging the sections.

The thickness of the cryo-sections, around 100 nm, thinner than the optical resolution in the Z- dimension, additionally facilitates the accuracy of this correlative method as the super-resolution microscopy signal is coming only from this thin layer and the scanning electron microscope signal is displaying the topography of the sample. This method could also be combined with multicolor imaging. However, special care must be taken that the sample can be imaged under same conditions (*e.g.* imaging buffer) and cross talk should be prevented.

One limitation of the method is its two dimensional approach, since only a limited number of serial sections (about 3 to 7 per wafer) can be collected. Thus, projects dealing with volume analysis would not be ideal. However, it is a method that can be applied to detect protein expression in any type of

tissue by simple sectioning of the sample. We provide a method without use of classical contrast agents like uranyl acetate or lead citrate. The contrast by platinum shadowing provides very informative topographical contrast, but in some cases membranes are difficult to resolve. This may pose problems for projects which need, for example, to determine the expression of proteins in small vesicles.

Our protocol, based on Tokuyasu cryo-sections, uses standard equipment to obtain correlative results from super-resolution and scanning electron microscopes. The collection of sections on silicon wafers and the use of platinum for contrast are simple steps to provide stability and reproducibility to the sample preparation.

Acknowledgements

Funding ION and RGB: Swiss National Science Foundation Ambizione-SCORE grant PZ00P3 142404/1 and PZ00P3 163979.

Disclosures

The authors have nothing to disclose.

References

Avanesov, A. & Malicki, J. Analysis of the retina in the zebrafish model. *Methods in cell biology* **100**, 153–204, doi:10.1016/B978-0-12-384892-5.00006-2 (2010).

Bachmann-Gagescu, R., Phelps, I. G., *et al.* The ciliopathy gene cc2d2a controls zebrafish photoreceptor outer segment development through a role in Rab8-dependent vesicle trafficking. *Human molecular genetics* **20** (20), 4041–55, doi:10.1093/hmg/ddr332 (2011).

Bachmann-Gagescu, R., Dona, M., *et al.* The Ciliopathy Protein CC2D2A Associates with NINL and Functions in RAB8-MICAL3-Regulated Vesicle Trafficking. *PLoS genetics* **11** (10), e1005575, doi:10.1371/journal.pgen.1005575 (2015).

Betzig, E., Patterson, G. H., *et al.* Imaging intracellular fluorescent proteins at nanometer resolution. *Science (New York, N.Y.)* **313** (5793), 1642–5, doi:10.1126/science.1127344 (2006).

Cardona, A., Saalfeld, S., *et al.* TrakEM2 software for neural circuit reconstruction. *PloS one* **7** (6), e38011, doi:10.1371/journal.pone.0038011 (2012).

Dempsey, G. T., Vaughan, J. C., Chen, K. H., Bates, M. & Zhuang, X. Evaluation of fluorophores for optimal performance in localization-based super-resolution imaging. *Nature Methods* **8** (12), 1027–1036, doi:10.1038/nmeth.1768 (2011).

Fölling, J., Bossi, M., *et al.* Fluorescence nanoscopy by ground-state depletion and single-molecule return. *Nature Methods* **5** (11), 943–945, doi:10.1038/nmeth.1257 (2008).

Hauser, M., Wojcik, M., Kim, D., Mahmoudi, M., Li, W. & Xu, K. Correlative Super-Resolution Microscopy: New Dimensions and New Opportunities. *Chemical Reviews* , acs.chemrev.6b00604, doi:10.1021/acs.chemrev.6b00604 (2017).

Kopek, B. G., Shtengel, G., Xu, C. S., Clayton, D. A. & Hess, H. F. Correlative 3D superresolution fluorescence and electron microscopy reveal the relationship of mitochondrial nucleoids to membranes. *Proceedings of the National Academy of Sciences of the United States of America* **109** (16), 6136–41, doi:10.1073/pnas.1121558109 (2012).

Kopek, B. G., Shtengel, G., Grimm, J. B., Clayton, D. A. & Hess, H. F. Correlative photoacti-

vated localization and scanning electron microscopy. ***PloS one*** **8** (10), e77209, doi:10.1371/journal.pone.0077209 (2013).

Mateos, J. M., Guhl, B., ***et al.*** Topographic contrast of ultrathin cryo-sections for correlative super-resolution light and electron microscopy. ***Scientific Reports*** **6**, 34062, doi:10.1038/srep34062 (2016).

Narayan, K. & Subramaniam, S. Focused ion beams in biology. ***Nature Methods*** **12** (11), 1021–1031, doi:10.1038/nmeth.3623 (2015).

Ovesny, M., K i ek, P., Borkovec, J., vindrych, Z. & Hagen, G. M. ThunderSTORM: a comprehensive ImageJ plug-in for PALM and STORM data analysis and super-resolution imaging. ***Bioinformatics*** **30** (16), 2389–2390, doi:10.1093/bioinformatics/btu202 (2014).

Paez-Segala, M. G., Sun, M. G., ***et al.*** Fixation-resistant photoactivatable fluorescent proteins for CLEM. ***Nature methods*** **12** (3), 215–8, 4 p following 218, doi:10.1038/nmeth.3225 (2015).

Schindelin, J., Arganda-Carreras, I., ***et al.*** Fiji: an open-source platform for biological-image analysis. ***Nature methods*** **9** (7), 676–82, doi:10.1038/nmeth.2019 (2012).

Slot, J. W. & Geuze, H. J. Cryosectioning and immunolabeling. ***Nature protocols*** **2** (10), 2480–91, doi:10.1038/nprot.2007.365 (2007).

Suleiman, H., Zhang, L., ***et al.*** Nanoscale protein architecture of the kidney glomerular basement membrane. ***eLife*** **2**, e01149, doi:10.7554/eLife.01149 (2013).

Thompson, R. E., Larson, D. R. & Webb, W. W. Precise nanometer localization analysis for individual fluorescent probes. ***Biophysical journal*** **82** (5), 2775–83, doi:10.1016/S0006-3495(02)75618-X (2002).

Tokuyasu, K. T. Immunochemistry on ultrathin frozen sections. ***The Histochemical journal*** **12** (4), 381–403at <http://www.ncbi.nlm.nih.gov/pubmed/7440248> (1980).

Westerfield, M. ***The zebrafish book. A guide for the laboratory use of zebrafish (Danio rerio)***. at <http://zfin.org/zf_info/zfbook/zfbk.html> (Univ. of Oregon Press: Eugene, 2000).

Wurm, C. A., Neumann, D., ***et al.*** Nanoscale distribution of mitochondrial import receptor Tom20 is adjusted to cellular conditions and exhibits an inner-cellular gradient. ***Proceedings of the National Academy of Sciences of the United States of America*** **108** (33), 13546–51, doi:10.1073/pnas.1107553108 (2011).

Supplementary material

Supplementary Figure 1: Alignment of light and electron microscopy images
(A) Screenshot from TrackEM2 interface with SEM image and numbered landmarks (yellow) along different nuclei. (B) Screenshot from TrackEM2 interface with fluorescence image and numbered landmarks (yellow) along different DAPI stained nuclei. To change layer transparency the sliders on the left upper part of the menu can be used. Scale bar: 1 µm.

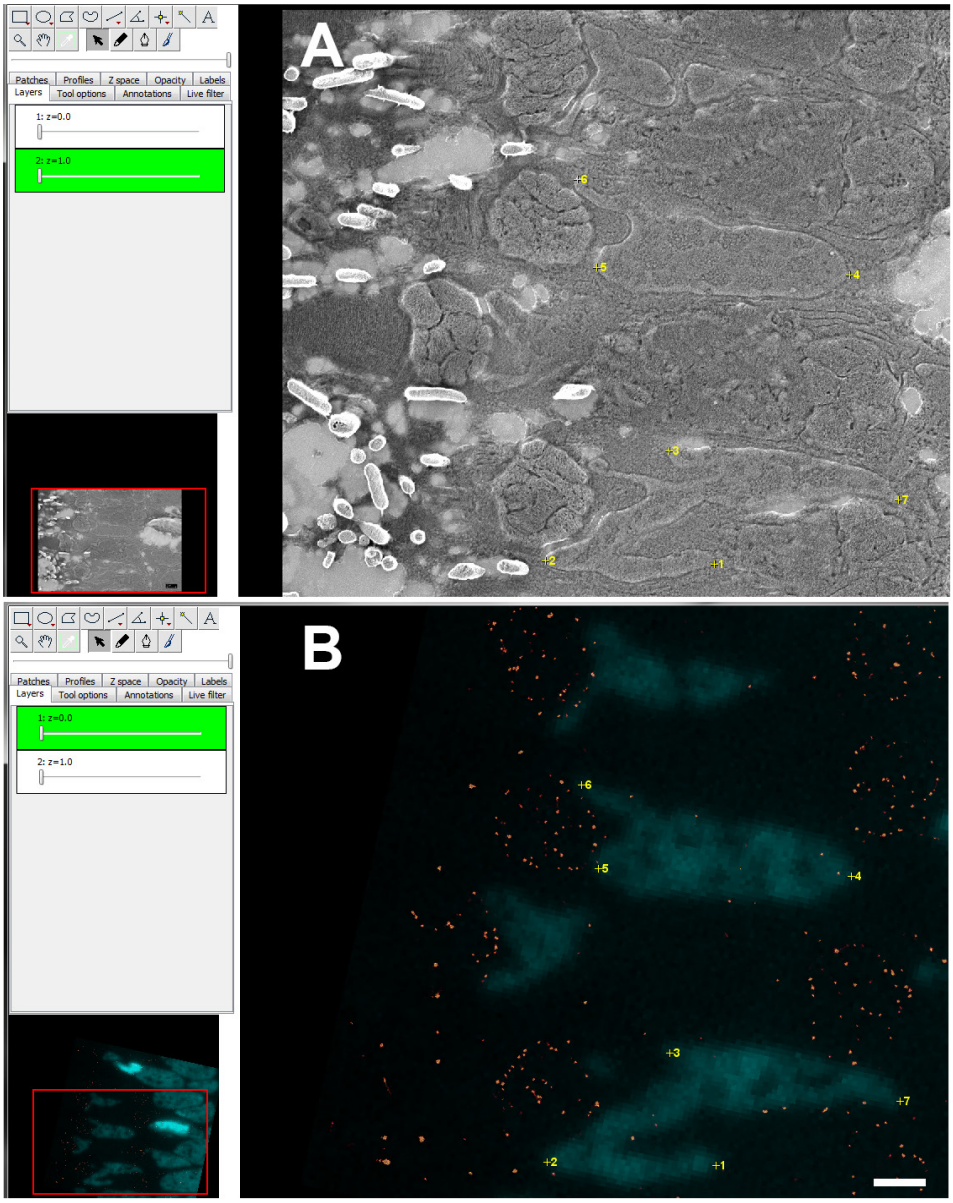

Chapter 4. The ciliopathy protein TALPID3/ KIAA0586 acts upstream of Rab8 activation in zebrafish photoreceptor outer segment formation and maintenance

Ojeda Naharros, I., Cristian, F.B., Zang, J., Gesemann, M., Ingham, P., Neuhauss, S.C.F. and Bachmann-Gagescu, R.*

University of Zurich, Institute of Molecular Life Sciences
Winterthurerstrasse 190, 8057
Zurich, Switzerland
Life Science Zurich Graduate School, PhD. Program in Neurosciences

* Corresponding author
Ruxandra Bachmann-Gagescu
ruxandra.bachmann@imls.uzh.ch

In submission

Personal contribution: Participated in testing of antibody, immunofluorescence staining and imaging, participation in manuscript preparation

Abstract

Ciliopathies are a group of human disorders caused by dysfunction of primary cilia, ubiquitous microtubule-based organelles involved in signal transduction. Cilia are anchored inside the cell through basal bodies (BBs), modified centrioles also acting as microtubule-organization centers. Photoreceptors (PRs) are sensory neurons, whose primary cilium has evolved into a highly specialized compartment called the outer segment (OS) responsible for sensing incoming light. Thus, ciliopathies often course with retinal degeneration.

KIAA0586/ TALPID3 (*TA3*) is a novel ciliopathy gene. Ta3 localizes to centrioles and is required for ciliogenesis in various model organisms through a role in BB docking dependent on the small GTPase Rab8. The requirement for Ta3 during ciliogenesis precludes the investigation of potential additional roles in ciliary function in mouse or chick models. To address this question, we analyzed the role of Ta3 in retinal photoreceptors of zygotic *ta3-/-* zebrafish mutants, in which maternally-derived Ta3 contribution partially rescues ciliogenesis at early developmental stages.

Zygotic *ta3-/-* zebrafish undergo progressive retinal degeneration, with a majority of PRs showing undocked BBs and lack of OSs with concomitant intracellular accumulation of the photopigment opsin and progressive loss of cell polarity. A subset of PRs display normally docked BBs and extended OSs, due to persistence of maternally-deposited Ta3. However, even in PRs with normally docked BBs, we observe progressive shortening of OSs, intracellular accumulation of opsins and loss of polarized cell shape, suggesting roles for Ta3 beyond BB docking in ciliary-directed trafficking or cytoskeletal maintenance. While we observe no substantial defects in Rab8a recruitment, overexpression of constitutively active Rab8a rescues OS formation but not cell shape abnormalities. Together, these results indicate that the role of Ta3 in early ciliogenesis is upstream of Rab8a activation but that its putative role in cell shape maintenance is independent of Rab8a function.

Author summary

Ciliopathies are a group of human disorders caused by dysfunction of ubiquitous organelles called primary cilia which are important for signal transduction. Photoreceptors (PRs) sense incoming light through the outer segment (OS), a specialized compartment that arises from a modified primary cilium. Thus, retinal degeneration is frequent in ciliopathies.
Mutations in the ciliopathy gene *KIAA0586/TALPID3* cause Joubert syndrome and lethal ciliopathies. To elucidate the function of TALPID3 in PRs, we studied *talpid3* (*ta3)* mutant zebrafish, which undergo progressive retinal degeneration. The majority of *ta3-/-* PRs do not form OSs due to a defect in the initial steps of cilium formation. In a small subset of PRs, persistence of maternally-deposited Ta3 rescues this phenotype. However, progressive abnormalities in cell shape and OS maintenance occur even in these initially normal-appearing PRs, indicating that Ta3 plays additional roles beyond cilium formation. We further show that a constitutively active form of the small GTPase Rab8 rescues the OS formation defect but not the subsequent cell shape defect. Together, our results indicate that Ta3 plays a role upstream of Rab8a activation in the initial steps of cilium formation and additional roles in ciliary function and cell shape maintenance that are independent of Rab8.

Introduction

Ciliopathies are a group of human disorders caused by primary cilium dysfunction and unified by a wide array of overlapping phenotypes including central nervous system (CNS) malformations, kidney cysts or retinal degeneration (Badano et al., 2006; Goetz and Anderson, 2010; Hildebrandt et al., 2011). Primary cilia are ubiquitous organelles that consist of a mother centriole-derived basal body (BB), a microtubule-based axoneme and a specialized membrane that harbors proteins required for signal detection (Singla and Reiter, 2006). Indeed, the main function of primary cilia lies in transduction of a wide range of extracellular signals, including important morphogens such as Hedgehog (Hh) (Goetz and Anderson, 2010) or environmental stimuli such as light (Fliegauf et al., 2007; Insinna and Besharse, 2008). Light transduction is carried out by retinal photoreceptors (PRs), which are highly polarized sensory neurons with a synaptic terminal, a cell body, an inner segment (IS) and a modified primary cilium called the outer segment (OS) (Bloodgood, 1990; Kennedy and Malicki, 2009). The OS consists of stacks of membranous disks which are organized around a microtubule-based axoneme and which contain proteins required for phototransduction, such as the photopigment opsin (Khanna, 2015). The connecting cilium, equivalent to the transition zone in other primary cilia (Bloodgood, 1990), joins the OS with the IS. The OS is, like all cilia, devoid of protein synthesis machinery (Nachury et al., 2010; Khanna, 2015).

Thus, the specialized protein enrichment of the OS membranes is enabled by polarized vesicle trafficking from the IS, which is in part regulated by the small GTPase Rab8 (Deretic et al., 1995; Nachury et al., 2007; Ward et al., 2011).

Trafficking to the ciliary compartment is coupled to cilium formation, since many proteins, including Rab8, are involved in both processes (Kobayashi and Dynlacht, 2011). Ciliogenesis occurs in quiescent cells, when the BB is released from its centrosomal spindle-forming role in cell division (Ishikawa and Marshall, 2011). It is, therefore, a highly regulated process that involves centriolar satellite dispersion, centriole maturation, ciliary vesicle (CV) docking onto the BB, docking of the whole structure to the plasma membrane and extension of the nascent axoneme and membrane (Reiter et al., 2012). Rab8 has been shown to play a crucial role in the docking steps of ciliogenesis (Kobayashi et al., 2014).

KIAA0586, orthologue of *talpid3 (ta3)*, is a novel ciliopathy gene (Alby et al., 2015; Bachmann-Gagescu et al., 2015c; Malicdan et al., 2015; Roosing et al., 2015; Stephen et al., 2015), thought to be involved in the early steps of ciliogenesis (Yin et al., 2009; Stephen et al., 2013). Mutations in *KIAA0586* lead to Joubert syndrome (JBTS) (Bachmann-Gagescu et al., 2015c; Roosing et al., 2015), a canonical ciliopathy characterized by a pathognomonic hindbrain malformation (Doherty, 2009; Romani et al., 2013; Poretti et al., 2014) and associated with variable retinal dystrophy and fibrocystic renal disease, among other typical ciliopathy phenotypes (Bachmann-Gagescu et al., 2015c; Bachmann-Gagescu et al., 2015a). More severe ciliopathies with fetal lethality such as hydrolethalus phenotype, consisting of major hydrocephaly and brain malformations, and short-rib polydactyly, including skeletal dysplasia, have also been associated with causal *KIAA0586* mutations (Alby et al., 2015).

The *KIAA0586/TALPID3* (*TA3*) gene was originally identified in a spontaneous chicken mutant displaying phenotypes characteristic of defective Hh signaling: craniofacial malformations, left-right asymmetry defects, polydactyly and neural tube mispatterning (Buxton et al., 2004; Davey et al., 2006). These Hh defects were subsequently shown to be secondary to a defect in ciliogenesis (Yin et al., 2009), since Hh cannot be transduced properly in the absence of a functional primary cilium (Goetz and Anderson, 2010). Indeed, a crucial role for Ta3 in BB-migration and docking was identified in neural tube cells of a *Ta3* conditional knock-out mouse model (Bangs et al., 2011) and in ependymal cells in the chick mutant, in which newly generated BBs remain undocked in the cytoplasm (Stephen et al., 2013). Consistent with these findings, cell culture studies revealed that Ta3 localizes to a rim crowning both the mother and daughter centrioles in RPE1 cells, and that it plays an essential role in early ciliogenesis steps including centriolar satellite dispersal, recruitment of Rab8 and BB docking to the plasma membrane (Kobayashi et al., 2014).

While the severe human phenotypes of hydrolethalus and short-rib polydactyly syndromes may be consistent with a severe ciliogenesis defect, the

mechanisms underlying the relatively milder phenotypes of JBTS caused by *KIAA0586/TA3* mutations are unlikely to be explained by complete absence of cilia. In particular, the role of TA3 in retinal photoreceptors remains unexplored. To address this question, we analyzed the retinal phenotypes of zebrafish *ta3* mutants, which display normal PR differentiation but progressive PR cell death. We found OS formation to follow an all-or-nothing pattern in *ta3-/-* PRs, whereby the majority of PR formed no OS at all, due to a defect in BB positioning, while a subset formed structurally normal OSs due to the presence of maternally-deposited Ta3. However, even PRs with an initially normal-appearing OS progressively developed intracellular opsin accumulation, abnormalities in cell shape and polarity and shortening of the OS, indicating that Ta3 plays additional roles beyond BB docking in maintenance of cell shape and/or ciliary-directed transport of ciliary components. Finally, while we observed no substantial defects in Rab8a recruitment, overexpression of constitutively active Rab8a rescued OS formation but not cell shape abnormalities. Together, these results indicate that the role of Ta3 in early ciliogenesis is upstream of Rab8a activation but that its putative role in cell shape maintenance is independent of Rab8a function.

Results

Normal PR differentiation followed by progressive degeneration in ta3 zebrafish mutants

Previously reported phenotypes of zebrafish *ta3* mutants include cystic kidneys in zygotic mutants and curved body shape, mild cyclopia and left-right asymmetry disruption in maternal-zygotic (mz) mutants (Ben et al., 2011). To investigate the role of Ta3 in retinal photoreceptors (PRs), we studied these three previously generated *ta3* alleles: *i262*, *i263* and *i264*, each of which harbours a small indel leading to frameshifts in exon 11, encoding part of the fourth coiled-coil domain (Ben et al., 2011). The phenotypes of these three mutants were indistinguishable from each other and will be referred to hereafter as *ta3-/-* or *ta3* mutants. Given that mz *ta3* mutants die at 4 days post fertilization (dpf), a stage at which PRs are still differentiating, we focused our analysis on zygotic mutants that live until 12-14 dpf. Initial stages of eye development up to 2 dpf were unaffected in *ta3* mutants, with normal retinal lamination (Fig. 1 A-F) and formation of the PR cell layer. Differentiation into various specialized PR subtypes was unaffected, as seen with zpr1 (Fret43) antibody staining (Fig. 1 G-H'), to mark the cell bodies of red-green cones (Zou et al., 2008) and with the *tg(zfRH1-3.7B:EGFP)* transgenic line that highlights rods (Hamaoka et al., 2002) (Fig. 1 I-J'). At 3 dpf, a time point when the rod photoreceptors start to differentiate in a ventral patch of the eye, the number of RH1-3:EGFP

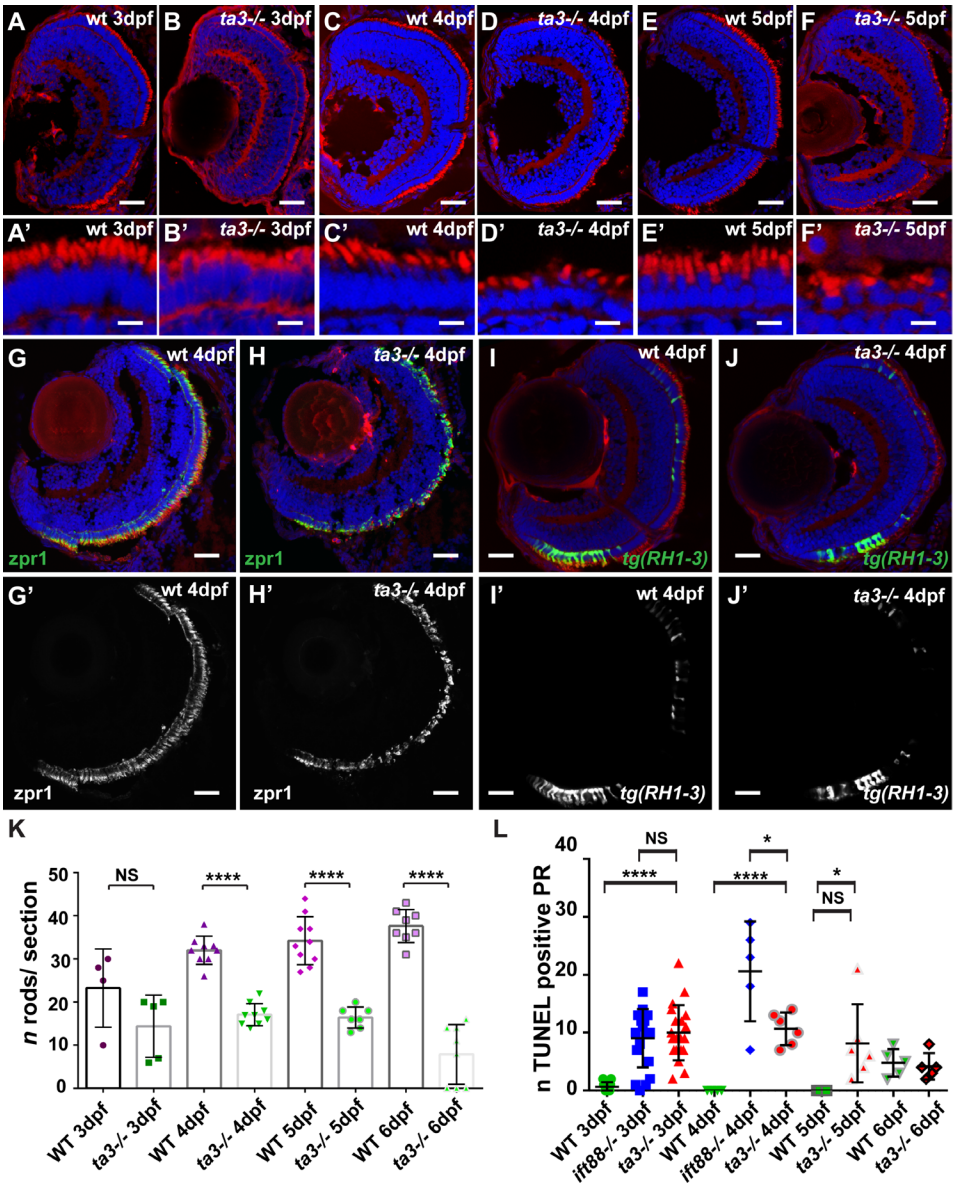

Figure 1: *ta3* mutants show normal PR differentiation followed by progressive retinal degeneration
(A-F) Retinal lamination is unaffected in *ta3* mutants as seen on cryosections at 3-4-5 dpf stained with the lipophilic dye BODIPY (red) to mark cell membranes and outer segments and DAPI (blue) to mark nuclei. Note the reduced number of PRs with OSs and the progressive cell shape changes in *ta3* mutants (B'-D'-F') compared to wildtype (wt) (A'-C'-E'). (G-J') Photoreceptors differentiate into specific subtypes: red-green cones marked by anti-zpr1 staining (green in G-H) and rods marked by the *tg(zfRH1-3.7B:EGFP)* line (green in I-J). (K) Numbers of rods per single confocal section, quantified using the *tg(zfRH1-3.7B:EGFP)* line, are initially not significantly different between wt and *ta3* mutants but decrease in mutants over time. ****$p<0.0001$, Student's t-test. (L) Progressive PR cell death is moderate in *ta3* mutants compared to *ift88* mutants as seen with a TUNEL assay. Quantification was performed on confocal stacks of identical thickness on stained cryosections. *$p<0.05$, ****$p<0.0001$, Student's t-test. In (K) and (L) each data point represents the number of positive cells on a single section for one larva. Scale bars are 30 µm in A-F, 4 µm in A'-F' and 20 µm in G-J').

positive PRs was not significantly different compared to controls (Fig. 1 I-J', Fig. 1 K and Fig. S1). At this stage however, PR cell death became apparent as seen with TUNEL assay (Fig. 1 L and Fig. S2). The extent of cell death was compared to that observed in the ciliary mutant *oval*, which harbours a nonsense mutation in the intraflagellar transport gene *ift88* that causes substantial PR cell death (Tsujikawa and Malicki, 2004; Sukumaran and Perkins, 2009), leading to quasi-absence of PRs in the central retina by 5 dpf. Compared to *oval* mutants, *ta3* mutant retinae showed a similar extent of PR cell death at 3 dpf, but less severe cell death at 4 dpf (Fig. 1 L and Fig. S2). Consequently, PRs were still present in the central retina at 5 dpf and beyond in *ta3* mutants, despite a thinning of the PR cell layer (Fig. 1 E-F' and Fig. S3). Together, these data indicate that PRs differentiate normally in *ta3* mutants but that moderate PR cell death occurs starting at 3 dpf, leading to a reduction in the number of PRs.

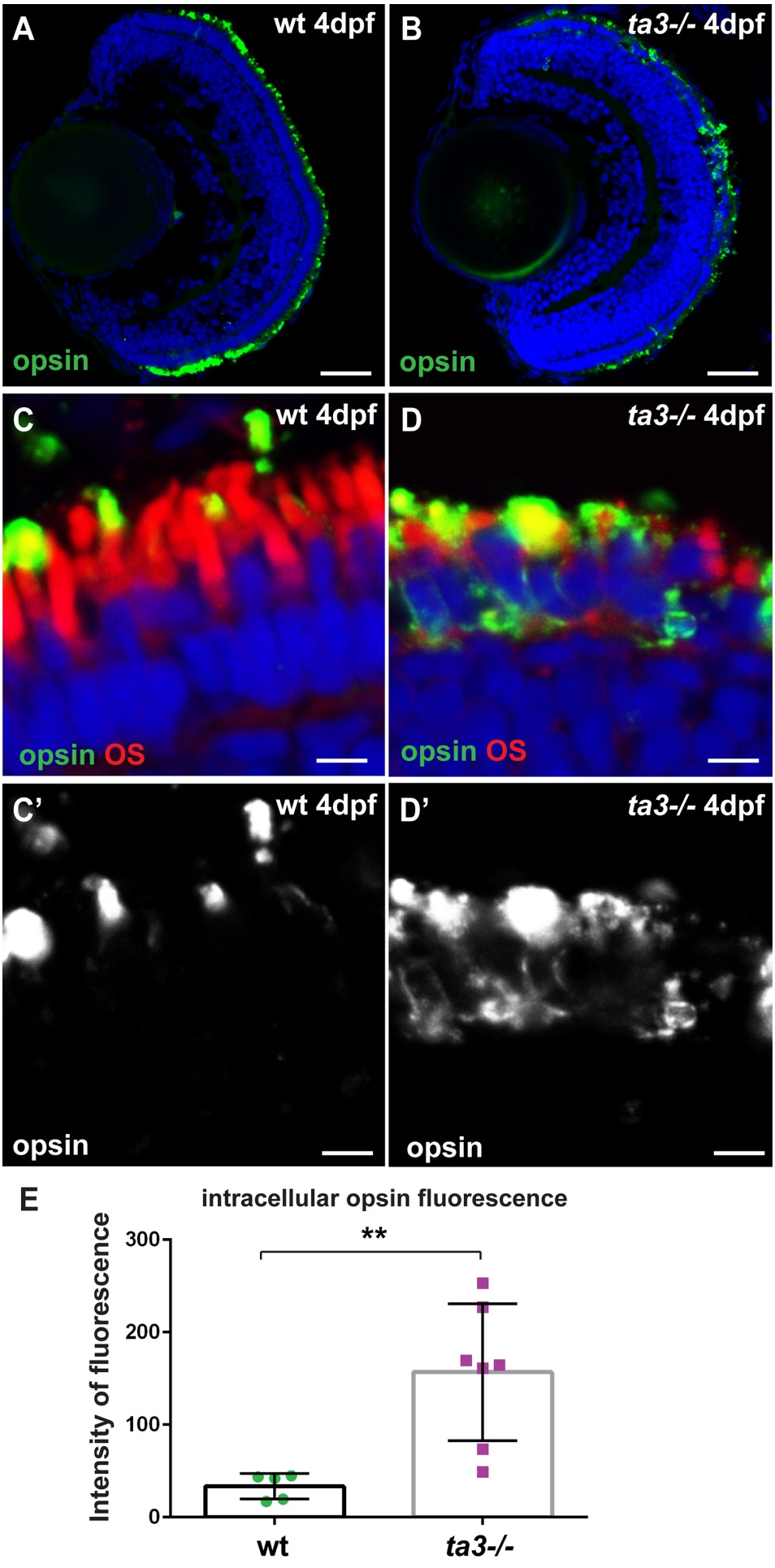

Figure 2: Marked intracellular opsin mislocalization as a cause for PR cell death

(A-B) Marked intracellular opsin accumulation on 4 dpf cryosections stained with 4D2 antibody (green) recognizing rhodopsin and red-green cone opsin on whole eye cryosections. Nuclei are counterstained with DAPI. (C-D') Higher magnification image of the PR cell layer on wildtype (C) and *ta3* mutant (D) cryosections at 4 dpf stained with the 4D2 antibody (green in C-D and white in C'-D') and with BODIPY (red in C-D) to highlight the outer segments (OS). Note the substantial intracellular opsin accumulation in mutant PRs in D-D'. (E) Quantification of the intracellular fluorescence demonstrates significantly increased levels in *ta3* mutants. Each data point represents the average intracellular fluorescence of approximately 20 PRs from one larva; the fluorescence intensity is normalized for area. ***p=0.0046*, Student's t-test. Scale bars are 30 µm in A-B and 4 µm in C-D'.

Marked intracellular opsin mislocalization as a cause for PR cell death

PR cell death in ciliary mutants is thought to be caused by intracellular opsin accumulation, since activation of the photopigment upon light exposure in the cytoplasm exerts a toxic effect (Marszalek et al., 2000; Chinchore et al., 2009; Lopes et al., 2010). We therefore determined whether opsins accumulate intracellularly in *ta3* mutant photoreceptors by immunohistochemistry using antibodies against opsin (4D2 antibody recognizing rhodopsin and red-green cone opsin). We observed significant intracellular accumulation of opsins in *ta3-/-* rods and cones at 4 dpf (Fig. 2; quantification of fluorescence in the cell body Fig. 2 E; $p=0.0046$, Student's *t*-test). This intracellular opsin accumulation was already visible at 3 dpf and persisted until 6 dpf, the latest stage analysed. Substantial variability was observed in the amount of intracellular opsin accumulation even between PRs in the same retina, with some PRs demonstrating normal opsin localization to the OS, while strong signal was mainly detected in the cell body of other PRs. Thus, the observed intracellular opsin accumulation may account at least in part for the observed PR cell death in *ta3* mutants.

Loss of Ta3 leads to visual function loss

To assess the consequences of intracellular opsin accumulation and PR cell death on visual function, we performed electroretinograms (ERG) at 6 dpf to determine the electrical response of the retina to bright light stimuli. The ERG response was highly significantly decreased in *ta3* mutants compared to wildtype (wt) even at the brightest light intensities (representative curves for wt and *ta3-/-* larvae in Fig. 3 A, quantification in Fig. 3 B; $p<0.0001$, Student's *t*-test). Therefore, the observed retinal PR degeneration and opsin mislocalization are associated with strongly decreased visual sensitivity in *ta3* mutant zebrafish.

Deficient outer segment development in ta3-/- larvae

Mutations in cilia-related genes frequently lead to abnormal formation and/or function of PR OSs given that these arise from highly specialized primary cilia (Kennedy and Malicki, 2009). At 3 dpf, the majority of wildtype (wt) PRs have started developing OSs as seen on cryosections stained with the lipophilic dye BODIPY which highlights the stacks of membranes composing the OSs (Fig. 4 A). In *ta3* mutants however, we observed a significant reduction in the proportion of PRs forming OSs compared to wt (Fig. 4 B; quantification in Fig. 4 C, $p<0.01$, Student's *t*-test). These findings were confirmed with transmission electron microscopy (TEM), showing that the majority of wt PRs had already elongated OSs at 3 dpf (Fig. 4 D) and that those PRs that appeared to still lack OSs on cryosections had started the process of membrane stacking (Fig. 4 D'). In contrast, no attempt

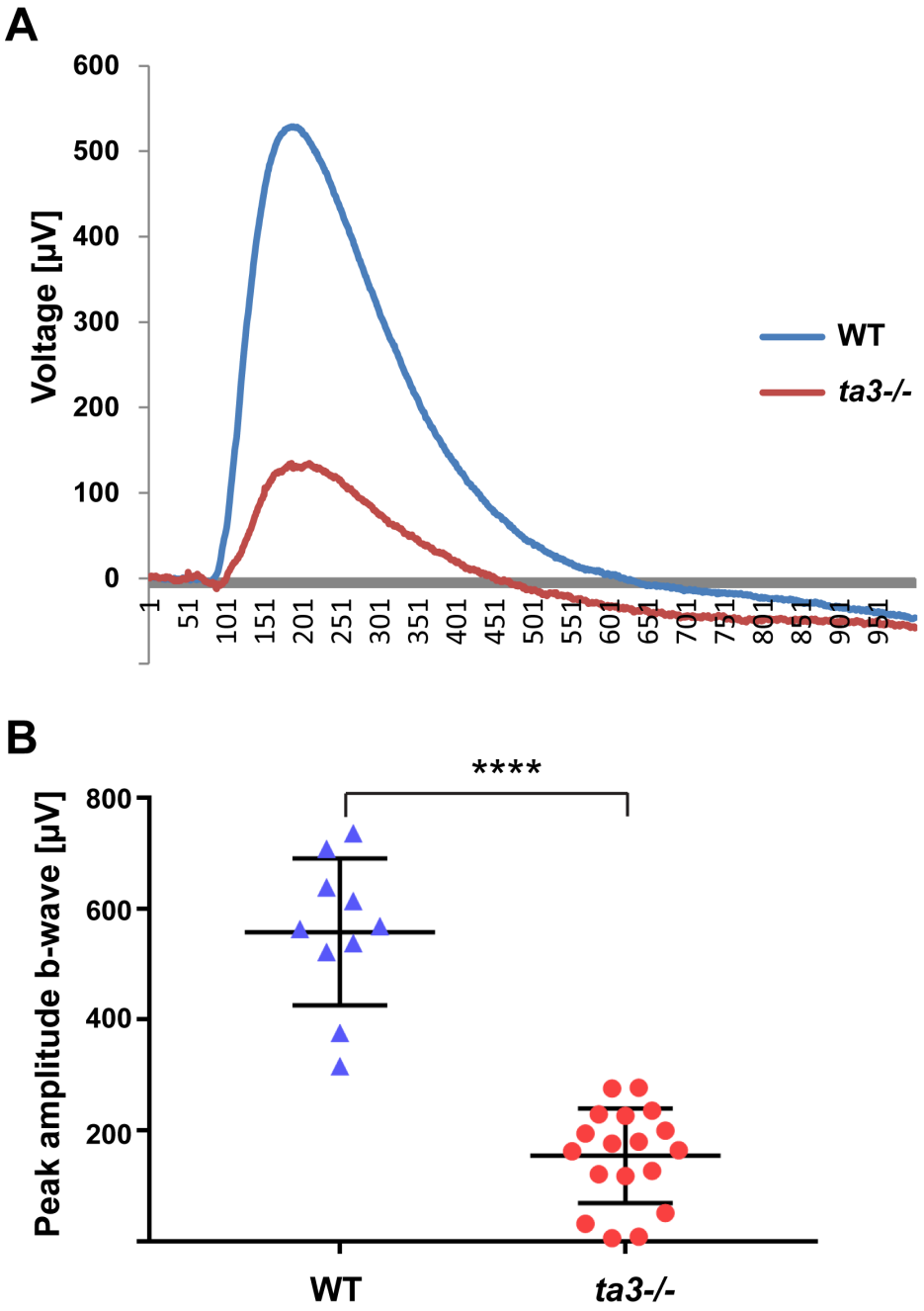

Figure 3: Loss of Ta3 leads to visual function loss
(A) Representative electroretinogram (ERG) recordings of wildtype (WT, blue curve) and *ta3* mutant (red curve) 6 dpf larvae exposed to light stimuli of 7000 lux (bright light intensity). (B) Average b-wave peak responses for WT and ta3 mutants (n = 18 *ta3* mutant animals and 10 WT animals). Bars represent standard deviation. *****p<0.0001*, Student's t-test.

at OS formation with membrane stacking was observed in the majority of *ta3-/-* PRs (Fig. 4 E-E'). However, the OSs that did develop in *ta3* mutants had normal morphology, as can be appreciated both on cryosections (Fig. 4 B) and with TEM (Fig. 4 E-F'). The stacks of membrane disks were regularly organized and the basal body and connecting cilium indistinguishable from those seen in wt. Moreover, OS length was not significantly different between wt and *ta3* mutants, as measured on 3 dpf cryosections (Fig. 4 G). Together, these results indicate that OS development in *ta3* mutants follows an "all or nothing" pattern: while the majority of PRs do not develop any OSs, those that do develop appear morphologically normal initially.

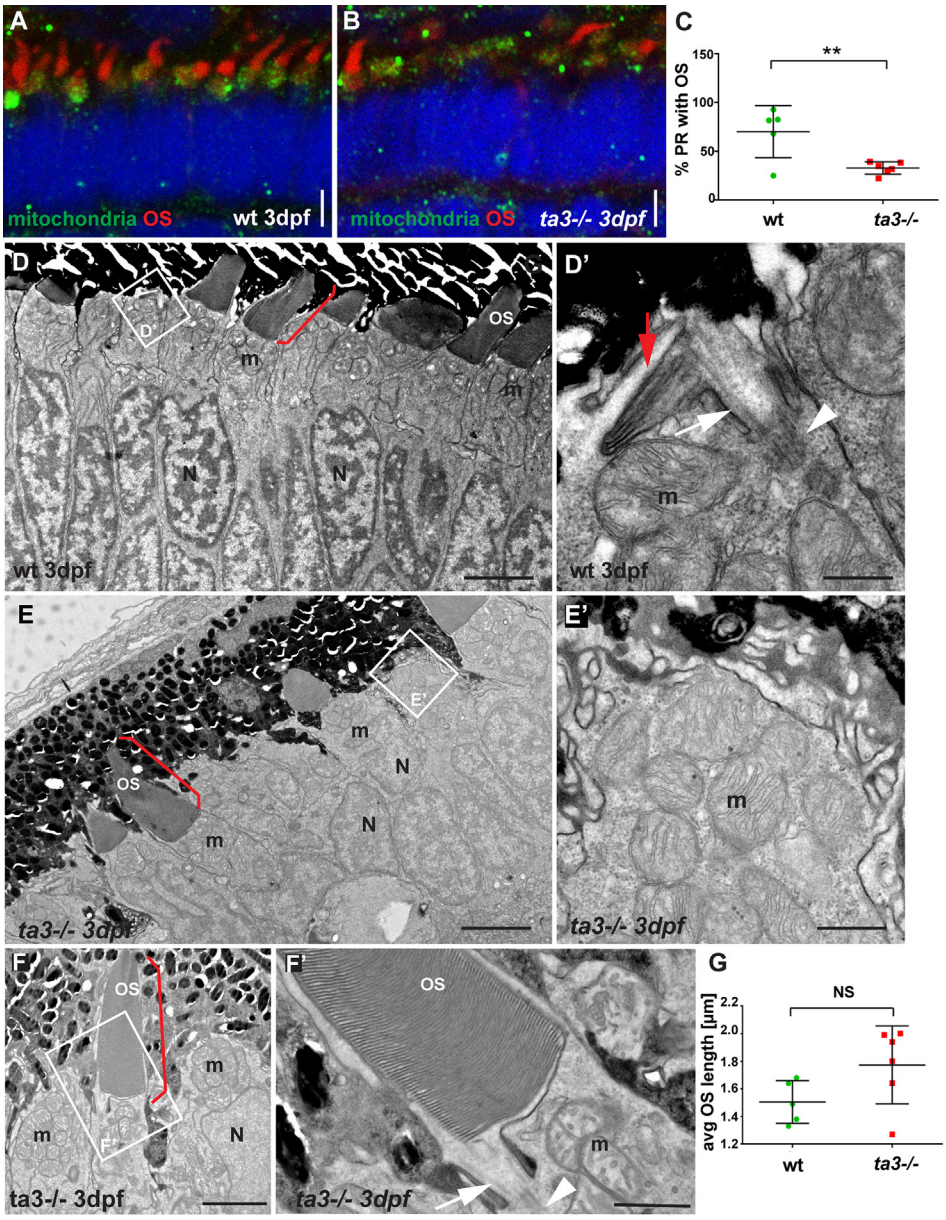

Figure 4: Deficient OS development in ta3-/- larvae
(A-B) 3 dpf cryosections stained with BODIPY to mark the OSs (red) and using the VDAC1 antibody to mark the mitochondrial cluster (green) show reduced numbers of OSs in *ta3* mutants (B) compared to wildtype (wt) (A). (C) Quantification of the proportion of PRs with extended OSs in wt (green circles) compared to ta3 mutants (red squares) shows significantly reduced PRs with OSs in mutants (***p<0.01*, t-test). (D-F') Transmission electron microscopy images of 4 dpf wt (D-D') and *ta3* mutant (E-F') retinae. (D-D') The majority of wt PRs have extended OSs (red bracket in D) or are starting to stack membranes to do so (red arrow in D'). Note the BB (arrowhead in D') and the connecting cilium (white arrow in D') in wt photoreceptors. (E-E') In contrast, in *ta3-/-* PRs, only a minority of PRs have extended OSs (red bracket in E), and no attempt at membrane stacking is observed in the other PRs (E'). (F) Note the normal appearance of the OSs that have extended in the mutants, including the structurally normal connecting cilium (arrow in F') and basal body (arrowhead in F'). (G) Quantification of average OS length on cryosections (from A-B) shows no significant difference between 3 dpf wt and *ta3* mutants (*p=0.899*, Student's t-test). Each data point represents a single larva. N nuclei, m mitochondria, OS outer segments. Scale bars are 4 µm in A-B, 3 µm in D and E, 0.5 µm in D', 2 µm in F, 1 µm in E'-F'.

Abnormal BB localization and impaired docking in ta3-/- PR underlie the OS development defect

OS development requires docking of the BB and extension of the axoneme before stacking of membrane disks can occur (Pearring et al., 2013). Given the described role for Ta3 in ciliogenesis, we evaluated if lack of OS development in *ta3-/-* PR was due to impaired BB docking. Indeed, while BBs marked with anti-Centrin antibodies were observed almost exclusively apically to the mitochondrial cluster and just below the BODIPY-marked OSs in wildtype (wt) retinae (Fig. 5 A-A' and 5 C), we observed a significantly increased proportion of PR with more basally located BBs in *ta3* mutants (Fig. 5 B-B', 5 D and quantification in 5 E; **** $p<0.0001$, Student's *t*-test). BBs were seen below and sometimes within the mitochondrial cluster by TEM (Fig. 5 F-F''), supporting a role for Ta3 in BB docking in retinal PRs and explaining the lack of OS development in these PRs.

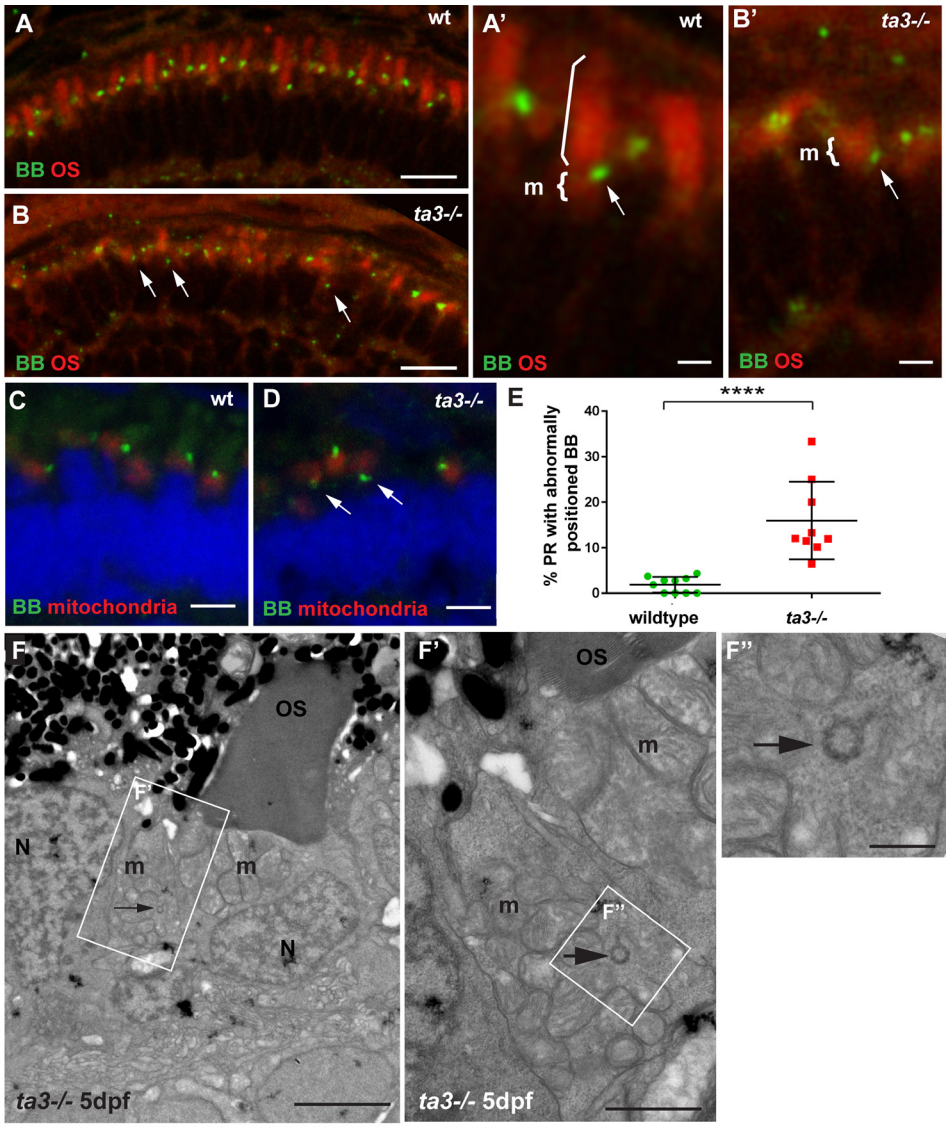

Figure 5: Abnormal BB localization in *ta3-/-* PRs underlies the OS development defect

(A-B) 4 dpf cryosections stained with BODIPY (red) to mark the membranes of the outer segment and mitochondrial cluster and with anti-Centrin antibody (green) to mark the basal bodies, show aberrant localization of BB below the mitochondria in *ta3-/-* PRs. In wildtype (wt) PRs, the centrin-marked BB is located just basal to the OS and apical to the mitochondrial cluster (arrow in A'), while this localization is lost in a substantial number of *ta3* mutant PRs (arrow in B'). (C-D) Immunohistochemistry on 4 dpf cryosections with anti-VDAC1 antibody (red) to mark the mitochondria and anti-Centrin antibody to mark the BB showing aberrant basal positionings of BBs in *ta3* mutants (arrows in D) compared to wt (C). (E) Quantification of the proportion of 4 dpf PRs with aberrant BB positioning based on immunohistochemistry with anti-Centrin antibody, reveals a statistically highly significant increase of aberrantly positioned BBs in *ta3* mutants (*****p<0.0001*, Student's t-test). Each data point represents one larva. (F-F") TEM images of 5 dpf PRs showing presence of a BB in cross-section (arrow) within a mitochondrial cluster. (F') is the boxed area in (F) and (F") is the boxed area in (F'). N nuclei, m mitochondria, OS outer segments. Scale bars are 10 µm in A-B, 3 µm in A'-B', 4 µm in C-D, 3 µm in F, 1 µm in F' and 0.5 µm in F".

Maternal Ta3 contribution rescues OS development in a subset of PRs of zygotic ta3-/-

While the majority of PRs in *ta3-/-* retinae lack OS, which can be explained by impaired ciliogenesis secondary to BB positioning defects, a minority of PRs in these mutants do develop OSs that initially appear normal. We hypothesized that in these PRs, maternally-derived Ta3 might rescue the ciliogenesis defect and allow normal extension of OSs. Indeed, mRNA and proteins from maternal origin, provided in the zebrafish egg, may persist and function several days into larval development. To test this hypothesis, we developed an antibody directed against the zebrafish Ta3 protein and co-stained cryosections with anti-Centrin antibody marking the BBs (Fig. 6 A-B). In wildtype zebrafish, Ta3 was found to co-localize with Centrin in retina and brain on sections from 2 dpf to 5 dpf (latest stage analysed; Fig. 6 A-B and Fig. S4) as previously described in RPE1 cells. While endogenous Ta3 protein was detected in both mother and daughter centriole, as previously reported for an EGFP-Ta3 fusion protein in zebrafish (Ben et al., 2011), it appeared to be unequally distributed between them (Fig. 6

A-B"). Given the lack of antibodies against mother centriole-specific proteins in zebrafish, we cannot determine with certainty if Ta3 staining is more pronounced at the mother or at the daughter centriole. However, the strong Ta3 staining observed at the base of acetylated tubulin-marked axonemes suggests that Ta3 is certainly abundant at the mother centriole (Fig. 6 C-C"). In *ta3* mutants, staining using our anti-Ta3 antibody was strongly reduced at 2 dpf in retina and brain, supporting specificity of the antibody and indicating that most *ta3-/-* PRs lack Ta3 protein (Fig. S4). However,

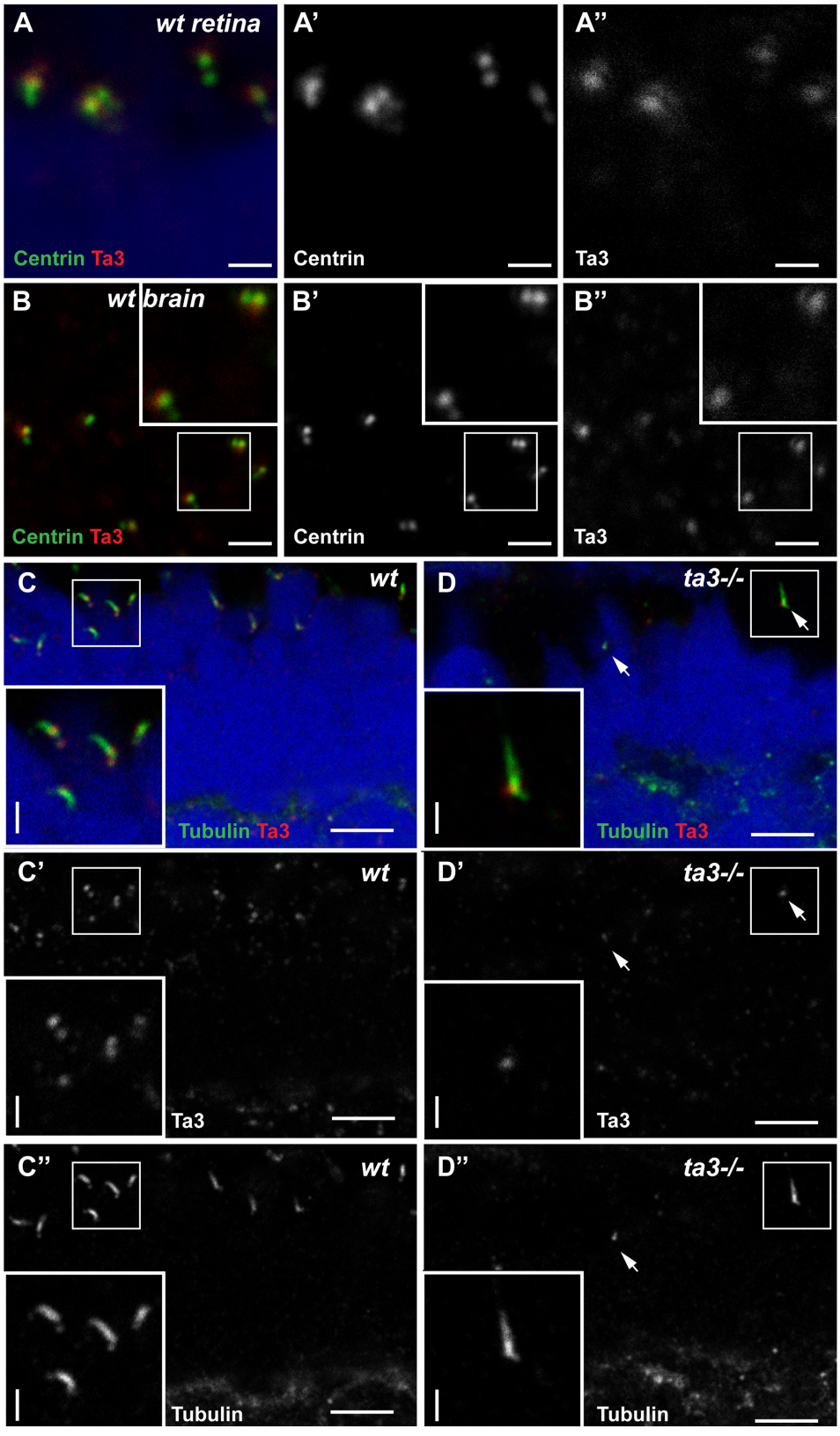

Figure 6: Maternal Ta3 contribution rescues OS development in a subset of PRs of zygotic *ta3-/-*
(A-A") 2 dpf retinal cryosections stained with anti-Centrin to mark BBs (green) and anti-Ta3 show co-localization in wildtype (wt) larvae. Of note, while both mother and daughter centrioles are stained with anti-Ta3 antibody, the staining appears to be asymmetrically distributed. (B-B") 2 dpf cryosections of wt brain stained with anti-Centrin and anti-Ta3 shows similar asymmetric co-localization at the BBs. (C-C") Immunohistochemistry of 4 dpf retinal cryosections shows presence of Ta3 (red) at the base of ciliary axonemes stained with anti-acetylated tubulin antibody in wt larvae. (D-D") While in *ta3* mutant larvae, the Ta3 signal is mostly abolished, isolated BBs still have positive Ta3 signal (arrow) and in those cases an acetylated-tubulin marked axoneme is visible. Scale bars are 3 µm in A-A", 6 µm in B-B", 4 µm in C-D" and 2 µm in the insets in C-D".

we observed persistent Ta3 staining up to 4 dpf in isolated mutant PRs and in these PR, extended axonemes were present as highlighted with anti-acetylated Tubulin staining (Fig. 6 D-D''). Together, these results indicate that Ta3 is located at both centrioles with likely predominance at the mother centriole in zebrafish PRs, and that isolated PRs of zygotic mutants have maternally-derived Ta3, which rescues the ciliogenesis defects in these cells.

Opsin mislocalization and cell shape abnormalities in PRs with normally formed OSs support roles for Ta3 beyond BB docking

The temporary rescue by maternally derived Ta3 in zebrafish PRs offers the unique opportunity to determine if Ta3 plays additional roles in ciliary function beyond the initial BB docking step required for ciliogenesis. We therefore focused on *ta3* mutant PRs that had extended an initially normal-looking OS at 3 dpf. In these PRs, we observed mislocalization of opsins in the cell body starting at 4 dpf, despite presence of an elongated OS (Fig. 7 A-A''), similar to our observation in PRs that lacked an OS. Even more strikingly, the cell shape of these PRs became abnormal starting at 4 dpf: instead of the typical elongated shape of PRs with clear apico-basal polarity as seen in wildtype PRs, *ta3* mutant PRs took on a rounded morphology, with quasi-disappearance of inner segment space, aberrant localization of the mitochondrial cluster lateral to the now rounded nucleus and progressive shortening of the OS (Fig. 7 C-C', 7 F and Fig. S5). To determine if this phenotype was secondary to non-cell autonomous consequences such as loss of tissue integrity, we compared the *ta3* mutants with the *ift88* mutant *oval*. Despite higher rates of PR cell death in *oval* mutants than in *ta3* mutants, *ift88-/-* PR remained more elongated in the apico-basal direction at the same stage as quantified by measuring the ratio of nuclear width over height in immunostained sections of wildtype and in the two mutants (Fig. 7 E). In addition, the loss of elongated cell shape in *ta3-/-* PRs with OSs is already obvious at 4 dpf (Fig. 7 C,F), a stage when PR cell death is less prominent in *ta3* mutants than in *ift88* mutants (Fig. 1 L and Fig. S1). Moreover, while OS length was initially normal at 3 dpf (Fig. 4 G), OSs progressively shorten subsequently, suggesting secondary deficiencies in transport of OS components to the ciliary base in addition to loss of cell polarity and shape (Fig. S5). Together, our results support a role for Ta3 beyond the initial stages of ciliogenesis, possibly in maintenance of cytoskeletal integrity and in ciliary-directed trafficking.

Outer segment development is rescued by constitutively active Rab8a

Initial stages of ciliogenesis require docking of the ciliary vesicle onto the mother centriole, a process in part controlled by the small GTPase Rab8 (Kobayashi et al., 2014). After docking of the BB at the apical membrane, ciliary membrane biogenesis depends on Rab8 as well (Nachury et al.,

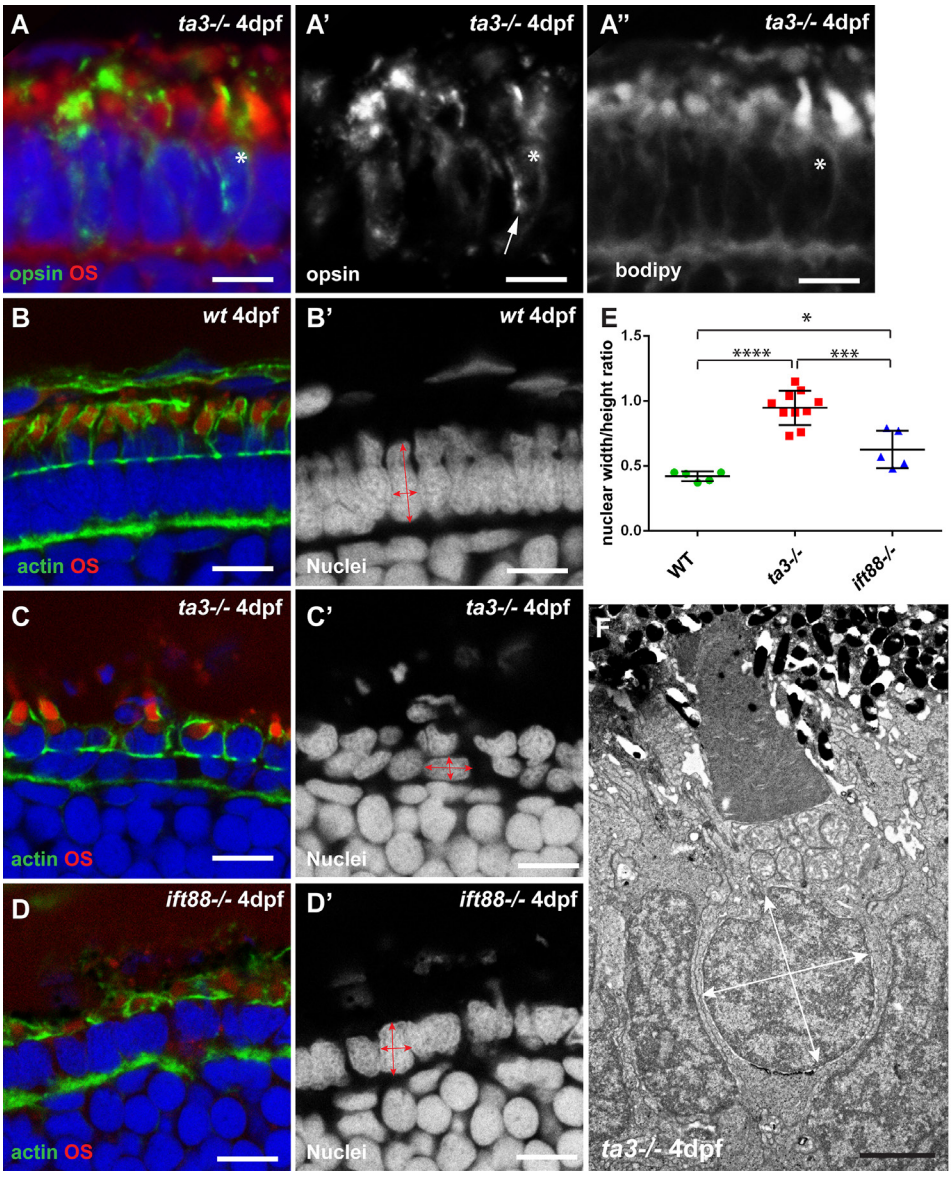

Figure 7: Opsin mislocalization and cell shape abnormalities in PRs with normally formed OSs indicate roles for Ta3 beyond BB docking
(A-A") 4 dpf retinal cryosections stained with BODIPY to highlight the OSs and with anti-opsin antibody (4D2) show intracellular accumulation of opsins also in PRs that have extended a normal-looking OS (arrow in A' and star in A-A"). (B-C') Cell shape abnormalities, highlighted with phalloidin (green) to mark the actin cytoskeleton, become obvious at 4 dpf in *ta3-/-* PRs. While wildtype (wt) PRs display nuclei with clear apico-basally elongated cell shape, highlighted with DAPI (B'), the nuclei become rounded in *ta3* mutant PRs (C') even in the presence of developed OSs (marked by BODIPY). In comparison, nuclei remain oriented more apico-basally in *ift88* mutants (D'), despite lack of any OS. (E) Quantification of the nuclear width/nuclear height ratio (arrows in B'-D') demonstrating strongly significant aberration in nuclear cell shape in *ta3* mutants compared to wt and to *ift88* mutants. Each data point represents the average of ratios for one larva. * $p<0.05$, *** $p<0.001$, **** $p<0.0001$, Student's t-test. (F) TEM image of a 4 dpf *ta3-/-* PR displaying a strikingly abnormal cell shape with loss of inner segment compartment space and rounded nuclear shape (arrows) despite well-stacked membrane disks in the OS. Note in particular the aberrant position of the mitochondrial cluster that becomes more lateral to the nucleus instead of the normal apical position. Scale bars are 4 µm in A-A", 8 µm in B-D and 2 µm in E.

2007). To test whether loss of Ta3 in PRs affects Rab8 localization, as described in RPE1 cells, we transiently expressed a mCherry-tagged version of Rab8a in rods (*rhod:mCherry-Rab8a*) and cones (*TaCP:mCherry-Rab8a*) (Bachmann-Gagescu et al., 2011). In wildtype PRs, punctate localization of Rab8a was observed in the majority of expressing PRs at 4 dpf (Fig. S6). In *ta3* mutants, the proportion of PR with punctate expression was slightly reduced in rods and unaffected in cones, indicating that loss of Ta3 has only a minor effect on Rab8a localization (Fig. 8 D and Fig. S6). Moreover, expression of these transgenic Rab8 forms had no effect on the presence or absence of OS in the expressing PRs (Fig. 8 C, green squares). However, when we transiently expressed a constitutively active form of Rab8a, using the same promoter (*TaCP:mCherry-Rab8aCA*), we observed highly significant rescue of OS development in the PRs expressing this transgene (quantification in Fig. 8 C, $p<0.0001$, Student's *t*-test). Indeed, the vast majority of expressing PRs now displayed a nicely elongated OS (Fig. 8 B-B''). Interestingly, the cell shape defect was not rescued in these PRs, which took on the same rounded appearance as *ta3-/-* PRs that developed OS independently of Rab8aCA expression. Together, these results indicate that the role of

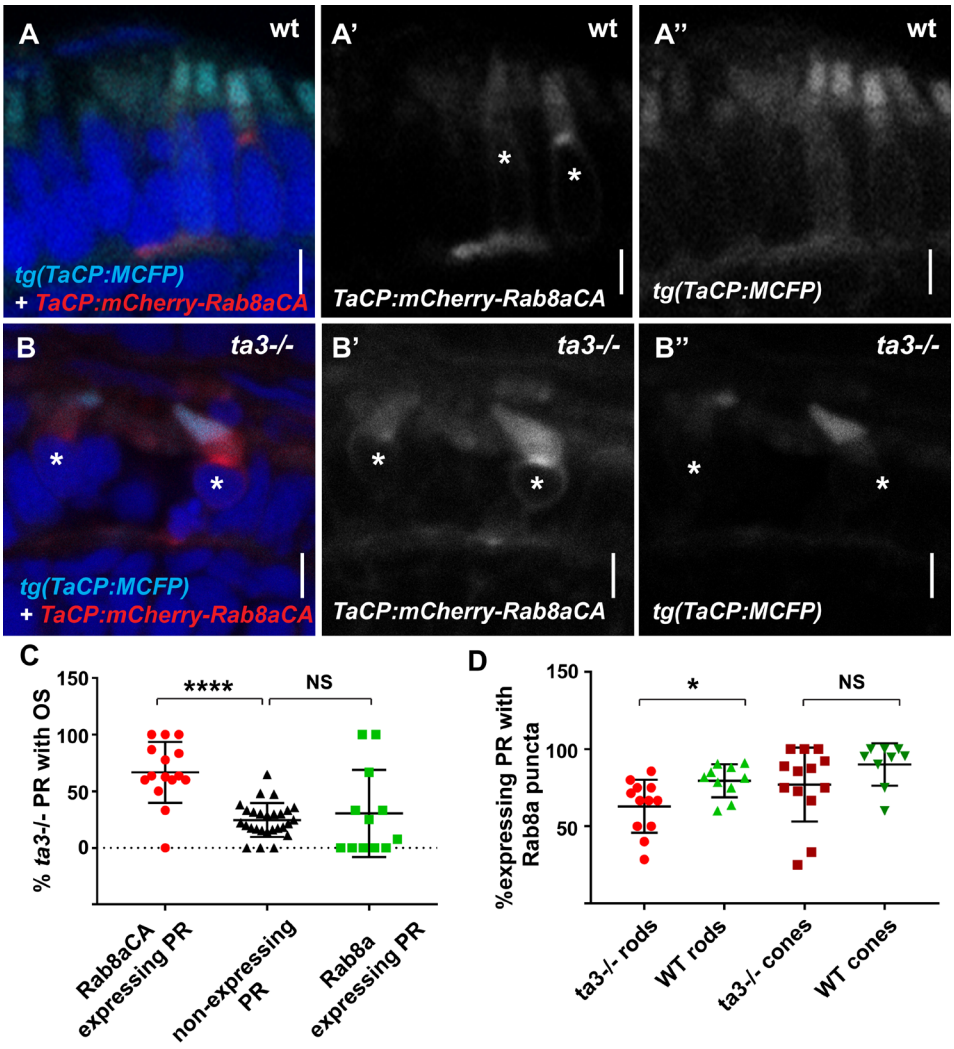

Figure 8: OS development is rescued by constitutively active Rab8a

(A-B) Transient expression of a mCherry-tagged, constitutively active form of Rab8a in cones *(TaCP:mCherry-Rab8aCA)* in the stable transgenic line *tg(TaCP:MCFP)* in which all cone OSs are cyan at 4 dpf. In wildtype (wt) PRs (A-A"), this form of Rab8a accumulates in the inner segment and in the outer segment. In *ta3* mutant PRs (B-B"), a similar expression pattern is visible and the majority of expressing PRs display OSs with normal morphology. (C) Quantification of the proportion of PRs with extended OSs at 4 dpf in ta3 mutants with expression of the constitutively active form of Rab8a (red circles), expression of wt Rab8a (green squares) or without transgenic Rab8a expression (black triangles). Only the constitutively active form of Rab8a rescues OS formation in *ta3* mutants (*****p<0.0001*, Student's t-test). (D) Quantification of the proportion of PRs expressing a mCherry-tagged Rab8a construct in a punctate pattern in rods or cones in wt and *ta3* mutants. Rab8a localization was not significantly different between wt and mutant cones and only marginally altered in *ta3-/-* rods (**p<0.05*, t-test).

Ta3 in early ciliogenesis is upstream of Rab8a activation but that a putative role in cell shape maintenance is not dependent on Rab8a function.

Discussion

KIAA0586/TA3 mutations cause a wide range of ciliopathies in humans, ranging from the milder Joubert syndrome (Bachmann-Gagescu et al., 2015c; Malicdan et al., 2015; Roosing et al., 2015; Stephen et al., 2015), which courses with retinal dystrophy in a subset of individuals, to syndromes associated with fetal lethality such as hydrolethalus syndrome or short-rib polydactyly (Alby et al., 2015). Our analysis using a zebrafish *ta3* mutant is the first model for Ta3-related retinal dystrophy, identifying a role for Ta3 in the development and function of retinal PRs and providing an opportunity for exploring putative roles for Ta3 beyond the initial steps of ciliogenesis. Our findings confirm the previously ascribed function of Ta3 in BB positioning and docking (Yin et al., 2009; Bangs et al., 2011; Stephen et al., 2013) and indicate that this function is upstream of Rab8a activation, since OS extension can be rescued by a constitutively active form of this small GTPase.

While studies in RPE1 cells also indicated a role for Ta3 in ciliary locali-

zation of Rab8 (Kobayashi et al., 2014), we did not observe significantly altered Rab8 localization in zebrafish PRs. This inconsistency may be explained by differences in methodology: during cilium extension, which can be visualized as it proceeds in cultured cells after serum starvation, Rab8 enters the ciliary compartment in control but not in siTa3 treated cells. In zebrafish larvae, cilium extension cannot be induced and thus followed dynamically and Rab8 is not seen within the ciliary compartment (OS) but only as puncta in the cytoplasm, which may represent a different aspect of Rab8 function during ciliary maintenance as opposed to its function during initial ciliary extension.

Indeed, some proteins play important roles both in the initial formation of cilia and in subsequent ciliary maintenance and function (Kobayashi and Dynlacht, 2011). The small GTPase Rab8 for instance is required for the initial steps of ciliogenesis (Yoshimura et al., 2007; Westlake et al., 2011) but also for continuous transport of ciliary cargo, predominantly opsins in PRs (Moritz et al., 2001; Wang et al., 2012; Pearring et al., 2013), essential for the function of the OS. Likewise, Ta3 may play a role not only in the initial steps of cilium formation but also in the long-term maintenance and function of cilia. These additional roles could not be investigated previously, since disrupted ciliogenesis in Ta3-deficient mouse, chick or cell models precluded analysis of further functions for this protein. The partial rescue of OS formation in a subset of PRs by persistent maternally-derived Ta3 in zebrafish zygotic mutants has allowed us to adduce evidence for additional roles for Ta3 beyond BB docking. Indeed, the progressive deterioration of initially normal appearing PRs indicates that Ta3 is also required for maintenance of OSs, cell shape and polarity.

The observed progressive loss of cell shape morphology, intracellular accumulation of opsins and shortening of OSs in initially normal appearing PRs are unlikely to be caused by non-specific causes, such as loss of tissue integrity, for a number of reasons. First, cell death in *ta3-/-* retinae is only moderate when compared to other ciliary mutants such as the *ift88* mutant *oval* which displays massive loss of PRs at 5 dpf. Nevertheless, loss of the typical apico-basally elongated cell shape of PRs is much more pronounced in *ta3* mutants compared to *ift88* mutants. Moreover, this cell shape loss is obvious even at early stages (4 dpf) in PRs that have extended an OS, when the PR cell layer is only little disrupted by cell death. Finally, we observe progressive intracellular polarity defects with displacement of the mitochondrial cluster next to the nucleus instead of its normal apical position, suggesting a loss in cytoskeletal organization. In addition, the progressive shortening of the initially normal OSs and the intracellular accumulation of opsins in PRs with OSs suggest a defect in transport of membranes and cargo towards the ciliary compartment. This could be secondary to loss of cytoskeletal organization as transport of opsin-carrier vesicles, which provide both the cargo and the membranes for the OS stacks, is thought to occur along microtubules (Tai et al., 1999; Lopes et al., 2010; Deretic and Wang, 2012).

Our findings are consistent with recent work which identified TA3 as an interaction partner of the microtubule actin crosslinking factor 1 (MACF1), whose deficiency leads to similar PR phenotypes in mouse retina as we observe in zebrafish (May-Simera et al., 2016). Indeed, mice lacking MACF1 function display deficient ciliogenesis due to lack of BB migration and docking as well as defects in OS maintenance in adult PRs. Moreover, defects in PR cell polarity are observed, leading the authors to propose that TA3 is involved in the coordination of microtubule and actin interactions. A possible model (Fig. 9) supported by our findings would therefore propose that Ta3 plays a role as microtubule-organization center at the BB after it has docked to the apical membrane. Lack of Ta3 function would thus lead to disorganization of the microtubule network and secondary deficits in ciliary-directed transport along these microtubules. In an alternative model, Ta3 could also play a more direct role in ciliary-directed trafficking to explain the intracellular accumulation of opsins and the progressive OS shortening. While we do observe some intracellular accumulation of vesicular structures on transmission electron microscopy, these do not appear to predominate, making this second hypothesis less likely.

Further work will be required to investigate these possible models and un-

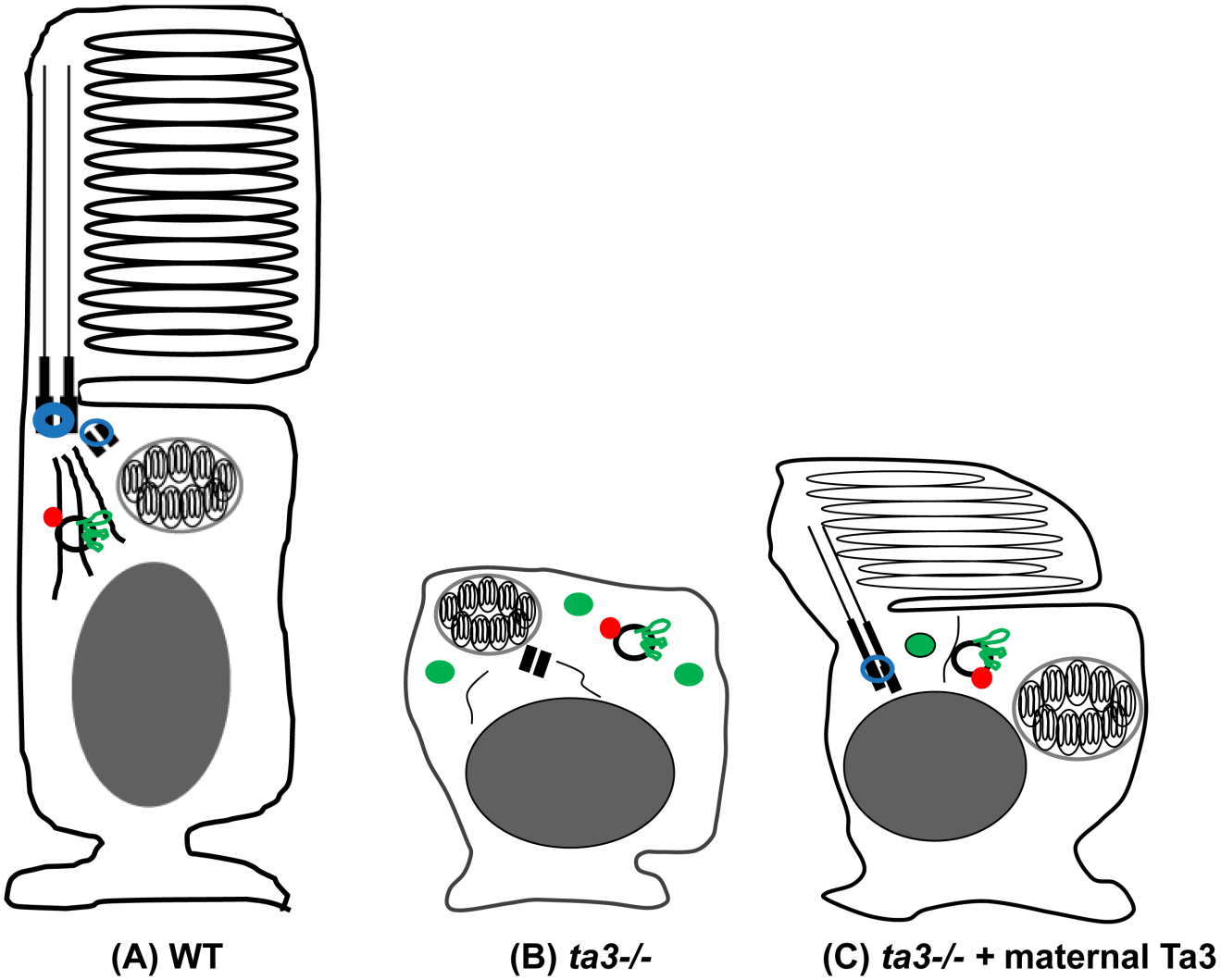

Figure 9: Ta3 function in zebrafish photoreceptors

(A) In wildtype PRs, Ta3 localizes to mother and daughter centrioles (blue ring). The axoneme and OS have extended after Ta3 allowed docking of the BB. The microtubule network is oriented towards the BB and opsin-carrier vesicles (opsins in green), coated with Rab8 (red) move towards the OS to deliver their cargo and membrane. (B) In the majority of PRs in zygotic ta3 mutants, Ta3 loss-of-function leads to aberrant BB positioning and subsequent lack of OS formation. Opsins accumulate in the cytoplasm, microtubules are mis-oriented, the cells lose their elongated shape. (C) In a subset of PRs in ta3 zygotic mutants, Ta3 function persists up to 4 dpf, allowing BB docking and extension of the axoneme and OS. However, as Ta3 vanishes, the OS shortens, opsins accumulate in the cell body and the cell shape becomes abnormal with loss of cell polarity.

ravel the additional functions for Ta3 beyond BB docking, which may be of prime importance for understanding and treating human disease caused by mutations in *KIAA0586/TA3*. Indeed, while a major ciliogenesis defect may underlie the more severe human ciliopathies caused by mutations in this gene, as suggested by analysis of fibroblasts from one fetus with short rib-polydactyly which showed a severe reduction in the proportion of cells extending cilia (Alby et al., 2015), the milder phenotypes of Joubert syndrome may be caused by more subtle ciliary dysfunction, which may in turn be more amenable to specific therapies.

Material and methods

Zebrafish

Zebrafish *(Danio rerio)* were maintained as described (Westerfield). The *talpid3* $^{i262, i263, i264}$ mutants (referred to as *ta3* mutant or *ta3-/-*) were previously described (Ben et al., 2011). The *ift88*^{tz288} *oval* mutant was previously described (Bahadori et al., 2003; Tsujikawa and Malicki, 2004; Sukumaran and Perkins, 2009). The *tg(zfRH1-3.7B:EGFP)* line (Hamaoka et al., 2002), the *tg(TaCP:MCFP)* line (Lewis et al., 2010) and the *tg(TaCP:mCherry-Rab8a)* lines were previously described (Bachmann-Gagescu et al., 2011; Bachmann-Gagescu et al., 2015b). The *tg(Rhod:mCherry-Rab8a)* line was generated by Gateway® (Invitrogen) cloning using a 5'entry clone with the zebrafish Rhodopsin promoter (gift from the Link lab) and a 3' entry clone with Rab8a (Accession number NM_001089562.2). Site targeted mutagenesis using overlapping complementary primers was employed to generate the Q67L (CAG to CTG codon) point mutation leading to constitutively active Rab8a (Peranen et al., 1996; Moritz et al., 2001). The primer sequences used were (modified nucleotides are indicated in lower case): 5'-CCGCAATACGTTCAGTATG-3' and 5'-CCGAAATCGTTCCaGTC-3' to amplify from the 5'UTR to the mutation site, and 5'-CAGGACtGGAACGATTTC-3' and 5'-GAGAGATGGGATAAAAGAGG-3' to amplify from the mutation site to the 3'UTR. cDNA obtained from whole zebrafish larvae at 5 dpf was used as template. Gateway® (Invitrogen) recombination using the Tol2kit (Kwan et al., 2007) was performed to generate the *TaCP:mCherry-Rab8aCA* construct which was co-injected with Tol2 transposase as previously described (Kawakami, 2007) into 1-cell stage offspring of incrossed *ta3+/-* zebrafish.

Embryos were raised at 28°C in embryo medium and pigment development was inhibited by phenylthiourea for immunohistochemistry as described in Westerfield (Westerfield). All animal protocols were in compliance with internationally recognized guidelines for the use of fish in biomedical research and experiments were approved by the local authorities (Veterinäramt Zürich TV4206).

Immunohistochemistry and Light microscopy

Zebrafish larvae were fixed in 4% PFA overnight at 4°C, embedded in OCT and cryosectioned following standard protocols. For Ta3 antibody staining, zebrafish larvae were anesthesized with tricaine, washed unfixed in 30% sucrose for 30 minutes and embedded in OCT for cryosectioning. Sections were blocked using PBDT (PBS, 1% DMSO, 0.5% Triton X-100, 2mg/ml BSA) with 10% goat serum for 30 minutes at RT before incubation with primary antibodies overnight. Primary antibodies were mouse monoclonal anti-acetylated Tubulin (1:500, Sigma T6793), mouse anti-Centrin (1:200, clone 20H5 Millipore), mouse anti-Opsin 4D2 (1:100, gift from R. Molday, University of British Columbia), zpr1 (1:100, ZIRC), VDAC1 (1:100 abcam, ab15895). Secondary antibodies were Alexa Fluor goat anti-rabbit or goat anti-mouse IgG (Life Technologies) used at 1:400. BODIPY® TR Methyl Ester (1:300, Invitrogen) was applied for 20 minutes and nuclei were counterstained with DAPI. Confocal imaging was performed on a Leica HCS LSI or a Leica SP5 microscope.

Transmission electron microscopy

For Transmission Electron Microsopy, larvae were fixed overnight at 4°C in a freshly prepared mixture of 2.5% glutaraldehyde and 2% paraformaldehyde in 0.1 M sodium cacodylate buffer (pH 7.4). After rinsing in buffer, specimens were washed in 1% osmium tetroxide in 0.1 M sodium cacodylate buffer (pH 7.4), during 2 h at room temperature. After rinsing, tissues were dehydrated through a graded series of ethanol ranging from 50% to 100% and embedded in Epon. Ultrathin sections (70 nm) comprising zebrafish eyes were obtained using a Leica Ultracut UCT ultramicrotome and collected on formvar coated grids and examined with a Philips CM-100 scope. Images were acquired using the Gatan Microscopy Software.

Ta3 antibody generation

Custom polyclonal peptide antibodies were raised by Eurogentec (Seraing, Belgium) using their standard 87-day protocol. Rabbits were immunized with the Ta3 peptide H2N-CRR LSD DAF FGA DEK GED T-COOH2. Antibodies were affinity-purified against the corresponding peptide.

Electroretinography (ERG)

Normal (white) ERG was recorded on 6 dpf larvae as previously described (Zang et al., 2015). Briefly, larvae were dark adapted for at least 30 min, the eye ball was isolated and placed in the middle of the recording chamber which was filled with 1.5% agarose. The recording electrode was positioned against the central cornea while the reference electrode was inserted into the recording chamber and underneath the eye. Each larva was submitted

to three bright light stimuli (7000 lux) with an inter stimulus interval of 10 seconds. The average of the 3 responses was calculated.

Quantifications and stats

Graphpad Prism software was used for statistical analysis and generation of plots. Unpaired t-test was applied for comparisons between groups. Data were pooled from at least 2-3 independent experiments. Fluorescence intensity was measured in ImageJ and normalized for area. Cell counts were performed on single confocal sections or on stacks of identical sizes.

Acknowledgements

The authors thank Yuya Sugano and the Center for Microscopy and Image Analysis, University of Zurich (ZMB), for their assistance with Transmission Electron Microscopy, in particular Gery Barmettler and Ursula Lüthi. We also thank Kara Dannenhauer and Martin Walther for expert fish care and members of the Neuhauss lab for constructive discussions. Many thanks for reagents go to research groups mentioned in the methods section (Robert Molday for the 4D2 antibody, Brian Link for the Rhod promoter 5'E clone, Brian Perkins for the *ift88*^{tz288} mutant line and Susan Brockerhoff for the *tg(TaCP:MCFP)* line).

References

Alby, C., Piquand, K., Huber, C., Megarbané, A., Ichkou, A., Legendre, M., Pelluard, F., Encha-Ravazi, F., Abi-Tayeh, G., and Bessières, B., et al. (2015). Mutations in KIAA0586 Cause Lethal Ciliopathies Ranging from a Hydrolethalus Phenotype to Short-Rib Polydactyly Syndrome. The American Journal of Human Genetics ***97***, 311-318.

Bachmann-Gagescu, R., Dempsey, J.C., Phelps, I.G., O'Roak, B.J., Knutzen, D.M., Rue, T.C., Ishak, G.E., Isabella, C.R., Gorden, N., and Adkins, J., et al. (2015a). Joubert syndrome: a model for untangling recessive disorders with extreme genetic heterogeneity. Journal of Medical Genetics, 514-522.

Bachmann-Gagescu, R., Dona, M., Hetterschijt, L., Tonnaer, E., Peters, T., Vrieze, E. de, Mans, D.A., van Beersum, S.E.C., Phelps, I.G., and Arts, H.H., et al. (2015b). The Ciliopathy Protein CC2D2A Associates with NINL and Functions in RAB8-MICAL3-Regulated Vesicle Trafficking. PLoS Genet ***11***, e1005575.

Bachmann-Gagescu, R., Phelps, I.G., Dempsey, J.C., Sharma, V.A., Ishak, G.E., Boyle, E.A., Wilson, M., Marques Lourenco, C., Arslan, M., and Shendure, J., et al. (2015c). KIAA0586 is Mutated in Joubert Syndrome. Human mutation ***36***, 831-835.

Bachmann-Gagescu, R., Phelps, I.G., Stearns, G., Link, B.A., Brockerhoff, S.E., Moens, C.B., and Doherty, D. (2011). The ciliopathy gene cc2d2a controls zebrafish photoreceptor outer segment development through a role in Rab8-dependent vesicle trafficking. Human Molecular Genetics ***20***, 4041-4055.

Badano, J.L., Mitsuma, N., Beales, P.L., and Katsanis, N. (2006). The Ciliopathies: An Emerging Class of Human Genetic Disorders. Annu. Rev. Genom. Human Genet. ***7***, 125-148.

Bahadori, R., Huber, M., Rinner, O., Seeliger, M.W., Geiger-Rudolph, S., Geisler, R., and Neuhauss, S.C.F. (2003). Retinal function and morphology in two zebrafish models of oculo-renal syndromes. European Journal of Neuroscience ***18***, 1377-1386.

Bangs, F., Antonio, N., Thongnuek, P., Welten, M., Davey, M.G., Briscoe, J., and Tickle, C. (2011). Generation of mice with functional inactivation of talpid3, a gene first identified in

chicken. Development *138*, 3261-3272.

Ben, J., Elworthy, S., Ng, A.S.M., van Eeden, F., and Ingham, P.W. (2011). Targeted mutation of the talpid3 gene in zebrafish reveals its conserved requirement for ciliogenesis and Hedgehog signalling across the vertebrates. Development *138*, 4969-4978.

Bloodgood, R.A. (1990). Ciliary and Flagellar Membranes. The Photoreceptor Connecting Cilium: A Model for the Transition Zone. pp 389-417 (Springer US).

Buxton, P., Davey, M.G., Paton, I.R., Morrice, D.R., Francis-West, P.H., Burt, D.W., and Tickle, C. (2004). Craniofacial development in the talpid3 chicken mutant. Differentiation; research in biological diversity *72*, 348-362.

Chinchore, Y., Mitra, A., and Dolph, P.J. (2009). Accumulation of rhodopsin in late endosomes triggers photoreceptor cell degeneration. PLoS genetics *5*, e1000377.

Davey, M.G., Paton, I.R., Yin, Y., Schmidt, M., Bangs, F.K., Morrice, D.R., Smith, T.G., Buxton, P., Stamataki, D., and Tanaka, M., et al. (2006). The chicken talpid3 gene encodes a novel protein essential for Hedgehog signaling. Genes Dev. *20*, 1365-1377.

Deretic, D., Huber, L.A., Ransom, N., Mancini, M., Simons, K., and Papermaster, D.S. (1995). Rab8 in retinal photoreceptors may participate in rhodopsin transport and in rod outer segment disk morphogenesis. Journal of Cell Science *108*, 215-224.

Deretic, D., and Wang, J. (2012). Molecular assemblies that control rhodopsin transport to the cilia. Retina Ciliopathies: From Genes to Mechanisms and Treatment *75*, 5-10.

Doherty, D. (2009). Joubert Syndrome: Insights Into Brain Development, Cilium Biology, and Complex Disease. Developmental Disorders of the Central Nervous System: Bench to Bedside and Back Again *16*, 143-154.

Fliegauf, M., Benzing, T., and Omran, H. (2007). When cilia go bad: cilia defects and ciliopathies. Nature reviews. Molecular cell biology *8*, 880-893.

Goetz, S.C., and Anderson, K.V. (2010). The primary cilium: a signalling centre during vertebrate development. Nat Rev Genet *11*, 331-344.

Hamaoka, T., Takechi, M., Chinen, A., Nishiwaki, Y., and Kawamura, S. (2002). Visualization of rod photoreceptor development using GFP-transgenic zebrafish. Genesis (New York, N.Y. : 2000) *34*, 215-220.

Hildebrandt, F., Benzing, T., and Katsanis, N. (2011). Ciliopathies. N Engl J Med *364*, 1533-1543.

Insinna, C., and Besharse, J.C. (2008). Intraflagellar transport and the sensory outer segment of vertebrate photoreceptors. Dev. Dyn. *237*, 1982-1992.

Ishikawa, H., and Marshall, W.F. (2011). Ciliogenesis: building the cell's antenna. Nature reviews. Molecular cell biology *12*, 222-234.

Kawakami, K. (2007). Tol2: a versatile gene transfer vector in vertebrates. Genome Biology *8*, S7.

Kennedy, B., and Malicki, J. (2009). What drives cell morphogenesis: A look inside the vertebrate photoreceptor. Dev. Dyn. *238*, 2115-2138.

Khanna, H. (2015). Photoreceptor Sensory Cilium: Traversing the Ciliary Gate. Cells *4*, 674-686.

Kobayashi, T., and Dynlacht, B.D. (2011). Regulating the transition from centriole to basal body. The Journal of Cell Biology *193*, 435-444.

Kobayashi, T., Kim, S., Lin, Y.-C., Inoue, T., and Dynlacht, B.D. (2014). The CP110-interacting proteins Talpid3 and Cep290 play overlapping and distinct roles in cilia assembly. The Journal of Cell Biology *204*, 215-229.

Kwan, K.M., Fujimoto, E., Grabher, C., Mangum, B.D., Hardy, M.E., Campbell, D.S., Parant, J.M., Yost, H.J., Kanki, J.P., and Chien, C.-B. (2007). The Tol2kit: a multisite gateway-based construction kit for Tol2 transposon transgenesis constructs. Developmental dynamics : an official publication of the American Association of Anatomists *236*, 3088-3099.

Lewis, A., Williams, P., Lawrence, O., Wong, R.O.L., and Brockerhoff, S.E. (2010). Wild-type cone photoreceptors persist despite neighboring mutant cone degeneration. J. Neurosci. *30*, 382-389.

Lopes, V.S., Jimeno, D., Khanobdee, K., Song, X., Chen, B., Nusinowitz, S., and Williams, D.S. (2010). Dysfunction of heterotrimeric kinesin-2 in rod photoreceptor cells and the role of opsin mislocalization in rapid cell death. Molecular Biology of the Cell *21*, 4076-4088.

Malicdan, M.C.V., Vilboux, T., Stephen, J., Maglic, D., Mian, L., Konzman, D., Guo, J., Yildi-

rimli, D., Bryant, J., and Fischer, R., et al. (2015). Mutations in human homologue of chicken talpid3 gene (KIAA0586) cause a hybrid ciliopathy with overlapping features of Jeune and Joubert syndromes. Journal of Medical Genetics ***52***, 830-839.

Marszalek, J.R., Liu, X., Roberts, E.A., Chui, D., Marth, J.D., Williams, D.S., and Goldstein, L.S. (2000). Genetic Evidence for Selective Transport of Opsin and Arrestin by Kinesin-II in Mammalian Photoreceptors. Cell ***102***, 175-187.

May-Simera, H.L., Gumerson, J.D., Gao, C., Campos, M., Cologna, S.M., Beyer, T., Boldt, K., Kaya, K.D., Patel, N., and Kretschmer, F., et al. (2016). Loss of MACF1 Abolishes Ciliogenesis and Disrupts Apicobasal Polarity Establishment in the Retina. Cell reports ***17***, 1399-1413.

Moritz, O.L., Tam, B.M., Hurd, L.L., Peränen, J., Deretic, D., and Papermaster, D.S. (2001). Mutant rab8 Impairs Docking and Fusion of Rhodopsin-bearing Post-Golgi Membranes and Causes Cell Death of TransgenicXenopus Rods. Molecular Biology of the Cell ***12***, 2341-2351.

Nachury, M.V., Loktev, A.V., Zhang, Q., Westlake, C.J., Peränen, J., Merdes, A., Slusarski, D.C., Scheller, R.H., Bazan, J.F., and Sheffield, V.C., et al. (2007). A Core Complex of BBS Proteins Cooperates with the GTPase Rab8 to Promote Ciliary Membrane Biogenesis. Cell ***129***, 1201-1213.

Nachury, M.V., Seeley, E.S., and Jin, H. (2010). Trafficking to the Ciliary Membrane: How to Get Across the Periciliary Diffusion Barrier? Annu. Rev. Cell Dev. Biol. ***26***, 59-87.

Pearring, J.N., Salinas, R.Y., Baker, S.A., and Arshavsky, V.Y. (2013). Protein sorting, targeting and trafficking in photoreceptor cells. Progress in Retinal and Eye Research ***36***, 24-51.

Peranen, J., Auvinen, P., Virta, H., Wepf, R., and Simons, K. (1996). Rab8 promotes polarized membrane transport through reorganization of actin and microtubules in fibroblasts. The Journal of Cell Biology ***135***, 153-167.

Poretti, A., Boltshauser, E., and Valente, E.M. (2014). The Molar Tooth Sign Is Pathognomonic for Joubert Syndrome! Pediatric Neurology ***50***, e15-e16.

Reiter, J.F., Blacque, O.E., and Leroux, M.R. (2012). The base of the cilium: roles for transition fibres and the transition zone in ciliary formation, maintenance and compartmentalization. EMBO reports ***13***, 608-618.

Romani, M., Micalizzi, A., and Valente, E.M. (2013). Joubert syndrome: congenital cerebellar ataxia with the molar tooth. Lancet Neurol. ***12***, 894-905.

Roosing, S., Hofree, M., Kim, S., Scott, E., Copeland, B., Romani, M., Silhavy, J.L., Rosti, R.O., Schroth, J., and Mazza, T., et al. (2015). Functional genome-wide siRNA screen identifies KIAA0586 as mutated in Joubert syndrome. Elife ***4***.

Singla, V., and Reiter, J.F. (2006). The primary cilium as the cell's antenna: signaling at a sensory organelle. Science (New York, N.Y.) ***313***, 629-633.

Stephen, L.A., Davis, G.M., McTeir, K.E., James, J., McTeir, L., Kierans, M., Bain, A., and Davey, M.G. (2013). Failure of centrosome migration causes a loss of motile cilia in talpid(3) mutants. Dev. Dyn. ***242***, 923-931.

Stephen, L.A., Tawamie, H., Davis, G.M., Tebbe, L., Nürnberg, P., Nürnberg, G., Thiele, H., Thoenes, M., Boltshauser, E., and Uebe, S., et al. (2015). TALPID3 controls centrosome and cell polarity and the human ortholog KIAA0586 is mutated in Joubert syndrome (JBTS23). eLife ***4***, 1161.

Sukumaran, S., and Perkins, B.D. (2009). Early defects in photoreceptor outer segment morphogenesis in zebrafish ift57, ift88 and ift172 Intraflagellar Transport mutants. Vision Res. ***49***, 479-489.

Tai, A.W., Chuang, J.-Z., Bode, C., Wolfrum, U., and Sung, C.-H. (1999). Rhodopsin's Carboxy-Terminal Cytoplasmic Tail Acts as a Membrane Receptor for Cytoplasmic Dynein by Binding to the Dynein Light Chain Tctex-1. Cell ***97***, 877-887.

Tsujikawa, M., and Malicki, J. (2004). Intraflagellar Transport Genes Are Essential for Differentiation and Survival of Vertebrate Sensory Neurons. Neuron ***42***, 703-716.

Wang, J., Morita, Y., Mazelova, J., and Deretic, D. (2012). The Arf GAP ASAP1 provides a platform to regulate Arf4- and Rab11–Rab8-mediated ciliary receptor targeting. The EMBO Journal ***31***, 4057-4071.

Ward, H.H., Brown-Glaberman, U., Wang, J., Morita, Y., Alper, S.L., Bedrick, E.J., Gattone, V.H.2., Deretic, D., and Wandinger-Ness, A. (2011). A conserved signal and GTPase complex are required for the ciliary transport of polycystin-1. Molecular Biology of the Cell ***22***, 3289-3305.

Westerfield, M. The Zebrafish Book. A Guide for the Laboratory Use of Zebrafish (Danio rerio) (University of Oregon Press, Eugene, OR.).

Westlake, C.J., Baye, L.M., Nachury, M.V., Wright, K.J., Ervin, K.E., Phu, L., Chalouni, C., Beck, J.S., Kirkpatrick, D.S., and Slusarski, D.C., et al. (2011). Primary cilia membrane assembly is initiated by Rab11 and transport protein particle II (TRAPPII) complex-dependent trafficking of Rabin8 to the centrosome. Proceedings of the National Academy of Sciences *108*, 2759-2764.

Yin, Y., Bangs, F., Paton, I.R., Prescott, A., James, J., Davey, M.G., Whitley, P., Genikhovich, G., Technau, U., and Burt, D.W., et al. (2009). The Talpid3 gene (KIAA0586) encodes a centrosomal protein that is essential for primary cilia formation. Development *136*, 655-664.

Yoshimura, S.-I., Egerer, J., Fuchs, E., Haas, A.K., and Barr, F.A. (2007). Functional dissection of Rab GTPases involved in primary cilium formation. The Journal of Cell Biology *178*, 363-369.

Zang, J., Keim, J., Kastenhuber, E., Gesemann, M., and Neuhauss, S.C.F. (2015). Recoverin depletion accelerates cone photoresponse recovery. Open biology *5*.

Zou, J., Lathrop, K.L., Sun, M., and Wei, X. (2008). Intact retinal pigment epithelium maintained by Nok is essential for retinal epithelial polarity and cellular patterning in zebrafish. The Journal of neuroscience : the official journal of the Society for Neuroscience *28*, 13684-13695.

Supplementary material

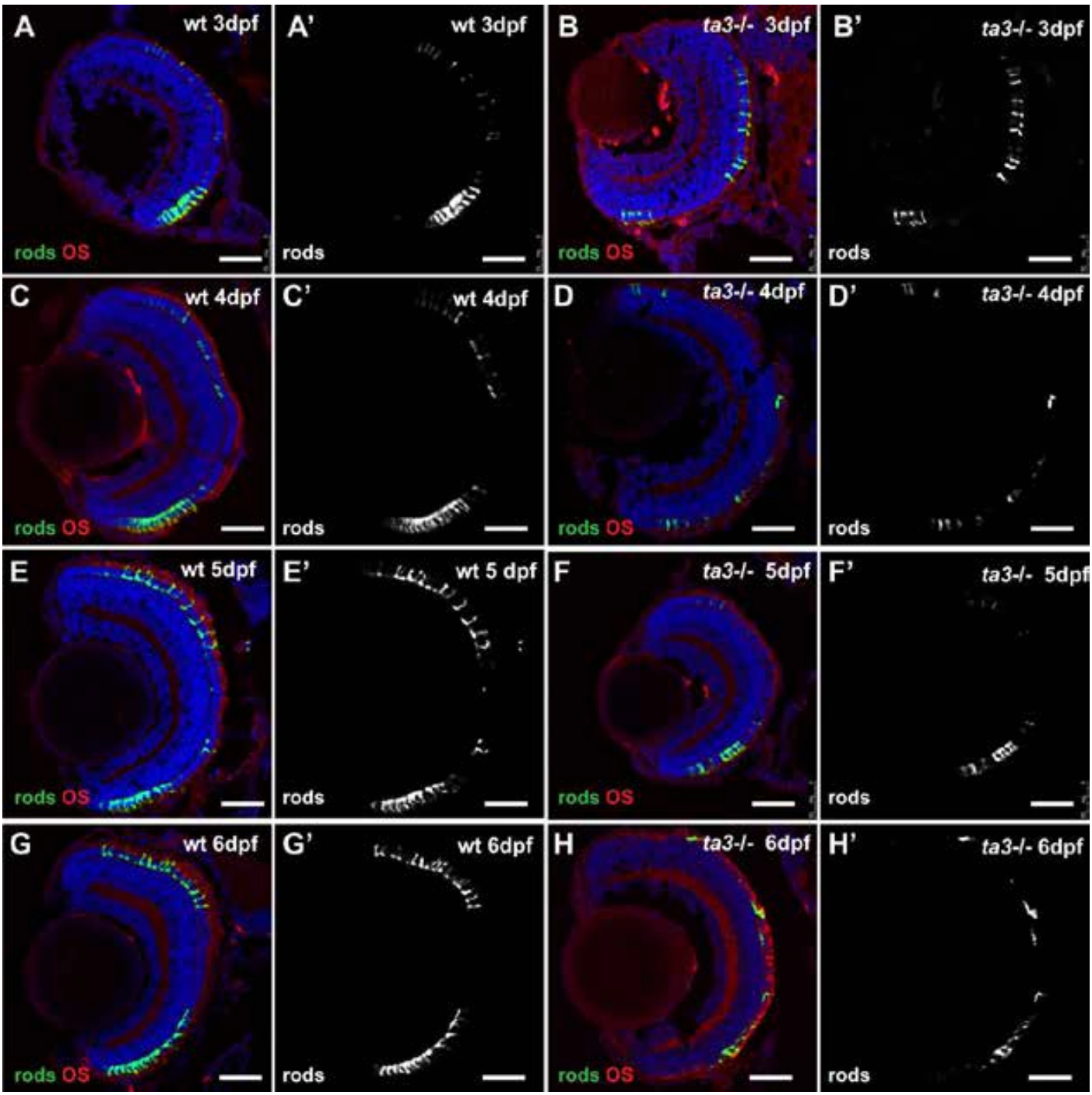

Figure S1: Time course of Rod PR development in *ta3* mutants
Retinal cryosections of the transgenic line *tg(zfRH1-3.7B:EGFP)* marking rod photoreceptors (PRs) at 3dpf **(A-B)**, 4dpf **(C-D)**, 5dpf **(E-F)** and 6 dpf **(G-H)**, in wildtype (A,C,E and G) and talpid3 mutant (B,D,F,H) zebrafish. Nuclei are counterstained with DAPI and membranes (including outer segments) are highlighted with BODIPY. Rod PRs are initially present in comparable numbers in mutants and wild-type but decrease in mutants as time progresses. Scale bars are 30 µm in all panels.

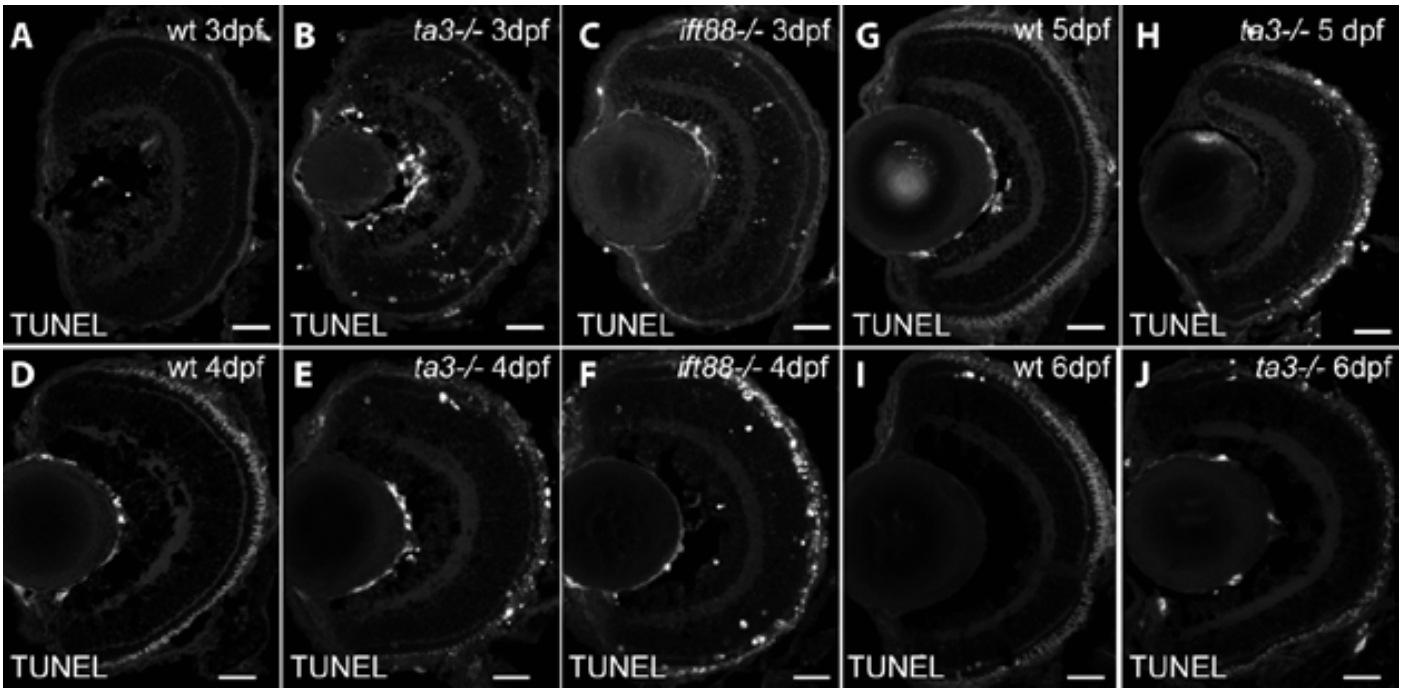

Figure S2: PR cell death in *ta3* mutant retinae
TUNEL staining on retinal cryosections at 3 dpf **(A-C)**, 4 dpf **(D-F)**, 5 dpf **(G-H)** and 6 dpf **(I-J)**, in wildtype (A,D,G and I), *talpid3* mutants (B, E, H and J) and *ift88* mutants (C and F). Note the strong signal in *ift88* mutants at 4 dpf and the comparatively lower amount of cell death in *ta3* mutants at the same stage. Scale bars are 20 µm in all panels.

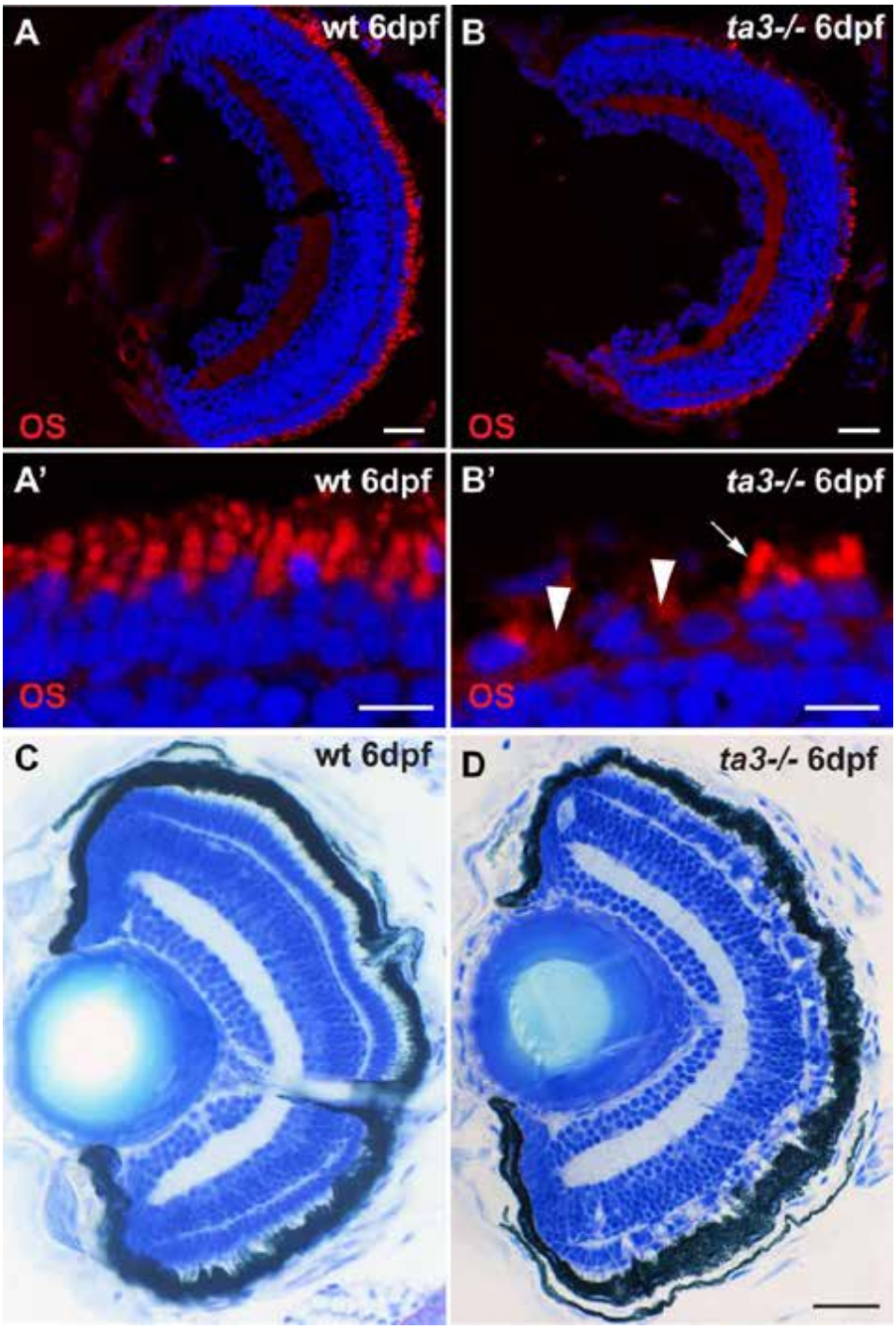

Figure S3: Retinal morphology of *ta3-/-* larvae

(A-B) 6 dpf cryosections through wildtype (A) and *ta3-/-* (B) retinae, where the membranes composing the outer segments (OS) are highlighted with the lipophilic dye BODIPY. (A'-B') Higher magnification images of (A-B). Note the absence of OS in a subset of mutant photoreceptors (PRs) in (B), alongside PRs with still elongated OSs (arrow). Also note the gaps in the outer nuclear layer (arrowheads). (C-D) Technovit histological sections through eyes of wildtype (wt) and *ta3-/-* larvae. Gaps are visible in the mutants in the PR layer (arrowheads). Note how the retinal pigment covers any residual OS in the mutants. Scale bars are 20 µm in (A-B and C-D) and 10 µm in (A'-B').

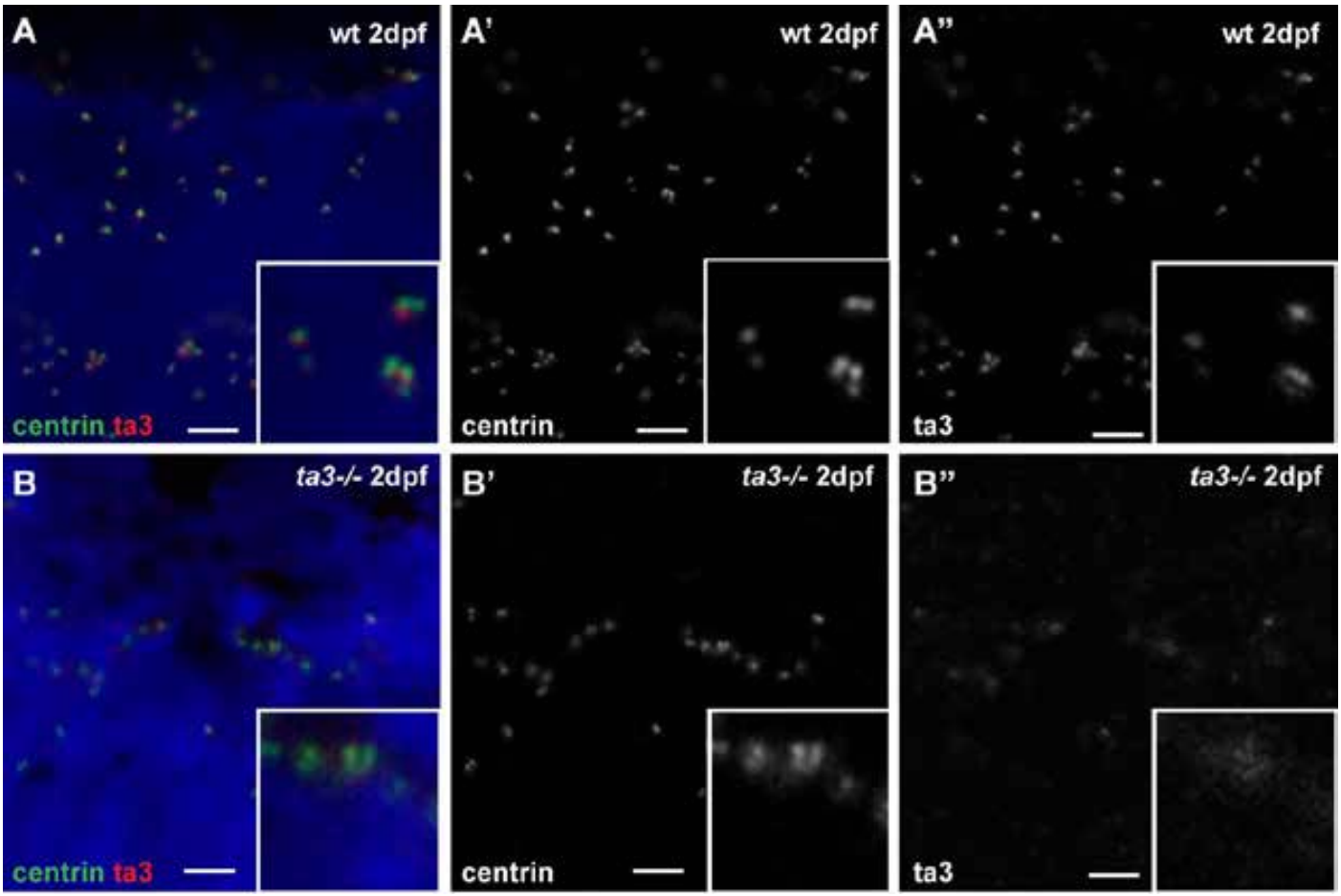

Figure S4: Talpid3 protein is strongly decreased in 2 dpf retina
(A-B) Retinal cryosections on 2 dpf wildtype (A-A") and *ta3-/-* (B-B") larvae, stained with an antibody against Centrin to mark the basal bodies (green in A,B) and an antibody against Talpid3 (red in A,B). Note the loss of signal in the *ta3-/-* retina B"). Scale bars are 4 µm in all panels.

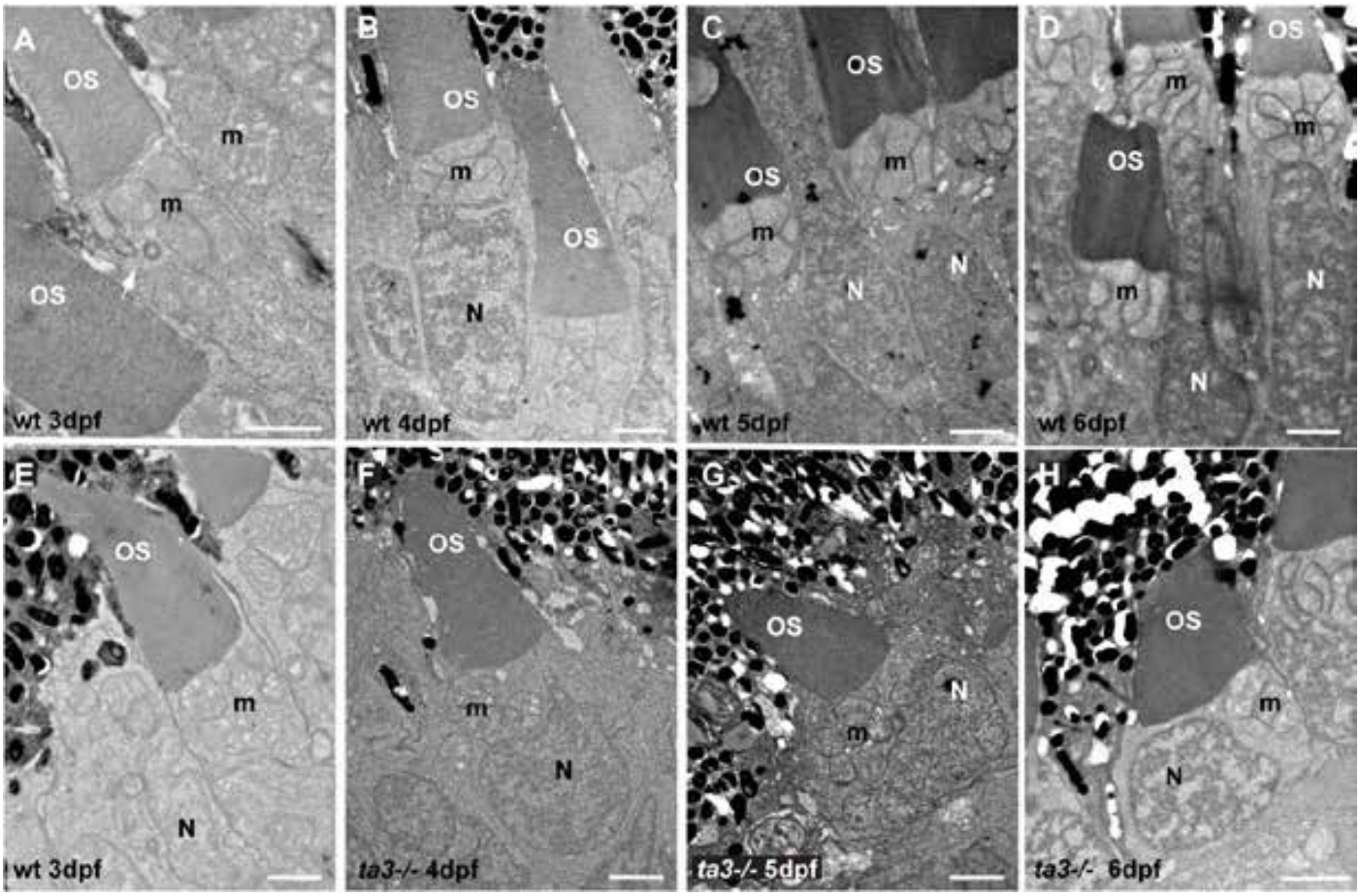

Figure S5: Progressive loss of photoreceptor cell shape in *ta3* mutants visible on transmission electron microscopy (TEM)
TEM time course focusing on retinal photoreceptor (PR) cell morphology at 3 dpf **(A, E)**, 4 dpf **(B, F)**, 5 dpf **(C,G)** and 6 dpf **(D-H)** in wild-type (A-D) and zygotic ta3 mutants (E-H). Note the normal elongated cell shape of *ta3* PRs at 3 dpf (E) compared to wildtype (A), and the progressive collapse of the cell: at 4dpf the nucleus (N) is already rounded **(F)**, at 5dpf the inner segment space becomes strongly reduced **(G)** and at 6 dpf, the mitochondrial cluster (m) is lateral to the nucleus **(H)** instead of being apical to it as in wildtype (D). Also note the progressive shortening of the outer segments (OS) from 3 to 6 dpf. The arrow points to the basal body in (A). Scale bars are 2 µm in all panels.

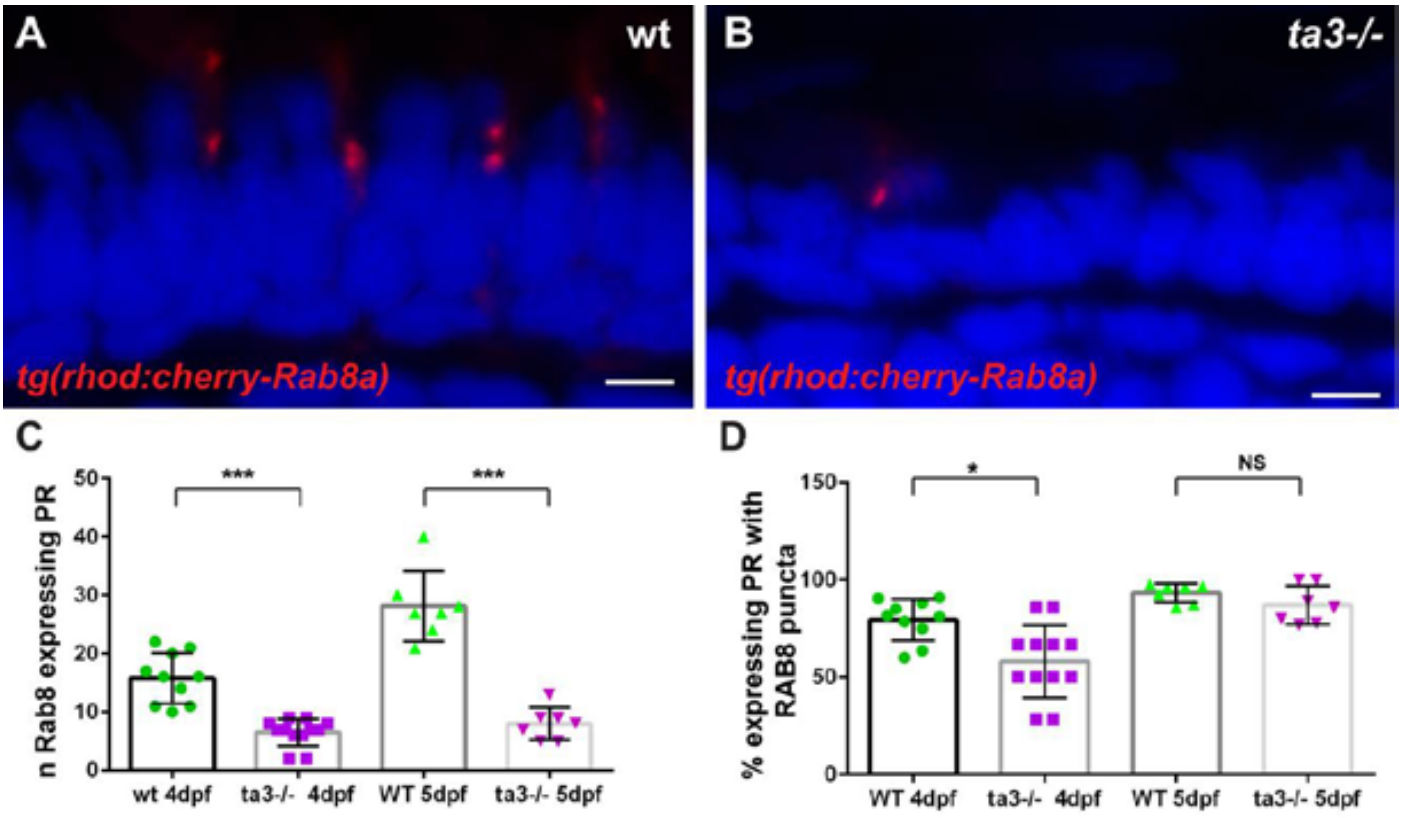

Figure S6: Punctate Rab8 localization is little affected in *talpid3* mutant PRs

(A-B) Cryosections through wildtype (A) and *ta3-/-* (B) retinae expressing mCherry-tagged Rab8a under the control of the Rhodopsin promoter in rods. Note the punctate expression pattern in both wildtype and mutant PRs and the decreased number of expressing cells in mutants. Scale bars are 4 µm in (A-B). (C) Quantification of the number of PRs per analysed section expressing the transgene. Each datapoint represents one individual larva. ****p<0.001*, Student's t-test. (D) Quantification of the proportion of expressing PRs that display a punctate pattern (as opposed to a diffuse expression pattern). **p<0.05*, NS not significant, Student's t-test.

Chapter 5. General discussion

During my thesis, I have used the zebrafish and exploited its many advantages in an attempt to identify the molecular mechanisms underlying the pathogenesis of JBTS. Specifically, I have investigated the disease pathways associated with loss of function of two JBTS proteins localizing to distinct compartments within the cilium, the transition zone protein Cc2d2a and the basal body protein Talpid3. In the following paragraphs I will summarize, integrate and discuss results from my studies and lay out possible future directions to continue the line of investigations developed during my thesis.

The role of the TZ protein Cc2d2a in photoreceptor ciliary function

In Chapter 2, dedicated to the role of Cc2d2a in zebrafish PRs, we have proposed a model whereby Cc2d2a provides a docking point for incoming OCVs through its interaction with NINL (Bachmann-Gagescu et al., 2015a) and controls the localization of the t-SNAREs required for fusion, thereby bringing all components required for vesicle fusion in proximity with each other at the periciliary region. Although the mechanism by which SNAP25 mislocalizes in the absence of Cc2d2a function remains unknown, we hypothesize that changes in the ciliary membrane lipid composition may be underlying this observation. Indeed, protein-lipid interactions have been the focus of intensive research in the past years and a number of findings would support our hypothesis: 1) SNAP25 is inserted in the target membrane through palmitoylation; thus, its localization might be influenced by the lipid composition of the periciliary membrane (Loranger and Linder, 2002). 2) SNAREs are arranged around cholesterol and PIP_2-rich membrane microdomains (Lang et al., 2001; Davletov et al., 2007; Balla et al., 2012). 3) OCV delivery was shown to depend on PIP_2 recognition by FIP3 (Mazelova et al., 2009; Wang and Deretic, 2015). 4) The Rab8 effector MICAL3 recognizes membrane-associated proteins bound to specific PIPs as the vesicle "landing site" (Lansbergen et al., 2006; Grigoriev et al., 2011). 5) Finally, the JBTS protein INPP5E, whose ciliary localization depends on the TZ (Garcia-Gonzalo et al., 2015; Slaats et al., 2016), plays a crucial role in regulating ciliary PIP content.

To test this hypothesis, specific phosphoinositide-binding domains fused to fluorescent reporters can be expressed in zebrafish PRs following the same paradigm I have employed to express Rabs. Several such sensors have been tested already (Hammond and Balla, 2015). Furthermore, the phosphatidylinositol 4-phosphate (PIP)-binding P4M domain of the secreted effector protein SidM from the bacterial pathogen *Legionella pneumophila* (Hammond et al., 2014) and the phosphatidylinositol 4,5-bisphosphate (PIP_2)-binding pleckstrin homology domain of PLCδ1 (Stauffer et al., 1998) have been successfully used by J. Reiter's group to determine the different lipidic domains of the ciliary membrane in IMCD3 cells and MEFs (Garcia-Gon-

zalo et al., 2015). In wild-type conditions, restricted areas of fluorescence with a clear border are expected to appear at the OS and at the periciliary membrane. Changes in this fluorescence pattern in *cc2d2a-/-* PRs would advocate for changes in the membrane composition.

A role for PIP composition in controlling the periciliary membrane localization of vesicle fusion machinery components such as SNAP25 would further be supported if targeted mutagenesis of the JBTS ciliary phosphatase INPP5E (or of PDE6δ which is required to transport INPP5E into the ciliary compartment) (Humbert et al., 2012; Fansa et al., 2016) would lead to a vesicle fusion defect in photoreceptors. Likewise, overexpression of a ciliary targeted constitutively active PIP 5-kinase (Falkenburger et al., 2010) could similarly potentially phenocopy loss of Cc2d2a function.

Identification of other protein or lipid interaction partners of CC2D2A in addition to NINL would further clarify the mechanism by which this TZ protein exerts its function in wild-type and disease conditions. Likewise, identification of other players involved in OCV docking and fusion would refine the model for Cc2d2a function in photorceptors that we propose. Most exocystosis processes are triggered upon the aperture of Ca^{2+}-channels and the subsequent local intracellular Ca^{2+} concentration increase (Barclay et al., 2005; Oheim et al., 2006). At the synapse, these channels are tightly coupled to the docking and fusion machinery of synaptic vesicles to ensure a rapid fusion reaction upon an action potential (Simms and Zamponi, 2014; Ehmann et al., 2015). It is likely that a similar mechanism operates for highly-demanding exocytic processes, such as OCV delivery, where an unidentified Ca^{2+}-channel could be in close proximity to the fusion machinery and its organizers. Besides, Cc2d2a, like other proteins in the TZ compartment, possesses a C2 domain that is predicted to bind to ceramide 1-phosphate and PIP_2 phospholipids in a Ca^{2+}-dependent/reversible manner (Stahelin, 2009). Clustering of missense mutations in the C2 domain in patients with JBTS supports an important functional role of this particular protein domain of CC2D2A (Bachmann-Gagescu et al., 2012). Does Ca^{2+} trigger a conformational change in Cc2d2a or other TZ proteins that promotes facilitator or gatekeeper functions? What L-type voltage-gated Ca^{2+}-channel regulates OCV exocytosis? These questions could be addressed through different approaches: yeast two hybrid or tandem affinity purification may be useful approaches to identify the Ca^{2+}-channel (should it exist) and other SNARE regulators associated with the binomial Syntaxin3/SNAP25 system. Zebrafish could be used to confirm the co-localization of thereby identified interaction partners using immunohistochemical assays or reporter-fused protein overexpression both in wild-type and *cc2d2a-/-* backgrounds. The candidate partner proteins could be additionally knocked-down in a *cc2d2a-/-* background to address whether this modifies the *cc2d2a-/-* phenotype. Alternatively, knock-outs of candidate interactors and comparison of the resulting phenotypes with those of the *cc2d2a-/-* mutant, and generation of double mutant lines could provide valuable information on epistasis. Investigation of the localization

of Cc2d2a and other ciliary proteins in knock-outs for candidate interactors would further determine a localization hierarchy. Dissecting the role of the CC2D2A C2 domain could be done by overexpression of a truncated mutant protein version in a *cc2d2a-/-* background. However, based on my own experience trying to generate a stable transgenic line overexpressing GFP-Cc2d2a in zebrafish (see Appendix I), this last experiment may not be feasible in this model (possibly given the large size of the Cc2d2a protein which made generation of a stable transgenic line challenging). A cell culture approach, where the CRISPR/Cas9 system can be employed with ease to mutate the endogenous *CC2D2A* gene (Bauer et al., 2015), might be more successful.

The role of Rab8 in ciliary transport

In addition to investigating the role of Cc2d2a in ciliary-directed trafficking in zebrafish, the stable transgenic lines expressing Rab8 paralogs in rods and cones have allowed me to address the recent controversy on the role of the small GTPase Rab8 in opsin trafficking (Ying et al., 2016) by providing the first live characterization of Rab8 movement in photoreceptors (PRs) in a whole tissue context. Our work supports a role for Rab8 paralogs in rhodopsin transport based on co-localization of transgenically tagged Rabs with opsins on vesicular structures using a cutting-edge correlative and light electron microscopy imaging technique (Mateos et al., 2016). Furthermore, the movement pattern of Rab8 particles with apico-basal directionality is consistent with the current model on the disposition of the microtubule-based cytoskeleton network (Besharse et al., 2010); and occurs at a speed that is consistent with the ascribed dynein-dependent OCV transport (Howard, 2001). Thus, our work supports the proposed universal role for Rab8 in ciliary transport (Nachury et al., 2007; Westlake et al., 2011; Wang and Deretic, 2015) and we suggest that the discrepancy with the double *rab11a;rab8a* knock-out mouse model could be explained by a compensatory mechanism carried out by another RabGTPase expressed at PRs, such as the closest paralogs Rab13 (this study), Rab10 (Babbey et al., 2010), Rab17 (Lim et al., 2011), Rab23 (Yoshimura et al., 2007; Boehlke et al., 2010) and/or Rab28 (Jensen et al., 2016). The authors of this double knock-out mouse model propose a species-specific difference governing the rhodopsin transport mechanisms in mammals compared to the general model proposed in frog (Wang and Deretic, 2015) based on the different PR morphologies (and assumed different transport needs). However, because of the large body of evidence involving Rab8 in ciliary trafficking in human cells and the fact that mutations in Rab8 effectors/interactors have been linked to ciliopathy disease causality in humans and animal models (Omori et al., 2008; Fogelgren et al., 2011; Kobayashi and Dynlacht, 2011; Dixon-Salazar et al., 2012; Shaheen et al., 2013; Martin-Urdiroz et al., 2016; Seixas et al., 2016), it is difficult to believe a spe-

cies-specific difference in mouse, especially when RabGTPase orthologue functions are evolutionarily conserved (Brighouse et al., 2010). Our results even support conserved Rab8 function in rods and cones, thus differences cannot be attributed to rod-dominant or cone-dominant retina types.

The large number of RabGTPase proteins in high eukaryotes (close to 70 members in humans) has been proposed to obey the necessity of increasing complexity of cellular compartmentalization to facilitate separation of major biochemical processes and allow much finer control and sophistication of cell function in evolution, especially after the acquisition of multicellularity (Brighouse et al., 2010). In that sense, the genetic expansion of the RabGTPase superfamily follows subfunctionalization or neofunctionalization of the individual Rab genes that would have otherwise been lost from the genome (Rastogi and Liberles, 2005; Glasauer and Neuhauss, 2014). However, this concept is not excluding punctual or relative redundancy between subsets RabGTPases as previously shown in other studies (Sato et al., 2014) and our own study demonstrates redundancy between Rab8a and Rab8b-like in rhodopsin transport.

Because of the overexpression nature of our assays, the interpretation of our results must proceed with caution. Indeed, we cannot conclude if Rab8a, Rab8b-like, and by extension Rab8b, function in PRs at the same time under the same circumstances. It is possible that one of the paralogs is solely involved in rhodopsin transport function but their redundant capacity allows the other two to perform this task in case of loss of function of the first one. mRNA and protein expression profiles would be required in PRs and other ciliated cell types to clarify the major Rab paralog functioning in ciliary transport and redundancy could be evaluated by full or conditional knock-out of Rab paralogs and subsequent profiling of the expression and localization of other RabGTPases. The CRISPR-Cas9 system could be employed in zebrafish could to generate the Rab knock-outs and isolate different tissues for their mRNA and protein profiling.

Is the Rab8-mediated transport mechanism universally used in all cilia types? Rab10 was found to co-localize with the Exocyst at the ciliary base of renal epithelial cells (Babbey et al., 2010), which would suggest otherwise. This question can be addressed in zebrafish, as it displays a similar variety of cilia types as in humans. Furthermore, I have generated transgenic lines expressing Rab8a and Rab8b-like ubiquitously (see Appendix I). Using these lines, co-localization assays using antibody staining or transient heat-shock inducible expression of reporter-fused specific cell-type ciliary cargoes (e.g.: Adenylyl cyclase III in olfactory pits, Polycystin1 in renal cells, possibly Patched1 in neurons) could be employed to determine the involvement of Rab8 in ciliary trafficking in other cells than photoreceptors.

The hidden roles of Talpid3 in photoreceptor cell shape maintenance

In 2015, mutations in the *KIAA0586/TALPID3* gene were found to be causal for JBTS and other more severe ciliopathies in humans (Alby et al., 2015; Bachmann-Gagescu et al., 2015b; Malicdan et al., 2015; Roosing et al., 2015; Stephen et al., 2015). Talpid3 (Ta3) had been previously shown to localize to the centrosome and to be necessary for ciliogenesis in chick and mouse models (Yin et al., 2009; Bangs et al., 2011). This role in ciliogenesis is dependent on the interaction of Ta3 with Rab8 during initial docking of the ciliary vesicle (Kobayashi et al., 2014). Given the ascribed function of Rab8 in ciliary trafficking (Nachury et al., 2007; Knodler et al., 2010; Westlake et al., 2011) confirmed for rhodopsin transport in PRs in our study, and the published interaction between Rab8 and Ta3, we hypothesized that zebrafish carrying mutations in *ta3* would display defects in ciliary-directed trafficking in photorceptors similar to *cc2d2a* mutants, if Ta3 played additional roles in ciliary function/maintenance beyond ciliogenesis. To test this hypothesis, we used a *ta3* zygotic zebrafish mutant line (Ben et al., 2011), in which early embryos benefit from maternal contribution of wild-type Ta3 which rescues ciliogenesis and allows mutant embryos to undergo early developmental stages normally. However, when we characterized the phenotype in *ta3-/-* PRs, we observed very limited vesicle accumulation in a subset of PRs, in contrast with the massive vesicle accumulation occurring in *cc2d2a-/-* PRs. This observation suggested little involvement for Talpid3 in vesicle trafficking towards the cilium.

However, besides confirming the previously ascribed function of Ta3 in BB docking, we observed a very interesting and specific phenotype that could not be seen previously due to the fundamental role of Ta3 in ciliogenesis: progressive loss of cell shape morphology even in PRs that had extended OSs thanks to maternally-derived Ta3. This phenomenon is concomitant to intracellular polarity defects with displacement of the mitochondrial cluster and nuclear collapse. Furthermore, there is progressive shortening of the initially normal OSs and intracellular accumulation of opsins in PRs with OSs. These findings are consistent with recent work that identified TA3 as an interaction partner of the microtubule actin crosslinking factor 1 (MACF1), whose deficiency leads to similar PR phenotypes in mouse retina as those observed in *ta3-/-* zebrafish (May-Simera et al., 2016). Indeed, mice lacking MACF1 function display deficient ciliogenesis due to lack of BB migration and docking as well as defects in OS maintenance and defects in cell polarity in adult PRs when MACF1 is inactivated after OS extension. The authors propose that TA3 is involved in the coordination of microtubule and actin interactions, which is consistent with our findings and our proposed model.

The PR cell shape phenotype, which was previously unrecognized in *ta3* mutant models given, indeed suggests a cytoskeleton defect, which would be consistent with the role of the centrosome, to which Ta3 loalizes, as

microtubule organization center (MTOC). The progressive shortening of the initially normal OSs suggests a defect in transport of membranes and cargo towards the ciliary compartment, which could be secondary to loss of cytoskeletal organization, since transport of OCVs is thought to occur along microtubules (Tai et al., 1999; Lopes et al., 2010; Deretic and Wang, 2012). The fact that we observe only limited vesicle accumulation in *ta3-/-* photoreceptors, suggests that Ta3 does not play a direct or predominant role in ciliary-directed trafficking. A possible model would postulate that the microtubule network is initially present and well-formed and in zebrafish *ta3-/-* photoreceptors is slowly deteriorating over time because of reduced tubulin polymerization dynamics, a role formerly tested for Ta3 in cell culture (Yin et al., 2009). A number of future experiments can be performed to test the involvement of Ta3 in cytoskeleton formation and dynamics. Preliminary immunohistochemistry results with α-tubulin staining did not provide sufficient spatial resolution, despite use of STED microscopy, to accurately follow the microtubule network in photoreceptor inner segments, in wild-type or mutant cells. To overcome this problem, the CLEM technique presented in this work could be employed on *ta3-/-* fish expressing *tacp:EB3-GFP*, a construct that I have generated (see Appendix I) which labels microtubule plus ends (Stepanova et al., 2003). This technique could potentially shed light on the amount and disposition of the microtubules in the cytoskeleton network of the inner segment. Because the section thickness on CLEM may not be sufficient to clearly follow the microtubule lattice, another possibility would be to fully reconstruct and compare the 3D microtubule network in wild-type and *ta3-/-* PRs by focused ion beam combined with transmission electron microscopy (FIB-TEM). To test whether the microtubule dynamics are impaired, I propose two possible approaches: live imaging of microtubule re-polymerization using animals expressing the *tacp:EB3-GFP* transgene (either transiently or stably) after transient exposure to nocodazole to depolymerize microtubules.

Given the described interaction in mouse between TA3 and MACF1 (May-Simera et al., 2016), which has a single orthologue annotated in the zebrafish genome, it would be interesting to analyze the expression pattern of this gene and localization of its protein product, should an antibody be available. If *macf1* mRNA is found in PRs, it could be tested by knockdown or knock-out whether it can function as a modifier for the loss of Ta3 phenotype. Whether this is or is not the case, the interaction between the actin microfilament-based and the tubulin microtubule-based cytoskeleton is a consolidated fact, also in PRs (Besharse et al., 2010; Besharse and Bok, 2011). Thus, it could also be worth testing if the microtubule dynamics in *ta3-/-* PRs are affected by microfilament de-polymerization and recovery upon transient treatment with cytochalasin D.

Genetic heterogeneity and phenotypic variability in ciliopathies

Ciliopathies arise from primary cilium dysfunction. Mutations in one ciliopathy gene can give rise to different clinical presentations and mutations in multiple genes, whose protein product localizes in different ciliary compartments, thereby likely serving different functions, can lead to the same clinical phenotype (Badano et al., 2006). How is this even possible? How can mutations in *CC2D2A* and *KIAA0586/TALPID3 (TA3)* give rise to the well-defined JBTS cerebellar phenotype when their functions and their disease mechanisms seem so dissimilar? This paradox is still far from being solved, and exists for many genetic diseases with genetic heterogeneity and phenotypic variability. Phenotypic variability is a common problem in Mendelian genetics; therefore increasing our understanding in ciliopathies could potentially have a broader impact extended to genetics of other rare disorders.

There are different explanations that can be used as a platform to approach this intricate question:

1. Different disease mechanisms lead to a common failed function. In other words, if the same organelle is affected then the same readouts/pathways will be involved. While this is an obvious statement, it does not explain the different phenotypic manifestations of each ciliopathy (why do patients with defects in ciliary genes have different disorders?).
2. There is a convergent mechanistic link common to all the disease-causing genes involved in the same disease. This does not explain why the same gene can be involved in different clinical presentations. Then, genetic modifiers and nature of the mutations would come into play (see the general introduction section for more information on the genotype-phenotype correlation of ciliopathies).
3. In both cases, it is possible that the same gene has tissue-specific roles, which would account for a common failed function or a convergent mechanistic link in one tissue type (i.e. the cerebellum in JBTS) and different extracerebellar phenotypes. This hypothesis would be supported by a *cc2d2a* mutant mouse which displays ciliogenesis defects in neurons but not in MEFs (Garcia-Gonzalo et al., 2011).

Following the hypothesis of a shared pathway affected by dysfunction of genes causing the same disorder, in the case of the JBTS proteins CC2D2A and TA3, the common read-out could lie in impaired Shh signaling during brain development. This in turn would lead to hypoproliferation of the cerebellar cells and defective axon guidance (Doherty, 2009; Romani et al., 2013; Guemez-Gamboa et al., 2014; Poretti et al., 2014) resulting the pathognomonic brain malformation, the MTS. In this case, reduced ciliogenesis due to loss of BB docking caused by loss of TA3 function would result in a similar impairment of Shh signaling as impaired Shh activator smoothened translocation in the ciliary membrane derived from loss of CC2D2A function. Consistent with this hypothesis, animal models for

both Cc2d2a and Ta3 loss of function display neural tube mispatterning phenotypes, known to be governed by Shh (Garcia-Gonzalo et al., 2011).

Having focused only the zebrafish retina, we have not investigated tissue-specific fucntions for the studied JBTS genes. In the case of *cc2d2a*, preliminary data suggest that ciliary transport of adenylyl cyclase III in the olfactory cilia of *cc2d2a-/-* zebrafish is unaffected. Tissue-specific functions in ciliary transport could be examined with the aforementioned ready-to-use transgenic zebrafish lines: *ubi:mCherry-rab8a* and *ubi:mCherry-rab8b-like* (with *bactin:centrin-GFP* for the BB reference, see Appendix I). We have established the conditions for the analysis of live imaging time-lapse videos using ILASTIK, thus evaluating trafficking defects in cilia at the olfactory pits, kidneys, otic vesicles or brain tissue would be a matter of optimizing the imaging conditions for each cell population. This analysis could be extended to any of the JBTS gene zebrafish mutants where a trafficking defect is suspected. Given the presence of kidney cysts in *cc2d2a-/-* fish, analyzing transport of ciliary proteins to the cilium (such as polycystins), determining if vesicle accumulation is present through TEM and identifying vesicle fusion machinery components could indicate whether the mechanisms we identified for Cc2d2a dysfunction in photoreceptors are at play in kidney tubule cells as well.

Could *cc2d2a-/-* and *ta3-/-* share a common mechanistic link (not only consequence) in a specific cell type? Besides the common Rab8 node, shared by Ta3 to engage ciliogenesis and Cc2d2a to promote membrane and protein delivery in the ciliary compartment (and addressed in the previous paragraph), this is a scenario worth investigating. This could be performed through transcriptomic and proteomic approaches by comparison of either mutant with wild-type and with each other. Ideally, analyses should rely on comparisons of specific tissues/cell-types, which could be obtained through manual dissections (whole eyes) or relying on transgenic lines fluorescently marking specific cell types (i.e. *tg(wtb1:GFP)* marking renal tubular cells) and FACS sorting.

Despite the unifying molar tooth sign phenotype common to all patients diagnosed with JBTS, we have not seen a gross morphological hindbrain defect in the zebrafish larvae harboring homozygous mutations for the genes at question. Nonetheless, the phenotype could be much more subtle in the zebrafish compared to the human. A transgenic line available in the Neuhauss lab expressing an RFP reporter in Purkinje cells in the cerebellum *(tg(RFP-T:4xCa8:GCaMP5g))* (Matsui et al., 2014) could be crossed to our mutant lines to determine if a cerebellar phenotype is present in either or both mutants. While brain phenotypes have been not reported *per se* in zebrafish ciliopathy mutants at larval stages, a recent publication by Grimes and collaborators (Grimes et al., 2016) described defective motile cilia in brain ventricles and linked the resulting abnormal cerebrospinal fluid flow to curved bodies in adult zebrafish. Since our *cc2d2a* mutant adults present a similar body curvature, this warrants investigation of the ependymal cilia in this mutant through scanning electron microscopy. Unfortuna-

tely, because of the lethality of *ta3-/-* fish, which die around 12 dpf, it is not possible to carry out this experiment on this mutant. Movement of ependymal cilia can also be evaluated through the movement of fluorescent beads injected in the ventricular space at adult or larval stages.
These proposed experiments, which can be extended to other JBTS zebrafish mutants, will help to untangle the shared roles from the gene-specific and tissue-specific roles for each gene. Molecular dissection of the divergent and convergent functions will be crucial for understanding the phenotypic variability of JBTS and potentially other complex Mendelian disorders.

Concluding remarks and perspective

In this thesis, I have described different molecular mechanisms underlying the retinal phenotypes of *cc2d2a* and *ta3* mutant zebrafish and provided a new CLEM technique that, because of its ease, can be used in the future to localize any protein of interest at the ultrastuctural level, with better tissue conservation compared to immunogold. Furthermore, I have provided a useful toolkit to analyze ciliary trafficking *in vivo*, that can be applied to other cell types or mutants.
Since the association of primary cilia with disease in 2000, the ciliopathy field has been an ever expanding research field. However, while answers seem to be obtained in a linear fashion, the questions that these answers open increase in an exponential manner. Molecular dissection of the different components of the cilium will lead us to unraveling the common mechanisms underlying JBTS as well as explaining the sources of its phenotypical variability. This could impact our understanding of other genetically heterogeneous Mendelian disorders. With the future perspective exposed in the previous paragraphs and the inherent advantages that zebrafish possesses as a model to study ciliopathies, this small teleost provides a powerful tool and offers a great opportunity to research these mechanisms *in vivo*. Furthermore, identifying the molecular mechanisms underlying dysfunction of JBTS proteins will allow development of chemical screens to reverse the phenotypes that are more amenable to treatment and identify therapeutic targets in the future.

References

Alby, C., Piquand, K., Huber, C., Megarbane, A., Ichkou, A., Legendre, M., Pelluard, F., Encha-Ravazi, F., Abi-Tayeh, G., and Bessieres, B., et al. (2015). Mutations in KIAA0586 Cause Lethal Ciliopathies Ranging from a Hydrolethalus Phenotype to Short-Rib Polydactyly Syndrome. American journal of human genetics ***97***, 311-318.

Babbey, C.M., Bacallao, R.L., and Dunn, K.W. (2010). Rab10 associates with primary cilia and the exocyst complex in renal epithelial cells. American journal of physiology. Renal physiology ***299***, F495-506.

Bachmann-Gagescu, R., Dona, M., Hetterschijt, L., Tonnaer, E., Peters, T., Vrieze, E. de,

Mans, D.A., van Beersum, S.E.C., Phelps, I.G., and Arts, H.H., et al. (2015a). The Ciliopathy Protein CC2D2A Associates with NINL and Functions in RAB8-MICAL3-Regulated Vesicle Trafficking. PLoS genetics ***11***, e1005575.

Bachmann-Gagescu, R., Ishak, G.E., Dempsey, J.C., Adkins, J., O'Day, D., Phelps, I.G., Gunay-Aygun, M., Kline, A.D., Szczaluba, K., and Martorell, L., et al. (2012). Genotype-phenotype correlation in CC2D2A-related Joubert syndrome reveals an association with ventriculomegaly and seizures. Journal of medical genetics ***49***, 126-137.

Bachmann-Gagescu, R., Phelps, I.G., Dempsey, J.C., Sharma, V.A., Ishak, G.E., Boyle, E.A., Wilson, M., Marques Lourenco, C., Arslan, M., and Shendure, J., et al. (2015b). KIAA0586 is Mutated in Joubert Syndrome. Human mutation ***36***, 831-835.

Badano, J.L., Mitsuma, N., Beales, P.L., and Katsanis, N. (2006). The ciliopathies: an emerging class of human genetic disorders. Annual review of genomics and human genetics ***7***, 125-148.

Balla, T., Wymann, M., and York, J.D. (2012). Phosphoinositides II: The Diverse Biological Functions (Springer).

Bangs, F., Antonio, N., Thongnuek, P., Welten, M., Davey, M.G., Briscoe, J., and Tickle, C. (2011). Generation of mice with functional inactivation of talpid3, a gene first identified in chicken. Development (Cambridge, England) ***138***, 3261-3272.

Barclay, J.W., Morgan, A., and Burgoyne, R.D. (2005). Calcium-dependent regulation of exocytosis. Cell calcium ***38***, 343-353.

Bauer, D.E., Canver, M.C., and Orkin, S.H. (2015). Generation of genomic deletions in mammalian cell lines via CRISPR/Cas9. Journal of visualized experiments : JoVE, e52118.

Ben, J., Elworthy, S., Ng, A.S.M., van Eeden, F., and Ingham, P.W. (2011). Targeted mutation of the talpid3 gene in zebrafish reveals its conserved requirement for ciliogenesis and Hedgehog signalling across the vertebrates. Development (Cambridge, England) ***138***, 4969-4978.

Besharse, J., and Bok, D. (2011). The Retina and its Disorders (Elsevier Science).

Besharse, J., Dana, R., and Dartt, D.A. (2010). Encyclopedia of the Eye (Elsevier Science).

Boehlke, C., Bashkurov, M., Buescher, A., Krick, T., John, A.-K., Nitschke, R., Walz, G., and Kuehn, E.W. (2010). Differential role of Rab proteins in ciliary trafficking: Rab23 regulates smoothened levels. Journal of cell science ***123***, 1460-1467.

Brighouse, A., Dacks, J.B., and Field, M.C. (2010). Rab protein evolution and the history of the eukaryotic endomembrane system. Cellular and molecular life sciences : CMLS ***67***, 3449-3465.

Davletov, B., Connell, E., and Darios, F. (2007). Regulation of SNARE fusion machinery by fatty acids. Cellular and molecular life sciences : CMLS ***64***, 1597-1608.

Deretic, D., and Wang, J. (2012). Molecular assemblies that control rhodopsin transport to the cilia. Vision research ***75***, 5-10.

Dixon-Salazar, T.J., Silhavy, J.L., Udpa, N., Schroth, J., Bielas, S., Schaffer, A.E., Olvera, J., Bafna, V., Zaki, M.S., and Abdel-Salam, G.H., et al. (2012). Exome sequencing can improve diagnosis and alter patient management. Science translational medicine ***4***, 138ra78.

Doherty, D. (2009). Joubert syndrome: insights into brain development, cilium biology, and complex disease. Seminars in pediatric neurology ***16***, 143-154.

Ehmann, N., Sauer, M., and Kittel, R.J. (2015). Super-resolution microscopy of the synaptic active zone. Frontiers in cellular neuroscience ***9***, 7.

Falkenburger, B.H., Jensen, J.B., and Hille, B. (2010). Kinetics of PIP2 metabolism and KCNQ2/3 channel regulation studied with a voltage-sensitive phosphatase in living cells. The Journal of general physiology ***135***, 99-114.

Fansa, E.K., Kosling, S.K., Zent, E., Wittinghofer, A., and Ismail, S. (2016). PDE6delta-mediated sorting of INPP5E into the cilium is determined by cargo-carrier affinity. Nature communications ***7***, 11366.

Fogelgren, B., Lin, S.-Y., Zuo, X., Jaffe, K.M., Park, K.M., Reichert, R.J., Bell, P.D., Burdine, R.D., and Lipschutz, J.H. (2011). The exocyst protein Sec10 interacts with Polycystin-2 and knockdown causes PKD-phenotypes. PLoS genetics ***7***, e1001361.

Garcia-Gonzalo, F.R., Corbit, K.C., Sirerol-Piquer, M.S., Ramaswami, G., Otto, E.A., Noriega, T.R., Seol, A.D., Robinson, J.F., Bennett, C.L., and Josifova, D.J., et al. (2011). A transition zone complex regulates mammalian ciliogenesis and ciliary membrane composition. Nature genetics ***43***, 776-784.

Garcia-Gonzalo, F.R., Phua, S.C., Roberson, E.C., Garcia, G.3., Abedin, M., Schurmans,

S., Inoue, T., and Reiter, J.F. (2015). Phosphoinositides Regulate Ciliary Protein Trafficking to Modulate Hedgehog Signaling. Developmental cell ***34***, 400-409.

Glasauer, S.M.K., and Neuhauss, S.C.F. (2014). Whole-genome duplication in teleost fishes and its evolutionary consequences. Molecular genetics and genomics : MGG ***289***, 1045-1060.

Grigoriev, I., Yu, K.L., Martinez-Sanchez, E., Serra-Marques, A., Smal, I., Meijering, E., Demmers, J., Peränen, J., Pasterkamp, R.J., and van der Sluijs, P., et al. (2011). Rab6, Rab8, and MICAL3 Cooperate in Controlling Docking and Fusion of Exocytotic Carriers. Current Biology ***21***, 967-974.

Guemez-Gamboa, A., Coufal, N.G., and Gleeson, J.G. (2014). Primary cilia in the developing and mature brain. Neuron ***82***, 511-521.

Hammond, G.R., and Balla, T. (2015). Polyphosphoinositide binding domains: Key to inositol lipid biology. Phosphoinositides ***1851***, 746-758.

Hammond, G.R.V., Machner, M.P., and Balla, T. (2014). A novel probe for phosphatidylinositol 4-phosphate reveals multiple pools beyond the Golgi. The Journal of cell biology ***205***, 113-126.

Howard, J. (2001). Mechanics of Motor Proteins and the Cytoskeleton (Sinauer Associates, Publishers).

Humbert, M.C., Weihbrecht, K., Searby, C.C., Li, Y., Pope, R.M., Sheffield, V.C., and Seo, S. (2012). ARL13B, PDE6D, and CEP164 form a functional network for INPP5E ciliary targeting. Proceedings of the National Academy of Sciences of the United States of America ***109***, 19691-19696.

Jensen, V.L., Carter, S., Sanders, A.A.W.M., Li, C., Kennedy, J., Timbers, T.A., Cai, J., Scheidel, N., Kennedy, B.N., and Morin, R.D., et al. (2016). Whole-Organism Developmental Expression Profiling Identifies RAB-28 as a Novel Ciliary GTPase Associated with the BBSome and Intraflagellar Transport. PLoS genetics ***12***, e1006469.

Knodler, A., Feng, S., Zhang, J., Zhang, X., Das, A., Peranen, J., and Guo, W. (2010). Coordination of Rab8 and Rab11 in primary ciliogenesis. Proceedings of the National Academy of Sciences of the United States of America ***107***, 6346-6351.

Kobayashi, T., and Dynlacht, B.D. (2011). Regulating the transition from centriole to basal body. The Journal of cell biology ***193***, 435-444.

Kobayashi, T., Kim, S., Lin, Y.-C., Inoue, T., and Dynlacht, B.D. (2014). The CP110-interacting proteins Talpid3 and Cep290 play overlapping and distinct roles in cilia assembly. The Journal of cell biology ***204***, 215-229.

Lang, T., Bruns, D., Wenzel, D., Riedel, D., Holroyd, P., Thiele, C., and Jahn, R. (2001). SNAREs are concentrated in cholesterol-dependent clusters that define docking and fusion sites for exocytosis. The EMBO journal ***20***, 2202-2213.

Lansbergen, G., Grigoriev, I., Mimori-Kiyosue, Y., Ohtsuka, T., Higa, S., Kitajima, I., Demmers, J., Galjart, N., Houtsmuller, A.B., and Grosveld, F., et al. (2006). CLASPs attach microtubule plus ends to the cell cortex through a complex with LL5beta. Developmental cell ***11***, 21-32.

Lim, Y.S., Chua, C.E.L., and Tang, B.L. (2011). Rabs and other small GTPases in ciliary transport. Biology of the cell ***103***, 209-221.

Lopes, V.S., Jimeno, D., Khanobdee, K., Song, X., Chen, B., Nusinowitz, S., and Williams, D.S. (2010). Dysfunction of heterotrimeric kinesin-2 in rod photoreceptor cells and the role of opsin mislocalization in rapid cell death. Molecular biology of the cell ***21***, 4076-4088.

Loranger, S.S., and Linder, M.E. (2002). SNAP-25 traffics to the plasma membrane by a syntaxin-independent mechanism. The Journal of biological chemistry ***277***, 34303-34309.

Malicdan, M.C.V., Vilboux, T., Stephen, J., Maglic, D., Mian, L., Konzman, D., Guo, J., Yildirimli, D., Bryant, J., and Fischer, R., et al. (2015). Mutations in human homologue of chicken talpid3 gene (KIAA0586) cause a hybrid ciliopathy with overlapping features of Jeune and Joubert syndromes. Journal of medical genetics ***52***, 830-839.

Martin-Urdiroz, M., Deeks, M.J., Horton, C.G., Dawe, H.R., and Jourdain, I. (2016). The Exocyst Complex in Health and Disease. Frontiers in cell and developmental biology ***4***, 24.

Mateos, J.M., Guhl, B., Doehner, J., Barmettler, G., Kaech, A., and Ziegler, U. (2016). Topographic contrast of ultrathin cryo-sections for correlative super-resolution light and electron microscopy. Scientific reports ***6***, 34062.

Matsui, H., Namikawa, K., Babaryka, A., and Koster, R.W. (2014). Functional regionalization of the teleost cerebellum analyzed in vivo. Proceedings of the National Academy of Sciences of the United States of America ***111***, 11846-11851.

May-Simera, H.L., Gumerson, J.D., Gao, C., Campos, M., Cologna, S.M., Beyer, T., Boldt, K., Kaya, K.D., Patel, N., and Kretschmer, F., et al. (2016). Loss of MACF1 Abolishes Ciliogenesis and Disrupts Apicobasal Polarity Establishment in the Retina. Cell reports *17*, 1399-1413.

Mazelova, J., Ransom, N., Astuto-Gribble, L., Wilson, M.C., and Deretic, D. (2009). Syntaxin 3 and SNAP-25 pairing, regulated by omega-3 docosahexaenoic acid, controls the delivery of rhodopsin for the biogenesis of cilia-derived sensory organelles, the rod outer segments. Journal of cell science *122*, 2003-2013.

Nachury, M.V., Loktev, A.V., Zhang, Q., Westlake, C.J., Peränen, J., Merdes, A., Slusarski, D.C., Scheller, R.H., Bazan, J.F., and Sheffield, V.C., et al. (2007). A Core Complex of BBS Proteins Cooperates with the GTPase Rab8 to Promote Ciliary Membrane Biogenesis. Cell *129*, 1201-1213.

Oheim, M., Kirchhoff, F., and Stuhmer, W. (2006). Calcium microdomains in regulated exocytosis. Cell calcium *40*, 423-439.

Omori, Y., Zhao, C., Saras, A., Mukhopadhyay, S., Kim, W., Furukawa, T., Sengupta, P., Veraksa, A., and Malicki, J. (2008). Elipsa is an early determinant of ciliogenesis that links the IFT particle to membrane-associated small GTPase Rab8. Nature cell biology *10*, 437-444.

Poretti, A., Boltshauser, E., and Doherty, D. (2014). Cerebellar hypoplasia: differential diagnosis and diagnostic approach. American journal of medical genetics. Part C, Seminars in medical genetics *166C*, 211-226.

Rastogi, S., and Liberles, D.A. (2005). Subfunctionalization of duplicated genes as a transition state to neofunctionalization. BMC evolutionary biology *5*, 28.

Romani, M., Micalizzi, A., and Valente, E.M. (2013). Joubert syndrome. Congenital cerebellar ataxia with the molar tooth. The Lancet Neurology *12*, 894-905.

Roosing, S., Hofree, M., Kim, S., Scott, E., Copeland, B., Romani, M., Silhavy, J.L., Rosti, R.O., Schroth, J., and Mazza, T., et al. (2015). Functional genome-wide siRNA screen identifies KIAA0586 as mutated in Joubert syndrome. eLife *4*, e06602.

Sato, T., Iwano, T., Kunii, M., Matsuda, S., Mizuguchi, R., Jung, Y., Hagiwara, H., Yoshihara, Y., Yuzaki, M., and Harada, R., et al. (2014). Rab8a and Rab8b are essential for several apical transport pathways but insufficient for ciliogenesis. Journal of cell science *127*, 422-431.

Seixas, C., Choi, S.Y., Polgar, N., Umberger, N.L., East, M.P., Zuo, X., Moreiras, H., Ghossoub, R., Benmerah, A., and Kahn, R.A., et al. (2016). Arl13b and the exocyst interact synergistically in ciliogenesis. Molecular biology of the cell *27*, 308-320.

Shaheen, R., Faqeih, E., Alshammari, M.J., Swaid, A., Al-Gazali, L., Mardawi, E., Ansari, S., Sogaty, S., Seidahmed, M.Z., and AlMotairi, M.I., et al. (2013). Genomic analysis of Meckel-Gruber syndrome in Arabs reveals marked genetic heterogeneity and novel candidate genes. European journal of human genetics : EJHG *21*, 762-768.

Simms, B.A., and Zamponi, G.W. (2014). Neuronal Voltage-Gated Calcium Channels: Structure, Function, and Dysfunction. Neuron *82*, 24-45.

Slaats, G.G., Isabella, C.R., Kroes, H.Y., Dempsey, J.C., Gremmels, H., Monroe, G.R., Phelps, I.G., Duran, K.J., Adkins, J., and Kumar, S.A., et al. (2016). MKS1 regulates ciliary INPP5E levels in Joubert syndrome. Journal of medical genetics *53*, 62-72.

Stahelin, R.V. (2009). Lipid binding domains: more than simple lipid effectors. Journal of lipid research *50 Suppl*, S299-304.

Stauffer, T.P., Ahn, S., and Meyer, T. (1998). Receptor-induced transient reduction in plasma membrane PtdIns(4,5)P2 concentration monitored in living cells. Current Biology *8*, 343-346.

Stepanova, T., Slemmer, J., Hoogenraad, C.C., Lansbergen, G., Dortland, B., Zeeuw, C.I. de, Grosveld, F., van Cappellen, G., Akhmanova, A., and Galjart, N. (2003). Visualization of microtubule growth in cultured neurons via the use of EB3-GFP (end-binding protein 3-green fluorescent protein). The Journal of neuroscience : the official journal of the Society for Neuroscience *23*, 2655-2664.

Stephen, L.A., Tawamie, H., Davis, G.M., Tebbe, L., Nurnberg, P., Nurnberg, G., Thiele, H., Thoenes, M., Boltshauser, E., and Uebe, S., et al. (2015). TALPID3 controls centrosome and cell polarity and the human ortholog KIAA0586 is mutated in Joubert syndrome (JBTS23). eLife *4*.

Tai, A.W., Chuang, J.Z., Bode, C., Wolfrum, U., and Sung, C.H. (1999). Rhodopsin's carboxy-terminal cytoplasmic tail acts as a membrane receptor for cytoplasmic dynein by binding to the dynein light chain Tctex-1. Cell *97*, 877-887.

Wang, J., and Deretic, D. (2015). The Arf and Rab11 effector FIP3 acts synergistically with ASAP1 to direct Rabin8 in ciliary receptor targeting. Journal of cell science *128*, 1375-1385.

Westlake, C.J., Baye, L.M., Nachury, M.V., Wright, K.J., Ervin, K.E., Phu, L., Chalouni, C., Beck, J.S., Kirkpatrick, D.S., and Slusarski, D.C., et al. (2011). Primary cilia membrane assembly is initiated by Rab11 and transport protein particle II (TRAPPII) complex-dependent trafficking of Rabin8 to the centrosome. Proceedings of the National Academy of Sciences of the United States of America ***108***, 2759-2764.

Yin, Y., Bangs, F., Paton, I.R., Prescott, A., James, J., Davey, M.G., Whitley, P., Genikhovich, G., Technau, U., and Burt, D.W., et al. (2009). The Talpid3 gene (KIAA0586) encodes a centrosomal protein that is essential for primary cilia formation. Development (Cambridge, England) ***136***, 655-664.

Ying, G., Gerstner, C.D., Frederick, J.M., Boye, S.L., Hauswirth, W.W., and Baehr, W. (2016). Small GTPases Rab8a and Rab11a Are Dispensable for Rhodopsin Transport in Mouse Photoreceptors. PloS one ***11***, e0161236.

Yoshimura, S.-I., Egerer, J., Fuchs, E., Haas, A.K., and Barr, F.A. (2007). Functional dissection of Rab GTPases involved in primary cilium formation. The Journal of cell biology ***178***, 363-369.

Appendix I. Transgenic lines and constructs

Additionally to the lines and constructs described in Chapters 1 and 3, I have generated a number of transgenic lines and constructs that will be useful to perform future experiments proposed in Chapter 5. They are summarized in this appendix.

Materials and methods

RT-PCR was performed using cDNA obtained from whole larvae at 5 dpf to generate Gateway® (Invitrogen) p3' entry clones including the full length coding sequence for Rabin8 (also called Rab3IP, NM_001020581.2). The following primers were used (attB site sequences are written in lowercase):
Rabin8 attB2r:
5'-ggggacagctttcttgtacaaagtgggtATGAAGATCTTTTGGGCTAT-3'
Rabin8 attB3:
5'-ggggacaactttgtataataaagttgtTCACAGCTCATCTTTGTAGA-3'

Site targeted mutagenesis using overlapping complementary primers was employed to generate the T22N (ACC to AAC codon) point mutation leading to dominant Rab8a. The primer sequences used were (modified nucleotides are indicated in lower case): 5'-GAAGCCAAGTCTATTGAAGG-3' and 5'-TGAACAGCACACAGtTCTTC-3' to amplify from the 5'UTR to the mutation site, and 5'-GGGAAGAaCTGTGTGCTG-3' and 5'-GAGAGATGGGATAAAAGAGG-3' to amplify from the mutation site to the 3'UTR. cDNA obtained from whole zebrafish larvae at 5 dpf was used as template. The mutant sequence was assembled using the following primers (attB site sequences are written in lowercase):
Rab8a attB2r: 5'-ggggacagctttcttgtacaaagtgggtATGGCGAAGACCTACGATTA-3'
Rab8a attB3: 5'-ggggacaactttgtataataaagttgtTCACAGTAGCACACAGCGAA-3'

Gateway® (Invitrogen) recombination using the Tol2kit was performed to generate the constructs summarized in the table below. p5' entry clones included the rod-specific rhodopsin promoter (gift from the Link lab), the cone-specific alpha-transducin promoter (tacp, (Lewis et al. 2010)) and the ubiquitously expressed ubiquitin promoter (ubi, Zon lab). mCherry or GFP middle-entry clones and the aforementioned p3' entry clones as well as another p3' entry clone containing the zebrafish cc2d2a sequence (cloned by R. Bachmann-Gagescu) and p3' Rab8a zebrafish sequence (NM_001089562; gift from Beales lab). The resulting constructs were co-injected with Tol2 transposase mRNA as previously described (Kawakami 2007) into 1-cell stage embryos. Injected fish were raised and further generations (when obtained) outcrossed to *casper* zebrafish for at least two generations.

Results

Construct	Injected	Fish line	Status
ubi:mCherry-rab8b-like	Yes, by R. Bachmann-Gagescu	*Tg(ubi:mCherry-rab8b-like;bactin:GFP-centrin)*	Stable (F2)
rhod:GFP-rab11	Yes, by R. Bachmann-Gagescu	*Tg(rhod:mCherry-rab8a;rhod:GFP-rab11)*	Stable (F2)**
tacp:GFP-rab11	Yes, by R. Bachmann-Gagescu	*Tg(tacp:GFP-rab11)*	Stable (F1)**
ubi:mCherry-rab8a	Yes	*Tg(ubi:mCherry-rab8a;bactin:GFP-centrin)*	Stable (F2)
ubi:mCherry-rab8a	Yes	*Tg(ubi:mCherry-rab8a)*	Stable (F2)
rhod:mCherry-rab8aT22N	Yes	*Tg(rhod:mCherry-rab8aT22N)*	Mosaic (F0)*
tacp:EB3-GFP	Yes, by R. Bachmann-Gagescu		
rhod:GFP-cc2d2a	Yes	*Tg(rhod:GFP-cc2d2a;rhod:mCherry-rab8a)*	Mosaic (F0)*
rhod:GFP-rabin8	Yes	*Tg(rhod:mCherry-rab8a;rhod:GFP-rabin8)*	Mosaic (F0)*

The lines labeled with one asterisk (*) did not produce any positive F1 fish (>15 fish screened). The lines labeled with two asterisks (**) are viable and positive, but the imaging was not informative so far.

We aimed to have the platform to analyze Rab8-mediated trafficking (T22N dominant negative forms) in multiple cilia types (ubi-promoter) and extend the analysis of Rab8-mediated trafficking to its activation cascade (co-expressing GFP-tagged Rab11 or Rabin8) in PR. However, only the ubiquitin-driven lines have proven useful within this collection and can be used in the future to study trafficking in other cell types in different ciliary mutants.

The rhod:GFP-cc2d2a construct had a dual purpose: 1) Specifically rescue the cc2d2a phenotype in PRs of zebrafish mutants and 2) Provide a TZ reference marker. However, transiently injected animals have very few positive cells, which have strong cytoplasmic GFP expression. No F1 positive animals were obtained, likely due to the enhanced difficulty of incorporating large DNA fragments.

Appendix II. List of Abbreviations

Abbreviated name	Long name
ADPKD	Autosomal dominant polycystic kidney disease
ALMS	Alstrom syndrome
Arf4	ADP Ribosylation Factor 4
ARPKD	Autosomal recessive polycystic kidney disease
ASAP1	ARF GTPase-Activating Protein 1
ATP	Adenosine-5'-triphosphate
BB	Basal body
BBS	Bardet-Biedl syndrome
BBS17	Bardet-Biedl syndrome protein 17
BODIPY	Boron-dipyrromethene
Cas9	CRISPR associated protein 9
CC2D2A	Coiled-coil C2 containing domain protein 2 A
CDK	Cyclin dependent kinase
Cep290	Centrosomal Protein 290
Cep97	Centrosomal Protein 97
CFP	Cyan fluorescent protein
CLEM	Correlative light and electron microscopy
CNS	Central nervous system
CP110	Centriolar Coiled-Coil Protein 110
CRISPR	Clustered regularly interspaced short palindromic repeats
C-ter	Carboxy-terminus
CTS	Ciliary targeting sequence
CV	Ciliary vesicle
DAPI	4′,6-diamidino-2-phenylindole dihydrochloride
DNA	Deoxyribonucleic acid
dpf	days post fertilization
ERG	Electroretinogram
FIP3	RAB11 family interacting protein 3
GAP	GTPase activating protein
GDP	Guanosine-5'-diphosphate
GEF	Guanidine exchange factor
GFP	Green fluorescent protein
GTP	Guanosine-5'-triphosphate
GTPase	Guanosine-5'-triphosphatase
Hh	Hedgehog

hpf	hours post fertilization
hsp70	Heat-shock protein family A
IFT	Intraflagellar Transport
IFT88	Intraflagellar transport protein 88
INPP5E	Inositol Polyphosphate-5-Phosphatase E
IS	Inner segment
JBTS	Joubert syndrome
Kif24	Kinesin Family Member 24
LCA	Leber congenital amaurosis
MACF1	Microtubule actin crosslinking factor 1
MICAL3	Microtubule associated monooxygenase, calponin and LIM domain containing protein 3
MKS	Meckel-Gruber syndrome
MTOC	Microtubule organization center
MTS	Molar tooth sign
NINL	Ninein-like protein
NPHP	Nephronophthisis
NSF	N-ethylmaleimide-sensitive factor
N-ter	Amino-terminus
OCV	Opsin-Carrier-Vesicle
OMIM	Online Mendelian Inheritance in Man
OS	Outer segment
PCP	Planar cell polarity
PFA	paraformaldehyde
PIP	Phosphatidylinositol 4-phosphate
PIP2	Phosphatidylinositol 4,5-bisphosphate
PR	Photoreceptor
PTU	1-phenyl-2-thiourea
PVDF	Polyvinylidene difluoride
qRT-PCR	Quantitative reverse transcription polymerase chain reaction
rhod	Rhodopsin
RPE1	Human retinal pigmented epithelial cells
RT	Room temperature
RTC	Rhodopsin transport carrier (OCV synonymous)
SEM	Scanning electron microscopy
Shh	Sonic hedgehog
SNARE	SNAP Soluble NSF Attachment Protein REceptor

SRTD	Short-rib thoracic dysplasia with or without polydactyly
Stx3	Syntaxin 3
Ta3	Talpid3
TaCP	Transducin alpha cone promoter
TALEN	Transcription activator-like effector nuclease
TEM	Transmission electron microscopy
t-SNARE	target membrane SNARE
TUNEL	Terminal deoxynucleotidyl transferase dUTP nick end labeling
TZ	Transition zone
VAMP7	Vesicle associated membrane protein 7
VDAC1	Voltage dependent anion channel 1
v-SNARE	vesicular membrane SNARE
Wnt	Wingless type pathway
WT	Wild-type
ZFN	Zinc finger nuclease
ZIRC	Zebrafish international resource center
ZMB	Center for microscopy and image analysis (original in German)

Appendix III. Curriculum Vitae

Personal Information

Name	Irene OJEDA NAHARROS
Present address	Zürichholzstrasse 5, 8057, Zürich
Phone	+41(0)766811087
e-mail	irene.ojedanaharros@uzh.ch
Date of Birth	04.10.1987
Place of Birth	Cuenca, Spain
Citizenship	Spanish

Academic Education

2013-present	PhD thesis in Neuroscience, in the laboratory of Prof. Dr. Stephan Neuhauss at the Institute of Molecular Life Sciences, University of Zurich, Switzerland **Thesis:** Modelling ciliopathies in the zebrafish: elucidating the role of Cc2d2a and Talpid3 in photoreceptor development and function
2011-2012	Postgraduate M.Sc. in Biochemistry, Molecular Biology and Biomedicine. Molecular Biology Option, Biomedicine Minor, Faculty of Medicine. Universidad Autónoma de Madrid, Spain. Thesis completed at the lab of Dr. Helena Mira Aparicio **Thesis:** Determination of the mouse SVZ proliferative status during ageing
2005-2011	B.Sc. + M.Sc. in Biology. Biotechnology and Medical Biology Specializations, Faculty of Biology and Geology. Universidad Complutense de Madrid, Spain. One year abroad in Georg-August Universität Göttingen. Thesis completed at the lab of Prof. Dr. Ernst A. Wimmer **Thesis:** Biochemical characterization of the odoriferous glands of the red flour beetle
1999-2005	High school (Matura), Instituto de Educación Secundaria Rafael Alberti, Coslada, Madrid, Spain

Presentations at international research meetings

2016	**Poster presentation:** EMBO 2016 Cilia, Amsterdam, Netherlands The role of the ciliopathy protein CC2D2A in ciliary trafficking in zebrafish photoreceptors

2015 **Poster presentation:** Radboud New Frontiers in Cilia Medicine, Nijmegen, Netherlands

The role of the ciliopathy protein CC2D2A in ciliary trafficking

2015 **Poster presentation:** 9th European Zebrafish Meeting, Oslo, Norway

Live imaging of Rab8 trafficking in photoreceptors of a zebrafish ciliopathy model

Publications and manuscripts in preparation

- **Ojeda Naharros, I**., Gesemann, M., Mateos, J.M., Barmettler, G., Neuhauss, S.C.F., and Bachmann-Gagescu, R. The ciliopathy protein CC2D2A organizes the vesicle fusion machinery at the periciliary membrane of zebrafish photoreceptors. *In preparation.*
- **Ojeda Naharros, I.**, Cristian, F.B., Zang, J., Gesemann, M., Neuhauss, S.C.F. and Bachmann-Gagescu, R. The ciliopathy protein Talpid3 acts upstream of Rab8 activation in outer segment formation and maintenance in zebrafish retinal photoreceptors. *In preparation.*
- Mateos, J.M., Barmettler, G., Doener, J., **Ojeda Naharros, I.**, Guhl, B., Neuhauss, S.C.F**.,** Kaech, A., Bachmann-Gagescu, R., & Ziegler, U. Correlative super-resolution and electron microscopy to resolve protein localization in zebrafish retina. *JoVE. In press*
- Li, J., Lehmann, S., Weißbecker, B., **Ojeda Naharros, I.**, Schütz, S., Joop, G. & Wimmer, E.A. (2013) Odoriferous defensive stink gland transcriptome to identify novel genes necessary for quinone synthesis in the red flour beetle, *Tribolium castaneum*. *PLoS Genet*. e1003596
- De Munck, E., Muñoz-Sáez, E., Miguel, B.G., Solas, M.T., **Ojeda, I.**, Martínez, A., Gil, C. & Arahuetes, R.M. (2013) β-N-methylamino-l-alanine causes neurological and pathological phenotypes mimicking Amyotrophic Lateral Sclerosis (ALS): the first step towards an experimental model for sporadic ALS. *Environ Toxicol Pharmacol.* 36: 243-255

Acknowledgements

First of all and foremost, I would like to express my gratitude to both my supervisors, Stephan Neuhauss and Ruxandra Bachmann-Gagescu for giving me the opportunity to do my PhD in their lab. Thank you, Stephan, for hosting and supporting our cilia mini-group, keeping an open door for scientific and non-scientific discussions and inviting us to nice (and delicious) Thanksgiving dinners, birthdays and "becoming swiss" events. Ruxandra, you have been a great mentor to me and "thank you" are two words that cannot express for how much I appreciate you… thank you for believing in me, for teaching me science, life lessons, survival in the scientific world and for introducing and promoting my work to important people in the field during conferences. As your first PhD student, I hope you always remember these four years with fondness. I wish you success and hope that the mini-group becomes really big and distinguished in the years to come.

Many thanks go to Ronald Roepman, Esther Stoeckli and Stefan Luschnig for being members of my PhD thesis committee and for their valuable scientific input. Ronald, thank you for your career advice and for encouraging me to pursue a scientific career.

Thanks also to Irene Hoffman for always helping us with administrative issues.

Many warm thanks to all the present and past members of the Neuhauss group. It has been a pleasure being your colleague and sharing time both inside and outside the lab with you. Thanks to Thomas, Peter, Fränzi, Steven, Marco, Kaspar, Sabina, Manu, Pascal, Kulsum and Anja Naacke.

I would like to acknowledge people who have immensely facilitated my job: our technicians, Kara and Martin, for taking good care of our fish and keeping everything under control in the lab even in times of crisis. Matthias Gesemann, for sharing his expertise in antibody design, western and IP troubleshooting (and subsequent headache management), phylogenetic tree building and for showing me that I have a brilliant future as long as I do not choose ice skating as a career path. Marion and Jingjing, for their help with western blots, qRT-PCR and for invitations to the funniest Christmas events ever and the best Oktoberfest/Carnival pics respectively. Bianca, who started the Talpid3 project and kept me company in the solitary cilia lab during long working days. Marlen, who shared my tracking nightmare with dignity.

Special thanks go to all the people in the ZMB, who have helped me so much. Thanks to Txema Mateos, to whom I am so indebted, Gery Barmettler, Moritz Kirschmann, Caroline Aemisegger, Jana Doehner and Urs Ziegler.

A big warm thank you goes to my fellow PhD students: Steffi, Stella, André, Yuya and Domino. To Steffi, my best friend, for lending a hand whenever needed and being the most pragmatic and clever person in problem-solving situations, for inviting and showing me wonderful places in Switzer-

land, her spaghetti *a la Estefanía*, and not giving up on me ever… especially when it came to skiing. To Stella, with whom I have so much in common, for her patience, kind spirit and for selflessly sharing her time, her incredible amount of knowledge and her comfort in and outside the office. To André, for providing us with delicious home-brewed beer, cheerful company, for inviting me to beautiful concerts and teaching me the best German expression ever to show surprise. To Yuya, who immortalized me in his thesis acknowledgements as "Irene from Madrid" and provided countless laughs during lunchtime conversations and karaoke sessions. To Domino, for inviting me to beautiful singing ensembles and for "ensembling" herself the greatest volleyball team in the world. Go T-rex!

A special mention also goes to former lab members Jenny, Tanja, David and Valentin, for the many fun activities we have done together. I also want to thank Chiara for her thoughtful insights shared while riding the train to the easy slopes (now we are done with them!), Adriana for her kindness and offering her place for massive cookie baking events, Tamara for being the passionate-but-calm person our mini-group needed (I wish you a lot of success with your PhD!), Selin for making me crack up even in the most blue moments and for sharing so much good mood and gems of wisdom (I cannot top the acknowledgements section of your master thesis, I am afraid), Michelle for feeding me with candy when my brain entered energy-saving mode, and our newest master students Anja Enz and Valerio to whom I wish a great time in the lab.

Pablo, thank you so much for your loving care throughout the PhD and especially during the writing process. Thanks for feeding me in the past weeks and helping me in the past four years with your programming and software skills, which have helped me so much in accomplishing what is now summarized in this work. Thanks for the scientific discussions, for pushing me beyond my limits to improve myself, for your moral support and for always believing in me. Your supporting counsel could be worldly quoted from Winnie the Pooh: «*you are braver than you believe, stronger than you seem and smarter than you think*». I only expect great things from you.

Last but not least, I would like to thank my friends and my family. Miriam, thanks for staying by my side ever since we met and trusting my illustrating abilities. Lucía, the best sister one could wish for, thanks for your blind trust in me. I would quote any of the nice things you write and tell me to express your unconditional support but I am afraid this is supposed to be the kind of document that requires sobriety and political correctness. Thank you mom and dad for teaching me so many things, engaging my curiosity and encouraging me to do anything I wanted because "you make anything possible with your tenacity, Irene", even in situations where what I wanted to do completely messed up with your schedules and your peace. Thank you for enduring the long distance, your support and picking me from the airport. Finally, and also on my mother's behalf, thanks to the sequoia who gave its life for the printing of this thesis and the bibliography I needed during these four years to write it.